

UNIFIED CONSTITUTIVE EQUATIONS  
FOR CREEP AND PLASTICITY

# UNIFIED CONSTITUTIVE EQUATIONS FOR CREEP AND PLASTICITY

*Edited by*

ALAN K. MILLER

*Professor (Research) of Materials Science and Engineering, Stanford  
University, California, USA*



ELSEVIER APPLIED SCIENCE  
LONDON and NEW YORK

ELSEVIER APPLIED SCIENCE PUBLISHERS LTD  
Crown House, Linton Road, Barking, Essex IG11 8JU, England

*Sole Distributor in the USA and Canada*  
ELSEVIER SCIENCE PUBLISHING CO., INC.  
52 Vanderbilt Avenue, New York, NY 10017, USA

WITH 11 TABLES AND 92 ILLUSTRATIONS

© ELSEVIER APPLIED SCIENCE PUBLISHERS LTD 1987  
(except Chapter 1)

Softcover reprint of the hardcover 1st edition 1987

**British Library Cataloguing in Publication Data**

Unified constitutive equations for creep and plasticity.

1. Plasticity  
I. Miller, A.K.  
620.1'1233 TA418.14

**Library of Congress Cataloging-in-Publication Data**

Unified constitutive equations for creep and plasticity.

Includes bibliographies and index.

1. Deformations (Mechanics)—Mathematical models.  
2. Materials—Creep—Mathematical models. 3. Plasticity—Mathematical models.  
I. Miller, A. K. (Alan K.)

TA417.6.U55 1987 620.1'123'0724 87-8895

ISBN-13: 978-94-010-8039-2 e-ISBN-13: 978-94-009-3439-9

DOI: 10.1007/978-94-009-3439-9

No responsibility is assumed by the Publisher for any injury and/or damage to persons or property as a matter of products liability, negligence or otherwise, or from any use or operation of any methods, products, instructions or ideas contained in the material herein.

**Special regulations for readers in the USA**

This publication has been registered with the Copyright Clearance Center Inc. (CCC), Salem, Massachusetts. Information can be obtained from the CCC about conditions under which photocopies of parts of this publication may be made in the USA. All other copyright questions, including photocopying outside of the USA, should be referred to the publisher.

All rights reserved. No parts of this publication may be reproduced, stored in a retrieval system, or transmitted in any form or by any means, electronic, mechanical, photocopying, recording, or otherwise, without the prior written permission of the publisher.

## Preface

Constitutive equations refer to ‘the equations that constitute the material response’ at any point within an object. They are one of the ingredients necessary to predict the deformation and fracture response of solid bodies (among other ingredients such as the equations of equilibrium and compatibility and mathematical descriptions of the configuration and loading history). These ingredients are generally combined together in complicated computer programs, such as finite-element analyses, which serve to both codify the pertinent knowledge and to provide convenient tools for making predictions of peak stresses, plastic strain ranges, crack growth rates, and other quantities of interest.

Such predictions fall largely into two classes: structural analysis and manufacturing analysis. In the first category, the usual purpose is life prediction, for assessment of safety, reliability, durability, and/or operational strategies. Some high-technology systems limited by mechanical behavior, and therefore requiring accurate life assessments, include rocket engines (the space-shuttle main engine being a prominent example), piping and pressure vessels in nuclear and non-nuclear power plants (for example, heat exchanger tubes in solar central receivers and reformer tubes in high-temperature gas-cooled reactors used for process heat applications), and the ubiquitous example of the jet engine turbine blade. In structural analysis, one is sometimes concerned with predicting distortion *per se*, but more often, one is concerned with predicting fracture; in these cases the information about deformation is an intermediate result *en route* to the final goal of a *life* prediction. In manufacturing analysis, one is more often concerned with predicting deformation response (such as press loads and die filling during forging) but is also sometimes concerned with

predicting material failure (such as cracking during rolling and forging, tearing during sheet stretching and drawing, or fracture of metallic interconnects during integrated circuit fabrication).

Broadly speaking, the material phenomena pertinent to the above needs are governed by three physical processes: elastic deformation (stretching of interatomic bonds), non-elastic deformation (permanent switching of interatomic bonds among the various atoms in the solid), and decohesion (permanent breakage of bonds). The first process is predictable by the well-understood laws of elasticity and needs no further discussion in this book. The third category is so complex—because it depends not only on the material behavior at a point but also on the distribution of stresses and strains across the body—that few unified, generally applicable approaches for predicting fracture have emerged, other than the ‘laws’ of fracture mechanics which have well-known limitations. It is in the *second* category that the greatest progress has been made in the past several decades, in formulating equations that can predict the non-elastic deformation response under fairly general conditions; and this second category is the focus of the present volume.

The need to *predict* implies that the desired answer is not already available from experimental measurements. In most cases, this is not because of a total lack of test data on the material of interest; it is because of the notorious history or path dependence of non-elastic deformation response. Even though experiments spanning the entire temperature and strain rate regime of interest may have been run, it is impossible to explore all of the sequences and combinations of loadings that might be imposed in service. Interactions of ‘creep’ and ‘plasticity’ are one such complication; non-proportional multiaxial deformation is a second. Thus, a major purpose of modern constitutive equations is to extrapolate from simple test data to complex histories. Of course, extrapolation in the usual sense, e.g. from short-term tests to long-term service, or from a small number of test data to all of the temperatures and strain rates of interest, is also a major objective of the constitutive equations presented herein.

The principle that extrapolation is most accurately done using equations founded on the actual governing physical processes has been invoked so often that it is scarcely necessary to mention it at this point. This principle gives us a practical, utilitarian reason for using as much as possible the scientific knowledge about non-elastic deformation in developing these constitutive equations. Chapter 1, drawing on its

author's entire career in studying the physical mechanisms of non-elastic deformation, summarizes such knowledge. Most prominent among this knowledge is the fact that both 'plasticity' and 'creep' (at least creep due to slip) are controlled by the motion of dislocations; this leads directly to an obligation to *unify* 'plasticity' and 'creep' within a *single* set of equations, rather than taking the traditional engineering approach of one set of equations to predict 'time-independent plastic' strains and a separate set of equations to predict 'time-dependent creep' strains. Predicting both 'plasticity' and 'creep' within a single variable is the primary distinguishing feature of the unified constitutive equations approach.

Also prominent among our physical knowledge is the role of internal structure (e.g. dislocation density, state of internal stress, degree of solute clustering) in controlling non-elastic deformation. This leads directly to the use of internal structure variables, rather than only the external variables such as strain or time, to predict transient and steady-state responses with the unified equations.

Despite the fact that the above arguments make it incumbent upon us to try to simply *derive* a set of predictive equations from the actual physical mechanisms, it is impossible at the present time to do so. For one thing, despite the many great advances in our scientific knowledge about non-elastic deformation, the available 'first-principles' theories do not yet treat deformation under general loading histories, over wide ranges and changes in temperature, for multiaxial loadings, and in complex engineering materials. For another, even if they did, the resulting equations might be too cumbersome for structural or manufacturing analysis purposes. Faced with this situation, but still mindful of our obligation to build as much as possible of the physical knowledge into the equations, we are forced to make judgments of various sorts, such as:

- Which subset among all of the possible deformation phenomena deserves the most attention?
- Which types of internal variables should be used in the equations?
- Which are the most accurate quantitative expressions for predicting these phenomena?

As might be expected, various investigators differ in their judgments with respect to these and other factors. A natural consequence is the current existence of several unified constitutive equation approaches, all sharing a similar overall philosophy but differing in many details.

The major portion of this book (Chapters 2–6) is a presentation of five such approaches, each authored by its own ‘proponent’. Chapter 1 includes elements of a sixth set of constitutive equations. The reader is invited to browse through this smorgasbord of approaches, both to develop an appraisal of the overall state-of-the-art in unified constitutive equations, and also to select the approach best suited to his or her own needs.

As an aid in assessing the merits (and a few demerits) of the various approaches, Chapter 7 discusses the equations presented in the earlier chapters. This critique is mostly from the point of view of a potential *user* of such equations, and focusses on both their predictive capabilities and their numerical behavior.

The above discussion has concentrated on the pragmatic aspects of unified constitutive equations as a methodology for engineering predictions. There is also a scientific accomplishment within these covers, namely partial progress towards a unified, first-principles model that can predict all aspects of non-elastic deformation behavior, based on a detailed representation of the internal physical processes. Clearly we are not there yet, but equally clearly, the field is closer to that goal with unified constitutive equations than it has been with the previous ‘traditional’ approaches. Perhaps it is not too unrealistic to hope that some future edition may present *the* universally-accepted, first-principles based, set of unified constitutive equations for plastic deformation and creep of engineering alloys.

It is a pleasure to acknowledge assistance from a number of sources. First and foremost are the authors who have contributed chapters to this endeavor. Collectively, they represent a clear majority of the expertise in this field. The staff at Elsevier Applied Science Publishers have been most helpful. Ms Virginia Sills provided considerable assistance in the preparation and coordination of the book manuscript. Other individuals, acknowledged by the authors of each chapter, were equally helpful. Many agencies provided financial support for the sponsored research programs under which the constitutive equations presented herein were developed; these agencies are acknowledged in the individual chapters but special mention must be made of the US Department of Energy, Office of Basic Energy Sciences, Materials Sciences Division, which not only supported several of the individual efforts but also provided support for the Editor during the preparation of this book.

**Alan K. Miller**

# Contents

<i>Preface</i> . . . . .	v
<i>List of Contributors</i> . . . . .	xiii
<b>1 Constitutive Behavior Based on Crystal Plasticity</b> . . . . .	<b>1</b>
U. F. Kocks	
1 Introduction . . . . .	1
2 Some Important Realities . . . . .	4
2.1 Uniaxial Monotonic Deformation . . . . .	4
2.2 Multiaxial Deformation . . . . .	11
3 Flow Kinetics . . . . .	16
3.1 Non-uniform Deformation . . . . .	16
3.2 Uniform Deformation . . . . .	18
4 Polycrystal Plasticity . . . . .	28
4.1 Crystal Plasticity . . . . .	29
4.2 Averaging over a Polycrystal . . . . .	36
5 Evolution . . . . .	48
5.1 Texture Evolution . . . . .	48
5.2 Substructure Evolution . . . . .	51
6 Internal Stresses . . . . .	64
6.1 Two-phase Materials . . . . .	65
6.2 Single-phase Materials . . . . .	68
7 Application . . . . .	72
7.1 Diagnostics . . . . .	73
7.2 Constitutive Relations . . . . .	76
8 Summary and Recommendations . . . . .	81

<b>2</b>	<b>State Variable Theories Based on Hart's Formulation . . .</b>	<b>89</b>
	M. A. KORHONEN, S.-P. HANNULA and CHE-YU LI	
1	Introduction . . . . .	89
2	The Physical and Phenomenological Bases . . . . .	90
3	A State Variable Description . . . . .	95
	3.1 Hart's Model for Grain Matrix Deformation . . . . .	95
	3.2 An Extension of Hart's Model to a Multiaxial Loading Case . . . . .	98
	3.3 An Extension of Hart's Model to Transient Deformation . . . . .	98
	3.4 An Extension of the State Variable Description to Grain Boundary Sliding . . . . .	101
4	The Type of Data Utilized in Determining the Material Parameters . . . . .	103
5	Materials Tested . . . . .	107
6	Simulative and Predictive Powers of the State Variable Approach. . . . .	108
	6.1 Schematic Description of the Flow Chart . . . . .	109
	6.2 Simulations . . . . .	115
	6.3 Predictions . . . . .	116
7	Discussion . . . . .	122
	7.1 The Components of the Flow Stress . . . . .	122
	7.2 Work-hardening . . . . .	123
	7.3 Limitations of the Present State Variable Approach. . . . .	124
	7.4 Future Developments . . . . .	125
	Appendix 1 . . . . .	130
	Appendix 2 . . . . .	134
<b>3</b>	<b>The MATMOD Equations . . . . .</b>	<b>139</b>
	ALAN K. MILLER	
1	Introduction . . . . .	139
2	Development of the Equations . . . . .	141
	2.1 General Relations Between the Phenomena Ad- dressed and the Types of Equations Required . . . . .	141
	2.2 Physical and Phenomenological Bases for the Equations . . . . .	146
	2.3 Phenomenological Development of the Specific Equations . . . . .	164
3	Simulations and Predictions . . . . .	185
	3.1 Aluminum (emphasizing strain hardening and strain softening behaviors). . . . .	186

3.2	Austenitic Stainless Steel (emphasizing solute effects) . . . . .	198
3.3	Zircaloy (emphasizing irradiation effects) . . . . .	204
4	Numerical Integration Methods . . . . .	208
5	Calculation of the Material Constants . . . . .	211
6	Summary . . . . .	212
<b>4</b>	<b>The Mechanical Equation of State . . . . .</b>	<b>221</b>
	J. H. GITTUS	
1	Yield Criteria . . . . .	221
1.1	Von Mises Yield Criterion . . . . .	221
1.2	Other Yield Criteria . . . . .	222
1.3	Yield Criteria Applicable to Polymers . . . . .	222
1.4	Yield Criteria Applicable to Metals . . . . .	223
2	Mechanical Equation of State for Dislocation Creep under Multiaxial Stresses . . . . .	224
2.1	Some Anticipated Features of the MEOS . . . . .	224
2.2	Anelasticity: the Delayed Elastic Strain Diagram . . . . .	225
2.3	Non-recoverable Strain . . . . .	231
2.4	Remobilisation by Stress Reversal . . . . .	234
2.5	Multiaxial Strain Rates and the Dislocation Velocity . . . . .	235
2.6	The Strain-Time Equation . . . . .	236
2.7	Computer Program that Solves the MEOS . . . . .	242
<b>5</b>	<b>A Physically Based Internal Variable Model for Rate Dependent Plasticity . . . . .</b>	<b>245</b>
	R. D. KRIEG, J. C. SWEARENGEN and W. B. JONES	
1	Introduction . . . . .	245
2	The General Problem . . . . .	248
2.1	Linear Model . . . . .	248
2.2	Non-Linear Model . . . . .	251
3	Proposed New Model . . . . .	253
3.1	The Kinematic Internal Variable . . . . .	253
3.2	The Isotropic Internal Variable . . . . .	254
3.3	Final Equations for the Model . . . . .	258
3.4	Determination of Constants . . . . .	260
3.5	Problems with Parameter Determination . . . . .	266
4	Behavior of the Model . . . . .	268

<b>6</b>	<b>Review of Unified Elastic–Viscoplastic Theory . . . . .</b>	<b>273</b>
	S. R. BODNER	
1	Introduction . . . . .	273
2	Constitutive Equations . . . . .	275
	2.1 Basic Equations . . . . .	275
	2.2 Evolution Equations . . . . .	278
	2.3 Temperature Dependence . . . . .	284
3	Interpretation and Evaluation of Material Constants . . . . .	286
4	Modeling of Metals . . . . .	290
5	Applications . . . . .	295
	5.1 Finite Element Computer Programs . . . . .	295
	5.2 Finite Difference Computer Programs . . . . .	296
	5.3 Special Problems . . . . .	297
<b>7</b>	<b>Summary and Critique . . . . .</b>	<b>303</b>
	D. BAMMANN and R. D. KRIEG	
1	Introduction . . . . .	303
2	Model by Krieg, Swearngen and Jones . . . . .	308
3	Model by Miller . . . . .	310
4	Model by Bodner . . . . .	312
5	Model by Korhonen, Hannula and Li . . . . .	316
6	Model by Gittus . . . . .	320
7	Numerical Difficulties with the Models . . . . .	324
8	Conclusion . . . . .	327
	Appendix A . . . . .	329
	Appendix B . . . . .	332
	<i>Index</i> . . . . .	337

## List of Contributors

D. BAMMANN

*Mechanics of Materials Division, Sandia National Laboratories,  
Livermore, California 94550, USA*

S. R. BODNER

*Department of Mechanical Engineering, Technion—Israel Institute  
of Technology, Haifa, Israel*

J. H. GITTUS

*Safety and Reliability Directorate, United Kingdom Atomic Energy  
Authority, Warrington, Cheshire WA3 4NE, UK*

S.-P. HANNULA

*Department of Materials Science and Engineering, Cornell  
University, Ithaca, New York 14853, USA*

W. B. JONES

*Physical Metallurgy Division, Sandia National Laboratories,  
Albuquerque, New Mexico 87185, USA*

U. F. KOCKS

*Centre for Materials Science, Los Alamos National Laboratory,  
Los Alamos, New Mexico 87545, USA*

M. A. KORHONEN

*Department of Materials Science and Engineering, Cornell University, Ithaca, New York 14853, USA. Present address: Department of Mining and Metallurgy, Helsinki University of Technology, 02150 Espoo 15, Finland.*

R. D. KRIEG

*Applied Mechanics Division, Sandia National Laboratories, Albuquerque, New Mexico 87185, USA*

CHE-YU LI

*Department of Materials Science and Engineering, Cornell University, Ithaca, New York 14853, USA*

A. K. MILLER

*Department of Materials Science and Engineering, Stanford University, Stanford, California 94305, USA*

J. C. SWEARENGEN

*Advanced Systems Division, Sandia National Laboratories, Livermore, California 94550, USA*

# 1

## Constitutive Behavior Based on Crystal Plasticity

U. F. Kocks

*Center for Materials Science, Los Alamos National Laboratory, Los  
Alamos, New Mexico, USA*

### 1. INTRODUCTION

Constitutive equations are the vehicle by which our knowledge of material behavior enters into engineering design. At the very least, they should be sufficiently accurate. This could be—and frequently is—achieved by an empirical description based on data obtained under conditions that essentially duplicate those of the specific application. Of more general usefulness are relations that can be applied under a wide range of conditions and for many materials, containing a number of materials parameters (the fewer the better), which can be measured in simple tests. Such general relations can be expected to be found only if they fulfill two conditions: they must be phenomenologically sound; and they should be based on as much of the underlying physics as can be ascertained with some confidence. The closer the phenomenological description reflects the actual physical processes involved, the further it can be extrapolated beyond the range of variables for which it was measured.

Phenomenological soundness reflects, *inter alia*, an appropriate choice of variables, and a formulation that exhibits the proper invariance against arbitrary frames of reference. For example, it recognizes that the material responds to stresses, not forces (thus separating parameters of the geometry from those of the material), and that the stress is a second-rank tensor; it takes proper account of the changes in geometry with finite deformations, usually by the use of matrix descriptions. These problems are by no means trivial, but they

are solvable. More subtle are judgments as to whether one should use history or state variables, integral or differential descriptions, and the like.

We will address some of these questions briefly but will, in the main, oversimplify the phenomenological aspects in order to concentrate on the material properties. Thus, we will inquire into the behavior of a *material element* (a convected volume element) under a macroscopically uniform stress during a macroscopically uniform, *infinitesimal* increment of strain. These (local, average) stresses and strain-increments are supposed to be related to surface tractions and surface displacements by the standard methods of solid mechanics. For this purpose, the medium in which the element is embedded is considered non-dissipative—though the element itself is essentially dissipative. By this convention, the local stresses and strain-increments become, in effect, the ‘applied’ variables (regardless of which is viewed as the independent and which as the dependent one). Their product is the work done by the environment on the material element under consideration, representative, in the end, of the lowering of weights at the surfaces.<sup>1</sup>

We will regard the material element as being at *constant temperature*, on the time scale for which the behavior is described. The *material response* is then principally the relation between the stress and the strain-increment. In addition, the stress increment, time-rates of change, and other variables may enter under certain circumstances.

The prime lesson to be learned from materials science is that there is not one material response, one ‘mechanical equation of state’, or even one set of differential constitutive equations. If such a completely general formulation were attempted, it would be too complicated to be of any use. A more effective approach is to look for *classes of materials*, *regimes of variables*, and *aspects of behavior*, for which a ‘universal’ constitutive description can be found. For example, in the present treatise, we will concentrate on polycrystalline, single-phase metals of cubic lattice structure that have been plastically deformed by, say, 1–100%, at temperatures between about 20 K and one-half to two-thirds of the melting temperature, at strain rates between about  $10^{-7}$  and  $10^3 \text{ s}^{-1}$ . Within this restricted (though very broad) ‘interest space’, deformation is governed by *crystallographic slip* in the grains of the material element or, on a finer scale, by *dislocation glide* and *dislocation storage*. This assessment of the physical mechanisms allows

one to formulate a meaningful set of stress/strain relations, with respect to both the kinetics and the multi-axial behavior.

An important input from an understanding of the physical mechanisms is the provision of *diagnostic tools* to assess whether a specific material under specific conditions in fact falls within the assumed 'regime'.<sup>1,2</sup> In Section 7 we will give some examples; in particular, it will be outlined how one can assess whether a material behaves, in its macroscopic properties, like a 'single-phase' or a 'multi-phase' material, which has important implications for the hardening rule to be expected.

A final decision one has to make is which *aspects of behavior* to include. Again, if one attempted to condense *all* aspects of the mechanical behavior into one general set of constitutive relations, these would quickly become unmanageable. This is the point in any complex problem where judgment becomes of paramount importance. For the purposes of the present treatise, considering the 'interest space' circumscribed above, it is our judgment that a sufficiently self-contained description of *plasticity* can be obtained by ignoring elasticity and anelasticity, unloading and reverse-loading effects, inertial effects and body-forces, and energy storage. We will give some justifications for this judgment in Section 2. The judgment concerns material properties only; for *calculational* purposes, an inclusion of elasticity is sometimes necessary (when pure plasticity relations cannot be inverted), and body forces are sometimes used explicitly as an algorithmic tool, etc.

Our primary concern will be with three aspects of material behavior:

- the *kinetics* of flow under the influence of thermal activation, which is well described elsewhere<sup>1,3</sup> and will only briefly be summarized in Section 3;
- the influence of polycrystal plasticity on the *multi-axial* stress-strain relations for *anisotropic* materials, for which we present new results in Section 4;
- the description of the *evolution* of the state parameters, which is given for both texture and substructure evolution in Section 5, including some new proposals for treating a specific second state parameter.

To round out these primary concerns, we will discuss various meanings of the term 'internal stress' in Section 6, and assess them with respect

to the necessity or usefulness of introducing such an extra parameter. Finally, in Section 7, we summarize diagnostic procedures to establish the type of behavior that controls a given material in a given regime of the variables, and summarize the constitutive relations for the interest sphere emphasized in this article. This leads to some general recommendations in Section 8.

A recurring theme in constitutive relations is scaling laws. We will give some general guidance to various stress and temperature scaling parameters. In addition, we discuss briefly the fundamental question of *scale*: the size of a meaningful material element (Section 3.1.1).

A major theme of this book is ‘unified’ constitutive equations for ‘plasticity’ and ‘creep’. In the physical theories of plastic deformation, this unification exists *ab initio*: whether the strain (rate) is prescribed and the stress is measured, or the stress is prescribed and the strain (rate) measured—the material response is the same, it must be independent of the boundary conditions.

The material response is also independent of the history; it is entirely determined by the current (micro-)structure, regardless of which path was taken to get there. This may be called the ‘article of faith’ of material scientists, and it will be assumed throughout this work: *current behavior depends only on the current state*. The current rate of evolution of the state is one aspect of current behavior.

## 2. SOME IMPORTANT REALITIES

For problems as complicated as plasticity, there is no hope of ever finding a ‘correct’ solution, from first principles, even for a restricted interest space. The most important decisions are made before one writes down the first equation: namely, what to consider important and what to neglect if necessary. It is not only approximations at the solution stage that are made (as anywhere in physics), but also judgments at the problem-setting stage. To be as wise as possible in making these judgments, it is imperative to have most of the basic realities in mind.

### 2.1. Uniaxial Monotonic Deformation

#### 2.1.1. Yield

Figure 1(a) shows the beginning of a typical stress/strain curve. It is drawn on a scale that emphasizes the transition from elastic to plastic

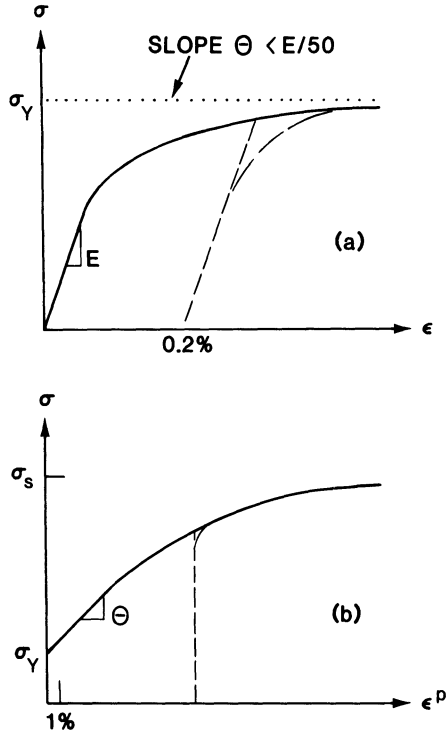


**Fig. 1.** The same stress/strain curve drawn schematically on two scales: (a) to emphasize the elastic–plastic transition, which is typically completed by about 5 times the elastic strain; (b) to emphasize the fully plastic state and strain hardening. The dashed lines show unloading/reloading behavior.

behavior. For about half of the stress range shown, the behavior is linear-elastic (modulus  $E$ ). The beginning of deviations from linearity coincides, for most materials,† with the beginning of plasticity: upon unloading, there would be a permanent ‘offset’. This first deviation from nonlinearity is sometimes used as the definition of ‘yield’; more succinctly, it is called the ‘proportional limit’. Since the first deviation from linearity is a matter of the resolution of the experiment, a definition in terms of the magnitude of the offset is often preferred. A typical choice for ‘microyield’ is an offset strain of  $10^{-5}$ .

† Nonlinear elasticity of the deviatoric components is important only in materials of exceptional strength.

The slope of the stress/strain curve then drops precipitously: typically, it changes by one or two orders of magnitude as the stress increases by a factor 2. For this reason, it is easy to define an *asymptotic* behavior: on the scale of Fig. 1(a) it is a horizontal line; this stress is normally defined as the *yield stress* (or yield strength, or macroyield stress, or flow stress). Another common definition uses an offset of 0.2%; this is, in practice, for many materials, equivalent to the asymptotic definition, because yield is so sharp. (A more general definition would be an offset of 5 times the elastic strain: then the material is essentially fully plastic.)

The asymptote is not exactly horizontal. Fortunately, it is approximately *straight* for many materials (single-phase, at low temperatures), with a slope of about  $E/50$ . Then, *back-extrapolation* is a straightforward procedure (or rather, a straight-backward one). The loading slope measured in a typical experiment is less than  $E$ , because of a finite machine compliance—but usually larger than  $E/5$ . Thus, the ratio between the two recorded slopes is usually larger than 10. This permits an accurate determination of the point of intersection between the two lines: the ‘yield stress’.

In two-phase materials, or at high temperatures, the initial strain-hardening behavior may not be linear. In such cases, a plot of the *square* of the stress against strain may well give an approximately straight asymptote near yield, and may then be used to determine a back-extrapolated yield stress.<sup>2,4</sup> Alternatively, one may here resort to a 0.2%-offset definition.

### 2.1.2. Strain Hardening: the Flow Stress

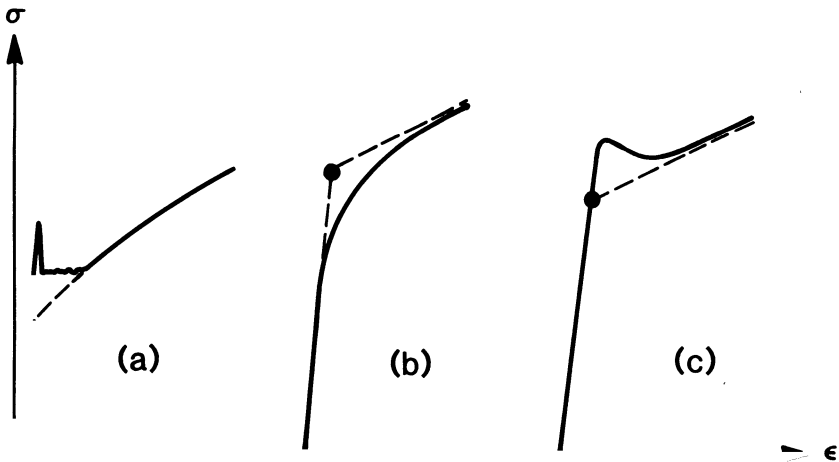
Figure 1(b) is a stress/strain curve drawn to a different scale; here the elastic slope appears infinite—but what was called the (‘horizontal’) asymptote above now appears with a definitely finite slope, displaying the effects of strain hardening. It tends to its own asymptote, at perhaps 2 to 20 times the yield stress: the ‘saturation stress’ or ‘steady-state stress’. (Actually, in many materials the asymptote is not truly horizontal, but its slope is typically another order of magnitude lower.<sup>5-8</sup>)

Figure 1(b) also shows the effect of unloading, after some significant plastic strain, and reloading. There is again an elastic–plastic transient, typically much sharper than at initial yield—but then the curve asymptotically approaches the continuous one. Thus, the back-extrapolated yield stress upon reloading is equal to the stress last

reached before unloading; this is usually called the *flow stress*. The *strain hardening* curve is then also the *locus of all flow stresses as a function of plastic prestrain*.<sup>9</sup> This differs, in principle, from the 'stress/strain' curve (Fig. 1(a)) in that the elastic-plastic transition region is not treated as 'strain hardening'. In practice, on any scale on which strain hardening can be seen (Fig. 1(b)), the two diagrams are indistinguishable, and so are the total strain and the plastic strain; this is how we will use 'strain' throughout this paper.

### 2.1.3. Transients

There are principally two types of transients in addition to the elastic-plastic transition described above.<sup>10</sup> Figure 2(a) illustrates a *yield drop*; it occurs in some materials, such as mild steel, at the beginning of testing (after an anneal), and in many other materials after unloading and reloading (with or without deliberate aging). Its length is typically much less than 1% strain, unless a Lüders band propagation is associated with it, in which case it may be of the order of 1% strain. We choose to ignore such transients here, and continue to consider 'yield' to occur at the stress obtained by back-extrapolating



**Fig. 2.** Some commonly observed loading transients: (a) sharp yielding in aged materials; (b) gradual yielding after recovery or a large increase in strain-rate or a reversal of the straining direction; (c) 'work softening' after a large decrease in strain-rate or a general straining-path change. (Similar behavior is observed in essentially dislocation-free materials.) None of these transients lasts longer than a few percent strain.

the steady stress/strain curve—either to the ‘lower yield point’ or, if feasible, beyond that to the elastic line.<sup>3</sup>

The other type of transient is longer (typically about 3% strain) and often difficult to ignore or extrapolate through. It occurs after *path changes*, and primarily when the strain-hardening rate is low (due to dynamic recovery). For example, after an increase in strain rate or decrease in temperature, it typically looks like Fig. 2(b), after the reverse path change like Fig. 2(c) (this is called ‘work softening’). A change in ‘stress path’ (i.e. in the ratios of the components of the stress and/or strain-rate tensors; see Section 2.2) may cause either one of these behaviors.

A special case of a path change is *stress reversal*: after previous straining in the reverse direction, a new loading curve looks about like Fig. 2(b). In a *microyield* definition, this amounts to a substantial lowering of the ‘yield stress’ upon reversal, and this is often referred to as the ‘Bauschinger effect’. It is seen that, from a macroscopic plasticity point-of-view, such a description does not capture the essence of the effect: the Bauschinger effect is primarily a *transient in the strain-hardening behavior*. The asymptotic behavior after the transient may or may not coincide with that without reversal, depending both on the details of the chosen description and on the type of material. We shall make use of this material dependence as a diagnostic tool to identify two-phase materials in Section 7.

#### 2.1.4. Rate Sensitivity

The rate sensitivity of the flow stress may be defined as

$$m = \left. \frac{\partial \ln \sigma_Y}{\partial \ln \dot{\epsilon}} \right|_T \quad (2.1)$$

where  $\sigma_Y$  may be the yield stress or the flow stress in a prestrained state of the material, as defined in Fig. 1(b). (However, it is *not* the flow stress attained after the same strain at different strain rates; see Section 5.2.4.) This ‘isostructural’ rate sensitivity  $m$  is usually negligible in magnitude, of order 0.01.<sup>11,12</sup> This fact has led to the common idealization of a rate-*independent* material, which is often useful. One case in which the rate sensitivity becomes of paramount importance is when it is *negative*: this causes instabilities (unless some other stabilizing factor intervenes).<sup>3</sup>

There is another rate sensitivity: that of the flow stress in the limit of

*steady state* (i.e. zero strain-hardening, which is controlled by the rate sensitivity of strain hardening. It is commonly characterized by a 'stress exponent'  $n$  (the inverse of a rate sensitivity):

$$\frac{1}{n} = \left. \frac{\partial \ln \sigma_s}{\partial \ln \dot{\epsilon}} \right|_T \quad (2.2)$$

$1/n$  is always much greater than  $m$ ; it increases more-or-less linearly with temperature,<sup>13</sup> from values around 0.03 near room temperature (strongly dependent on the specific material) to near 0.3 at high temperatures. This rate sensitivity is responsible for a significant increase in stability against necking.<sup>3</sup>

While all of these rate sensitivities may be quantitatively neglected in many applications, the *principle* of rate sensitivity is useful in two respects: (a) it eliminates phenomena such as bifurcations and vertices on yield surfaces that are really artifacts of the idealization of a *strictly* rate independent material;<sup>9</sup> and (b) it serves as a potent diagnostic tool to identify physical mechanisms.<sup>1</sup> We shall use these two effects of rate dependence in Sections 4 and 7, respectively.

All the rate sensitivities in the regime of interest we have circumscribed are intimately linked to temperature sensitivities, because they are due to thermal activation. We will summarize these relations in Section 3.

### 2.1.5. Pressure Dependence and Volume Changes

Yield stresses and flow stresses are almost always proportional to elastic constants—and elastic constants are pressure dependent. Thus, yield is, in principle, pressure sensitive. In many cases, experimental observations of pressure dependence are in quantitative agreement with this explanation.<sup>14</sup> It makes the yield strength go up with pressure.

Other pressure effects could be due to a change in dislocation core configuration with pressure, and a consequent change in the lattice resistance ('Peierls stress'). In this case, one would expect the yield stress to decrease as the pressure increases (since the cores get wider).

Neither of these pressure effects causes any plastic volume change. Volume changes are, however, possible through the accumulation of defects with deformation: dislocations themselves as well as vacancies (or voids) and self-interstitials cause some increase in the volume. An applied pressure could therefore decrease the rate of accumulation of these defects and thus influence *hardening* processes.

All of these effects are usually quite small and shall be neglected in the present treatise. They would be significant in materials of exceptional strength (such as high-strength steels<sup>14</sup>) or exceptional elastic nonlinearity (such as polymers<sup>15</sup>), or at very high pressures, or very large strains (when void generation becomes important).

Finally, we emphasize that *elastic* volume changes (as opposed to deviatoric elastic strains) can be quite large when the pressure is great: in strong shocks, the volume may decrease by a factor 2.

### 2.1.6. Energy Storage

The accumulation of dislocations during plastic deformation, and the possible changes in microstructural details such as precipitate size, shape, degree of order, etc., require some of the plastic work to go into stored energy. A simple estimate shows that the rate of energy storage divided by the rate of work done should be of order  $\theta/\mu$ :<sup>16</sup> the shear hardening rate (in crystallographic slip) divided by the shear modulus. This quantity is always less than 0.01 in single-phase materials of cubic lattice structure, although it may be quite high (especially at low strains) in two-phase materials and polycrystals of hexagonal or lower symmetry materials. Experimental determinations of the energy stored after deformation typically give about 3% of the work done.

The rate of energy storage provides a ‘thermodynamic threshold’<sup>9</sup> for flow: a minimum stress that must be applied to furnish the energy to be stored. Due to the above estimates, this stress can be safely neglected for all but the very lowest stresses, at high temperatures (for the materials of interest here). We shall therefore consider plastic processes to be essentially dissipative.

### 2.1.7. Conclusion

A good approximation for a description of the plastic response of many materials under many conditions is to treat them as *essentially* rigid-plastic, purely dissipative, rate independent, pressure independent, and isochoric: this we shall do in the present text. However, none of these idealizations is *strictly* true; thus, they should not be taken seriously when they lead to *qualitatively* different behavior. With these restrictions, we will emphasize the behavior under *multiaxial* deformations. We will also treat in some detail the description of *evolution* (including its rate dependence).

## 2.2. Multiaxial Deformation

### 2.2.1. The Yield Surface

The fact that yield is sharp and rate-insensitive makes the concept of a *yield* condition useful (as opposed to a treatment in terms of a plastic *modulus*, decreasing with strain, or a plastic *viscosity*, increasing with strain rate). This is true particularly when ‘yield’ is defined as the *asymptotic* behavior discussed in Fig. 1(a); for *small*-offset (‘micro-yield’) definitions, the concept of a yield surface is questionable—we shall return to this below (Section 2.2.3).

The yield condition is graphically described by a surface in stress space. Since the stress is a symmetric second-rank tensor, ‘stress space’ is six-dimensional; since the hydrostatic component of stress is considered irrelevant (or essentially irrelevant) for plastic flow, one usually uses the *five-dimensional* deviatoric stress space. In such a space, it is convenient to describe the stress as a *vector* (in the sense of a  $5 \times 1$  matrix, not in the sense of a first-rank tensor). The yield surface is, then, the locus of yield stresses for different directions of the stress vector (i.e. different ratios of the stress tensor components). Note that the ‘yield stresses’ do not transform as a tensor; their directional dependence is described by the yield surface. It is for this reason that the term ‘yield *strength*’ is sometimes preferred over ‘yield *stress*’.

Symmetry considerations can reduce both the dimensionality and the extent of the stress space in which the yield surface must (at least) be given for a complete description. For isotropic materials, as is well known, a  $60^\circ$  sector of the plane of principal deviatoric stresses suffices; if there is no sign-dependence of yield, a  $30^\circ$  sector suffices. In this sector, the demands of convexity (see further below) limit the possibilities severely. Two commonly used assumptions are the ‘Tresca hexagon’ (which is sometimes realistic, e.g. for the lower yield point in mild steel) and the von Mises circle. It must be emphasized that the *circle* in *stress space* is not a consequence of isotropy; it is an assumed shape of the yield surface within the bounds allowed by isotropic symmetry.

A point often made, and true, is that, were it only to discover the correct shape of the yield surface for isotropic materials, a great effort would not be worthwhile, since the differences are so small. The fact, however, is that experimental yield surfaces often depart very substantially from those allowed for isotropic materials—because many

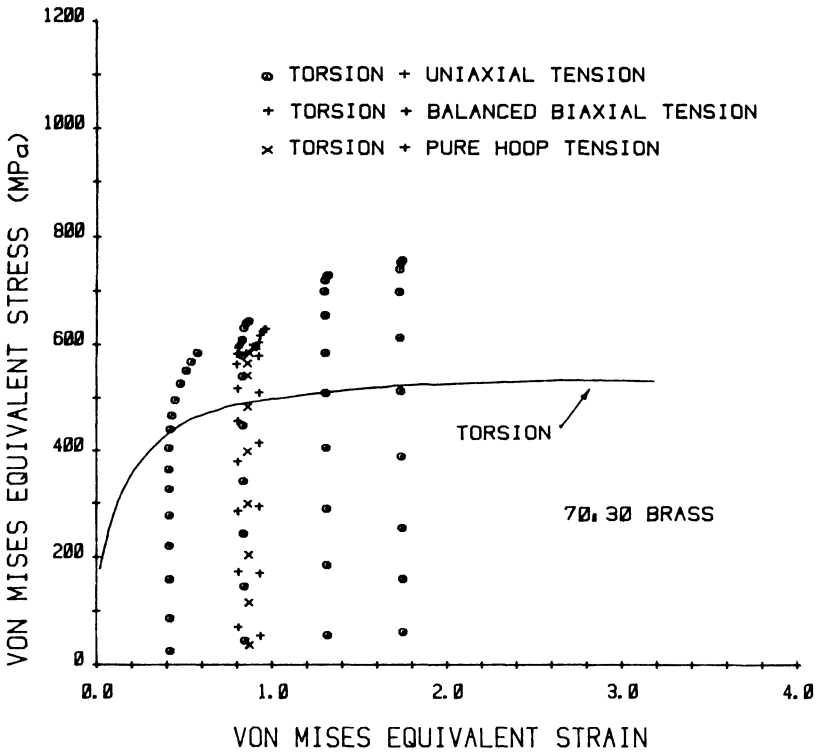


**Fig. 3.** Probes in different straining directions after various prestrains in torsion; long tubes of brass.<sup>17</sup> The ratio of yield stresses in any one state is considerably greater than allowed by an assumption of isotropy.

materials (e.g. all that have been heavily deformed) are *not* isotropic. An example is shown in Fig. 3,<sup>17</sup> which represents probes in various directions of stress space after various (large) amounts of prestrain in torsion. It is plotted so that, were the von Mises criterion valid, the reloading yield points would have to fall on the continuous curve. The departures are quite substantial.

### 2.2.2. Equivalent Stress and Equivalent Strain

The size of the yield surface defines a scalar parameter, the 'equivalent stress' (or 'effective stress'),  $\sigma_e$ . Its change with strain may be used to describe a form of *hardening* (called 'isotropic hardening'; see below). An 'equivalent strain' is usually defined as its work conjugate (so that  $\sigma_{ij} d\epsilon_{ij} = \sigma_e d\epsilon_e$ ). An unfortunate experimental fact, however, is that a

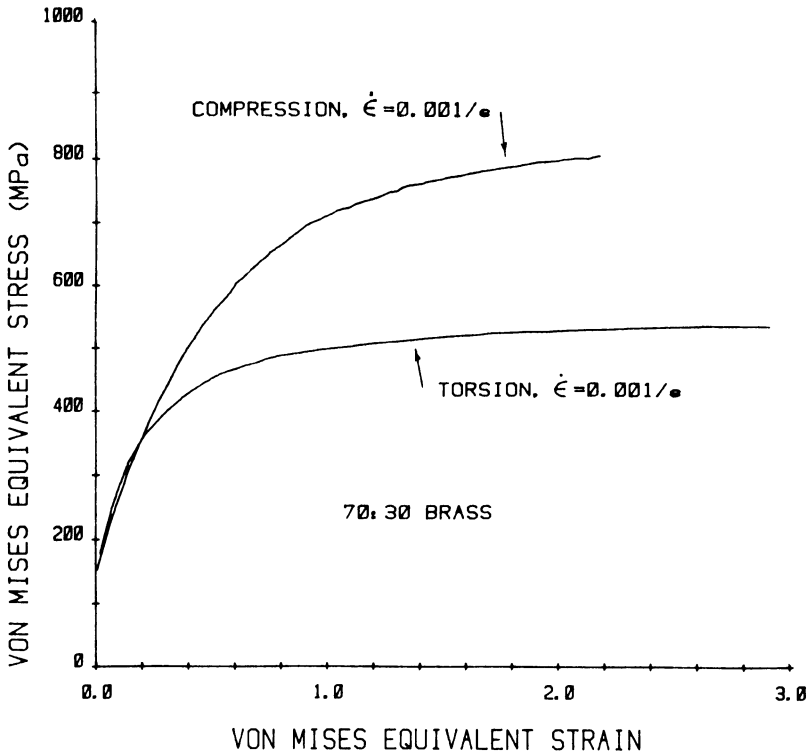


**Fig. 4.** Continuous straining in torsion and compression; brass.<sup>17</sup> The comparison is made on the basis of the von Mises equivalent stress and strain; it does *not* serve to unify the plots.

plot of equivalent stress versus equivalent strain does *not* usually give a unique hardening law for all deformation modes. Figure 4 shows this in an example for torsion and compression in brass, using the von Mises definitions of equivalent stress and equivalent strain.<sup>17†</sup> There are two plausible causes for this discrepancy: one that, as stated above, few metals are nearly isotropic; but more fundamentally that there is no reason to expect the state of the material to be the same when the 'equivalent strain' achieved along two different strain paths is the same (see Section 5.1.3).

† Sometimes the terms 'equivalent stress' and 'equivalent strain' are used as *identical* to those according to the von Mises postulate; we will discuss this in detail in Section 4.2.1.

### 2.2.3. Hardening Rules

This term is commonly used to describe changes in the *yield surface* with strain. (The *rate of change* with strain is 'strain hardening' or 'work hardening', discussed above). The two most common hardening rules are: 'isotropic hardening', a change in the *size* of the yield surface only (all dimensions being scaled by the same constant—whether the material is plastically isotropic or not); and 'kinematic hardening', a change in *location* of the yield surface only (which requires a *tensor* to be specified).

Figure 5 shows the results of an experimental probe of the yield surface after a significant prestrain in torsion.<sup>18</sup> 'Yield' was evaluated both in the small-offset definition ( $\epsilon = 5 \times 10^{-6}$ ) and as the back-extrapolated value. It is seen that the latter deviates little from 'isotropic hardening'. Microyield, on the other hand, involves a change

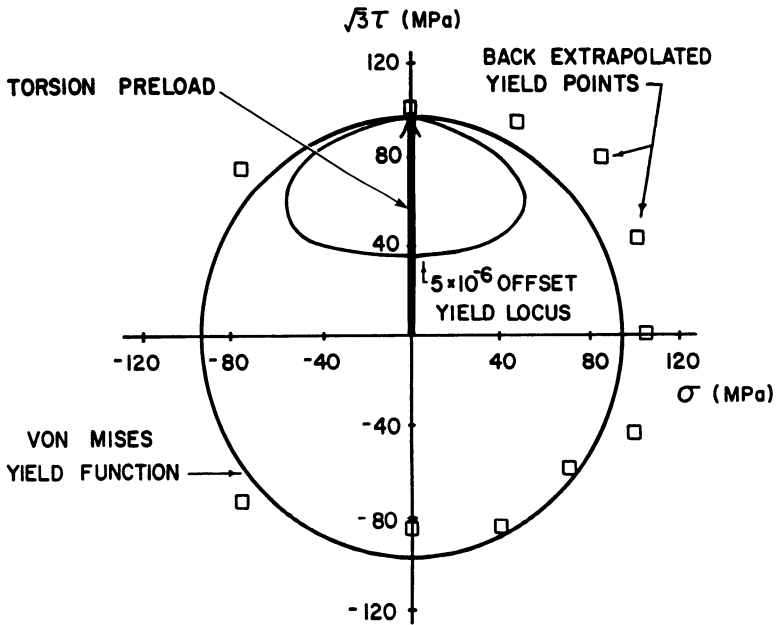


**Fig. 5.** Experimentally determined yield loci, after a pre-shear-strain of 0.5 in torsion of a long tube of 1100 aluminum.<sup>18</sup> The last stress reached during prestraining is shown as a heavy arrow. The small oval 'yield locus' was taken at a very small offset after unloading only into its interior. The von Mises circle is shown for reference. The squares show back-extrapolated yield points. (Yield stresses at 0.2% offset were the same.)

in size, location and, in fact, *shape* of the ‘yield surface’. Another way of describing the small-offset yield surface is that it is almost like the macroyield surface except for a drastic reduction in ‘yield’ in the reverse direction (to the point of occurring already during unloading, in this case). This is in congruence with the description of the Bauschinger effect we gave in Section 2.1.3: it is primarily a work-hardening transient.

Another hardening rule has been derived from ‘slip theory’.<sup>19</sup> here, only the direction of prestraining hardens, developing a vertex around it (and implying a Bauschinger effect, too). Such vertices around the loading point have been observed;<sup>20</sup> however, they appear to be a dynamic phenomenon only: they are not found after (even partial) unloading and reloading, for either definition of yield in aluminum (Fig. 5).

We shall focus our attention on back-extrapolated (macro)yield only. For this, ‘isotropic hardening’ is a good first approximation; deviations may be expected in two-phase materials (in which the Bauschinger effect has a more lasting component).

#### 2.2.4. *Plastic Anisotropy*

It was already mentioned in Section 2.2.1 that experimental yield surfaces deviate from the allowed range of possibilities in isotropic materials; this is true even when the yield surface is determined at a given state of the material.<sup>18</sup> Such discrepancies can only be explained on the basis of plastic anisotropy. There is also an anisotropy in the *strain* increments, which is in fact much more drastic: this corresponds to substantial deviations of the plastic potential from any possible isotropic yield surface. For example, if strips of rolled sheet are subjected to a uniaxial tensile stress, the two lateral strains will, in general, not be equal; their ratio is called the *R*-value or ‘Lankford coefficient’.<sup>21</sup> This anisotropy is a major cause of forming problems. Apart from the well known ‘earing’, it may be a cause of instabilities.<sup>22</sup>

#### 2.2.5. *Conclusion*

It is our judgment that, considering the ‘realities’ reviewed in Section 2.1, the concept of a yield surface is useful (in preference to a description in terms of a plastic modulus or a plastic viscosity)—but only for the back-extrapolation definition of yield. With this definition, ‘isotropic hardening’ may be a good first approximation, but plastic

isotropy is not. For the *rate* of hardening in different deformation modes, no good description is yet available.

### 3. FLOW KINETICS

Kinetics describes the rate at which processes occur under given driving forces (and given temperature)—or, conversely, the influence of an imposed rate of the process (such as straining), at a given temperature, on the forces required. The kinetics of a process is a consequence of the physical mechanisms that control it.

The physical mechanisms of plasticity occur on a microscopic scale; yet the kinetics is measured on a macroscopic scale. It is therefore important to have some understanding of the connection. Under certain conditions, the microscopic non-uniformities can give rise to macroscopic instabilities which in turn can lead to localization and thus return the process to a more microscopic scale. These questions will be briefly addressed in Section 3.1.

In plasticity, there are two different types of kinetics that are conveniently separated: *flow kinetics*, which describes dislocation glide at a given 'structure' or 'state' of the material; and *evolution kinetics*, which describes the influence of strain-rate and temperature on the rate of change of structure (state).

In Section 3.2, we will deal only with the kinetics of dislocation glide, and shall review only the most essential fundamentals. The statements that will be made may be regarded as well established, as a consequence of decades of research by many investigators. For a detailed treatment, see Kocks *et al.*<sup>1</sup>

#### 3.1. Non-uniform Deformation

##### 3.1.1. Microscopic Heterogeneities and Jerkiness

Deformation is always non-uniform on a microscopic scale: it is localized in specific slip planes and, on a finer scale yet, occurs by the motion of dislocations. It is also non-uniform in a temporal sense: both dislocation motion and slip on a whole plane are 'jerky'. For most macroscopic applications, these effects are averaged out over the extent of the material element and over the time scale of interest.

This microscopic non-uniformity has one major consequence on constitutive descriptions of plasticity: the material element that is

taken to represent a 'point' in the continuum sense must be *large enough* to encompass many dislocations and many slip planes. This typically means that it must be larger than about  $10\ \mu\text{m}$  on edge. A more stringent criterion for most materials, which are polycrystalline aggregates, is that the material element must contain many grains. This typically means that it must be larger than about 1 mm on edge. On the other hand, of course, it must be *small enough* to warrant its treatment under macroscopically uniform conditions: the gradients of stress and of strain-rate, for example, should not be too great over the extent of the chosen material element.

Similarly, the time step over which deformation of a material element may be considered uniform is limited by various processes. Experimentally, the time for a 'unit slip step' (corresponding to the motion of many dislocations throughout the whole slip plane) is typically of the order of 0.1–1 s in observations at 'normal' strain rates and temperatures<sup>23</sup>—but this may well depend on stress and temperature. It is limited at the lower end by dislocation vibrations in the phonon field, which occur on a time scale of the order of  $10^{-10}$  s. This is a regime of interest in shock deformation, which has not been explored sufficiently.

One macroscopic consequence of the ubiquitous microscopic non-uniformities is that they provide a basis for (spatial or temporal) *fluctuations*—which may, on occasion, lead to *unstable* behavior.

### 3.1.2. Acceleration and Localization

Instabilities of deformation are usually described in terms of a localization of flow: that is, when flow becomes easier in one place than another (and the two are compatible with each other). 'Easier', at constant load, means faster; at constant rate, it means with a drop in load (and thus unloading of the 'other' elements). A characterization of plastic instability in terms of decreasing loads is, therefore, special and requires a knowledge of the interaction between many material elements and far-away boundary conditions.

On a local and instantaneous scale, the stress is fixed; however, the strain-rate may undergo fluctuations. The question then is whether these fluctuations tend to be damped out or lead to continued acceleration. In the latter case, the germs of instability are present.

There are two different types of causes for acceleration.<sup>3</sup> One is in the evolution that would occur if the process went on: strain softening or texture softening, for example, leading to diffuse or localized

necking. The other possible cause of accelerations is instantaneous: e.g. if dislocation propagation is much easier than their generation; or if the propagation itself can occur in two modes—with or without continual aging. In both of these cases, the strain-rate may (and therefore will<sup>3</sup>) discontinuously jump to a higher value.

When there is a high generation stress for dislocations, such as in (aged) mild steel, there is a yield drop in tension (Fig. 2(a)), followed by a (perhaps jerky) stress plateau, while one or more Lüders bands propagate along the specimen. After the whole specimen has once been deformed, dislocation generation is no longer necessary and homogeneous deformation ensues.

When aging can occur dynamically during straining, there is a continual alternation between the two modes, leading to jerky flow (serrated stress/strain curves). This may occur essentially homogeneously, as in a compression test, or be accompanied by the rapid (non-steady) propagation of bands. It is associated with a macroscopically measurable negative rate sensitivity.

Neither of these processes is catastrophic, from a macroscopic point of view. The stress/strain/strain-rate relations are almost the same as under more uniform deformation. The main interest in the phenomena is in the surface irregularities that may be expected, for example in sheets that have deformed in a non-uniform manner.

From the point of view of constitutive relations, it is important to realize that macroscopic instabilities arise from within the regime of uniform behavior. One must therefore understand the plasticity of the material under presumed uniform conditions even if the primary interest were in the formation of instabilities.

## **3.2. Uniform Deformation**

### *3.2.1. The Mechanical Threshold*

The concept of a yield surface may be put as follows: it separates a region of equilibrium states, inside it, from a region outside it in which equilibrium is not possible. There is a very similar concept in dislocation theory, namely the 'mechanical threshold':<sup>1</sup> below this value of the stress, dislocations can always find a static equilibrium situation; above it, no such equilibrium configuration exists, at least in a statistical sense, for many slip planes. Note that some dislocation rearrangement may occur at very low stresses, and more and more as the stress increases: this is 'plasticity' in a sense, but it is akin to

'contained' plastic flow, the elastic-plastic transition region (Fig. 1(a)). The mechanical threshold corresponds exactly to the *asymptote* at which plasticity becomes general, macroscopic, as in Fig. 1(a). Thus, it is opportune to identify the 'yield surface' with the locus of mechanical thresholds.

The above considerations were strictly mechanical—to be exact: static. At stresses *above* the mechanical threshold, viscous and inertial forces come into play, and if these are included, a 'dynamic equilibrium' may be attained. On the other hand, *below* the mechanical threshold, thermal fluctuations (in 'thermodynamic equilibrium', at a constant, finite temperature) may release dislocations from their 'mechanical equilibrium' positions and give rise to 'thermally activated flow'.

Thus, the mechanical threshold serves as an important demarcation line: flow is in fact possible both below and above it, but the kinetics is quite different in the two regimes.<sup>1,24</sup> This is shown schematically in Fig. 6. In a strictly rate-independent material, the strain rate  $\dot{\gamma}$  would

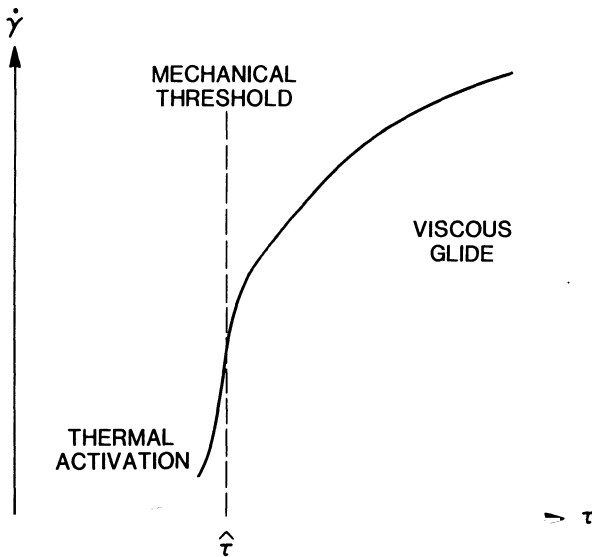


**Fig. 6.** Schematic linear strain-rate vs. stress diagram. The mechanical threshold  $\hat{\tau}$  serves as a demarcation between two kinetic regimes: thermal activation (by far the most common process) below it; viscous glide above it (presumably occurs at strain rates  $>10^5 \text{ s}^{-1}$ ). The mechanical threshold would be the yield stress in completely rate-independent flow.<sup>1,9,24</sup>

be zero at stresses below  $\hat{\tau}$ , and indeterminate at  $\hat{\tau}$ . The curve in Fig. 6 describes the effective smoothing-out of this step function in real materials (and also takes account of the upper limit set to all strain rates by the shear-wave velocity and the *de facto* maximum dislocation density).

The 'yield surface', if it is to refer to a rate-independent material, must then describe the mechanical threshold—and it will still be quite useful in rate-dependent materials. However, it is then no longer a limit between equilibrium (elasticity) and nonequilibrium (plasticity), but a limit between thermally activated plasticity (with little rate sensitivity) below this critical stress, and rate sensitive, quasi-viscous plasticity above.<sup>9</sup> In most applications (very high strain rates excepted), *plasticity occurs inside this yield surface*—though close to it, because of the very low value of the typical rate sensitivity. There is usually no finite stress below which absolutely no irreversible flow occurs anywhere. (See Section 2.1.6.)

The mechanical threshold can be measured experimentally by determining the quasi-static yield stress under elimination of thermal activation, i.e. at the absolute zero of temperature. In practice, of course, this means by back-extrapolation to 0 K.† Note that rate effects *cannot* be eliminated by going to very small rates: this would drive the 'yield stress' essentially to zero.

### 3.2.2. Normalization by the Shear Modulus (Temperature, Pressure)

The mechanical threshold can, in principle, be calculated on the basis of dislocation theory (and a lot of statistics).<sup>1</sup> In almost all cases, it comes out proportional to some elastic constant (the exception being some precipitation hardened or ordered alloys, in which some interface energy may be the 'strength' factor). Thus, it is really an elastic strain that reaches a critical value at yield.

The elastic constants are functions of the temperature, and this gives rise to a 'trivial' temperature dependence of the yield stress. For this reason, the demarcation line between the two kinetic regimes should not actually be taken as the (absolute) mechanical threshold (the yield stress back-extrapolated to 0 K), but as this stress divided by the (temperature dependent) modulus.

† This back-extrapolation should be done from temperatures that exclude the region of very small temperatures, because of various extra mechanisms that occur in this regime,<sup>25,26</sup> and it should be done on a plot of  $\sigma^{-1/2}$  vs.  $T^{2/3}$ .<sup>1,27</sup>

All plastic processes are *shear* processes. Thus, it is some shear modulus that is important; the bulk modulus should not matter. The isotropic shear modulus is quite adequate for the purpose; in more exact treatments, some modulus connected with dislocation properties is more appropriate.<sup>1</sup> We shall use the symbol  $\mu$  for whatever the appropriate shear modulus is. Similarly, we will generally characterize the mechanical threshold as a critical value of a *shear* stress, and label it  $\hat{\tau}$ . In this terminology, the important quantity is

$$\hat{\tau}/\mu(T, p) \quad (3.1)$$

Here, we have already incorporated another 'trivial' effect: the dependence of the shear modulus on the hydrostatic pressure  $p$  (the negative average normal stress). This is just one of the expressions of elastic non-linearity, and in very-high-strength materials this may be important (it is the major cause of the 'strength-differential effect').<sup>14</sup> The hydrostatic pressure plays a special role inasmuch as it can reach values much higher than the shear stresses, when these are limited by plasticity.

For a rough estimate for close-packed metals, the following two relations are useful:

$$\left. \frac{\partial \mu / \mu_0}{\partial T / T_m} \right|_p \approx -0.5; \quad \left. \frac{\partial \mu}{\partial p} \right|_T \approx 2 \quad (3.2)$$

where  $\mu_0$  is the value of the shear modulus back-extrapolated to zero temperature, and  $T_m$  is the melting temperature.

### 3.2.3. Overstress, Dynamics

At stresses above the mechanical threshold, the rate of deformation is checked by viscous drag on dislocations (usually due to dislocation/phonon interactions). In this regime, it is useful to write the crystallographic shear rate  $\dot{\gamma}$  in terms of the average dislocation velocity  $v$  and the mobile dislocation density  $\rho_m$ :

$$\dot{\gamma} = b\rho_m v \quad (3.3)$$

where  $b$  is the magnitude of the Burgers vector. Under drag control,  $v$  is proportional to the 'effective' (local) stress, which is zero at the mechanical threshold and increases above. All quantitative calculations show, however, that this 'effective stress' is *not* the difference between the applied stress and the mechanical threshold, but a strongly *nonlinear* function which asymptotes to the applied resolved

shear stress  $\tau$  in the drag-controlled limit  $\tau \gg \hat{\tau}$  (in practice  $\tau > 2\hat{\tau}$  is ample).<sup>1</sup> Then

$$v = \tau b / B \quad (3.4)$$

The drag coefficient  $B$  has an important characteristic: it *increases* with temperature. (At high temperatures, it appears to reach a constant value according to experimental information, although it should be linear in  $T$  according to theory.<sup>1</sup>) Thus, it is here not true (as it is for thermally activated glide) that higher temperatures lead to higher strain rates at the same stress.

The mobile dislocation density is a variable that is difficult to assess independently; however, rather general theoretical considerations suggest that it can depend on stress at most to the second power. Thus, for *viscous glide*:

$$\left. \frac{\partial \ln \tau}{\partial \ln \dot{\gamma}} \right|_T \geq 1/3 \quad (3.5)$$

It is very rate sensitive. It can be distinguished from other processes of high rate sensitivity (e.g. diffusional flow at high temperatures and low stresses) by the necessity that the applied stress be larger than the quasi-static flow stress at 0 K. In practice, this happens only at very high strain rates. (Follansbee<sup>28</sup> comes to the conclusion that this process has not as yet been observed in macroscopic deformation of polycrystals, in experiments up to about  $10^5 \text{ s}^{-1}$ .) We shall not be concerned with this regime in the remainder of this article.

Two other physical effects are important in some regimes of dislocation dynamics: relativistic behavior, for dislocation velocities in excess of, approximately, one-third the shear wave velocity; and dislocation inertia, in the regime where drag is small, at low temperatures (typically  $< 20 \text{ K}$ ). Neither of these falls within our present 'interest space'.

#### 3.2.4. Thermal Activation

By far the most common cause for rate sensitivity is a *lowering* of the flow stress (from the purely mechanical threshold) due to the help from thermal activation. The degree of lowering is the greater the higher the temperature, and the longer the time available for thermal activation (i.e. the lower the enforced strain rate). A quantitative link between temperature effects and rate effects is always given, in this

regime, by some form of Arrhenius law:

$$\dot{\gamma} = \dot{\gamma}_0 \exp(-\Delta G/kT) \quad (3.6)$$

involving a 'pre-exponential factor'  $\dot{\gamma}_0$  and an 'activation energy' (more exactly, activation free enthalpy)  $\Delta G$ . Both may depend on stress and also on the mechanical threshold. Thus, the rate dependence of the flow stress may be expressed (in its inverse) as

$$\frac{1}{m} \equiv \left. \frac{\partial \ln \dot{\gamma}}{\partial \ln \tau} \right|_{T, \hat{\tau}} = \left. \frac{\partial \ln \dot{\gamma}_0}{\partial \ln \tau} \right|_{T, \hat{\tau}} + \frac{1}{kT} \left( - \left. \frac{\partial \Delta G}{\partial \ln \tau} \right)_{T, \hat{\tau}} \right) \quad (3.7)$$

The first term is typically small (0, 1, or 2), while the second term is typically of order 100. Note that we have here specified the partial differentiation to be at constant mechanical threshold: this is a quantitative way of specifying 'constant structure' or 'constant state', as was done in words in the introduction of the rate sensitivity in eqn (2.1). (An observed rate sensitivity much greater than 0.01 almost certainly indicates an observation not at constant structure, but under control of evolution processes; see Section 5.2.4.)

The relation between activation energy and stress depends on the specific interaction profile between dislocation and obstacle, and on the way these are averaged over glide by many dislocations over many obstacles. It turns out that certain limiting considerations make the final relation rather insensitive to all these details. A sufficient approximation under most circumstances where temperature and strain-rate play a significant role, namely when short-range obstacles are rate-controlling, is<sup>1</sup>

$$\Delta G = \mu b^3 g_0 [1 - (\tau/\hat{\tau})^p]^q = kT \ln(\dot{\gamma}_0/\dot{\gamma}) \quad (3.8)$$

where the exponents  $p$  and  $q$  are typically 1/2 and 3/2, respectively (generally,  $0 < p < 1$  and  $1 \leq q \leq 2$ ). The normalization with  $\mu b^3$  is necessary when  $\hat{\tau} \propto \mu$ ;  $g_0$  is the total activation energy (if no stress were aiding) in units of  $\mu b^3$ . We have also repeated eqn (3.6) in inverted form at the end of eqn (3.8);  $\dot{\gamma}_0$  is typically  $10^8 \text{ s}^{-1}$ .<sup>1</sup>

Figure 7 shows this behavior schematically (as a thin drawn-out line) for a value of  $g_0$  that is far off-scale on the right. The heavy line indicates typical real behavior. (For many examples, see reference 29.) At very low temperatures (<50 K) dislocation-inertia effects may lower the flow stress slightly.<sup>25,26</sup> At very high temperatures (typically above  $T_m/2$ ), the flow stress is influenced by concurrent dynamic (and

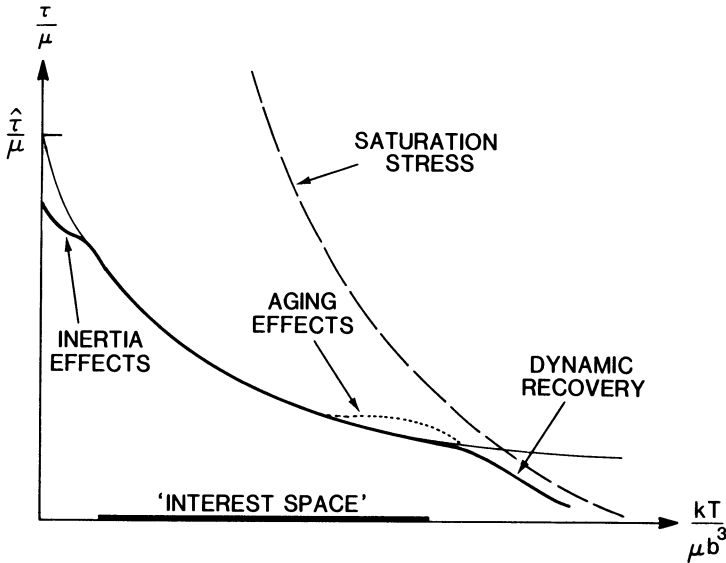


**Fig. 7.** Schematic temperature dependence of the yield stress (solid curve) and the (extrapolated) saturation stress (dashed), after appropriate normalization with the (temperature-dependent) shear modulus  $\mu$ . Our 'interest space' covers the typically the range of temperatures from 50 K to half the melting point.

eventually also static) recovery: the drop occurs near where the saturation stress (shown dashed) becomes lower than the extrapolated 'constant-structure flow-kinetics' curve. This regime is not well understood. Thus, the 'interest space' we have chosen is approximately as outlined by a heavy line in the abscissa. Temperatures above this are treated only under evolution.

At intermediate temperatures, there is often a 'plateau' in flow stress—at least apparently. This could have a number of reasons. First, it can merely be an effect of a large  $g_0$ , as plotted. Often, however, it is assumed that there is an athermal contribution  $\tau_0$  to the flow stress; then,  $\tau$  in eqn (3.8) would have to be replaced by  $\tau - \tau_0$ , and  $g_0$  could be much smaller. The plateau itself is not sufficient reason for such an introduction of an additional parameter; we shall discuss methods to assess when this is warranted (Section 6.2.5).

When there are any solutes in the material, there are two further reasons for plateau-like behavior at intermediate temperatures. First, there should be a regime of dynamic strain-aging, which leads to the 'hump' above what would be the normal curve; this is indicated by a

dotted line in Fig. 7. Second, there are theories of solution hardening<sup>29,30</sup> that predict a dependence of the activation energy on  $1/\tau$  (times some short-range function as in eqn (3.8)): this gives a very slow decrease at higher temperatures.

Expressing the kinetic effects as influences on the flow stress, we have

$$\tau = \mu \cdot \frac{\hat{\tau}}{\mu_0} \cdot s \left( \frac{kT}{\mu b^3} \ln \frac{\dot{\gamma}_0}{\dot{\gamma}} \right) \quad (3.9)$$

(perhaps plus additional terms such as a  $\tau_0$ ). Here,  $s$  is the inverse of the function given in eqn (3.8).

While the semi-logarithmic dependence of the flow stress on the strain rate is thus founded in the physical mechanism of deformation, the relation is often expressed as a power law:

$$\tau = \tau_1 (\dot{\gamma}/\dot{\gamma}_1)^m \quad (3.10)$$

The exponent  $m$  is not identical to the rate sensitivity used in eqns (2.1) and (3.7): it is the same only when  $m$  is independent of  $\tau$ ; in other words, when the activation energy  $\Delta G$  is proportional to the logarithm of the stress. This is often sufficiently accurate over a substantial regime. Note, however, that  $m$  should be expected to depend on temperature if eqn (3.10) is merely a phenomenological approximation to eqn (3.6).<sup>1</sup>

The quantities  $\tau_1$  and  $\dot{\gamma}_1$  in eqn (3.10) are meant to be pairs of values under reference conditions within the regime of validity of eqn (3.10). They could, in principle, be replaced by  $\hat{\tau}$  and  $\dot{\gamma}_0$ ; but note that neither eqn (3.10) nor indeed eqn (3.6) holds near  $\tau = \hat{\tau}$ , so that  $\dot{\gamma}_0$  is not a limiting value. In fact, in the neighborhood of the mechanical threshold, thermal activation and dislocation drag superpose in a complicated way.<sup>27</sup>

### 3.2.5. Time Effects

In phenomenological plasticity, it is common to refer to 'time-independent' plasticity and, by implication, to possible 'time effects'. From the physical point of view, we have so far only referred to *rate* effects: these are in fact the most important ones.

However, there are some true *time* effects (which, of course, also reflect themselves dynamically as rate effects). They are of two kinds: recovery and aging. The first term is used for thermal softening (and may, in this context, also include recrystallization); it is important only

at temperatures above about  $T_m/2$ , at the upper end of our 'interest space', and we shall not consider it further here.

'Aging' refers to a change in the metallurgical structure with time: e.g. precipitation of solutes into small particles, or segregation of solutes to dislocations. It generally leads to a *hardening*—the more so the longer the time elapsed (or the higher the temperature: this is what led to the 'hump' in Fig. 7). When aging occurs dynamically, it leads to a *negative rate sensitivity*. While this is not truly a 'constant structure' effect, but rather a time evolution, the time scales involved may be so small that, for practical purposes, it acts like an 'instantaneous' rate sensitivity. Since this may lead to instabilities in deformation, it is a very important phenomenon. We will briefly discuss it in Section 3.2.

### 3.2.6. Stress Relaxation

The easiest test to measure kinetic effects is to merely stop the machine and watch the load relax. This relaxation is not usually due to a *time* effect, as discussed above (in fact, a *time-strengthening*, i.e. aging, effect can never be observed this way<sup>3</sup>), but is instead due to the decrease of strain-rate with stress. The plastic strain rate is proportional to the magnitude of the stress/time slope. Thus, a plot of this slope vs. stress gives a good first evaluation (more appropriate than stress vs.  $\log t$ ).

The low rate sensitivity of the flow stress means that the slope decreases very rapidly—until it is hard to distinguish from zero. This is another phenomenon that has tempted many observers to introduce an athermal, 'internal' stress level—although it can be easily explained without such a new parameter. (For further discussion of 'internal stresses', see Sections 3.2.7 and 6.)

At long times, the stress relaxation test is more difficult to do because it becomes very sensitive to temperature fluctuations; and it is more difficult to interpret because, at very low rates, simultaneous dynamic-recovery processes influence the results (much as they do the flow stress above  $T_m/2$ ).<sup>2,12</sup> On the other hand, if one is really interested in low rates, this is the quickest test.

The stress-relaxation test has other problems. The most important of these is that transients, which are so instructive for assessing material behavior, are very difficult to detect. Further, the small strains incurred do not guarantee that one is in the 'macroplastic' regime (Section 2.1.1); in fact, it is generally recognized that anelastic effects may play a significant role.<sup>31</sup> Finally, if the stress-rate is ever

important (which actually seems rarely if ever the case<sup>32,33</sup>), it has the opposite sign here.<sup>34,35</sup> In conclusion, this author believes the stress-relaxation test to be grossly overrated in its usefulness and reliability. (See also Section 6.2.3.)

3.2.7. Strain Dependence

The most useful test of the flow-kinetics behavior of a material is to investigate the rate sensitivity as a function of strain. The best way to evaluate it is in the ‘Haasen plot’:<sup>36</sup>  $m\tau$  ( $=\Delta\tau/\Delta \ln \dot{\gamma}$ ) versus  $\tau$ .<sup>37</sup> Note that this is not a relation between the ‘activation volume’ (which is proportional to  $1/m\tau$ ) and the *applied stress at constant structure*: that would give information on the obstacle profile, which is not very sensitive (Section 3.2.4). Instead, it describes the evolution of the (inverse) activation volume with *structure*, as measured by the flow stress under standard conditions of strain-rate and temperature.

Figure 8 sketches various types of material behavior in a Haasen plot, as abstracted from extensive work on pure and commercial alloys:<sup>37-40</sup> the data for pure materials (p) tend to back-extrapolate to the origin (this is called the Cottrell–Stokes law<sup>41</sup>); those for two-phase materials (t) back-extrapolate to zero rate sensitivity at a

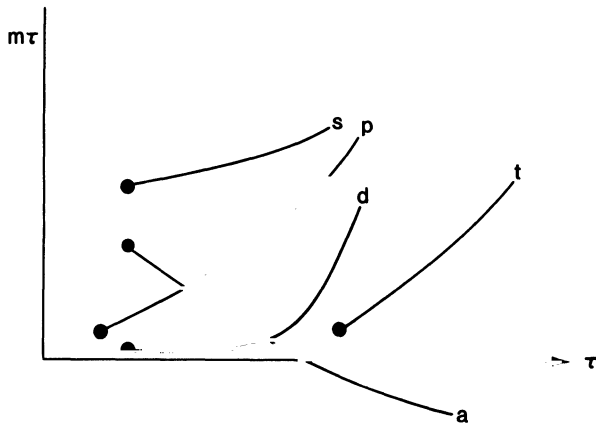


**Fig. 8.** Appropriate plot to diagnose the relative rate sensitivity of the flow stress,  $m$ , as a function of the flow stress itself (as both change with strain). Typical behavior, starting with the yield *point*, is shown for pure, solution hardened, and two-phase materials, as well as during dynamic strain-aging and under solute-dragging conditions. A negative rate sensitivity can cause instability.<sup>36-40</sup>

positive stress (this is *evidence* of the need for an additional 'internal stress' parameter); solution-strengthened alloys (s), on the other hand, have a relatively high rate sensitivity at the yield stress; dynamic strain-aging (a) causes a *decrease* of  $m\tau$  with strain (and may eventually lead to a negative rate sensitivity and ensuing instabilities). Finally, while all curves tend to start out as straight lines (which is in itself evidence for a linear superposition of flow-stress mechanisms), they all tend to give an accelerated rate of increase of the rate-sensitivity when dynamic recovery becomes important at higher strains. An extreme case of this is solute dragging (d), which occurs at temperatures above a dynamic-strain-aging regime: here, the rate sensitivity increases rapidly at high strains, but is quite close to zero for a significant range of stresses.

In conclusion, even though the rate sensitivity is small, its variation with strain provides important clues as to which of many possible mechanisms in a particular material actually contributes significantly to the flow stress.

### 3.2.8. Conclusion

By far the most common cause of rate sensitivity at constant structure in uniform deformation under 'normal' conditions (our chosen interest space) is thermal activation. The rate sensitivity is small and serves to lower the flow stress from the mechanical threshold. The effects of strain rate and temperature are linked by the 'Fisher variable'<sup>42</sup>  $kT \ln(\dot{\gamma}_0/\dot{\gamma})$ ; if the flow stress vs. strain-rate relation is expressed, for phenomenological convenience, as a power law, the exponent is temperature dependent. The smallness of these rate effects makes the concept of a yield surface applicable and appropriate; the most precise correspondence is to the *mechanical threshold* of dislocation theory. This mechanical threshold is usually proportional to a shear modulus, and through it depends on temperature (uncoupled from strain rate in this instance) and on pressure.

While the 'instantaneous' rate sensitivity is so small that it may often be neglected, its dependence on strain provides a valuable tool for an analysis of important strengthening mechanisms.

## 4. POLYCRYSTAL PLASTICITY

Most materials are crystalline—but polycrystalline: they consist of many grains, each of which consists of an ordered array of atoms (on a

'lattice'). Typical grain sizes are between about  $10\ \mu\text{m}$  and  $1\ \text{mm}$ . (Grain sizes beyond these limits do occur, but we wish to exclude them from consideration here, because the large ones would usually not be small compared to the macroscopic body dimensions, and the small ones smaller than normal slip plane spacings.) The grain boundary thickness is of atomic dimensions; thus, the deformation of the polycrystal must be carried by the deformation of the grains.

The predominant mode of plastic deformation in single crystals is crystallographic slip; twinning plays a role at low temperatures, at very high strain rates, and in materials of low crystal symmetry (including, however, hexagonal lattice structures); and diffusive flow is important at high temperatures and very low stresses. Our 'interest space' was chosen such that slip is the controlling mechanism. The deformation of polycrystals then is some average over the crystallographic slips in each grain.

The deformations in the various grains cannot be independent of each other: certain conditions must be met at the interfaces between them, and this is in fact the major role of grain boundaries. The theory of polycrystal deformation consists essentially of treating these interactions—once the properties of the grains are known. The interaction may, however, influence the deformation mechanisms inside the grains themselves and make them different from single crystals. Thus, when we describe the plasticity of 'crystals' in the following sections, we mean that of *representative grains*.

## 4.1. Crystal Plasticity

### 4.1.1. Kinematics

Crystallographic slip has one very handy characteristic: it leaves the crystal lattice invariant (whereas elasticity changes both the spacings and the angles in the crystal lattice). Thus, our choice of omitting elasticity from the aspects of behavior we wish to treat (by concentrating on strains larger than, say,  $0.2\%$ ) affords us a major bonus: an ingrown coordinate system. In fact, even if elasticity were added, it is an entirely appropriate way (see Sections 2.1.2 and 4.2.6) to treat plastic properties as those remaining after unloading (and to consider continuous deformation as a series of loadings and unloadings). Then, all the following relations are to be viewed as being in the unloaded state.

In general, the material properties are given in terms of the crystallographic axes (or in terms of axes of anisotropy for non-

random polycrystals) and must be related to the macroscopic coordinates for the solution of any particular boundary-value problem. This is the general meaning of ‘orientation’. The material constitutive relations specify the relation between the ‘true’ (Cauchy) stress and the (true) strain rate, as well as the evolution with a (true) strain increment, *in these property-reference axes*.

Slip occurs on various ‘slip systems’: crystallographic planes and directions in which ‘simple shear’ takes place. If there is more than one such system (as always in grains of a polycrystal), the best coordinate system to choose is not usually one aligned with the slip elements, but one coincident with the crystallographic axes. We shall imply a cubic lattice here, and choose our coordinate system parallel to the cubic axes. (When the lattice coordinate system is not Cartesian, all relations are still valid, so long as one describes *plane* inclinations and spacings in the *reciprocal* coordinate system.)

If the incremental amount of simple (‘engineering’) shear in slip system  $s$  is called  $d\gamma^s$ , then the incremental (plastic) ‘distortion tensor’ (displacement gradient tensor) *in the crystal coordinate system* is given by

$$d\beta_{ij} \equiv \frac{\partial du_i}{\partial x_j} = l_{ij}^s d\gamma^s \quad (4.1)$$

where  $du$  is an incremental displacement of a point at location  $\mathbf{x}$  (in the crystal lattice) and  $l_{ij}$  is the tensor transformation matrix from the coordinates of the slip system to the ‘crystal coordinates’. (If the components of the slip direction in the crystal system are  $b_i$ , and those of the slip plane normal are  $n_j$ ,  $l_{ij} = b_i n_j$ .)

In eqn (4.1), we have introduced *incremental* quantities related to distortions and strains. These are meant to be infinitesimal, but not necessarily total differentials of (state) functions.<sup>43,44</sup> Another common practice (more common presently) is to use *rates*. These can be obtained by dividing both sides of eqn (4.1)—and of all following equations that employ the differential symbol  $d$ —by  $dt$ , again without implying that deformation ‘rates’ are total derivatives of any quantity that measures finite strain. In this article, we use increments in order to keep clear of the implication that directions in strain space have anything to do with the physical speed with which a process occurs (a *scalar* rate). Either increments or rates are appropriate in the spirit of state-plus-evolution descriptions; it is imperative that history variables such as *any* measure of finite strain be avoided.

The change in all material lines with respect to the crystal lattice is fully described by eqn (4.1): both in their length as in their orientation with respect to the crystal lattice (and, by implication, their change in angle with respect to each other). Since the element does not generally remain cubic in shape, a specification of its ‘orientation change’ (or its ‘rotation’ with respect to the lattice) requires further thought.<sup>51</sup> What is actually meant by the orientation change of a grain is the change in the relative orientation of the lattice and *certain material lines and/or planes*. In simple cases, these are the plane and line kept constant in the macroscopic experiment. For example, in rolling, the rolling plane and the rolling direction are kept constant (and are the coordinates in which the stress and strain state are related to the boundary conditions); but, for example, a plane that was initially perpendicular to the rolling direction need not remain so.

If the incremental displacement gradient tensor *in machine coordinates* is labelled  $dB_{ij}$ , then when a *plane*  $i$  remains parallel to itself,  $dB_{ij} = 0$  ( $j \neq i$ ); and when a *material line*  $j$  remains parallel to itself,  $dB_{ij} = 0$  ( $i \neq j$ ). The components of the (‘relevant’) *orientation change*  $d\Omega_{ij}$  are given by the values of  $d\beta_{ij}$  for those three components in which  $dB_{ij} = 0$ . Thus, the orientation change is *not*, in general, the antisymmetric part of the distortion tensor  $d\beta_{ij}$ .<sup>51</sup>

The incremental strain, on the other hand, is always the symmetric part of the incremental distortion tensor. We write

$$d\varepsilon_{ij} = m_{ij}^s d\gamma^s, \quad m_{ij}^s \equiv \frac{1}{2}(l_{ij}^s + l_{ji}^s) \quad (4.2)$$

The ‘Schmid factor’  $m_{ij}$  plays the role of a ‘strain direction’: a unit ‘vector’ (Section 2.2.1) in strain-increment space for each slip system.

#### 4.1.2. Work Increment and ‘Resolved’ Stress

Consider now the increment of plastic work per unit volume:†

$$dW = \sigma_{ij} d\varepsilon_{ij} = \sigma_{ij} m_{ij}^s d\gamma^s \quad (4.3)$$

where  $\sigma$  is the true stress applied to the volume element under consideration. Use of eqn (4.2) in the second part of this equation has produced a scalar

$$\sigma^s \equiv m_{ij}^s \sigma_{ij} \quad (4.4)$$

† Summation over repeated (upper or lower) indices is always implied. When pairs of indices are repeated, a sum over all *pairs* is meant.

It is the value of the *resolved stress* in system  $s$ , or the projection of the stress vector on the direction of the strain-increment vector, or the work-conjugate to the crystallographically defined scalar strain-increment measure  $d\gamma$  in that system.

The ‘Schmid law’ states that this resolved stress must reach a critical value for system  $s$  to operate.<sup>53</sup> Then, the yield condition is

$$\sigma^s(\sigma_{ij}) = \tau^s(T, p, \dot{\gamma}^s, \dots) \quad (4.5)$$

Note the essential difference between  $\sigma^s$  and  $\tau^s$  (even though both are shear stresses; see eqn (4.4)). This difference is emphasized by the functional dependences written explicitly into eqn (4.5):  $\sigma^s$  is a function of the applied stresses (representing the weights on the body; see Section 1);  $\tau^s$  is a material property, a special case of the ‘plastic resistance’.<sup>45</sup> Ideally, it should be the mechanical threshold  $\hat{\tau}$  (the rate-independent value of  $\tau^s$  at  $T = 0$  K), but eqn (4.5) allows for the more realistic case of a flow stress at finite temperature—which is lower because of  $\mu(T)$  and, in addition, because of thermal activation. For the latter reason, the strain rate  $\dot{\gamma}^s$  on system  $s$  is also relevant. The pressure dependence of  $\tau^s$  is a stress dependence of a different nature from that of  $\sigma^s$ : it is an effect on the state of the material, for example because of  $\mu(p)$ , or because of a change in the dislocation core structure with pressure. In principle,  $\tau^s$  may even depend on deviatoric components of the applied stress.

*We shall always use  $\sigma^s$  for applied stresses (or functions thereof) and  $\tau^s$  for material properties.* The difference is crucial; if the particular terminology is not desired, two different symbols must in any case be found for ‘stress’ and for ‘strength’.† (For consistency, the yield strength should not have been called  $\sigma_Y$  in Fig. 1, but  $\tau_Y$ , with some orientation factor.)

#### 4.1.3. The Plastic Potential

Since the scalar stress measure  $\sigma^s$  was chosen as the work-conjugate of the scalar strain-increment measure  $d\gamma^s$  for single slip (eqns (4.2) and (4.4)), it follows immediately that‡

$$d\varepsilon_{ij} = \frac{\partial \sigma^s}{\partial \sigma_{ij}} d\gamma^s \quad (\text{no sum on } s) \quad (4.6)$$

† The new DIN norm uses  $R$  for the plastic resistance.

‡ The equation does hold for multiple slip when it is summed over  $s$ , but this is here not intended.

In words, if  $\sigma^s$  is known as a function of  $\sigma_{ij}$ , it acts like a plastic potential for single slip: the direction of the plastic strain increment is parallel to the gradient of  $\sigma^s$ ; it is *normal* to a surface

$$\sigma^s(\sigma_{ij}) = \text{constant} \quad (4.7)$$

where constant means independent of stress. In the *yield condition* (4.5), the right-hand side was  $\tau^s$ —which may or may not be independent of stress; we have seen that  $\tau^s$  does, in principle, depend on pressure, at least through the shear modulus. ‘*Normality*’ (of the strain increment on the yield surface) holds when the material strength parameter is insensitive to stress. This is generally true for metals in the regime of interest here, but it is, for example, grossly untrue in polymers.<sup>15</sup>

It should also be mentioned that normality may be violated for another reason: namely, when some strain increment component may be indirectly caused by plastic deformation; for example, a change in volume because of vacancy or dislocation generation. This is also usually negligible (see Section 2.1.5).

In summary, the ‘resolved stress’, i.e. the scalar stress measure that is work-conjugated to the scalar plastic strain-increment, is the plastic potential (for which normality is true by definition). Normality of the strain-increment on the *yield surface* is not a general principle, but may or may not hold depending on the class of material and the range of the imposed conditions. It generally holds for the ‘interest space’ we have defined in Section 1, and we will thus be lax in keeping plastic potential and yield surface separate.

#### 4.1.4. The Yield Surface of Single Crystals<sup>53</sup>

Descriptions in stress space are most convenient in ‘vector’ ( $5 \times 1$  matrix) notation (Section 2.2.1). With some fixed assignment of the single (Greek) subscripts to the five independent pairs of double subscripts, one can then write eqns (4.4) and (4.5) as

$$m_v^s \sigma_v = \tau^s \quad (4.8)$$

This is a set of planes (if  $\tau^s$  is independent of the stress component  $\sigma^s$ ), † one plane for each slip system  $s$ . The yield condition specifies not only that eqn (4.8) must be fulfilled for every active system, but also

† When  $\tau^s$  depends on the stress state, the yield surface may even be concave; the plastic potential is convex by definition.

that  $\sigma^s \leq \tau^s$  for every other system. Thus, the yield surface is the *inner envelope* of the planes specified by eqn (4.8). Each of these planes has intercepts  $\tau^{(s)}/m_v^{(s)}$  on the  $v$ -axis.

Figure 9 illustrates the typical topology for three slip systems (a, b, c). The inner-envelope construction means that systems 'a' and 'c' cannot operate simultaneously under any stress state. Whenever more than one system is active, the stress vector must be at a 'vertex' in a space the dimension of which equals the number of *independent* systems operative. Some slip system combinations are not independent; imagine the vertex of an octahedron in three dimensions: four planes meet, but only three (non-coplanar) strain directions are necessary to compose an arbitrary strain vector.

Vertices in the single-crystal yield surface play a major role in polycrystal plasticity. It is convenient to define normalized vertex vectors  $M_v^v$  such that the stress for a particular vertex  $v$  is

$$\sigma_v^v \equiv M_v^v \tau \quad (4.9)$$

where  $\tau$  is a single scaling parameter for the yield surface. To fulfill the yield condition, we must have (eqn (4.8))

$$M_v^v m_v^s = \tau^s / \tau \quad (4.10)$$

for each active slip system  $s$  in the vertex  $v$ . The right-hand side is equal to 1 when all slip systems have the same critical resolved shear stress (and then the left-hand side is 0 for all non-active slip systems in the case of fcc crystals).

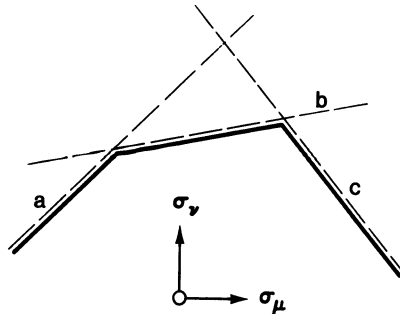


**Fig. 9.** Schematic single-crystal yield surface: three facets for the slip systems a, b, and c (each in *one* of their possible signs). To activate two systems simultaneously, the stress must be at a vertex; some systems (such as a and c) cannot be activated simultaneously.<sup>57</sup>

Another relevant quantity is the work-conjugate of  $\tau$ ; in the special case outlined above, it becomes the algebraic sum of shears:

$$d\Gamma \equiv dW/\tau = M_v^\gamma d\varepsilon_v = M_v^\gamma m_v^s d\gamma^s \quad (4.11)$$

Observe the following duality. A stress vector of arbitrary direction will generally produce slip on a single system (it will touch a single facet of the yield surface); thus, it will produce one of a few *discrete* directions of *straining*. This is, for example, seen in free single crystals under tension. On the other hand, if one imagines the direction of the strain-increment vector as given, the *stress* must be one of a small number of *discrete* values: the vertex vectors. It is evident from the plastic potential concept that the prescribed strain direction must be contained in the cone of normals of the active vertex.

There are two dual kinds of non-uniqueness associated with the facets-plus-vertices nature of the single crystal yield surface: if one happened to prescribe a strain direction that is identical to one of the facet normals, the stress direction is not unique; and if one happened to prescribe a stress vector that points precisely into a vertex, the resulting strain-increment direction is not unique.

Finally, there is an ambiguity at those vertices in which more facets meet than is the 'order' (dimensionality) of the vertex: then, a given strain-increment vector cannot uniquely be decomposed into shears on the activated slip systems. This has been a topic of much discussion in the theory of polycrystal plasticity, since the strain in the grains is presumed completely prescribed (in 5 dimensions) in the most prominent model,<sup>46</sup> whereas the vertices in highly symmetric materials always activate more than 5 slip systems.

#### 4.1.5. Rate Sensitivity

As we have pointed out above (Section 3.6), the most precise definition of the yield surface is as the (rate-independent) mechanical threshold; but the typical rate sensitivities are so low that a 'flow surface' can be defined for a constant strain rate, which differs only very little from the limit yield surface.<sup>9</sup>

Figure 6 showed (exaggerated) the typical rate effect: a slight lowering of the flow stress from the mechanical threshold. Thus, for each single slip system, a constant shear rate  $\dot{\gamma}$  will correspond to a plane parallel to the rate-independent yield facet, slightly inside it (Fig. 10).

When two or more slip systems operate, however, each one can

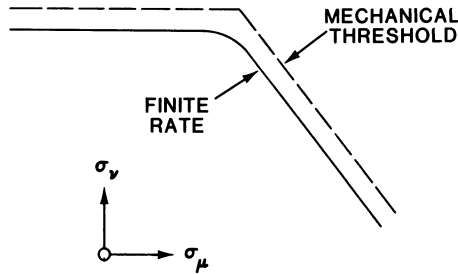


**Fig. 10.** The mechanical threshold provides a 'true' yield surface, in the rate-independent limit. Thermal activation lowers the stress needed for a given strain rate. Where two slip systems operate simultaneously, the yield surface vertices become rounded.<sup>9</sup> The relative decrease in stress is proportional to the relative rate sensitivity, typically of order 0.01.<sup>48</sup>

operate at a lower shear rate to produce the same macroscopic strain rate, and thus at an even slightly lower stress. Thus, *the 'flow surface' near a vertex gets rounded; this eliminates all problems of non-uniqueness.* Note that, in order to achieve this very convenient result, the rate sensitivity need not be large; it only must exist in principle (and be positive definite). Thus, the concept of an *essentially* rate-independent (a 'rate-insensitive') plasticity, but not a strictly rate-independent one, allows one to use the methods of classical plasticity theory, including (sharp) yield surfaces, while avoiding some of its pitfalls.<sup>47,48</sup>

When the rate sensitivity is low, the (true) vertices become sharp 'noses' (Fig. 10). These still have the characteristic that a very small variation in stress direction can produce a very large variation in strain-increment direction. This property of a vertex is important in the consideration of instabilities. The change from a true vertex to a sharp nose eliminates the possibility of bifurcation; but it leaves intact the sensitivity to small fluctuations, which may (or may not, depending on other factors) lead to instability.<sup>49</sup>

We shall, in the following, use the term 'vertex' to signify a sharp nose, whether it be continuous or discontinuous.

## 4.2. Averaging over a Polycrystal

### 4.2.1. Nomenclature

We have already introduced the vector notation for stress and strain-increment, which we write in extended form with single (Greek)

subscripts that go from 1 to 5. The particular association of one Greek subscript with one pair (or an independent combination) of Latin ones is arbitrary; different ones have been used. Two conditions should, however, be met: that the stress vector and strain-increment vector be work-conjugated, so that

$$dW = \sigma_\nu d\epsilon_\nu \quad (4.12)$$

and that, if the coordinate system is not Cartesian, the strain-increment vector be measured in reciprocal space, i.e. by the inverse axis intercepts of a plane perpendicular to it.

The relation between stress and strain-increment on the yield surface does not involve the magnitude of the strain increment, only its direction. It is convenient to define such a 'magnitude' and 'direction':<sup>55</sup>

$$d\epsilon_\nu = \epsilon_\nu^0 d\epsilon \quad (4.13)$$

The *straining direction*  $\epsilon^0$  should be normalized in some fashion. It has become common to do this such that, in uniaxial tension, the scalar  $d\epsilon$  is equal to the measured increment in tensile strain; then

$$\epsilon_\nu^0 \epsilon_\nu^0 = 3/2 \quad (4.14)$$

Inserting eqn (4.13) into eqn (4.12) leads to the definition of a scalar stress measure:

$$\sigma \equiv \sigma_\nu \epsilon_\nu^0 \quad (4.15)$$

which, when multiplied by the scalar  $d\epsilon$ , again gives the work. It is equivalent to the *resolved stress* in single crystals, and we will retain this descriptive nomenclature for the general case.  $\sigma$  is the distance in stress space from the origin to a plane perpendicular to  $\epsilon^0$  that is tangent to the plastic potential surface. In fact, the scalar  $\sigma$  is the plastic potential, much as the resolved stress on a slip system was shown to be the plastic potential for single slip (Section 4.1.3). If the resolved stress is *constant*, you get the von Mises sphere in deviatoric stress space; but, in general, the distance  $\sigma$  may depend on the direction  $\epsilon^0$ .

One may also define a *stress direction*  $\sigma^0$  so that

$$\sigma_\nu = \sigma_\nu^0 \sigma \quad (4.16)$$

Note that  $\sigma^0$  is not normalized to its length, but to its projection on  $\epsilon^0$  (eqn (4.15)). If one gave  $\sigma$  as a function  $\sigma(\sigma^0)$ , it would be a plastic potential in the conventional sense.

For *vertex* stress vectors, one may finally write, with eqns (4.10) and (4.15):

$$\sigma = M_v \varepsilon_v^0 \tau \equiv M \tau \quad (4.17)$$

where a scalar  $M$ , *the normalized Taylor factor*, has been defined as the projection of a vertex vector on the prescribed normalized strain direction.<sup>55</sup> (Note that this normalized definition differs from the standard one for deformation modes other than uniaxial tension or compression.)  $M$  is the spacing of tangent planes of the yield surface normalized to the scalar  $\tau$ . The stress direction becomes

$$\sigma_v^0 = M_v / M \quad (4.18)$$

The ‘maximum work’ postulate by Bishop and Hill<sup>57</sup> gives a prescription for the derivation of the correct value of  $M$  for any given strain direction: it is the greatest of all those for any vertex on the yield surface; this guarantees that the prescribed strain direction is contained in the cone of normals of the activated vertex.

#### 4.2.2. The Model

A grain in a polycrystal finds itself under a number of boundary conditions on stress and strain-increment. (In this section, we address total, not deviatoric, stresses and use the symbol  $\sigma$  for these.) A useful idealization is that some strain-increment components are prescribed and some (the complementary) stress components are prescribed. If we mark the prescribed components by an overwritten double bar, and furthermore assume that any prescribed component is equal to the average (single bar), we have

$$\begin{aligned} d\bar{\bar{\varepsilon}}_v &= d\bar{\varepsilon}_v & (p \text{ values of } v) \\ \bar{\bar{\sigma}}_\kappa &= \bar{\sigma}_\kappa & (6 - p \text{ values of } \kappa \neq v) \end{aligned} \quad (4.19)$$

where any prescribed stress component is usually zero.

There is an easy case in which eqns (4.19) in fact give the complete (approximate) solution: that of plate-like grains, with large planar interfaces (the interactions across the other interfaces being neglected). Across a planar interface, there are three continuity conditions on strain and three (the complementary ones) on stress. Thus, both compatibility and equilibrium can be fulfilled.<sup>50-52</sup>

Another easy case is the upper bound solution: all plastic strain increments are considered prescribed ( $p = 5$ ); the one remaining stress

condition is on the hydrostatic stress (which is here conveniently set to zero). In this case, compatibility is fulfilled *a fortiori*, but one renounces on fulfilling equilibrium. This upper bound has been considered a good approximation for large-strain plasticity. A justification can be given as follows:<sup>53</sup> The internal stress distribution necessary to fix up the violations of local equilibrium will disturb the compatibility conditions only by elastic strains, small compared to the plastic ones. On the other hand, violations of compatibility that are being fixed up elastically would add enormous stresses. Thus, a sensible approach to approximate polycrystal plasticity theory is: '*compatibility first*'. This is the essence of Taylor's model,<sup>46</sup> which is used as a basis for most current simulations of polycrystal plasticity.<sup>47,54-56</sup>

Compared to this completely constrained upper-bound solution, the more general approach of eqns (4.19) has been called 'relaxed constraints' (RC): only the most important compatibility conditions for a given grain shape are fulfilled by prescribing the respective strain components to be uniform; equilibrium is fulfilled for the remaining components.<sup>52,55</sup>

#### 4.2.3. The Calculation<sup>55</sup>

For each grain, one must determine which stress components can be prescribed (to be zero) and then investigate the yield surface in the subspace  $\sigma_\kappa = 0$  for  $6 - p$  values of  $\kappa$ . This subspace is  $p$ -dimensional. The yield subsurface has vertices of order  $p$ , with vertex vectors  $\sigma^\nu = \mathbf{M}^\nu \tau$ . Among them, the right one (components  $\sigma_\nu$ ) for the prescribed strain-increment in this subspace (components  $d\bar{\epsilon}_\nu$ ) follows from the geometric criterion

$$(\sigma_\nu - \sigma_\nu^\nu) d\bar{\epsilon}_\nu \geq 0 \quad (p \text{ values of } \nu)$$

or, normalizing both the stress and the strain increment:

$$(M_\nu - M_\nu^\nu) \bar{\epsilon}_\nu^0 \geq 0 \quad (4.20)$$

This is an extension of Bishop and Hill's<sup>57</sup> maximum work hypothesis to relaxed constraints, proved by Renouard and Wintenberger.<sup>58</sup>

As a result of the calculation, the unknown stress components  $\sigma_\nu$  of the correct vertex fulfill the conditions

$$\sigma_\nu \bar{\epsilon}_\nu^0 = M \tau \quad (4.21)$$

and, according to the model (or at least as an upper limit), the

polycrystal stresses must fulfill the same condition for the averages:

$$\bar{\sigma} \equiv \bar{\sigma}_v \bar{\epsilon}_v^0 = \bar{M} \bar{\tau} \quad (4.22)$$

In truth, the right-hand side should be averaged as a product; however, it has been found that the error is small. (Alternatively, one may interpret the quantity  $\bar{\tau}$  as a *weighted* mean, weighted by  $\bar{M}$ ; this has been called  $\bar{\tau}$ .<sup>55</sup>)

Equation (4.22) is, again, for arbitrary stresses, an equation of a plane perpendicular to the direction  $\bar{\epsilon}_v^0$ , at a spacing  $\bar{M} \bar{\tau}$  from the origin.  $\bar{M}$  depends on the crystallographic orientation distribution function of the grains in the polycrystal, and on the direction of the prescribed strain increment  $\bar{\epsilon}_v^0$ ;  $\bar{\tau}$  depends on the substructural state of each grain. The inner envelope of all these planes constitutes the yield subsurface for the polycrystal in this space.

While this ‘inner-envelope construction’ of the (upper-bound) yield surface follows directly from the maximum-work principle (4.20), it is sometimes more convenient (and will be needed later here) to know the locus of the stress vector itself. In fact, Hutchinson<sup>59</sup> has described the polycrystal yield surface by

$$\bar{\sigma}_v = \bar{M}_v \bar{\tau} \quad (4.23)$$

(again with the proviso that  $\bar{\tau}$  is a weighted mean). This can be shown to hold under at least one of the following two assumptions: (a) equilibrium everywhere, which would seem to be inconsistent with an upper-bound model; or (b) normality assumed for the polycrystal independently from the single crystal. (Normality for the polycrystal can be derived from that of the single crystal only by assuming equilibrium.) As we have shown, normality does not need to hold (and in fact does not hold when  $\tau$  depends on the stress state). However, for the plastic potential, normality holds by definition— for the polycrystal too. Thus, we will make use of relation (4.23) *without* the factor  $\bar{\tau}$ : *the plastic potential of the polycrystal is the five-dimensional locus of the vector  $\bar{\mathbf{M}}$ .*

The strain components in the *unprescribed* directions (where the stress is zero) follow, with eqn (4.2), from the crystallographic shears, which are a solution to the  $p$  equations (see eqn (4.19))

$$d\epsilon_v = m_v^s d\gamma^s \quad (4.24)$$

(modified near vertices at which the number of slip systems  $s$  exceeds the number of prescribed components  $\lambda$  according to the rate-

sensitivity criterion; Section 4.1.5). These crystallographic shears also determine the orientation change, according to eqn (4.1).

The average algebraic sum of shears (or, more generally, the work conjugate of  $\tau$ ) follows easily, as in eqn (4.11) and using eqn (4.17):

$$d\bar{\Gamma} = \bar{M} d\bar{\epsilon} \quad (4.25)$$

In some theories of hardening,  $d\Gamma$  plays a physical role;<sup>46</sup> but even when it does not it can serve as a handy ‘microscopic equivalent strain increment’.<sup>60</sup>

#### 4.2.4. *The Yield Surface of Polycrystals*

The method described above has been used to calculate polycrystal yield surfaces after various simulated deformations<sup>61</sup> (and also to calculate stress/strain curves for various proportional tests<sup>55</sup>). Figure 11(a) shows one of the most interesting applications: the yield surface after a torsional shear of 1.0, in the subspace that also displays the normal stress and strain-increment along the torsion axis. It is seen that, if the longitudinal stress is kept to zero (‘free ends’), there results a component of the strain-increment direction in the ‘lengthening’ direction: this, we feel, is the best explanation of this well known effect so far. Conversely, when the ends are fixed (which is the boundary condition under which the prestrain was run), an axial compressive stress develops.

The two effects are shown quantitatively in Fig. 11(b). The surprising result is that they are not proportional to each other—and this is actually observed.<sup>62</sup> Thus, they are not just two ways of expressing the same thing. The yield surface in Fig. 11(a) may help in understanding this phenomenon.<sup>61</sup> The length change of a ‘free’ tube is proportional to the inclination of the yield surface at the loading point; but the compressive stress in fixed-end torsion depends on the location of the apex. The two are not necessarily related (except in sign); the shape of the yield surface is quite irregular.

The irregularity of the yield surface is a very general observation. Figure 12(a) shows one after simulated rolling to a true through-thickness strain of 3.0, in a space of two shear stresses. In an isotropic material, the yield surface would have to be a circle in this space, regardless of any assumptions (von Mises or otherwise). In classical treatments of anisotropy, it would be an ellipse<sup>63</sup> or an oval of some kind.<sup>64,65</sup> It is neither, it has vertices. At this strain, the texture is not

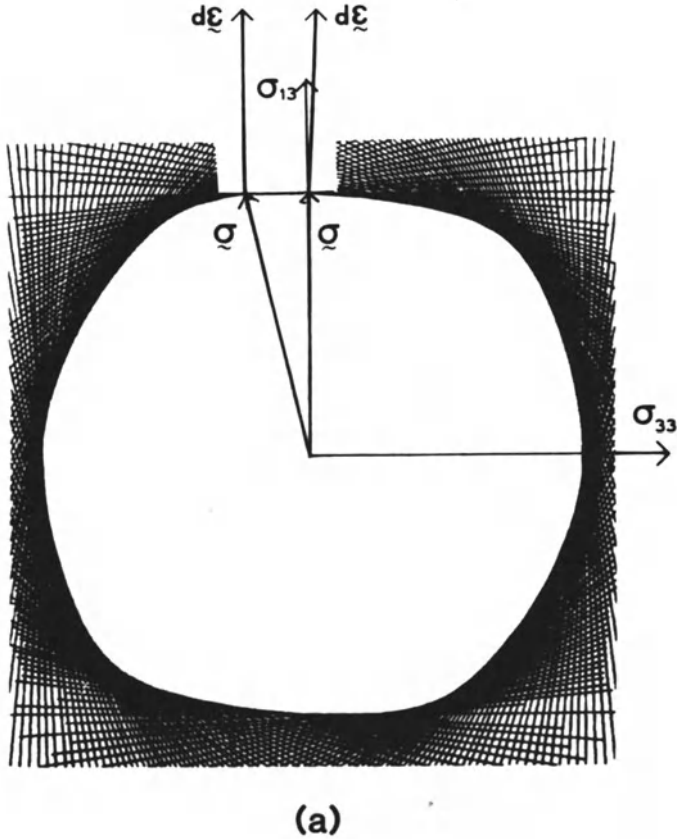


**Fig. 11.** (a) A polycrystal yield surface derived by computer simulation,<sup>61</sup> after torsion to  $\gamma_{31} = 1$ , with fixed ends. Continued shear with fixed ends demands a compressive stress (at the apex to the left); continued shear with free ends would give the length change corresponding to the inclination of the normal at the top.

yet very sharp—not at all like a single crystal (for which one would expect vertices).

Finally, Fig. 12(b) shows the same yield surface, but now in the ‘ $\pi$ -plane’: where the three interdependent normal stresses make a tristar. Note that the normal stresses are here meant to lie in the directions of the (orthotropic) texture symmetry, *not* necessarily in the

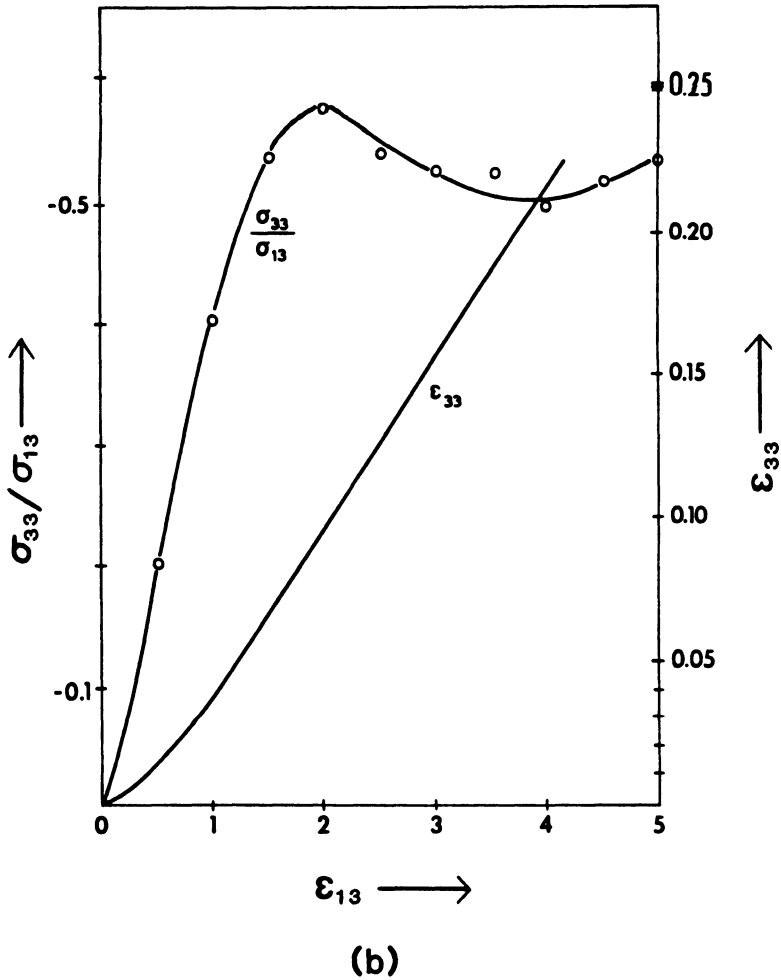
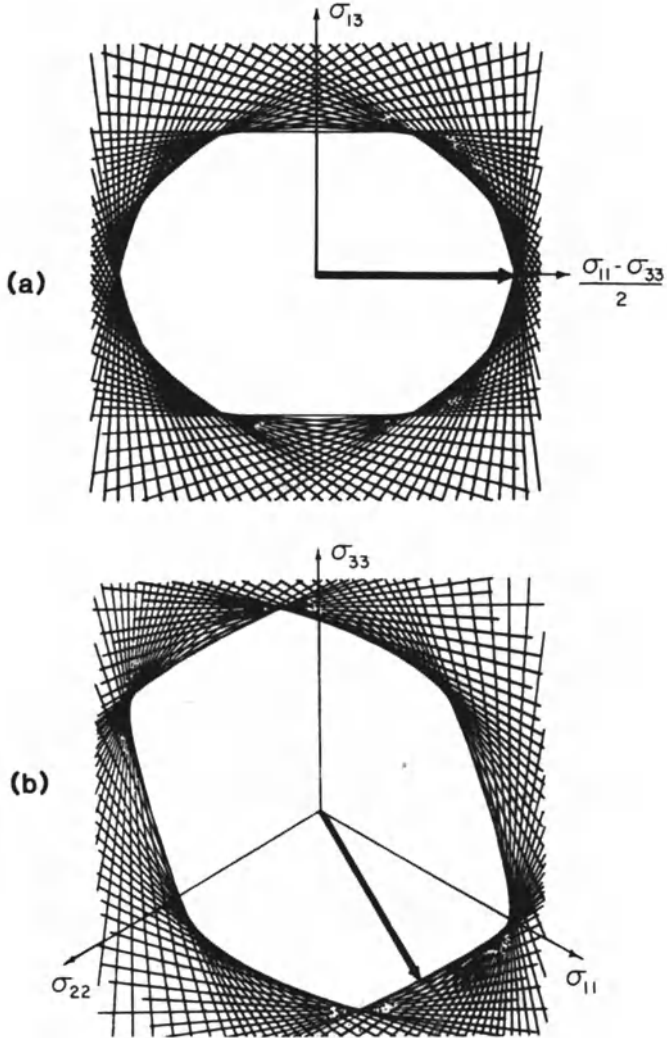


Fig. 11. contd. (b) Experimental results<sup>62</sup> for both cases.

*principal* axes. The most obvious feature of this yield surface is the sharpness of its vertices. Note also that the long flat region perpendicular to the previous rolling direction is the *edge* that corresponds to the vertex in the direction of the abscissa of Fig. 12(a).

The yield surfaces shown here were derived on the basis of a computer code at various stages of its development: they are not to be taken as quantitatively reliable results. However, *all* polycrystal yield surfaces we have ever derived, after strains in excess of about 50%



**Fig. 12.** Calculated polycrystal yield surface after plane-strain rolling to a thickness reduction of 95%. An isotropic yield surface would have to be circular in the shear space (a) and would be circular under the von Mises assumption in the normal-stress-deviator plane (b). The calculated yield surface shows vertices and flat spots.

from an isotropic start, had vertices, ridges, and flat spots. (It appears that they are particularly prominent under 'relaxed-constraints' (flat-grain) conditions.) Vertices are very hard to observe experimentally; nevertheless, some indications have been seen. More clearly, 'flat' regions have been identified in some cases.<sup>66</sup>

The most important consequence of vertices is that they may lead to instabilities.<sup>67</sup> This has been treated in some detail both for the ridge perpendicular to the rolling direction (using the plane-strain idealization for the rolling process), which can be one cause of 'shear bands',<sup>68</sup> and for localized necking in sheets, which can be explained on the basis of the sharp vertex in Fig. 12(b).

As in the case of single-crystal plasticity, rate dependence will round off any polycrystal vertices. However, the corner would (because of the quantitatively low rate sensitivity) remain very sharp. Then, minute internal stresses could lead, in practice, to the same kind of non-uniqueness that true vertices represent.

All the yield surfaces shown so far have been projections into a particular two-dimensional space. The most general yield surface would have to be plotted in five dimensions. However, in two interesting cases, three dimensions are actually sufficient (and only one octant of three-dimensional space, when there is no sign dependence of yield). One of these is a *fiber* texture, the other an orthotropic texture (such as in a rolled sheet) when only *plane-stress* conditions are encountered (such as in sheets). In both cases, these subspaces are 'closed': an arbitrary stress in this space gives rise to strain-increment components *only* in this space, and vice versa. The figures are simultaneously sections and projections of the five-dimensional yield surface.<sup>61</sup> Such symmetry relations can be of crucial help in treating anisotropic materials.

#### 4.2.5. Constitutive Relations for Anisotropic Plasticity

The rapid development of extensive flat spots and rather sharp ridges and vertices on the plastic-potential surface of polycrystals during deformation makes a description in terms of *functions* difficult if not impossible. Perhaps some scheme will eventually be found that abstracts the essential features of realistic yield surfaces in a useful way. For now, it would seem that one must employ a *tabular approach*. What is needed is a table of the stress direction  $\sigma^0$  for each strain-increment direction  $\epsilon^0$ . Unfortunately, this table will change with strain, since the *shape* of the yield surface changes. A help is that

the symmetries of the material (if known) and of the test to be performed can substantially reduce the space in which  $\epsilon^0$  must be scanned (Section 4.2.4).

The relation between  $\sigma^0$  and  $\epsilon^0$  may be expressed in matrix form:

$$\sigma_\mu^0 = P_{\mu\nu} \epsilon_\nu^0 \quad (4.26)$$

Note, however, that  $P$  is in general different for each direction  $\epsilon^0$ ; it does not transform like a fourth-rank tensor as Hart assumed.<sup>31</sup> Also note that it is substantially different from a 'plastic modulus': it links strain-increments (or rates) with (total) stresses. This is because we elected to treat plasticity only, and in terms of a flow-rule-type theory, not a modification of an elastic one. Dimensionally, it is like a viscosity; but it has nothing to do with kinetics.

A table of the  $5 \times 5$  matrix  $\mathbf{P}$  for each vector  $\epsilon^0$  may sound more cumbersome than a table of the vector  $\sigma^0$  vs.  $\epsilon^0$ . However, under many symmetry conditions,  $\mathbf{P}$  may have simple properties. For example, in *isotropy*

$$P_{\mu\nu} = \delta_{\mu\nu} \quad (4.27)$$

in any subspace defined by shear axes only (including differences between diagonal components), as a consequence of isotropy itself, and further in the deviatoric principal plane *under the assumption of a von Mises potential*. In anisotropic materials, eqn (4.27) may hold exactly for some subspaces, and may be an acceptable approximation for some other regions. Conceivably, one needs to explore the real nature of  $\mathbf{P}$  only near extensive flat spots or sharp vertices that may be reached in the expected application.

Given the table  $\mathbf{P}(\epsilon^0)$  and, as we shall need,  $\bar{M}(\epsilon^0)$ , we now imagine a polycrystalline material element under strain-increment boundary conditions in a  $p$ -dimensional subspace:

$$d\bar{\epsilon}_\nu = \bar{\epsilon}_\nu^0 d\bar{\epsilon} \quad (p \text{ values of } \nu) \quad (4.28)$$

where the double-bar, as before, means 'prescribed'. The average deviatoric stress in this subspace follows from

$$\bar{\sigma}'_\mu = P_{\mu\nu} \bar{\epsilon}_\nu^0 \bar{M} \bar{\tau} \quad (p \text{ values of } \mu) \quad (4.29)$$

The evolution of  $\mathbf{P}$  and  $\bar{M}$  must be calculated or measured and is to be tabulated. That of  $\bar{\tau}$  follows from the strain-hardening rate  $\theta \equiv d\tau/d\Gamma$  to be discussed in the next section, where

$$d\Gamma = M d\bar{\epsilon} \quad (4.30)$$

We have implied above that the subspace in which the strain-increments are prescribed may have  $p < 5$  dimensions. This applies only when a relaxed-constraints theory is appropriate. For example, in a cold-rolled sheet, all grains are likely to be flat and parallel to the sheet; then, the normal stress in the thickness-direction may be relaxed on the individual grains and prescribed (to be zero) on the surface. To allow, in general, for such a case, let us specify that *stresses* are prescribed in  $6 - p$  dimensions; one of these prescribes the hydrostatic pressure. From the others follows

$$\varepsilon_\lambda^0 = P_{\lambda\kappa}^{-1} \bar{\sigma}_\kappa^0 \quad (5 - p \text{ values of } \lambda \text{ and } \kappa)$$

and

$$d\varepsilon_\lambda = \varepsilon_\lambda^0 d\bar{\varepsilon} \quad (4.31)$$

At this point, the entire (average) stress state is known; it can be inserted into  $\tau(\boldsymbol{\sigma})$ , if there is such a dependence, and then the *yield surface* is described by the five-dimensional locus of

$$\bar{\boldsymbol{\sigma}}' = \bar{\mathbf{M}}(\boldsymbol{\varepsilon}^0, \{\Omega\}) \cdot \bar{\tau}(T, \dot{\Gamma}, \boldsymbol{\sigma}, \boldsymbol{\varepsilon}^0) \quad (4.32)$$

while the *plastic potential* is just the locus of  $\bar{\mathbf{M}}$ . Here, the vector  $\bar{\mathbf{M}}$  has been re-introduced for  $\boldsymbol{\sigma}^0 \cdot \bar{\mathbf{M}}$  (eqns (4.18) and (4.23)), and its dependence on the *orientation distribution* has been expressed by the set  $\{\Omega\}$  of orientations  $\Omega$ . Furthermore, the dependence of the plastic resistance  $\tau$  on its primary variables temperature and strain rate, on the stress state, and possibly on the straining direction has been explicitly stated.

#### 4.2.6. Adding Anisotropic Elasticity

So far, we have deliberately ignored elasticity. The strain-increment, whose direction played such a crucial role in determining the stress state necessary for plasticity, was taken to be the *total* (deviatoric)  $d\varepsilon$ . In truth, this should have been the *plastic* strain increment.

The following iterative procedure, in a step-wise calculation, may be used to take account of the change in the direction of the plastic strain-increment  $\Delta\boldsymbol{\varepsilon}^p$  at a given total strain-increment  $\Delta\boldsymbol{\varepsilon}^t$ , due to the direction of the elastic strain-increment  $\Delta\boldsymbol{\varepsilon}^e$ . Assume first (as we have) that  $\Delta\boldsymbol{\varepsilon}^p = \Delta\boldsymbol{\varepsilon}^t$ , and calculate the values of  $\boldsymbol{\sigma}'$  both before and after the step. Then use the difference between these two stress values to calculate the deviatoric part of the elastic strain-increment, and finally subtract it from  $\Delta\boldsymbol{\varepsilon}^t$  to determine a better approximation of  $\Delta\boldsymbol{\varepsilon}^p$ :

$$\Delta\boldsymbol{\varepsilon}^p = \Delta\boldsymbol{\varepsilon}^t - \mathbf{S} \Delta\boldsymbol{\sigma}' \quad (4.33)$$

where  $\mathbf{S}$  stands for the anisotropic deviatoric elastic compliance (a fourth-rank tensor). All quantities are written in the (stress-free) lattice coordinate system; elastic rotations may safely be neglected.

There is one set of problems where adding elasticity is not an option but a necessity (even though only the plastic response may be of interest): that is when parts of a body, at some time, may not actually be plastic. This could well occur in cases where the single crystal yield surface is very elongated (or even open in some directions of stress space), or is simply very large in some places (e.g. in a two-phase material). None of this would pose any problem if the local stress were completely known: one could check whether it is inside the yield surface or not. But, under prescribed straining conditions, the yield condition could only be verified by assuming the total strain increment to be elastic and checking for the location of the resulting stress. As in all cases, incorporation of rate dependence alleviates the problem also here.

## 5. EVOLUTION

It is part and parcel of a state-parameter description that the evolution of the parameters must be described: that is how history makes its impact on the future behavior. There have been many discussions of flow-stress evolution and various transients in strain-hardening that make further parameters necessary.<sup>69</sup> However, there has been very little discussion concerning the effects of the *change* of textures, and thus of average orientation factors, during deformation.<sup>55</sup> Instead the multiaxial behavior has been described by various postulates. We will compare these with physically expected behavior.

### 5.1. Texture Evolution

#### 5.1.1. Hardening Rules

The most evident effect of deformation on the calculated yield surfaces of the last section is a change in their *shapes*. This is not accounted for by any of the classical assumptions on 'hardening rules': they have postulated only a change in *size* ('isotropic hardening') and a change in *location* of the yield surface in stress space ('kinematic hardening').<sup>70</sup>

The difference between these postulates and the 'real' behavior, as exemplified in the foregoing section, is not negligible, because of the

developing vertices: while the difference in the absolute value of the resolved stress  $\sigma$  may not vary too much with direction in stress space, the angle between the stress direction and the strain-increment direction varies widely and abruptly. (In the von Mises model, this angle is zero and  $\sigma$  is constant for all directions.)

It would appear that a new formulation that takes some account of *angular yield surface shapes* must be developed. Until such a comprehensive treatment is available, a realistic assessment of yield surface evolution can only be obtained by direct measurement (which is especially difficult near vertices)—or by the measurement or calculation of textures, from which yield surfaces are to be calculated.

To calculate texture changes, one must carry the polycrystal model (Section 4) further: the distortion rate (eqn (4.1)) must be calculated from the slips on all systems, which can be unambiguously obtained by using rate dependence (eqn (3.10)) to invert the yield condition (eqns (4.4) and (4.5)).

In addition to changes in *shape*, there is, of course, a change in *size* of the yield surface: it increases with strain as  $\tau$  does ('isotropic hardening'; Section 5.2). For two-phase materials, one would, in addition, expect some 'kinematic hardening' (Section 7). Finally, there is some evidence for a phenomenon that may be called 'lateral hardening':<sup>71</sup> a slight additional growth of the yield surface in directions perpendicular to the previously applied straining direction. It would be expected as a consequence of 'latent hardening' in single crystals (see Section 5.2.1).

### 5.1.2. Texture Hardening and Texture Softening

In eqn (4.15), we defined a scalar stress parameter  $\sigma$  that characterizes the spacing of a tangent plane to the yield surface (and *depends* on the strain-increment direction, i.e. the inclination of the tangent plane). The change of this 'resolved stress' with the scalar equivalent strain increment  $d\varepsilon$  is an expression of (multiaxial) yield stress evolution. With eqn (4.22) it is

$$\Theta \equiv \frac{d\sigma}{d\varepsilon} = \bar{\tau} \frac{d\bar{M}}{d\varepsilon} + \bar{M} \frac{d\bar{\tau}}{d\varepsilon} \quad (5.1)$$

These are averages over the polycrystal, but we have dropped the bar over the  $\sigma$ . (Also, the possible dependence of  $\bar{\tau}$  on strain rate, temperature, etc. has not been explicitly stated in eqn (5.1).) The first term on the right-hand side is due to a change in texture, the second to

a change in dislocation structure. The latter is actually related to the crystallographic shears in the grains, so that eqn (5.1) is better written, with the aid of eqns (4.11) and (4.16), as†

$$\Theta \equiv \frac{d\sigma}{d\varepsilon} = \bar{\tau} \frac{d\bar{M}}{d\varepsilon} + \overline{M^2} \frac{d\bar{\tau}}{d\bar{\Gamma}} \equiv \bar{\tau}\bar{M}' + \overline{M^2}\theta \quad (5.2)$$

Here, the standard symbol,  $\theta$ , has been used for the microscopic strain-hardening rate, and  $\bar{M}'$  has been used for the change with strain in the average Taylor factor due to texture development. This change is due not only to the change in orientation of each grain *per se*, but also to the abrupt change in the activated vertex that such an orientation change occasionally entails.

The texture development can cause additional hardening; for example, in the tension (or wire drawing) of fcc metals, a  $\langle 111 \rangle$  fiber texture develops, which has the highest Taylor factor for uniaxial tests. On the other hand, it is also possible for a material to exhibit *texture softening* under certain conditions, and that has the most serious consequences: it can lead to instabilities even at a positive (microscopic) strain-hardening rate  $\theta$ .<sup>72</sup> The most potent combination for such a development is a vertex in the yield surface with texture softening occurring for one of the strain paths allowed in the vertex.

### 5.1.3. Path Dependence

Until now, it has been common to treat yield surface evolution as consisting of two aspects: the change in the yield surface (size, location, shape, etc.), and the rate of change with strain of the scalar parameter (or parameters) that describe it. It is, however, realized that this rate of change may itself depend on the strain path. For example, the texture that develops in torsion is different from that in tension, and the latter is different from that developed in compression. The change in yield surface shape will consequently also be different: sometimes the direction of prestraining is the hardest, sometimes not. (This is possible even when *microscopic* hardening is isotropic.) Unfortunately, there seems, at present, no general way of accounting for all these different possibilities—except by explicit texture calculation (or measurement) at every step.

† Note that this hardening is scalar in nature; an introduction of tensor stress-rates is not necessary when the lattice orientation change has been accounted for in this way (and when there is no kinematic hardening). However,  $\Theta$  may well depend on  $\varepsilon^0$  (or  $\sigma^0$ ).

A path dependence of macroscopic strain hardening can, in addition, be due to a path dependence of microscopic hardening. For example, the rate of dislocation accumulation appears to be smaller in torsion than in tension, perhaps because of the smaller number of slip systems that are significantly active.<sup>55</sup>

Both of these types of path dependence can, finally, make themselves felt during *path changes*: here one would expect significant *transients*. For example, since the range of orientation space that is filled after some heavy deformation is quite small, the re-orientation under the new test conditions may not lead to the same end texture as would be expected from a random start—or it may take much strain to convert to the new ‘equilibrium’ texture.

More potently, dislocation structures accumulated under one set of conditions tend to be unstable under other conditions; thus, one would expect a temporary softening, possibly an instability, upon a change in straining path.<sup>73</sup>

This is another set of problems that needs major theoretical and experimental attention.

## 5.2. Substructure Evolution

### 5.2.1. Strain Hardening and Latent Hardening

The microscopic (and major) aspect of strain hardening is the change of the local flow stress with strain. This is what is primarily meant by the term strain hardening:

$$\theta \equiv \left. \frac{\partial \tau}{\partial \Gamma} \right|_{\dot{\Gamma}, T} = \theta(\dot{\Gamma}, T, \tau, \epsilon^0) \quad (5.3)$$

Note that it is written in differential form, and as a function of state parameters and current conditions only.† Any relation that involves strain as an explicit, integral variable (as most of the common ones) is subject to additional path dependences.<sup>9,75–77</sup>

Equation (5.3) has been written in terms of a single grain. Truly, the average behavior of many grains (not considering orientation effects) should be described;<sup>78</sup> we have found<sup>55</sup> that the different ways of averaging do not change the result significantly, presumably because

†  $\theta$  could also depend on the current state of stress; this may, for example, explain its orientation dependence in single crystals.<sup>74</sup>

the spread of flow stresses in different grains at any one time does not cover a wide range of  $\theta$ 's.

The strain hardening rate, eqn (5.3), has been written in terms of  $\Gamma$ , the algebraic sum of shears (or, more generally, the work conjugate of  $\tau$ ). This is the quantity that can be directly related to the macroscopic strain by the Taylor factor (eqn (4.11)). Equation (5.3) does not imply that  $\theta$  is unique for all combinations of slip increments that make up the same  $d\Gamma$  (as was originally assumed by Taylor<sup>46</sup>); in fact, the inclusion of the straining direction  $\epsilon^0$  in the list of arguments explicitly allows for such non-uniqueness. Unfortunately, not much is known about the general behavior under the type of constrained flow (multiple slip) that occurs in grains of a polycrystal.

There have been attempts to describe single-crystal hardening in more detail by allowing for different hardening coefficients for different slip system interactions. Specifically, if two slip systems are labelled  $s$  and  $t$ , the interaction has been written in matrix form:

$$d\tau^s = h^{st} d\gamma^t \quad (5.4)$$

(and sometimes the orientation-change part of hardening, from eqn (5.2), has been built into this form<sup>79,80</sup>). This is probably grossly oversimplified. For a realistic description, one must at least separate two effects:<sup>80</sup> the ratio of the flow stresses on different systems *at the same structure* (*this* is the 'latent hardening ratio'); and the rate of development of various components of dislocation densities with slip on one slip system.

Equation (5.4) would have serious (beneficial) consequences on the theory of polycrystal plasticity if the hardening matrix were positive definite,<sup>81</sup> that is, roughly speaking, if the off-diagonal terms were smaller than the diagonal terms. The part of  $h^{st}$  that is due to the latent-hardening ratio can be tested in single crystals, operating single slip systems alternately.<sup>82,83</sup> The observations are that latent hardening is always equal to or *larger* than direct hardening. (It is never much greater: typical latent-hardening ratios are at most 1.4, except after easy glide in single slip.)

In summary, the global formulation (5.3) is, for now, as realistic as anything available.

For a quantitative description of strain hardening of any particular material, it is best to plot the differential relation (5.3). In the spirit of our description of polycrystal behavior, this should actually be a single-crystal relation. However, representative grains in a polycrystal

are not likely to behave exactly the same as free single crystals. The most important difference is that they are forced to slip on many slip systems, whereas most free single crystals deform in single slip. In fcc metals, the most appropriate single-crystal curve to use is that for tension or compression in a  $\langle 111 \rangle$  direction,<sup>84</sup> since here slip actually occurs on many slip systems throughout the straining.

Figure 13(a) shows a set of  $\theta(\tau)$  diagrams for Al  $\langle 111 \rangle$  crystals at different temperatures,<sup>85</sup> and Fig. 13(b) demonstrates the behavior of polycrystalline pure Ni and two Ni alloys in torsion.<sup>8</sup> The latter is, in our terminology, a  $\Theta(\sigma)$  diagram: textural effects have not been taken out. From a stress-dependence point of view, Figs 13(a) and 13(b) exhibit similar behavior: plasticity begins at  $\theta \approx \mu/200$  ('stage II'); then  $\theta$  decreases in a gradual fashion ('stage III'). In polycrystals at very large strains, one generally finds an eventual stage of constant, very low hardening rate, of the order of  $\mu/5000$  (or at  $\Theta \approx \sigma/4$  for two-phase materials).<sup>5-8</sup> This region (called 'stage IV'<sup>6</sup>) is little understood,<sup>78</sup> and we exempt it from discussion here.

The decrease of  $\theta$  with  $\tau$  may sometimes be approximated, over a meaningful range, as being linear; then, this corresponds to a Voce law of the stress/strain curve.<sup>86,13</sup> More generally, however, it is the actual curve  $\theta(\tau)$  that must be tabulated if the behavior of a particular material is to be described accurately; no generally applicable function is likely to be found.

### 5.2.2. Dynamic Recovery and Saturation

An interesting result of crystal plasticity investigations is that the strain-hardening rate consists of two components<sup>12,13,76</sup>

$$\theta = \theta_a - \theta_r(\dot{\Gamma}, T, \tau, \epsilon^0) \quad (5.5)$$

The first is an *athermal hardening* component, the second *dynamic recovery*; all the temperature and rate sensitivity lies in the latter (and some dependence on the straining direction is also admitted).

Athermal hardening was first found in free single crystals in single slip and was there labelled 'stage II'.<sup>87</sup> Its prime characteristics are, however, present in multi-slip deformation and in polycrystals;<sup>12</sup> they are: a value of about  $\mu/200$  (within, say,  $\pm 50\%$ ), and an insensitivity to temperature, strain rate, and material (within the same class, such as cubic, single-phase materials). When this stage is extensive,  $\theta_a$  is also virtually constant with stress; more generally, it is defined as *limiting behavior at low strains and low temperatures*. The value  $\mu/200$

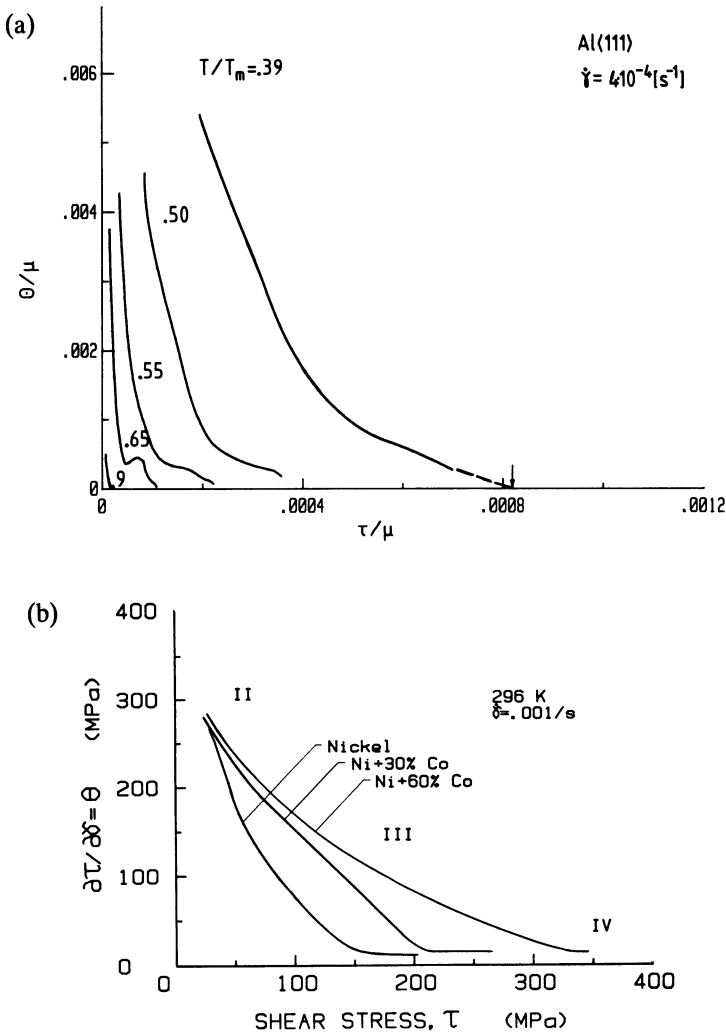


**Fig. 13.** The strain-hardening rate  $\theta$  versus the flow stress  $\tau$ , both normalized by the shear modulus  $\mu$  and plotted as an implicit function of strain: (a) aluminum  $\langle 111 \rangle$  single crystals in tension for various temperatures;<sup>85</sup> (b) nickel and nickel-cobalt polycrystals in short torsion.<sup>8</sup> There is a general decrease that may, over some regime, be approximated as linear and extrapolated to some 'saturation stress' limit; however, the strain-hardening rate eventually reaches a low constant value in many cases.

is what led to the statement, in Section 2.1.1, that  $d\sigma/d\epsilon \leq E/50$ : the square of the Taylor factor is of order 10, and  $E/\mu \approx 2.5$ .

The athermal hardening component has been explained on the basis of a geometrical-statistical dislocation storage rate.<sup>88</sup> It leads to a more-or-less random (tangled) arrangement of dislocations. *Dynamic recovery*, on the other hand, is associated with the rearrangement of the previously stored dislocations, under the action of stress, temperature, and the effects of continued straining. It leads to cellular, and eventually subgranular, substructures.<sup>5,89</sup>

The curves in Fig. 13(a) exhibit an example of an interesting scaling relation: to a good approximation, all the temperature dependence is in a stress-scale factor. This type of behavior is found quite generally, also for effects of strain-rate and even solute concentration (Fig. 13(b)). Thus, one may write (with a yield stress  $\tau_0$ )

$$\theta = \theta_a - \theta_r \left( \frac{\tau - \tau_0}{\tau_s} \right) \quad (5.6)$$

$$\tau_s = \tau_s(T, \dot{\Gamma})$$

When the function  $\theta_r$  is linear, we recover the Voce law, and  $\tau_s$  may be a saturation stress; in general, it is just a stress-scaling factor.

The rate- and temperature-sensitivity of  $\tau_s$  is different, both in cause and in magnitude, from the rate- and temperature-sensitivity of the flow stress (compared at constant structure). It is, in fact, about an order of magnitude larger. This is particularly important in the *limit of steady-state or flow-stress saturation*: if the limit  $\theta = 0$  can be operationally defined by extrapolation (even if it may not actually be reached), then the rate- and temperature-dependence of this steady-state limit is controlled by that of dynamic recovery, not by that of glide kinetics.

The stress exponent (eqn (2.2)) can now be expressed as

$$n \equiv \left. \frac{\partial \ln \dot{\epsilon}}{\partial \ln \sigma} \right|_{T, \Theta=0} = \left. \frac{\partial \ln \dot{\Gamma}}{\partial \ln \tau} \right|_{T, \theta=0} \quad (5.7)$$

A useful approximation to this steady-state value is that at the 'ultimate tensile strength', where  $\Theta = \sigma$  (not  $\Theta = 0$ ). Note that this relation between stress and strain-rate is due to thermal activation; thus,  $n$  should be expected to be temperature dependent (see Section 3.2.4). Within our 'interest space', it is of order 10, varying from about

20 or 30 at room temperature (depending on material) to a very-high temperature limit of 3 or 4.<sup>90</sup>

### 5.2.3. Temperature/Material Scaling

The temperature dependence of dynamic recovery, and thus of strain-hardening, can be expressed as that of the stress-scaling parameter  $\tau_s$  (eqns (5.6)). An example of such a description is given in Fig. 14, which refers to a series of pure fcc  $\langle 111 \rangle$  single crystals; the saturation stress from a 'long' extrapolation was used for  $\tau_s$ ,<sup>85</sup> and it is plotted as  $\tau_s/\mu$  versus  $kT/\mu b^3$ .

The stress and temperature were normalized by a further, constant scaling factor each, depending only on the material. It was found that then all these four materials could be brought into coincidence. The two scaling factors  $s^*$  and  $t^*$  (normalized to Al) in fact were correlated with each other and with the parameter  $\chi/\mu b$ , where  $\chi$  is the

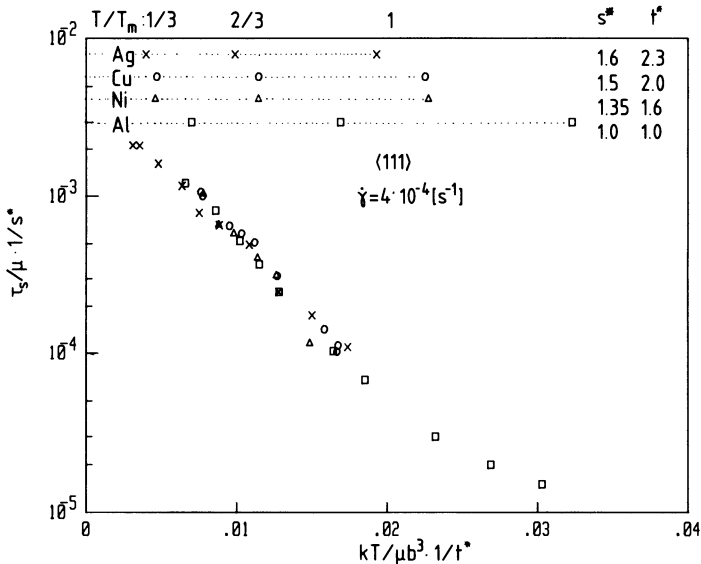


**Fig. 14.** The saturation stress  $\tau_s$  (or any other scaling parameter for the stress axis in diagrams like Fig. 13) decreases approximately linearly with temperature, in a semi-logarithmic plot. Different materials may be unified by using scaling parameters  $s^*$  and  $t^*$  for the axes on this plot, which correlate with each other and with the stacking-fault energy.<sup>85</sup> Note also that there is a maximum saturation shear stress of about  $5 \times 10^{-3} \mu$  at zero temperature for these pure fcc materials.

stacking-fault energy (SFE). This is a quantitative expression of the well known fact<sup>91</sup> that dynamic recovery is faster for high-SFE materials than for low-SFE materials, at the same homologous temperature. In fact, some parameter linked to  $\chi/\mu b$ , not to  $T_m$ , provides the appropriate normalization of temperature for plastic flow.

A surprising observation from Fig. 14 was<sup>85</sup> that this same normalization appears to hold over the *entire* temperature range, without ever requiring the introduction of parameters related to self-diffusion. In fact, Fig. 14 indicates that the functional dependence is essentially straight:

$$\ln \frac{\tau_s}{\mu} = \ln \frac{\tau_{s_0}}{\mu_0} + \frac{kT}{\mu b^3 g_s} \ln \frac{\dot{\Gamma}}{\dot{\gamma}_{s_0}} \quad (5.8)$$

where the two scaling parameters are labelled  $\tau_{s_0}$  and  $g_s$  for each material. (They are proportional to  $s^*$  and  $t^*$ .) The expected strain-rate dependence is also introduced. The strain-rate constant  $\dot{\gamma}_{s_0}$  is not well established and probably depends on  $\tau_s$ .<sup>85</sup> It was measured to be of order  $10^5 \text{ s}^{-1}$  in Al,<sup>13,85</sup> and of order  $10^{10} \text{ s}^{-1}$  in Cu.<sup>92</sup>

The first interesting observation to be made about eqn (5.8) is that there exists an absolute maximum saturation stress, corresponding to mechanical collapse of the dislocation structure (in the zero temperature limit). Its value is approximately  $10^{-2} \mu_0$  (as a crystallographic shear stress), for all fcc metals.<sup>13</sup>

Equation (5.8) expresses that the activation energy depends logarithmically on the stress, and a power-law stress/strain-rate relation is obeyed, with the exponent (eqn (5.7)) independent of stress and strain-rate, but  $n \propto 1/T$ .

A detailed scrutiny of this abstraction<sup>85</sup> revealed that, above  $T/T_m \approx 2/3$ , the data can also be described in a diffusion-related way. For the case of aluminum, it was in fact shown from strain-rate data over a sufficient range that the relationship

$$n = n_0 + \frac{\mu b^3}{kT} g_s \quad (5.9)$$

with  $n_0 \approx 3.7$  provides an even better fit over the entire temperature range, and gives a constant high-temperature limit of the activation energy, which agrees with that of self-diffusion.<sup>85</sup> In other materials, similar superposition laws for the steady-state stress-exponent have also been found;<sup>93</sup> the data tend to fit a value  $n \approx 4$  (although 3 would be easier to explain<sup>1,94</sup>).

In summary, eqn (5.8) gives a good first-order description of dynamic-recovery kinetics, at least up to  $T/T_m = 2/3$ . For a more accurate tabulation, especially for high-temperature applications, one must record the function  $S$  in

$$\ln \frac{\tau_s}{\mu} = \ln \frac{\tau_{s_0}}{\mu_0} + S \left( \frac{kT}{\mu b^3} \ln \frac{\dot{\gamma}_{s_0}}{\dot{\Gamma}} \right) \quad (5.8')$$

with  $\dot{\gamma}_{s_0}$  either constant or possibly dependent on  $\tau_s/\mu$ . In any case, it seems appropriate from these considerations to leave the value and functional form of the activation energy open, and not prejudice the data by normalizing with the self-diffusion energy  $Q$ ; the Fisher<sup>42</sup> parameter  $kT \ln(\dot{\epsilon}_0/\dot{\epsilon})$  should be preferred over the Zener parameter  $\dot{\epsilon} \exp(Q/kT)$ , because the result is much less sensitive to the value of the free parameter ( $\dot{\epsilon}_0$  vs.  $Q$ ) chosen for the evaluation.

#### 5.2.4. Creep

This term is used in two ways. Its definition, for us, is deformation at constant stress (or at least constant load); then the observed behavior is strain versus time, or strain-rate versus strain—different from a ‘stress/strain test’. But the term ‘creep’ is also used for ‘slow deformation at high temperature’—because these are the conditions under which its observation is easy.

In the first (‘true’) definition, ‘creep’ and ‘plasticity’ are merely different expressions of the *same* material behavior. That is why this book is one of the efforts to attain a ‘unified’ description of creep and plasticity. We, in fact, use the term plasticity for both: plasticity is, *ab initio*, allowed to be rate-dependent.

But there is another difference: creep is usually studied *near steady state*, with the initial loading strain and the transient creep strain held to about the same order as the ‘steady’ strain or less. Thus, the behavior is almost always dominated by recovery (dynamic or static); this may bring in special problems related to ‘hardening transients’, which we will discuss in Section 5.2.6 but ignore for now. In addition, there is a good possibility that the ‘rearrangement strain’ that occurs during dynamic recovery<sup>95,96</sup> contributes substantially to the total strain-rate near steady state.<sup>2,12</sup> Only tentative descriptions have been given for its relation to flow stress and strain-hardening.

The material response measured in a creep test is the *creep deceleration*

$$\delta \equiv - \left. \frac{\partial \ln \dot{\epsilon}}{\partial \epsilon} \right|_{\sigma, T} \quad (5.10)$$

We have written it, in the usual form, in terms of the macroscopic variables  $\sigma$  and  $d\varepsilon$ , not in the microscopic  $\tau$  and  $d\Gamma$ ; this is acceptable because the strains during typical creep deformation in metals are not large enough to cause any significant *change* in texture; thus, there is only a constant orientation factor to be taken care of. Note, however, that the symbols  $\sigma$  and  $d\varepsilon$  are in fact supposed to mean the *equivalent* stress and strain-rate defined in Section 5.2.1.

An unfortunate fact is that in creep the material parameter ( $\delta$  in eqn (5.10)) can only be obtained by *double* differentiation of the experimentally obtained  $\varepsilon(t)$  data; for this reason, stress/strain tests are easier to evaluate: only a single differentiation is needed to obtain  $\theta$  or  $m$ .

### 5.2.5. A Differential Constitutive Equation

Until now, we have discussed the material behavior in terms of two separable aspects: its properties in a given state (having a given structure); and the evolution of this state/structure with strain. The first is typically described by a relation  $\tau = \tau(\dot{\gamma}, T, \hat{\tau})$ , such as eqn (3.8), the second as one or more *differential* relations such as eqn (5.3).

One could, of course, differentiate the first relation and insert it into the second. The results could, for example, be

$$d \ln \tau = \left. \frac{\partial \ln \tau}{\partial \ln \dot{\gamma}} \right|_{\hat{\tau}} d \ln \dot{\gamma} + \left. \frac{\partial \ln \tau}{\partial \ln \hat{\tau}} \right|_{\dot{\gamma}} \frac{d \ln \hat{\tau}}{d \gamma} d \gamma \quad (5.11)$$

where we have left out the temperature as an explicit variable. This describes the dependence of the flow stress on both strain rate and strain in differential form.

The advantage of such a formulation comes when one writes it in a phenomenological form, for example

$$d \ln \sigma = m d \ln \dot{\varepsilon} + H d \varepsilon \quad (5.12)$$

Here, we have shifted to the macroscopic variables. The coefficients are measurable; in particular†

$$H \equiv \left. \frac{\partial \ln \sigma}{\partial \varepsilon} \right|_{\dot{\varepsilon}} = \frac{\Theta}{\sigma} \quad (5.13)$$

†  $H$  may be called the *work-hardening* rate, since it equals  $d\sigma/dW$ , as distinct from the *strain-hardening* rate  $\Theta = d\sigma/d\varepsilon$ . Which of these is preferred depends on the application. Note that both the strain and the work are used in differential form only.

If eqn (5.12) is viewed as the *primary* statement of constitutive behavior, and not as a derivative of the state formulation, as in eqn (5.11), then *it is not necessarily integrable*. One can, however, state the precise conditions under which it is:<sup>44</sup> when  $m$  and  $H$  are functions of  $\sigma$  and  $\dot{\epsilon}$  only, not of any further, 'hidden' variables; then an integrating factor for  $d\epsilon$  can be found, and the integral of the combination is a state parameter—there is only one.

There are many reasons why the differential constitutive equation (5.12) might not be integrable, why there should be 'hidden parameters'. For example, we know that, in general, the texture will change with strain; then  $H$  will depend on path, even when both  $\sigma$  and  $\dot{\epsilon}$  are fixed. Similarly,  $\sigma$  could depend on grain size—say, in particular, on the minimum dimension of the grains; this changes with strain, in a path dependent manner. In both of these cases, one could add extra terms to eqn (5.12). Unfortunately, no macroscopic way is available (at least as yet) to separate changes in these variables. On the other hand, fortunately, they are likely to become important only at very large strains, where regular strain hardening has virtually saturated out. Thus, one may be able to deal with a single state parameter at a time, but change their identity at some definable demarcation line.

Finally, there is evidence for another state parameter associated with dynamic recovery, and we will treat this in detail in the next section. It may be important for creep. If it is not, eqn (5.12) already describes creep in the 'primary' regime (and in the steady-state limit): comparison of eqns (5.10) and (5.12) shows that

$$\delta = H/m \quad (5.14)$$

The *instantaneous* (iso-structural) rate sensitivity  $m$  enters to translate stress/strain data into strain-rate/strain data.† Again, when  $\delta = \delta(\sigma, \dot{\epsilon})$  only, a single state parameter and an 'equation of state' exist; otherwise,  $\delta$  must be tabulated for different paths. But it is always measurable, by the operational definition of eqn (5.10).

In summary, the differential constitutive equation (5.12) is 'unified' in that it describes both creep and plasticity; and it is general in that it does not presume the existence of a *single* state parameter or an

† The best operational definition of  $m$  is in fact  $H/\delta$ , since  $H$  and  $\delta$  are well defined as rates of change at any instant, whereas  $m$  describes the result of an abrupt change 'at constant state', which requires back-extrapolation for the measurement.<sup>3</sup>

(integral) 'equation of state'. Since it is a (first-order) differential equation, it requires an initial value pair; this is equivalent to a parameter of the current state.

### 5.2.6. *Hardening Transients*

We already sketched in Fig. 3 (b and c) that fairly long transients sometimes occur after a strain-rate or temperature change; this is in fact a characteristic of dynamic recovery. Qualitatively, it has been explained as being due to an exhaustion, under the current conditions, of recoverable dislocation arrangements: when conditions 'improve' (lower rate, higher temperature) some extra recovery occurs; in the reverse case, some athermal dislocation storage must first take place before recoverable tangles are formed again. Thus, it is really a transient in the hardening rate (not in glide kinetics).<sup>10</sup>

The transient is evidence for some structural change that corresponds to the evolution of a 'second' state parameter (other than the flow stress, and not counting texture, grain size, and others). This state parameter seems to attain a steady-state value in equilibrium with the external conditions and the other state parameters after about 3–5% strain. It is now a question of judgment, for a specific application, whether one wants to describe this short-term evolution or not. If not, back-extrapolation from larger strains would give a self-consistent description—and a value of  $\Delta\sigma$  for the prescribed  $\Delta \ln \dot{\epsilon}$  or  $\Delta T$  that reflects the new *evolution* rate (and is much larger than the 'instantaneous' value, due to glide kinetics).

However, this hardening transient may be quite important in the neighborhood of steady-state deformation—and therefore for creep. It is not clear, at this point, whether transient creep (of the 'normal' kind) is more directly connected to the main part of strain hardening or more to the exhaustion of dynamic recovery—probably both, under different limiting circumstances.

Since we interpret this transient as due to the evolution of a *hardening* parameter, it seems appropriate to write a differential equation for  $H$  (which, in a way, is a *second-order* differential equation in the flow stress, and thus leads to *two* state parameters, even if it is path independent):

$$dH = -C d \ln \sigma + B d \ln \dot{\epsilon} - E d\epsilon \quad (5.15)$$

The coefficients have been defined so that they are normally positive. Without the evolution term at the end, the equation has been used

before to describe the dependence of work hardening on stress and strain-rate.<sup>97,98</sup> But without this evolution term, the hardening slopes at points A and B in Fig. 15 should be the same; the whole point of eqn (5.15) is to describe the fact that this is not true during some transient regime.

The new coefficient  $E$  can be defined as

$$E \equiv \left. \frac{\partial H}{\partial \epsilon} \right|_{\sigma, \dot{\epsilon}} \quad (5.16)$$

Combining eqn (5.16) with eqn (5.12), we have

$$dH = -(E + CH) d\epsilon + (B - Cm) d \ln \dot{\epsilon} \quad (5.17)$$

The coefficient of  $d\epsilon$  is the *curvature* of the  $\ln \sigma$  vs.  $\epsilon$  diagram (at constant  $\dot{\epsilon}$ ), and  $E$  is the excess of this curvature in the transient over that during 'steady-state work hardening' (i.e. steady state of the *second* state parameter). The second term on the right-hand side is the rate sensitivity of work hardening; the contribution  $Cm$  comes from glide kinetics and is negligible with respect to that due to evolution kinetics,  $B$ .

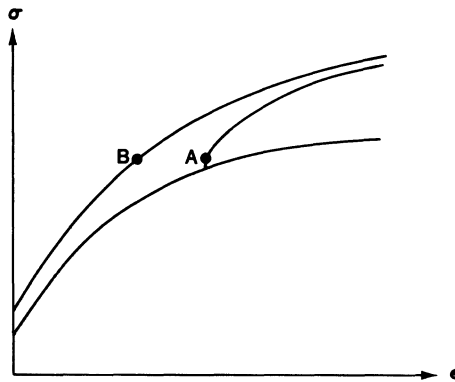


**Fig. 15.** Two continuous stress/strain curves and one with a change, near A, from one set of conditions (such as strain rate, temperature) to the other. If there were but a single state parameter, the 'future' starting from point A would look the same as from point B. The fact that this is generally not true is interpreted as a transient and as evidence of the need for an additional state parameter if this transient is to be described.

A completely equivalent 'second-order' evolution equation can be written in terms of the creep deceleration:<sup>3</sup>

$$d\delta = -c d \ln \sigma + b d \ln \dot{\epsilon} - e d\epsilon \quad (5.18)$$

which leads, with eqns (5.9) and (5.11), to

$$d\delta = (e + b\delta) d\epsilon + (b/m - c) d \ln \sigma \quad (5.19)$$

Here,  $c \ll b/m$ .

In (complete) steady state, the terms in  $d\epsilon$  in both equations (5.15) and (5.18) vanish, and we have for the stress exponent:

$$n = \left. \frac{\partial \ln \dot{\epsilon}}{\partial \ln \sigma} \right|_{H=0} = \left. \frac{\partial \ln \dot{\epsilon}}{\partial \ln \sigma} \right|_{\delta=0} = \frac{C}{B} = \frac{c}{b} \quad (5.20)$$

In steady state itself, there is no state parameter: they are all in equilibrium with external variables. *Near* steady state, one should expect *one* state parameter to be sufficient. It is an important question for a unified constitutive description at the present time whether this state parameter is the flow stress (so that eqn (5.12) can be used) or the hardening rate (which might be describable by eqn (5.15)). In the first case, it is the dislocation *density* that adjusts, in the second the dislocation *arrangement*.

### 5.2.7. Conclusion

The evolution of the state is best described by a strain-hardening rate  $\Theta$  as a function of state variables and parameters. Texture changes during straining can significantly contribute to  $\Theta$ , especially at intermediate strains where the changes are significant and have not yet saturated. No simple description of this influence is as yet available, nor is one likely to be found. Calculations in terms of polycrystal plasticity simulation are now possible (if the initial texture is known) and they may be necessary when anisotropic effects are of prime importance.

The 'physical' (rather than textural) hardening rate in the grains may usually be approximated by that of a representative ('average') grain. Its dependence on stress is primarily due to dynamic recovery, and it can be scaled by a stress parameter (the extrapolated 'saturation stress', or some other), which itself depends on temperature and strain-rate. For all of these dependences, simple linear relations in certain plots are often a good first approximation—but they are never

based on a compelling physical mechanism. In any case, the combination of variables that should be plotted or tabulated against each other is given with some generality.

An alternative that may sometimes be preferable to a description in terms of state parameters is an entirely differential constitutive relation in terms of external variables only (but not necessarily integrable). The number and order of such differential equations must be sufficient for the number of state parameters necessary, i.e. the number of transients identified as important for the material and conditions to be treated.

## 6. INTERNAL STRESSES

The term 'internal stress' has been used in many different meanings in plasticity.<sup>99</sup> These fall into two major classes: first, a 'true' stress, tensorial in character and with sign, to be added to (or subtracted from) the *applied stress*, and measurable in principle through the difference of the local elastic distortions from those expected on the basis of the applied stress alone. The spatial average of every component of this stress must be zero, but it may nevertheless be relevant, especially when the positive and negative contributions are spatially ordered. This is equivalent to the 'residual stress' used on a specimen scale to describe the consequence of macroscopically non-uniform deformation; but it also occurs as a consequence of microscopically non-uniform deformation, as it occurs in all polycrystals and especially in 'mixtures' of grains of different materials. It also occurs in 'two-phase materials', in which different components occur in each grain. This can be a strong effect and will be discussed first.

The other class of 'internal stresses' or 'back-stresses' that has been used frequently is an athermal and rate-independent contribution to the (scalar) *flow stress* or glide resistance; it need not be additive (though this is implied by using the term 'internal stress').

Finally, the term 'internal stress' has occasionally been used to describe local stress redistributions due to internal rearrangements caused by an applied stress, such as by the bowing-out of dislocations or dislocation walls.<sup>100</sup> As was discussed in Section 2.1.1, we wish to treat as state parameters only quantities that can be assessed in the unloaded state: they cause all subsequent behavior.<sup>10,89</sup>

## 6.1. Two-phase Materials

### 6.1.1. The Orowan Stress

Imagine a single-crystal matrix with a dispersion of spheres of a second phase that causes no misfit (and thus no ‘true’ internal stresses) and has the same elastic properties as the matrix; the only difference between the two phases is in their yield strengths. Then, at an applied stress between the two yield strengths, there will be a contribution to the yield strength of the aggregate due to the need for repeated, transient bowing-out of the dislocations to surround the particles. If the spacing between the particles is  $L$ , this ‘Orowan stress’<sup>101</sup> is approximately<sup>102</sup>

$$\tau_o \approx \mu b / L \quad (6.1)$$

It is quite insensitive to thermal activation (it is ‘athermal’, rate-independent), and it may superpose with other contributions to the flow stress either additively (e.g. with solution hardening<sup>103</sup>) or quadratically (with strain hardening<sup>2,4,104</sup>).

To summarize: the Orowan stress is an example of a scalar, athermal contribution to the yield strength (additive or not), but it does not correspond to any internal stress measurable in the crystal before loading.

### 6.1.2. Strain Hardening

The remnants of the dislocations that bowed around the impenetrable particles in the above example accumulate around the particles and make for an extra contribution to strain hardening. These extra dislocations have been described as ‘geometrically necessary’:<sup>104</sup> they accommodate, in the matrix, the (true, tensorial) internal stresses caused by a now misfitting particle. In fact, their density is initially proportional to the elastic strain in the particle, and thus to the plastic strain in the matrix. Their effect on strain hardening is essentially through this (scalar) dislocation density  $\rho$ ; since  $\tau \propto \sqrt{\rho}$ , the strain hardening they cause (if it is alone) is truly parabolic:  $\tau \propto \sqrt{\gamma}$ . This is, again, a (scalar) contribution to the flow stress (as rate insensitive as all strain-hardening contributions).

With increasing strain, the statistical accumulation of dislocations (both because of the above ‘geometrically necessary’ ones and because of all other obstacles) usually dominates strain-hardening behavior; thus, parabolic hardening is typically observed only until  $\theta$  has decreased to the value  $\theta_a$  (Section 5.2.2).

### 6.1.3. Forward and Backward Internal Stresses

When particles have to deform elastically while the matrix deforms plastically, a 'forward' internal stress must be generated inside each of them: forward in the sense that it is in the same direction as the macroscopic plastic strain. Note that it is the strain that counts, in this case, not the stress; for example, in a single crystal undergoing primarily single slip, the internal stress in any imbedded, non-deformable particles is of the same character as the shear strain caused by slip (even if the stress might be uniaxial tension), and in the same direction (assuming elastic isotropy).

Since all true internal stresses must average out to zero through the aggregate, it follows that the average internal stress in the matrix must be 'backward': against the prevailing strain direction. It is, for some applications, helpful to consider this *average* back-stress in the matrix; it has also been called 'image stress'.<sup>105</sup> It is a true, tensorial, internal stress. Its magnitude is proportional to the volume fraction of particles; typically, it is about 10–20% of the applied stress, and this part should truly be subtracted from the applied stress, *tensorially*, to get the glide resistance.

This is called the *kinematic hardening* component in the phenomenological plasticity literature and often labelled  $\alpha$ , signed as a back-stress; then, the yield condition becomes, instead of (4.32):

$$\sigma' - \alpha = \bar{M}\bar{\tau} \quad (6.2)$$

where  $\bar{\tau}$  is now the plastic resistance due to both particles and dislocations stored (and may include a contribution from  $\tau_0$ ).

### 6.1.4. The Bauschinger Effect

Since the plastic deformation in the matrix does not reverse upon unloading, the internal-stress distribution discussed above will essentially remain. Thus, it will also influence reverse loading. Of course, it must eventually change sign; but a reverse plastic strain of the same order as the previous forward strain is needed to achieve this loss of memory. Thus, there should be, and is, a significant Bauschinger effect in two-phase materials.<sup>106</sup> It seems that no systematic investigations of its tensor character have been undertaken as yet.

Figure 16 shows stress reversals in an Al–Cu alloy heat-treated in two different ways:<sup>107</sup> one to keep the alloy single-phase (solution treated), one to make it two-phase ( $\theta'$ ). The qualitative difference between the two 'Bauschinger effects' is obvious.

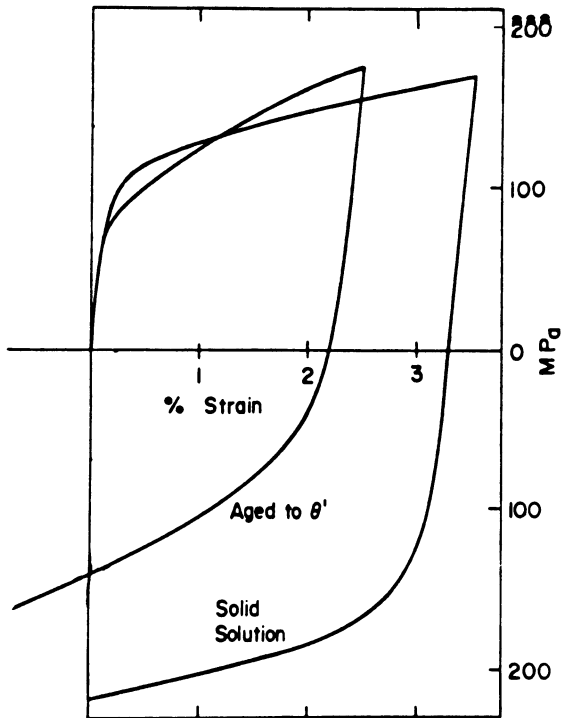


**Fig. 16.** Stress reversal behavior of single-phase (solution hardened) and two-phase ( $\theta'$ ) Al-Cu alloy.<sup>107</sup> Only the latter is a 'permanent' Bauschinger effect, the former is a strain-hardening transient.

'Kinematic hardening' was originally invented to describe Bauschinger effects.<sup>70</sup> In the spirit we use here (Section 2.1.1), it should best be used *only* for the type of 'permanent' softening upon reverse loading as is observed in two-phase materials: it is a hallmark of a true internal-stress contribution to the flow stress. The substantial lowering of the proportional limit (sometimes involving a change of sign) is better described as a strain-hardening transient (Section 2.1.3).

#### 6.1.5. Recovery

Both the internal-stress build-up and the unusually rapid accumulation of dislocations cause a high rate of energy storage in two-phase materials. This expresses itself in unusually effective recovery: upon annealing and reloading under the same conditions, there is an initial flow stress decrease of the order of 50% in two-phase materials (as

compared to ~10–20% in single-phase materials), and again a much longer transient to standard behavior. This is another characteristic of materials with ‘kinematic hardening’, and can be used as a diagnostic test.

#### 6.1.6. *Conclusion*

There is a class of materials, typified by dispersion-strengthened single crystals, in which internal stresses of opposite sign develop, with deformation, in the two phases. Their existence can be identified by a strong, ‘permanent’ softening upon either reverse loading or recovery. In addition, these materials show an athermal contribution to the glide resistance at yield, as well as initial parabolic strain-hardening. Thus, they should be described by both a ‘kinematic’ hardening component (to be subtracted tensorially from the applied stress) and a scalar one (to be accounted for in the plastic resistance). We believe this to be the *only* class of materials where a kinematic hardening component is justified; but note that even here the scalar resistance dominates quantitatively.

## 6.2. Single-phase Materials

### 6.2.1. *Polycrystal Effects*

The interactions between grains in a polycrystal cause internal stresses that vary roughly with a wavelength of the grain size. While these are true internal stresses, tensorial in nature, they are already made use of in all modern theories of polycrystal plasticity: namely such as to activate enough slip systems to satisfy compatibility. They are the reason for setting the effective orientation factor of polycrystals to something larger than the average of that of free single crystals. Thus, they should not be counted again as an internal stress of the kinematic-hardening kind. The same is true for the effects of the so-called geometrically necessary dislocations in polycrystals,<sup>108</sup> which are just another way of describing these very same stresses.<sup>78</sup>

In addition to these ‘true’ but irrelevant internal stresses, there is generally assumed to be some contribution to strain hardening that specifically relates to polycrystals, presumably due to an extra dislocation accumulation near grain boundaries, more ‘statistical’ than ‘geometrical’ in nature. This is probably the main cause of the mild grain-size effect in pure fcc materials.<sup>78</sup> Its rate sensitivity should be similar to that of other strain-hardening effects. Indeed, the rate-

sensitivity behavior of polycrystals and single crystals is quite similar, at least in pure fcc metals.<sup>12</sup>

Finally, there is a 'back-stress' effect that leads to the 'Hall–Petch' grain-size dependence of the polycrystal yield stress. It is strong only in materials in which dislocation generation or unlocking makes an important contribution to the flow stress (and is often associated with a sharp yield drop). The tensor character of this stress has not been investigated; probably, it is a scalar contribution to the glide resistance. It may sometimes have 'athermal' character, compared to more activatable contributions, but can also be very rate sensitive. In any case, it does not qualify as a kinematic hardening component.

### 6.2.2. *Forward and Backward Internal Stresses*

There are, of course, true internal stresses in *any* material; e.g. every dislocation is a source of a (tensorial) stress field, each component of which averages out to zero over the body (requiring certain 'image stresses' in finite bodies). In most materials—those that form dislocation tangles and cell walls of the 'thick', disordered kind—these internal stresses are actually ordered: they tend to be 'forward' inside the tangles or cell walls, 'backward' in the more-or-less dislocation-free cell interiors.<sup>95</sup> This distribution has some similarities to that in two-phase materials. However, its effects on macroscopic properties are quite different.

The polarity of the internal stresses in cellular dislocation structures has been made use of in a number of ways.<sup>89,109</sup> First, the forward stresses inside cell walls provide the driving force for dislocation rearrangements during dynamic and static recovery.<sup>95,110,111</sup> Second, the backward stresses in the cell interiors must be important during loading and unloading: during small-strain, contained plastic flow.<sup>96,112</sup> Finally, the very existence of the polarity makes some kind of asymmetry between forward and reverse straining possible.<sup>88</sup>

Where these internal stresses are different from those in two-phase materials is in their effect on the macroscopic flow stress: we claim they have no effect at all in single-phase materials. On a mechanistic basis, this is plausible because of the areal nature of glide in these materials:<sup>89</sup> the 'critical gates' through which dislocations must pass to achieve long-range slip<sup>9,88</sup> are precisely at the saddle points between the regions of forward and backward internal stresses, and are thus at least approximately at zero internal stress.

More potent, perhaps, is a macroscopic argument: the very fact that

the macroscopic flow stress *after any transient* is unaffected, in single-phase as opposed to two-phase materials, by a reversal of straining or by recovery is in itself evidence that internal stresses are not relevant for this particular property—and is, in fact, another justification for using the *macroscopic flow stress* as an important parameter to describe the plastic state.

A powerful tool to ascertain the presence of any separable, athermal contribution to the flow stress (whether tensorial or scalar) is the Haasen plot introduced in Section 3.1.7: when the rate sensitivity  $m\tau$  of the flow stress is proportional to the flow stress itself (i.e. when the ‘Cottrell–Stokes law’ is obeyed), then there is no such separable component—and this is the case e.g. for pure fcc metals, in which cell structures do develop. If there were an independent athermal contribution to the flow stress, there would have to be an intercept of the data such that the rate sensitivity vanishes at a finite stress.

### 6.2.3. *Stress Relaxation and Unloading Effects*

Stress relaxation after plastic deformation exhibits an ever decreasing *rate* of stress decrease, which is a consequence of the rapid decrease of strain rate with stress. The temptation is great to extrapolate to a finite stress level at which the rate would vanish. This interpretation does not hold up under more sophisticated evaluations.<sup>99</sup> In fact, in the best tests at the lowest rates,<sup>113</sup> the rate sensitivity increases again (due to the increasing influence of dynamic recovery at very low rates, in our interpretation).

When the specimen is unloaded rapidly but partially, one observes what might be called ‘negative stress relaxation’, and this terminology would lead one to believe in a finite stress where stress relaxation is zero, and to call this an ‘internal stress level’. This is, again, a misleading interpretation. The response on both sides of this presumed internal stress level is by no means symmetrical (as one should expect in such an interpretation); indeed, the ‘negative relaxation’ has all the marks of a transient effect: the behavior is not reproducible. We would interpret all ‘negative relaxation’ as just another expression of unloading effects: the reverse motion of some of the last dislocations to have moved forward. This occurs primarily in the cell interiors, and while these are, indeed, under a back-stress (Section 6.2.2), this is not an additive contribution to forward flow.

Of all the parameters that have been called an ‘internal stress’, the ‘relaxed level’ is perhaps the least deserving one. Further support for

this opinion is to be seen in the fact that it typically depends on temperature and actually tends to be a constant fraction ( $\sim 75\%$ ) of the current flow stress.

#### 6.2.4. Power-law Creep

The steady-state relation between stress and strain-rate is often adequately described as a power law (Section 5.2.3). When a direct fit of the data gives a stress exponent of order 10, another description is often tempting: namely, to subtract an 'internal stress' from the applied stress to form an 'effective stress', which then only requires a smaller exponent—which is easier to explain. This is very common practice. It is justified when there are other, independent reasons to postulate a lower-limit stress, such as in two-phase materials.

There is one cause for such a threshold that is always legitimate, but almost never important (certainly not in our regime of interest): namely, the thermodynamic threshold.<sup>1,9</sup> It represents the work necessary to provide whatever energy needs to be stored during plastic deformation. (See Section 2.1.6.)

#### 6.2.5. The Flow-stress Plateau at Intermediate Temperatures

A diagram of flow stress versus temperature almost invariably exhibits three regions (Fig. 7): a fairly rapid decrease at low temperatures, a more-or-less constant flow stress at intermediate temperatures (at least when divided by an elastic modulus), and another decrease at temperatures in excess of, typically, half the melting point. The high-temperature drop is almost certainly associated with concurrent dynamic recovery and its associated rearrangement strains (Section 5.2.4). But if it were not there, perhaps the temptation would be less to regard the low and intermediate temperature regimes as separate. Both regimes together certainly fall qualitatively into the category of mechanisms (all those discussed here) that get harder and harder to activate as the stress decreases. Thus, the so-called plateau could be merely a *very* slowly decreasing stress (similar to the late part of a stress-relaxation test).

In materials that contain substitutional solutes, there are two other reasons for 'plateau'-like behavior: one is that here the activation energy may well be proportional to the reciprocal of the stress, which makes for a much slower decrease with temperature,<sup>29</sup> the other reason lies in an expected mobility of solutes which, in extreme cases, would actually give a 'hump' in the  $\tau(T)$  diagram.

In conclusion, there are a number of at least qualitative explanations for the appearance of a more-or-less level flow stress at intermediate temperatures that do not require the introduction of a separate 'internal stress';<sup>33</sup> such a new parameter should only be used when there are other reasons for needing it. The easiest example of such another reason, as pointed out repeatedly, is a failure of the Cottrell–Stokes law in the direction that extrapolates to a zero rate- or temperature-sensitivity at a finite stress (Section 3.1.7).

#### 6.2.6. Conclusion

While there are many causes for true, tensorial internal stresses in real materials, most of these affect only transient behavior, but not the macroscopic flow stress. The latter is an appropriate quantity to characterize the deformed state of the material, using as many parameters as necessary. The first of these parameters is always the mechanical threshold: the flow stress back-extrapolated to zero temperature, *below* which most deformation happens. Sometimes, but by no means always, there is, in addition, a lower threshold or (scalar) 'athermal stress', which may superpose with other contributions to the plastic resistance in a linear or nonlinear fashion. Finally, and probably only in two-phase materials, there is a true long-range, tensorial internal back-stress (in the deforming matrix) which must be subtracted from the applied stress tensor before insertion into the yield criterion: this is the only legitimate cause for 'kinematic hardening'.

## 7. APPLICATION

As was pointed out in the Introduction, the most important lesson to be learned from materials science is that one cannot expect a single set of constitutive relations to hold for all materials and conditions. A worthy long-range aim of constitutive-relations development is to establish a systematic procedure by which it can be ascertained which class of materials and which regime of conditions a particular foreseen application falls into.

In this article, we have focussed on one such class and one such regime—even through we believe it to be a very broad and important case: uniform plastic deformation in (primarily single-phase) metals and alloys, at not too high or too low a temperature, at not too high or too low a strain rate, at not too small or too large strains. We have

stated in the Introduction the expected range of these variables under which (quasi-static) dislocation motion and accumulation dominate the behavior. In Section 7.1 we will outline some experimental tests that can be used to establish whether one indeed is in this regime, and what observations might warn one of special effects. Then, in Section 7.2, we will summarize the set of constitutive relations that appear to be most useful for this 'interest space'.

## 7.1. Diagnostics

### 7.1.1. *Stress/Strain/Strain-rate Test*

A very large amount of information can be derived from an analysis of the simplest test of all: a single tension test in which the whole stress/strain curve is recorded.† The only additional variable that must be introduced to assure this pay-off is the strain rate: it should be abruptly changed many times during the test. Good interpretability is ensured by using one of two procedures: either change the strain-rate up and down (by about a factor of 10) regularly every 3% strain or so; or make the slow rate the 'master' rate at which most of the straining is done and make occasional excursions to a higher strain rate and back. The amount of strain in any excursion must be large enough to have passed through any transient behavior, and the data acquisition system must be sufficiently sensitive to record the subtle changes. Even in materials in which the rate sensitivity is negligible in magnitude, a rate change can serve as a potent diagnostic tool.

First, an evaluation without rate changes. Assess whether there is a yield drop—in which case ignore that part of the stress/strain curve, since it relates to non-uniform deformation. Then see whether the slope of the load–elongation curve is reasonably constant for the first few percent strain, and of order  $E/50$  ( $E$  is Young's modulus): then you are certainly within our 'interest space'. If it is much smaller (by an order of magnitude or so) you probably have a pre-deformed material, or perhaps an aged one—not all is lost.

If the initial plastic part of the stress/strain curve looks more parabolic than linear, there are two easy possibilities: either (at high temperatures) you are close to flow-stress saturation, which will be

† A compression test is just as useful, especially when not enough material is available, or when the ductility is quite limited. Teflon or some other lubrication can usually assure homogeneous deformation, which can be checked by inspection of the shape of the deformed specimen.

obvious (and you may wish to treat everything before as a transient); or you have a material in which a second phase plays a significant role. In the latter case, plot  $\sigma^2$  vs.  $\epsilon$  to see whether you get an essentially straight initial part. In this case, Section 7.1.2 becomes important. (We always assume materials of cubic lattice structure; in non-cubic polycrystals, there may be an extended region of elasto-plastic transition, also linked to high internal stresses.<sup>114</sup>)

Next check the appearance of any transients upon an *increase* in strain-rate. If they are less than about 0.5% long, ignore them and extrapolate through them: they are due either to machine effects<sup>115</sup> or to some adjustments in the dynamic dislocation structure.<sup>10</sup> If the stress/strain curve after any such short transient is accurately parallel to the one at the lower strain rate, you have the easiest case of all: a single state parameter (which might as well be the strain in this case). On the other hand (which is more likely at larger strains), if you have a higher-than-normal strain-hardening rate for more than 1% strain, it is probably due to a significant influence of dynamic recovery, and thus more complicated kinetics: Sections 5.2.4 through 5.2.6 apply, and you must decide whether this transient is important for your application or may be extrapolated through.

Now for a quantitative evaluation of the rate sensitivity. First, assess whether  $\Delta \ln \sigma / \Delta \ln \dot{\epsilon}$ , the way you measure it (using the applied stress, no 'effective stress'), is smaller or larger than 0.03. If larger, you are probably measuring a steady-state rate-sensitivity  $1/n$  (eqn (5.7)), or at least one that is significantly influenced by dynamic recovery. For use in the following analysis, it would be better to try a more 'instantaneous' evaluation, i.e. a shorter back-extrapolation. If a truly iso-structural value is between, say, 0.03 and 0.01, the glide-controlling obstacle is probably quite small (a solute acting individually, or the 'Peierls stress'); in this case, nonlinear elastic effects are likely to be important and the parallelism of yield surface and plastic potential may well be violated (Section 4.2.1).

As a next step, plot  $m\sigma = \Delta\sigma / \Delta \ln \dot{\epsilon}$ , at various strains, versus the flow stress at that strain: the 'Haasen plot' (Section 3.1.7). Warning: if the slope of this line is negative, and  $m$  itself is not negative yet, it may become so at higher strains or temperatures or concentrations, and lead to jerky flow.<sup>38</sup>

If the data in the Haasen plot extrapolate to the origin, the Cottrell-Stokes law is obeyed and a single state parameter suffices to describe the monotonic-kinetic behavior. If the plot gives a fairly

straight line that does *not* extrapolate to the origin, two flow-stress contributions superpose linearly; one may be 'athermal' if the line extrapolates to a finite stress at zero rate sensitivity. In the latter case, there may be a kinematic-hardening component (to be ascertained by the tests under Section 7.1.2). In general, both contributions may be thermally activated.

Finally, assess the rate sensitivity of the ultimate tensile strength: a special case of  $1/n$ , as defined in eqn (5.7). If it is less than about 0.1, the formalism outlined in Section 5.2.3 can be used, without the need of introducing any 'pre-exponential' stress exponent, and most likely without a real influence of diffusion mechanisms.<sup>85</sup> When  $1/n > 0.1$  (and the temperature is larger than half the melting point) more caution is advised.

Last but not least, look at the specimen, for any evidence of grossly non-uniform deformation, or of anisotropic deformation. If the aspect ratio of the cross-section of a tensile sample has changed, the material was not isotropic at the start of deformation; in fact, it did not even have the symmetry of the tensile test: a fiber in the tensile axis. For this purpose, an initially cubic compression specimen is even more instructive, since shear strains can be seen that would not be expected on the basis of the test symmetry. When any initial anisotropy is discovered, the yield function to be used is unknown—and not likely to be well represented by a von Mises assumption.

### 7.1.2. Stress Reversal and Recovery

When there is suspicion of a kinematic hardening component (for example, because of initial parabolic hardening, or a positive stress intercept on the Haasen plot), two additional tests are advisable. The easiest is an annealing test, at a temperature where recrystallization does not occur (Section 6.1.5): is the flow stress upon reloading under the old conditions less than 80% of the one reached previously? Or, more to the point, does the new stress/strain curve fail, by a substantial margin and after many percent strain, to join up with the extrapolation of the previous one? (Actually, it is the behavior in a diagram of  $\Theta$  vs.  $\sigma$  that gives the best information.<sup>110</sup>) Then, a kinematic hardening component, of the order of this failure, may be appropriate.

Secondly, if possible, a Bauschinger test would be instructive: if the behavior is of a transient nature, 'normal' after a few percent strain, a kinematic hardening component is *not* indicated (Section 6.1.4).

### 7.1.3. *Temperature Dependence*

This is the hardest test to execute; it depends on the application whether, and in which range, it is worthwhile. At very low temperatures (say,  $<50$  K), one must assess whether dislocation inertia may be important;<sup>26</sup> this is indicated when the flow stress falls below the back-extrapolation from higher temperatures. At somewhat higher, yet subenvironmental temperatures, a strong decrease of stress with increasing temperature is probably due to an influence of the Peierls stress, and is possibly connected to a non-normality of the strain-increment on the yield surface.

At intermediate temperatures (typically at room temperature and above), one may wish to investigate the nature of an apparent stress plateau (Section 3.1.4), especially if the rate sensitivity indicated a negative trend in the Haasen plot: then, dynamic strain-aging and its instabilities may occur under slightly changed conditions. In solution-hardened alloys in general, one may wish to plot  $\sigma$  vs.  $T \cdot \sigma$ , to see whether this provides a reasonable description.<sup>29</sup> If the plateau is associated with a positive stress intercept in the Haasen plot, an investigation of the temperature dependence of the strain-rate sensitivity can be quite instructive.<sup>116</sup>

Finally, at high temperatures (say,  $>T_m/2$ ), the treatment of the yield stress becomes complicated (it being influenced by concurrent dynamic recovery), but near-steady-state behavior may be assessed reasonably well. Here again, it becomes important to study the temperature dependence of the rate sensitivity—except now the one in steady state,  $1/n$ . An instructive plot is the stress exponent  $n$  versus  $\mu b^3/kT$ : it is likely to extrapolate to a finite value (around 4) at infinite temperatures (eqn (5.9)). For values near there, some superposition of mechanisms is probably appropriate. But so long as  $n$  depends (in a continuous fashion) on temperature, this is evidence for a stress-dependent activation energy, and thus for inapplicability of diffusion-only mechanisms.

## 7.2. **Constitutive Relations**

We will now give, as an example, one set of constitutive relations for cubic metals or alloys fulfilling the following assumptions (using the symbol  $\in\{ , \}$  to mean ‘in the range of’). The specified ranges are not necessarily restrictive, as we have discussed other cases in the foregoing; we merely mean that within these ranges we should be

comfortably within the scope of the explicit or implicit assumptions made.

(a) Only macroscopic flow will be treated; loading and unloading transients will be ignored. This may be stated as

$$\Delta \varepsilon \gg \Delta \sigma / E \quad (E \text{ is the elastic modulus})$$

(b) There is no tensorial internal back-stress at this macroscopic flow level:

$$\alpha_{ij} \ll \sigma_{ij}$$

(Otherwise, perhaps all equations still hold if  $\alpha_{ij}$  is subtracted from  $\sigma_{ij}$ , whenever the stress appears as a tensor.)

(c) The 'instantaneous' rate sensitivity of the flow stress (as measured by the applied equivalent stress):

$$m \equiv \left. \frac{\partial \ln \sigma}{\partial \ln \dot{\varepsilon}} \right|_{T, \dot{\varepsilon}} = \varepsilon \{0, 0.01\}$$

(d) The strain-hardening rate (again measured by macroscopic variables):

$$\Theta \equiv \left. \frac{\partial \sigma}{\partial \varepsilon} \right|_{T, \dot{\varepsilon}} = \varepsilon \{\sigma/2, E/50\}$$

The upper limit,  $E/50$ , again suggests that there is no kinematic-hardening component. The lower limit,  $\sigma/2$ , is set beyond the 'ultimate tensile strength' (UTS), for which  $\Theta = \sigma$ ; but it is chosen at the safe side of the point where the strain-hardening behavior typically changes in a qualitative manner (at about  $\Theta \approx \sigma/4$  or perhaps  $E/500$ ). In creep, the minimum creep rate under constant load is included; the regime much beyond this level does require more scrutiny.

(e) The rate sensitivity of the UTS (the reciprocal of the stress exponent of the minimum creep rate at constant load):

$$\frac{1}{n_1} \equiv \left. \frac{\partial \ln \sigma_{\text{UTS}}}{\partial \ln \dot{\varepsilon}} \right|_T < 0.1$$

(Even 1/6 probably works.) This indicates a strong influence of *dynamic* recovery (and less, if any, of diffusion).

### 7.2.1. *Multiaxial Relations*

For simplicity, we only summarize the relations for the case that fully constrained conditions apply to all grains: an upper bound, and a good approximation for equi-axed grains. Then, as far as the material element is concerned, all strain increments are locally prescribed.† Split up into direction and magnitude, they may be labelled

$$d\epsilon_v = \epsilon_v^0 d\epsilon \quad (7.1)$$

(We now drop all bars for averages and double bars for prescribed components.)

The deviatoric stress becomes, in principle:

$$\sigma'_\mu = P_{\mu\nu} \epsilon_v^0 M \tau \quad (7.2)$$

In practice, as we have elaborated in Section 4.2.5, the matrix  $P_{\mu\nu}$  is known only for isotropy under the von Mises assumption, when it is  $\delta_{\mu\nu}$ . But plastic anisotropy is of major qualitative importance for any description of multiaxial behavior, and no simple description of its effects exists as yet. For a quantitative treatment, it is imperative that  $\mathbf{P}(\epsilon^0)$  be tabulated for the entire relevant subspace.

The values  $P_{\mu\nu}$  for each  $\epsilon^0$  can, in principle, be obtained in three ways: by experimental yield surface determinations under all expected conditions; by experimental texture measurements followed by a polycrystal calculation; or by a polycrystal calculation *ab initio*, assuming the initial texture to be known (e.g. isotropic). It is not impossible that the last method becomes feasible in the not-too-distant future. For now, only cases near isotropy can be explicitly treated: say, for 20–30% strain from an isotropic situation—or the trivial case of proportional loading of a specimen that already has (at least) the symmetry of the test.

Finally, to describe the evolution of  $\tau$ , one will need the microscopic equivalent strain increment

$$d\Gamma = M d\epsilon \quad (7.3)$$

### 7.2.2. *Kinetics and Evolution*

With respect to the kinetics of flow and strain-hardening, one may adopt the same point of view as for the multiaxial part of the constitutive relations: they are too complicated to expect a sufficiently

† If, in fact, some components of *stress* are locally prescribed, this requires an iterative procedure.

accurate description in terms of functions—tables are needed. The principal use of the results of physical plasticity is then a specification of what the normalized parameters are that should be tabulated or plotted against each other. This is what we shall do in the following; but we will also repeat the simple functions that have given a reasonable description in many cases, for the regime specified at the beginning of Section 7.2.

The flow stress may have more than one component; however, one cannot make use of this in a phenomenologically sound way unless one has an operational way to separate the components, such as by using the Haasen plot of rate sensitivity (Section 3.1.7), or the Hall–Petch plot of grain-size dependence. The appearance of ‘plateaus’ in flow-stress vs. temperature or vs. time diagrams is not sufficient cause.

Any one component of flow stress is likely to obey a law of the kind (eqn (3.9))

$$\frac{\tau}{\mu(T, p)} = \frac{\hat{\tau}}{\mu_0} \cdot s \left( \frac{kT}{\mu b^3} \ln \frac{\dot{\gamma}_0}{M\dot{\epsilon}} \right) \quad (7.4)$$

where (eqn (3.8) and using  $x$  for the argument of  $s$  above)

$$\begin{aligned} s(x) &\approx (1 - (x/g_0)^{2/3})^2 \\ \dot{\gamma}_0 &\approx 10^8 \text{ s}^{-1} \end{aligned} \quad (7.4')$$

and  $\hat{\tau}/\mu_0$  is obtained by back-extrapolation to  $s = 1$ , i.e.  $T = 0$ .

The dependence of the state parameter  $\hat{\tau}$  on history parameters such as strain is not explicitly stated; it must be given in differential form. Most easily, it is specified directly by the variation of  $\tau$  (not  $\hat{\tau}$ ) with strain at a standard  $T$  and  $\dot{\epsilon}$ , in which case the value of  $s$  in eqn (7.4) should, strictly, appear as a factor in the following equations.

The strain-hardening rate (eqns (5.3) and (7.3)) appears to have the general form (eqn (5.6))

$$\theta = \theta_a - \theta_r \left( \frac{\tau - \tau_0}{\tau_s} \right) \quad (7.5)$$

where the general function may have the special form

$$\begin{aligned} \theta_r(r) &\approx \theta_a r \\ \theta_a &\approx \mu/200 \end{aligned} \quad (7.5')$$

$\tau_0$  is the yield stress, and  $\tau_s$  is a scaling parameter that obeys the

relation (eqn (5.8'))

$$\ln \frac{\tau_s}{\mu} = \ln \frac{\tau_{s_0}}{\mu_0} + S \left( \frac{kT}{\mu b^3} \ln \frac{\dot{\gamma}_{s_0}}{M\dot{\epsilon}} \right) \quad (7.6)$$

where the general function  $S(x)$  approximately obeys (eqn (5.8))

$$\begin{aligned} S(x) &\approx x/g_s \\ \dot{\gamma}_{s_0} &\approx 10^5 \text{ s}^{-1} \end{aligned} \quad (7.6')$$

$\tau_{s_0}/\mu_0$  is obtained by back-extrapolation to  $T = 0$ , and  $g_s$  follows from the measured slope of the plot.

When eqns (7.5') and (7.6') apply, one can extrapolate to steady-state creep with a stress exponent  $n$  that is independent of stress and strain-rate, but inversely proportional to temperature. At higher temperatures, eqn (7.6') is not found to be sufficiently accurate, and a useful expression for  $n$  becomes (eqn (5.9))

$$n = n_0 + \frac{\mu b^3}{kT} g_s \quad (7.7)$$

with  $n_0 \approx 4$ .

Transient creep is best described by the deceleration parameter (eqns (5.10), (5.13), (5.14))

$$\delta = \frac{\Theta}{m\sigma} \quad (7.8)$$

However, it is at present not clear whether the strain-hardening rate measured in the 'macro-flow' way (past the 'long transient'; Section 5.2.6) is in fact relevant near steady state, or whether some measure of this strain-hardening transient is more appropriate. In general, one should use a differential description such as outlined in Section 5.2.5.

When the relations (7.4), (7.5) and (7.6) hold, but not their primed counterparts, a tabular description may be necessary—but one has gained a great deal from applying the physical principles appropriate for this regime: e.g. temperature and strain rate appear essentially as a single parameter,  $kT \ln \dot{\epsilon}$ , properly normalized by material constants; the strain-hardening rate depends on stress only, and the stress-scaling parameter depends on the strain-rate/temperature combination. Thus, one needs only three two-dimensional plots or tables, not the whole four-dimensional space spanned by  $\tau$ ,  $\theta$ ,  $T$  and  $\dot{\epsilon}$ .

### 7.2.3. Conclusion

We have presented a sample, a tentative example, of the procedure we envisage for future determinations of constitutive behavior: a series of diagnostic tests, proceeding from simple to more complex if necessary; and a set of normalized parameters between which, for the regime of interest, relations (in functional or tabular form) are to be found. This technique needs much development work.

## 8. SUMMARY AND RECOMMENDATIONS

### Article of Faith

The current behavior of a material depends only on its current state, which is embodied in its current structure (microstructure, substructure). History variables such as time and strain can enter the constitutive relations only in differential form: describing the evolution of the state. The current rate of evolution is one aspect of current behavior, determined by the current state. Rearrangements of the structure upon loading are also entirely determined by the structure in the unloaded state.

### Elastic-Plastic Transition

The elastic-plastic transition is very sharp; deviatoric elastic strains are negligible with respect to plastic ones except in the very vicinity of the yield stress. The constitutive behavior using a yield or flow stress defined by back-extrapolation of the strain-hardening curve is much simpler and more reproducible than the regime in which both plastic and elastic distortions must be taken into account, and the simpler description does capture the most important features of plasticity.

### Yield Surface for Rate-sensitive Materials

The concept of a yield criterion is useful even for rate-sensitive materials, especially when (as usual) the rate sensitivity is low. Overstress formulations may be appropriate at very high strain-rates ( $>10^5 \text{ s}^{-1}$ ). In the normal range, thermal activation dominates rate sensitivity, and it *lowers* the yield stress from the rate-independent (zero temperature) limit, the 'mechanical threshold', which is a primary parameter of the dislocation theory of flow.

### **Normality Flow Rule**

The strain-increment direction is normal to the yield surface if, and only if, the state of the material, as it affects the plastic resistance, does not depend on the state of stress. This is true for most metals in the normal range of applications, but is expected to be violated under conditions of non-negligible nonlinear-elastic effects (e.g. in very-high-strength materials, at very high pressures, and in polymers). In any case, a plastic potential exists and provides a useful description in terms of the relation between strain *rates* and (total) stresses (rather than stress rates).

### **Plastic Anisotropy**

The shape of the yield surface is strongly influenced by the crystallographic texture of the material. Even at mild textures, it departs significantly from a von Mises 'sphere' and 'oval' shapes: extensive flat regions and sharp (though not necessarily discontinuous) ridges and vertices develop, which are very important for plastic-stability considerations. It is unlikely that a useful *functional* relation for such realistic yield surfaces will be found; numerical descriptions appear mandatory. Appropriate subspaces have been identified in which, for a given texture symmetry, the yield surface must be derived (from experiment or simulation).

### **Hardening Rules**

The evolution of the yield surface is also strongly influenced by the texture changes accompanying plastic deformation. These expected changes in shape are superposed on a general increase in size. 'Kinematic hardening' is significant only in two-phase materials, so long as the macroscopic flow stress is being described.

### **Kinetics of Flow and Evolution**

The rate dependence of the flow stress is usually negligible, but it provides an important tool to identify deformation mechanisms; in particular whether more than one contribution to the flow stress can be operationally identified (such as an 'internal stress' in addition to the mechanical threshold). The rate dependence of strain hardening is more substantial and more important; it controls steady-state flow and, more generally, flow at a low strain-hardening rate (whether this be due to large prestrains or high temperature).

**Strain Hardening**

Strain hardening consists of an athermal and a dynamic-recovery part. The latter is primarily stress dependent, with a stress-scaling parameter that depends on temperature and strain rate. At very high strains, an additional, little-explored stage causes slow but steady hardening in many materials.

**Transients**

Noticeable transients in the strain-hardening behavior occur after changes such as rate-changes, stress reversal, and recovery. They last for about 3% strain. If they are significant for the particular application, an additional state parameter is necessary to describe the evolution of each type of transient.

**Differential Constitutive Relations**

An attractive alternative to constitutive descriptions in terms of (tentatively) identified state parameters and their evolution is an entirely differential description, in terms of external state variables only; in that case, the initial conditions are equivalent to state parameters, and the number and order of such differential equations must allow for the requisite number of initial conditions. A new formulation of this kind has been proposed that incorporates hardening transients.

**Temperature Dependence**

The most important temperature dependence is that of the steady-state limit stress, or other parameters characterizing dynamic recovery. In some cases at least, it obeys a single law over the entire temperature range up to at least  $2/3$  of the melting point; changes in mechanism need not then be postulated. The activation energy is stress dependent, over this regime, and correspondingly the stress exponent depends on temperature in a continuous fashion.

The temperature dependence of the yield stress is mild by comparison, but in most cases it is not nil, so that an athermal, 'internal' stress need not be postulated as an additional parameter. Solute hardening, and especially solute mobility, play an important role in this regime.

**Creep**

The view is taken here that plasticity is inherently rate sensitive and thus indistinguishable (except for the boundary conditions) from

creep. It is, however, an important open question whether the creep behavior near steady state is correlated with regular strain hardening or with the prominent hardening transients in this regime.

### **Internal Stresses**

There are reliable methods to test whether any macroscopic state parameter that fits any of the many meanings of this term needs to be introduced. This is expected in two-phase materials.

### **Normalized Variables**

Various external variables and material parameters occur, according to crystal plasticity theory, in certain combinations only. This can reduce significantly the amount of information that need be collected. Some such combinations are:  $\tau/\mu$ ,  $(kT/\mu b^3) \ln(\dot{\epsilon}/\dot{\epsilon}_0)$  (where only  $\dot{\epsilon}_0$  is a free parameter to which, however, the results are not sensitive), and  $\theta/\mu$  as well as  $\theta/m\tau$ , the deceleration rate in creep.

### **Functional versus Numerical Description**

In general, we have come to the conclusion that functional relations will rarely be easy and accurate enough to describe the various dependences outlined above. The most important task of physical constitutive relations development is the identification of the smallest space in which the relationships must be specified. Then, a numerical description (tabular or diagrammatic) may be feasible. Inasmuch as most applications in which realistic material descriptions are needed are in numerical, computer-code form anyway, a numerical approach to materials behavior is not inopportune.

## **ACKNOWLEDGMENTS**

It is a pleasure to acknowledge that the long-standing collaboration with Heinz Mecking has significantly contributed to the development of the ideas and abstractions summarized here. I have also benefitted from frequent interactions on these topics with A. S. Argon, M. F. Ashby, P. R. Dawson, P. S. Follansbee, J. W. Hutchinson, W. D. Nix and M. G. Stout. Comments on the manuscript by D. A. Hughes, A. K. Miller and D. Tonks are greatly appreciated. The research underlying this article has been sponsored for many years by the US Department of Energy, Division of Basic Energy Sciences.

## REFERENCES

1. U. F. Kocks, A. S. Argon and M. F. Ashby, *Prog. Mater. Sci.*, **19** (1975).
2. U. F. Kocks, in *The Strength of Metals and Alloys*, ed. P. Haasen *et al.*, Pergamon, 1980, p. 1661.
3. U. F. Kocks, in *Chalmers Anniv. Vol.*, *Prog. Mater. Sci.* (1981) 185.
4. U. F. Kocks, in *Physics of Strength and Plasticity*, ed. A. S. Argon, MIT Press, 1969, p. 143.
5. H. Mecking, in *Dislocation Modelling of Physical Systems*, ed. M. F. Ashby *et al.*, Pergamon, 1981, p. 197.
6. J. Gil Sevillano, P. van Houtte and E. Aernoudt, *Prog. Mater. Sci.*, **25** (1982) 69.
7. A. D. Rollett, U. F. Kocks and R. D. Doherty, *Formability and Metallurgical Structure*, The Metallurgical Society of AIME, 1987, in press.
8. D. A. Hughes, J. C. Gibeling and W. D. Nix, in *The Strength of Metals and Alloys*, ed. H. J. McQueen, J.-P. Bailon, J. I. Dickson, J. J. Jonas and M. G. Akben, Pergamon, 1985, p. 51.
9. U. F. Kocks, in *Constitutive Equations for Plasticity*, ed. A. S. Argon, MIT Press, 1975, p. 81.
10. U. F. Kocks and H. Mecking, in *Dislocation Modelling of Physical Systems*, ed. M. F. Ashby *et al.*, Pergamon, 1981, p. 173.
11. Z. S. Basinski, *Phil. Mag.*, **4** (1959) 393.
12. H. Mecking and U. F. Kocks, *Acta Metall.*, **29** (1981) 1865.
13. U. F. Kocks, *J. Eng. Mater. Tech.* (ASME-H), **98** (1976) 76.
14. W. A. Spitzig and O. Richmond, *Acta Metall.*, **32** (1984) 457.
15. A. S. Argon, in *The Inhomogeneity of Plastic Deformation*, ed. R. E. Reed-Hill, Amer. Soc. Metals, 1973, p. 161.
16. D. Kuhlmann-Wilsdorf, in *Work Hardening*, ed. J. P. Hirth and J. Weertman, AIME, 1968, p. 97.
17. M. G. Stout, Los Alamos National Laboratory, Los Alamos, NM 87545, USA, unpublished results
18. M. G. Stout, P. L. Martin, D. E. Helling and G. R. Canova, *Int. J. Plasticity*, **1** (1985) 163.
19. S. B. Batdorf and B. Budianski, *J. Appl. Mech.*, **21** (1954) 323.
20. S. S. Hecker, *Metall. Trans.*, **2** (1971) 2077.
21. W. T. Lankford, S. C. Snyder and J. A. Bauscher, *Trans. Amer. Soc. Metals*, **42** (1950) 1197.
22. G. R. Canova and U. F. Kocks, *Eighth International Conference of Textures of Materials*, ed. J. S. Kallend and G. Gottstein, The Metallurgical Society of AIME, 1987, in press.
23. H. Neuhäuser, in *Strength of Metals and Alloys*, ed. P. Haasen, V. Gerold and G. Kostorz, Pergamon, 1979, p. 1531.
24. R. J. Clifton, in *Shock Waves and the Mechanical Properties of Solids*, ed. J. J. Burke and V. Weiss, Syracuse Univ. Press, 1971, p. 73.
25. R. B. Schwarz, R. D. Isaac and A. V. Granato, *Phys. Rev. Lett.*, **38** (1977) 554.

26. R. B. Schwarz and R. Labusch, *J. Appl. Phys.*, **49** (1978) 5147.
27. P. S. Follansbee, G. Regazzoni and U. F. Kocks, in *Mechanical Properties of Materials at High Rates of Strain*, ed. J. Harding, Inst. Phys. Conf. Ser. 70, 1980, p. 71.
28. P. S. Follansbee, in *Metallurgical Applications of Shock Waves and High Strain-Rate Phenomena*, ed. L. E. Murr, K. A. Staudhammer and M. A. Meyers, Marcel Dekker, New York, 1986, p. 451.
29. U. F. Kocks, *Metall. Trans.*, **16A** (1985) 2109.
30. H. Suzuki, in *Dislocations and the Mechanical Properties of Crystals*, ed. J. C. Fisher *et al.*, Wiley, 1957, p. 361.
31. E. W. Hart, *J. Mater. Sci. Techn.* (ASME H), **98** (1976) 193.
32. J. H. Holbrook, R. W. Rohde and J. C. Swearingen, *Acta Metall.*, **29** (1981), 1099.
33. J. C. Gibeling and T. H. Alden, *Acta Metall.*, **32** (1984) 2069.
34. U. F. Kocks, in *Fundamental Aspects of Dislocations Theory*, ed. J. A. Simmons, R. deWit and R. Bullough, NBS Spec. Pub. 317, 1971, p. 1077.
35. T. H. Alden, *Phil. Mag.*, **25** (1972) 785.
36. P. Haasen, *Phil. Mag.*, **3** (1958) 384.
37. R. A. Mulford, *Acta Metall.*, **27** (1979) 1115.
38. R. A. Mulford and U. F. Kocks, *Acta Metall.*, **27** (1979) 1125.
39. R. A. Mulford, *Metall. Trans.*, **10A** (1979) 1527.
40. U. F. Kocks, R. E. Cook and R. A. Mulford, *Acta Metall.*, **33** (1985) 623.
41. A. H. Cottrell and R. J. Stokes, *Proc. Roy. Soc.*, **A233** (1955) 17.
42. C. W. MacGregor and J. C. Fisher, *J. Appl. Mech.*, **13** (1946) A11.
43. R. Hill, *The Mathematical Theory of Plasticity*, Oxford Univ. Press, Oxford, 1950.
44. E. W. Hart, *Acta Metall.*, **18** (1970) 599.
45. A. S. Argon, in *Constitutive Equations in Plasticity*, ed. A. S. Argon, MIT Press, 1975, p. 1.
46. G. I. Taylor, *J. Inst. Metals*, **62** (1938) 307.
47. G. R. Canova and U. F. Kocks, in *Int. Conf. on Textures of Materials*, ed. C. M. Brakman, P. Jongenburger and E. J. Mittemeijer, Netherlands Soc. Mater. Sci., Amsterdam, 1984, p. 573.
48. G. R. Canova, A. Molinari, C. Fressengeas and U. F. Kocks, *Acta Metall.*, in press.
49. U. F. Kocks, in *Plastic Instability; Considère Memorial Symposium*, Ponts et Chaussées Press, Paris, 1985, p. 309.
50. H. Honneff and H. Mecking, in *Textures of Materials*, ed. G. Gottstein and K. Lücke, Springer, 1978, vol. 1, p. 265.
51. U. F. Kocks and H. Chandra, *Acta Metall.*, **30** (1982) 695.
52. U. F. Kocks and G. R. Canova, in *Deformation of Polycrystals*, ed. N. Hansen, Risø National Laboratory, Denmark, 1980, p. 35.
53. U. F. Kocks, *Metall. Trans.*, **1** (1970) 1121.
54. P. van Houtte, in *Textures of Materials*, ed. C. M. Brakman, P. Jongenburger and E. J. Mittemeijer, Netherlands Soc. Mater. Sci., Amsterdam, 1984, p. 573.

55. C. Tomé, G. R. Canova, U. F. Kocks, N. Christodoulou and J. J. Jonas, *Acta Metall.*, **32** (1984) 1637.
56. R. J. Asaro and A. Needleman, *Acta Metall.*, **33** (1985) 923.
57. J. F. W. Bishop and R. Hill, *Phil. Mag.*, **42** (1951) 1298.
58. M. Renouard and M. Wintenberger, *Compt. Rend. Acad. Sci.*, **B290** (1980) 403.
59. J. W. Hutchinson, *Proc. Roy. Soc.*, **A319** (1970) 247.
60. J. J. Jonas, G. R. Canova, S. C. Shrivastava and N. Christodoulou, in *Plasticity of Metals at Finite Strain*, ed. E. H. Lee and R. L. Mallett, Stanford Univ., 1982, p. 206.
61. G. R. Canova, C. Tomé and U. F. Kocks, *J. Mech. Phys. Sol.*, **33** (1985) 371.
62. F. Montheillet, M. Cohen and J. J. Jonas, *Acta Metall.*, **32** (1984) 2077.
63. R. Hill, *Proc. Roy. Soc.*, **A193** (1948) 281.
64. W. F. Hosford, *J. Appl. Mech. (ASME-E)*, **39** (1972) 607.
65. J. L. Bassani, *Int. J. Mech. Sci.*, **19** (1977) 651.
66. M. G. Stout, Los Alamos National Laboratory, Los Alamos, NM 87545, USA, unpublished results
67. J. W. Hutchinson, *Adv. Appl. Mech.*, **14** (1974) 67.
68. G. R. Canova, U. F. Kocks and M. G. Stout, *Scripta Metall.*, **18** (1984) 437.
69. A. P. L. Turner and T. Hasegawa, in *Mechanical Testing for Deformation Model Development*, ed. R. W. Rohde and J. C. Swearingen, ASTM, 1982, STP-765, p. 322.
70. W. Prager, *Proc. Inst. Mech. Engrs*, **169** (1955) 41.
71. P. Franciosi, M. G. Stout, J. O'Rourke, B. Erskine and U. F. Kocks, *Acta Metall.*, in press.
72. D. Peirce, R. J. Asaro and A. Needleman, *Acta Metall.*, **31** (1983) 1951.
73. J. D. Embury, A. Korbelt, V. S. Raghunathan and J. Rys, *Acta Metall.*, **32** (1984) 1883.
74. P. Haasen, *Z. Physik*, **136** (1953) 26.
75. F. R. N. Nabarro, Z. S. Basinski and D. B. Holt, *Adv. Phys.*, **13** (1964) 193.
76. H. Mecking, in *Work Hardening in Tension and Fatigue*, ed. A. W. Thompson, AIME 1977, p. 67.
77. U. F. Kocks, in *Mechanical Testing for Deformation Model Development*, ed. R. W. Rohde and J. C. Swearingen, Amer. Soc. Testing Mater., STP 765, 1982, p. 121.
78. H. Mecking, in *Deformation of Polycrystals*, ed. N. Hansen, Risø National Laboratory, Denmark, 1980, p. 73.
79. K. S. Havner and A. H. Shalaby, *Proc. Roy. Soc.*, **A358** (1977) 47.
80. P. Franciosi, M. Berveiller and A. Zaoui, *Acta Metall.*, **28** (1980) 273.
81. R. Hill, *J. Mech. Phys. Sol.*, **14** (1966) 95.
82. U. F. Kocks and T. J. Brown, *Acta Metall.*, **14** (1966) 87.
83. Z. S. Basinski and P. J. Jackson, *Phys. Stat. Sol.*, **10** (1965) 45.
84. U. F. Kocks, *Acta Metall.*, **6** (1958) 85.
85. H. Mecking, B. Nicklas, N. Zarubova and U. F. Kocks, *Acta Metall.*, **34** (1986) 527.

86. E. Voce, *J. Inst. Metals*, **74** (1948) 537.
87. J. Diehl, *Z. Metallk.*, **47** (1956) 331.
88. U. F. Kocks, *Phil. Mag.*, **13** (1966) 541.
89. U. F. Kocks, in *Dislocations and the Properties of Real Materials*, Inst. Metals, London, 1985, p. 125.
90. H. Mecking, U. F. Kocks and H. Fischer, in *Strength of Metals and Alloys*, Lab. de Physique du Solide, E.N.S.M.I.M., I.N.P.L., Nancy, France, 1976, p. 334.
91. A. Seeger, J. Diehl, S. Mader and H. Rebstock, *Phil. Mag.*, **2** (1957) 323.
92. P. S. Follansbee and U. F. Kocks, *Acta Metall.*, in press.
93. W. Blum and B. Reppich, *Acta Metall.*, **17** (1969) 959.
94. J. Weertman, in *Rate Processes in Plastic Deformation of Materials*, ed. J. C. M. Li and A. K. Mukherjee, ASM, 1975, p. 315.
95. U. F. Kocks, T. Hasegawa and R. O. Scattergood, *Scripta Metall.*, **14** (1980) 449.
96. T. Hasegawa, T. Yakou and U. F. Kocks, *Acta Metall.*, **30** (1982) 235.
97. U. F. Kocks, H. Mecking and J. J. Jonas, *Acta Metall.*, **27** (1979) 419.
98. U. F. Kocks, in *Superplastic Forming of Structural Alloys*, ed. N. E. Paton and C. H. Hamilton, AIME, 1982, p. 41.
99. J. C. Gibeling and W. D. Nix, *Mater. Sci. Eng.*, **45** (1980) 123.
100. A. S. Argon and S. Takeuchi, *Acta Metall.*, **29** (1981) 1877.
101. E. Orowan, in *Symposium on Internal Stresses in Metals and Alloys*, Inst. Metals, London, 1948, p. 451.
102. U. F. Kocks, *Mater. Sci. Eng.*, **27** (1977) 291.
103. E. Nembach and M. Martin, in *The Strength of Metals and Alloys*, ed. P. Haasen *et al.*, Pergamon, 1979, p. 1407.
104. M. F. Ashby, in *The Physics of Strength and Plasticity*, ed. A. S. Argon, MIT Press, 1969, p. 113.
105. L. M. Brown and W. M. Stobbs, in *Constitutive Equations in Plasticity*, ed. A. S. Argon, MIT Press, 1975, p. 387.
106. J. D. Atkinson, L. M. Brown and W. M. Stobbs, *Phil. Mag.*, **30** (1974) 1247.
107. G. D. Moan and J. D. Embury, *Acta Metall.*, **27** (1979) 903.
108. M. F. Ashby, *Phil. Mag.*, **21** (1970) 399.
109. W. D. Nix and B. Ilschner, in *The Strength of Metals and Alloys*, ed. P. Haasen *et al.*, Pergamon, 1980, p. 1503.
110. T. Hasegawa and U. F. Kocks, *Acta Metall.*, **27** (1979) 1705.
111. U. F. Kocks and H. Mecking, in *The Strength of Metals and Alloys*, ed. P. Haasen *et al.*, Pergamon, 1980, p. 345.
112. T. Hasegawa, T. Yakou and U. F. Kocks, *Mater. Sci. Eng.*, **81** (1986) 189.
113. E. W. Hart and A. D. Solomon, *Acta Metall.*, **21** (1973) 295.
114. S. R. MacEwen and J. Faber, *Proc. Symp. Neutron Scattering*, ed. M. S. Lehmann *et al.*, Hahn-Meitner Inst. Report B411, p. 53.
115. H. Mecking and K. Lücke, *Mater. Sci. Eng.*, **1** (1967) 349.
116. R. A. Mulford and U. F. Kocks, *Scripta Metall.*, **13** (1979) 729.

# 2

## State Variable Theories Based on Hart's Formulation

M. A. KORHONEN,† S.-P. HANNULA and CHE-YU LI

*Department of Materials Science and Engineering, Cornell University,  
Ithaca, New York, USA*

### 1. INTRODUCTION

Constitutive equations based on state variables are very attractive in stress analysis because of their ability to characterize the consequences of mechanical history by current values of state variables. By virtue of this a state variable theory can organize and rationalize a wealth of accumulated data, and the ensuing economy in thought will automatically lead to economy in experiment.<sup>1</sup> Moreover, with the aid of state equations, material behavior under difficult or even unmanageable conditions may be predicted by more readily performable tests; for example, long-term creep behavior at high temperatures might be estimated based on combined short-term tensile and relaxation testing at a lower temperature.

The state variable theory reviewed in this chapter was proposed by Hart<sup>2-5</sup> who first suggested the existence of a plastic equation of state in terms of stress, non-elastic strain rate and a hardness parameter. The use of the hardness parameter as a state variable which characterizes the structural state of a material represented a new direction in the development of state variable theories. Extensive experimental work has been motivated by Hart's proposal (see e.g. reference 6). In general the effort was designed to verify the existence of mechanical equations of state and to develop a set of constitutive equations based

† Present address: Department of Mining and Metallurgy, Helsinki University of Technology, 02150 Espoo 15, Finland

on state variables to describe in a unified way a range of phenomena involving plastic deformation.

In addition to plastic deformation and anelasticity, which were treated in Hart's original model, a variety of loading and unloading effects such as microplasticity or the Bauschinger effect,<sup>6-9</sup> and phenomena involving grain boundary sliding,<sup>6,9-11</sup> have also been included in a state variable description. The latter phenomena necessitate the extension of Hart's original model and consideration of additional state variables. The attitude taken in this development has been to emphasize the experimental verification of any extension of the state variable concept, including justification of the introduction of new state variables as well as measurement of the material parameters involved.<sup>6</sup>

These state variable models have been shown to be capable of describing, rationalizing and predicting a wide class of deformation phenomena, observed at low homologous temperatures, where only dynamic recovery and grain boundary sliding need to be involved. Static recovery and other time-dependent phenomena such as strain aging can be accounted for and described by a time-dependent change of certain model parameters. The models are able to simulate and predict, besides simple loading histories, a variety of complex transients during loading, unloading and stress reversal or stress and strain rate changes in general.<sup>6-15</sup>

The present state variable approach has already been successfully applied to study essentially homogeneous deformation of isotropic mainly single-phase materials including pure metals, metal alloys of technological importance, ionic crystals and amorphous solids. Much of this testing has taken place in conditions bearing relevance to practical technological applications. Further, the models have been applied to complex thermomechanical histories in structural members of technological interest by using finite element method (FEM) and boundary element method (BEM) computer codes.

## 2. THE PHYSICAL AND PHENOMENOLOGICAL BASES

The central point of the state variable theory proposed by Hart is the existence of a state variable called the hardness parameter which specifies the plastic state of a material. Physically the hardness parameter measures the characteristics of the barrier structure to

plastic flow.<sup>5,6</sup> If the hardness parameter is uniquely specified by the operating stress and non-elastic strain rate, the relationship among these state variables is a plastic equation of state. This concept has been successfully tested experimentally.

In Hart's original model for grain matrix deformation, the reversible motion of dislocations between barriers to plastic flow as depicted in Fig. 1(a) results in anelastic deformation.<sup>2,5</sup> Anelastic strain, which is also a state variable, depends on the extent of effective dislocation pile-up between these barriers.<sup>4,6</sup> The back stress of the pile-up and the anelastic strain are linearly related through an anelastic modulus. This relationship is also a mechanical equation of state which requires experimental verification. In fact, these anelastic or internal stresses drive plastic deformation, and upon unloading and subsequent reverse loading they are responsible for a reduced resistance for back-flow.

The probability of leakage of the leading dislocation through the barriers is viewed as depending on the strength of the barrier as well as on the internal stress of the pile-up. Even if well developed pile-ups may not always exist, the essential point is that there arise dislocation configurations which lead to stress concentrations helping dislocations to overcome barriers. This leakage process in general requires thermal activation and produces irreversible plastic deformation. The rate of change of the pile-up structure, on the other hand, gives the anelastic strain rate which is a function of the friction stress, which in turn is caused by local glide resistance. The total or applied stress,  $\sigma$ , is considered to be the sum of the friction stress,  $\sigma_f$ , and the internal stress of the pile-up,  $\sigma_a$ . When the applied stress is sufficiently large,

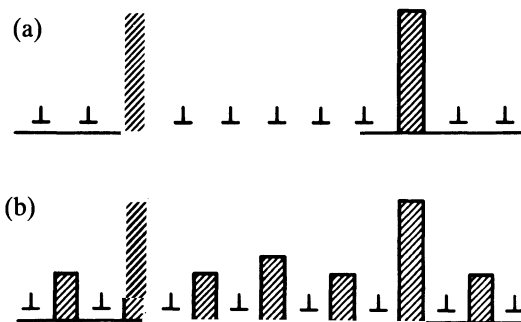


**Fig. 1.** Physical representation of (a) the Hart model and (b) the extension of the Hart model for transient deformation; shaded columns denote the barriers to dislocation glide.

the leakage through barriers will no longer be rate-limiting such that plastic deformation will be controlled entirely by glide friction. The phenomenological model for grain matrix deformation proposed by Hart can be taken to represent the physical processes described above by using appropriate constitutive equations.

In this description it is essential that the structural hardness appears as a divider between the decreasing and increasing strain rate sensitivities of low and high strain rate regimes, respectively. Figure 2 depicts this amply confirmed behavior; in this figure the components of the total stress are also shown schematically. The low strain rate or high homologous temperature behavior is governed by thermally assisted leakage of dislocations past barriers, even if  $\sigma \approx \sigma_a < \sigma^*$ . In this regime the glide friction is not important because the rate of the process is dominated by the activation kinetics. On the other hand, the high strain rate or low homologous temperature behavior is characterized by an essentially mechanical activation of dislocations through barriers, or  $\sigma_a \approx \sigma^*$ , so there is practically no waiting time at the barriers. Hence the glide friction remains the sole rate-limiting factor of the deformation, and ultimately at very high strain rates it accounts for most of the deformation resistance.

While it has been demonstrated that the concept of a single hardness parameter adequately characterizes the plastic state of a material and a

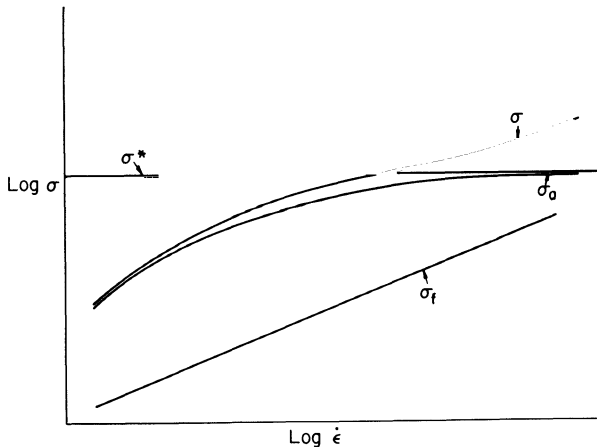


**Fig. 2.** A schematic representation of the strain rate dependence of the flow stress ( $\sigma$ ) and its components: internal stress ( $\sigma_a$ ) and friction stress ( $\sigma_f$ ).

variety of phenomena involving plastic deformation, it was realized that transient phenomena such as the Bauschinger effect cannot be satisfactorily described by Hart's model.<sup>7</sup> This should not be surprising since a single hardness parameter which corresponds to a mean spacing of barriers of the same strength throughout the specimen<sup>4</sup> represents a grossly simplified picture. In reality one should expect a distribution of barrier spacings and strengths. However, it is not always possible to specify experimentally the state variables and material parameters required by a more detailed model. The extension of Hart's model to describe transient deformation therefore represents a compromise between the desire for a realistic description and the experimental feasibility.

In the extension of Hart's model, a polycrystalline solid is viewed as consisting of two different types of barriers, strong and weak, to plastic deformation. The strong barriers can be identified with, for example, subgrain walls while the dislocation tangles may act as weak barriers.<sup>6,7</sup> Each type of barrier is characterized by a separate hardness parameter. The evolution of the two hardness parameters with mechanical history is generally different and the hard barriers are believed to be much more stable against thermally activated recovery. In fact, this description of a grain matrix consisting of 'hard' and 'soft' regions, each associated with an internal stress state of its own, comes close to some recent theoretical and experimental developments.<sup>16-18</sup>

The composite microstructure is schematically represented in Fig. 1(b). A uniformly distributed weak barrier structure is assumed over the slip zone. Upon loading, dislocations will pile up in front of the barriers. At sufficiently high stresses, leakage through the weak barriers will occur, contributing to the long-range pile-up across the zone against the strong barriers. When the pile-ups in front of the weak barriers are fully developed, macroplastic flow is impeded only by strong barriers as represented by Hart's original model.

A direct consequence of this composite microstructure is the so-called microplasticity which results from the dislocation penetration of weak barriers. The plastic behavior represented by Hart's original model is taken to correspond to dislocation penetration of strong barriers and is viewed as macroplastic behavior. Upon reversed loading of a specimen which has been deformed in the macroplastic region and unloaded, dislocations will first penetrate the weak barriers, resulting in a reduction in yield stress compared with that if the reloading were in the same forward direction. This reduction in

yield stress is usually taken as a manifestation of the Bauschinger effect.

At temperatures above about  $4/10$  of the absolute melting temperature, grain boundary sliding is expected to contribute to non-elastic deformation. The present state variable description that includes grain boundary sliding related deformation represents also a compromise between the desire for a physically realistic representation and the capabilities to evaluate the additional state variables and material parameters experimentally. Figure 3 depicts a segment of grain boundary between two neighboring grain corners. The sliding behavior of this basic unit of grain boundary and its interaction with grain matrix deformation are represented by an extended model.

Grain boundary sliding and grain matrix deformation are intimately related at various levels through compatibility considerations. For example, when the grain boundary sliding is accommodated by elastic and anelastic deformation in the grain matrix, the stored elastic and anelastic strain will be the driving force for reversed grain boundary sliding upon unloading, corresponding to the concept of grain boundary anelasticity introduced by Zener.<sup>19</sup> When the compatibility requirements are satisfied by plastic deformation in the grain matrix, grain boundary sliding enhanced deformation will take place. The interaction between grain boundary sliding and grain matrix deformation is expected to occur at grain boundary steps or other sites of inhomogeneity along this segment of the grain boundary (Fig. 3) as well as at grain corners. In the present treatment the interactions along the segment of grain boundary in Fig. 3 will appear as part of the flow behavior of the grain boundary which therefore will be expected to exhibit characteristics of grain matrix plasticity.

Since the stress dependence of the rate of grain matrix flow is usually stronger than that of grain boundary sliding, the interaction discussed above will vary depending on the magnitude of the applied stress.<sup>20,21</sup> At high stresses, grain boundary sliding is a more sluggish



**Fig. 3.** A schematic representation of a segment of the grain boundary between two neighboring grain corners.

process than grain matrix flow, such that a polycrystalline solid will exhibit behavior governed by grain matrix processes. At sufficiently low stresses, when grain boundary sliding becomes easy, a polycrystalline solid will again show grain matrix like flow characteristics with the grain boundaries acting like shear cracks. A range where both grain boundary sliding and grain matrix flow will contribute to the deformation occurs at stresses between the above two limits.

### 3. A STATE VARIABLE DESCRIPTION

The introduction of the present state variable theory will be made at three levels of increasing complexity. The basic level corresponds primarily to the original model proposed by Hart<sup>2-5</sup> for grain matrix deformation. It was later extended to describe more adequately a variety of transient phenomena<sup>6-9</sup> as well as phenomena involving grain boundary sliding.<sup>6,9-11</sup>

#### 3.1. Hart's Model for Grain Matrix Deformation

The model describes a synthesis of three deformation mechanisms and can be conveniently represented by the rheological diagram of Fig. 4(a). The three elements in the figure are often referred to as *a* (the

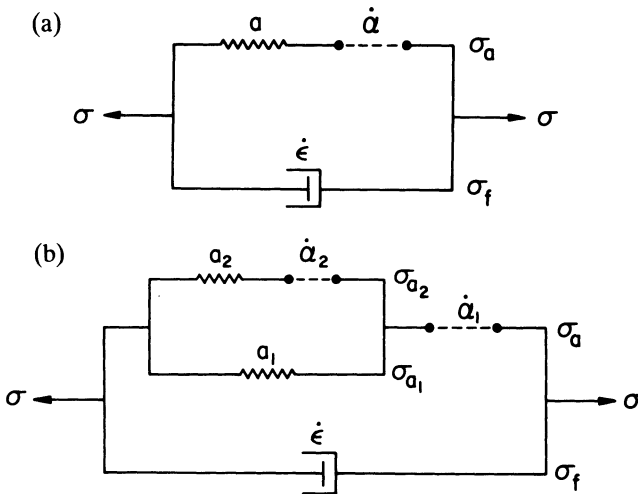


Fig. 4. Rheological diagrams of (a) Hart's model for grain matrix deformation and (b) the extension of the Hart model for transient deformation.

anelastic element),  $\dot{\alpha}$  (the plastic element), and  $\dot{\epsilon}$  (the glide friction element). All the elements contribute to the non-elastic deformation of a polycrystalline solid. The total strain at any time can be obtained simply by an addition of the elastic strain.

Physically, the  $a$  element and the  $\dot{\epsilon}$  element act together in parallel to represent anelastic deformation resulting from reversible motion of dislocations between barriers governed by glide friction, the  $a$  element being an anelastic spring and the  $\dot{\epsilon}$  element a flow element governed by glide friction. The  $\dot{\alpha}$  element is another flow element, representing plastic deformation. The  $\dot{\epsilon}$  element participates also in plastic deformation, acting in parallel with the  $\dot{\alpha}$  element.

The total non-elastic strain rate  $\dot{\epsilon}$  is the sum of the time rate of the recoverable anelastic strain  $a$  and the non-recoverable plastic strain rate  $\dot{\alpha}$ , such that

$$\dot{\epsilon} = \dot{a} + \dot{\alpha} \quad (1)$$

The anelastic strain can be shown to be a state variable of the material, while the plastic strain is not.<sup>4-6</sup>

The stresses operating in the two branches of the model satisfy a constraint equation

$$\sigma = \sigma_a + \sigma_f \quad (2)$$

where  $\sigma$  is the applied stress,  $\sigma_a$  is the internal stress of the dislocation pile-up and  $\sigma_f$  is identified as the friction stress.

The constitutive equations for the three elements are deduced from experimental measurements. The anelastic element is a linear element with a modulus  $M$  such that<sup>4</sup>

$$\sigma_a = Ma \quad (3)$$

The plastic element is represented by the flow equation<sup>4</sup>

$$\ln(\sigma^*/\sigma_a) = (\dot{\epsilon}^*/\dot{\alpha})^\lambda \quad (4)$$

where  $\sigma^*$  is a hardness parameter,  $\dot{\epsilon}^*$  is a rate parameter,  $\dot{\alpha}$  is the plastic strain rate as defined previously and  $\lambda$  is a constant.

A manifestation of the mechanical equation of state characteristics of the flow equation for  $\dot{\epsilon}$  is the scaling relation between  $\sigma^*$  and  $\dot{\epsilon}^*$ :

$$\dot{\epsilon}^* = (\sigma^*/G)^mf \exp(-Q/RT) \quad (5)$$

where  $m$  is the inverse of the slope of the scaling direction,  $f$  and  $Q$  are material parameters,  $G$  is the shear modulus and  $RT$  has the usual

meaning. The evolution of  $\sigma^*$  as governed by work-hardening and static recovery is incorporated in the model by<sup>4-6</sup>

$$d(\ln \sigma^*)/dt = \Gamma(\dot{\alpha}, \sigma^*)\dot{\alpha} - \mathcal{R}(\sigma^*, T) \quad (6)$$

where  $\Gamma$  represents an absolute work-hardening coefficient and  $\mathcal{R}$  represents static recovery.

The glide friction element is represented by a flow equation:

$$\dot{\epsilon} = \dot{\alpha}^*(T)(\sigma_f/G)^M \quad (7)$$

which is of similar form to the flow law proposed by Li and co-workers on a physical basis.<sup>22</sup> Here  $\dot{\alpha}^*$  is a rate parameter and  $M$  is a material parameter, the inverse of which gives the scaling direction  $\mu = d(\ln \sigma^*)/d(\ln \dot{\epsilon}^*)$ , in a logarithmic plot of stress against the strain rate, as in Fig. 2.

In the above equations  $M$ ,  $m$ ,  $\lambda$ ,  $f$  and  $Q$  are parameters specific for each material and  $\sigma^*$ ,  $\dot{\epsilon}^*$  and  $\dot{\alpha}^*$  are parameters characteristic of each state. Typical values for some of the parameters are  $\lambda \approx 0.15$ ,  $m = 3-8$ ,  $M = 3-15$ , and  $Q$  is usually close to the activation energy for atomic self-diffusion. A typical dependence of the total stress and its components  $\sigma_a$  and  $\sigma_f$  on the strain rate as described by eqns (4) and (7) is depicted in Fig. 2.

The work-hardening and recovery functions  $\Gamma$  and  $\mathcal{R}$  are also determined experimentally. Recent experimental work on a variety of metals has suggested that the function  $\Gamma$  can be represented by<sup>23</sup>

$$\Gamma \equiv \frac{d(\ln \sigma^*)}{d\alpha} = \Gamma^*(\sigma^*)\exp[-(\dot{\alpha}^*/\dot{\alpha})^\Lambda] \quad (8)$$

which is a generalized form of the absolute work-hardening function suggested previously.<sup>5</sup> In this equation  $\Gamma^*$  is the athermal part of the work-hardening coefficient, which depends on hardness only,  $\dot{\alpha}^*$  is an auxiliary parameter dependent on temperature and on hardness, and  $\Lambda$  is a material parameter which has a value close to  $\lambda$ .  $\Gamma^*$  was found to be given by

$$\Gamma^* = \left( \frac{A}{\sigma^* - \sigma_0^*} \right)^B \quad (9)$$

where  $A$ ,  $B$  and  $\sigma_0^*$  are material parameters to be measured for each material.

The function  $\mathcal{R}$ , which represents static recovery of the hardness

$\sigma^*$ , has not been studied systematically. Some recent investigations<sup>24,25</sup> show that  $\mathcal{R}$  depends principally on  $T$  and  $\sigma^*$ , as would be expected.

### 3.2. An Extension of Hart's Model to a Multiaxial Loading Case

In a multiaxial formulation<sup>4</sup> the tensorial non-elastic strain rate is composed of anelastic and plastic contributions as

$$\dot{\epsilon}_{ij} = \dot{a}_{ij} + \dot{\alpha}_{ij} \quad (10)$$

Correspondingly, the stress deviator is composed of an anelastic and a friction part as

$$s_{ij} = s_{ij}^a + s_{ij}^f \quad (11)$$

By using these variables, Levy–Mises type flow relations can now be defined between the corresponding stress and strain rate components:

$$\dot{\epsilon}_{ij} = (3/2)(\dot{\epsilon}/\sigma_f)s_{ij}^f \quad (12)$$

$$\dot{\alpha}_{ij} = (3/2)(\dot{\alpha}/\sigma_a)s_{ij}^a \quad (13)$$

$$\dot{a}_{ij} = (3/2)(\dot{a}/\sigma_a)s_{ij}^a \quad (14)$$

The scalar invariants appearing here are defined in the usual way as

$$\sigma = \sqrt{(3/2)s_{ij}s_{ij}} \quad \dot{\epsilon} = \sqrt{(2/3)\dot{\epsilon}_{ij}\dot{\epsilon}_{ij}} \quad (15, 16)$$

$$\sigma_a = \sqrt{(3/2)s_{ij}^a s_{ij}^a} \quad \dot{\alpha} = \sqrt{(2/3)\dot{\alpha}_{ij}\dot{\alpha}_{ij}} \quad (17, 18)$$

$$\sigma_f = \sqrt{(3/2)s_{ij}^f s_{ij}^f} \quad \dot{a} = \sqrt{(2/3)\dot{a}_{ij}\dot{a}_{ij}} \quad (19, 20)$$

These scalar invariants can be considered as effective stresses and strain rates, and they are postulated to be related by the uniaxial equations (1)–(7) given above.

Even if a plastic equation of state exists for a uniaxial deformation, the extension for the multiaxial case, as presented here, needs separate verification. Experimental results thus far support the existence of the plastic equation of state also in the triaxial formulation.<sup>26</sup>

### 3.3. An Extension of Hart's Model to Transient Deformation

A modification of Hart's model for grain matrix deformation was suggested by Jackson *et al.*<sup>7</sup> in order to allow the description of such phenomena as microplastic yielding and the Bauschinger effect. In the extended model the barrier structure of Hart's model is modified by allowing weaker barriers between the stronger ones as depicted in Fig. 1(b).

A rheological representation of the extended model is given in Fig. 4(b). This model requires two state variables for the stored strain, and thus two anelastic elements ( $a_1, a_2$ ) of different moduli. An additional flow element (microplastic element,  $\dot{\alpha}_2$ ) is incorporated for the penetration of weak barriers. The plastic element ( $\dot{\alpha}_1$ ) and the glide friction element ( $\dot{\epsilon}$ ) are the same as those in Hart's model, while the three elements ( $a_1, a_2, \dot{\alpha}_2$ ) can be viewed as replacing the anelastic element of the Hart model. The  $a_1$  element represents the long-range dislocation pile-ups between the strong barriers (Fig. 1(a)). The short-range pile-ups are represented by the  $a_1$  and  $a_2$  elements acting together, and the microplastic flow is represented by the  $\dot{\alpha}_2$  element.

The constraint equations of the model can be written as

$$\sigma = \sigma_f + \sigma_a = \sigma_f + \sigma_{a1} + \sigma_{a2} \quad (21)$$

and

$$\dot{\epsilon} = \dot{\alpha}_1 + \dot{a}_1 = \dot{\alpha}_1 + \dot{\alpha}_2 + \dot{a}_2 \quad (22)$$

where  $\sigma_{a1}$ ,  $\sigma_{a2}$  and  $\dot{a}_1$ ,  $\dot{a}_2$  are internal stresses and time rates of stored strains for the two anelastic elements. The constitutive relations for the two new anelastic elements are given as<sup>9</sup>

$$\sigma_{a1} = M_1 a_1 \quad (23a)$$

$$\sigma_{a2} = M_2 a_2 \quad (23b)$$

For the microplastic element, experimental results have suggested a flow relation that is of the same form as that for the macroplastic element of Hart's model.<sup>8,15</sup> The constitutive relations for the microplastic elements are

$$\ln(\sigma_2^*/\sigma_{a2}) = (\dot{\epsilon}_2^*/\dot{\alpha}_2)^{\lambda_2} \quad (24)$$

with the scaling relation

$$\dot{\epsilon}_2^* = (\sigma_2^*/G)^{m_2} f_2 \exp(-Q/RT) \quad (25)$$

In these formulas the state variable  $\sigma_2^*$  characterizes the weak barriers, and the other parameters are defined in the same way as those in eqns (4) and (5) with an appropriate subscript. The evolution of  $\sigma_2^*$  with  $\sigma_1^*$  has not yet been specified. For a given strong barrier structure  $\sigma_1^*$ , the value of  $\sigma_2^*$  is expected to vary also with the applied stress. This is because, during for example a tensile loading, the microplastic flow is controlled by successively more resistant weak barriers and the evolution of  $\sigma_2^*$  can therefore be thought of as a sampling effect.<sup>7,15</sup>

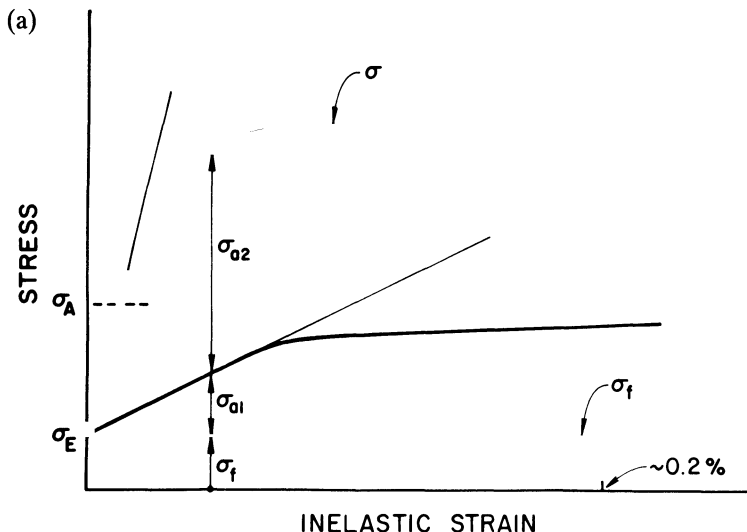


Fig. 5. (a) A schematic stress-strain curve for a constant strain rate tensile test.

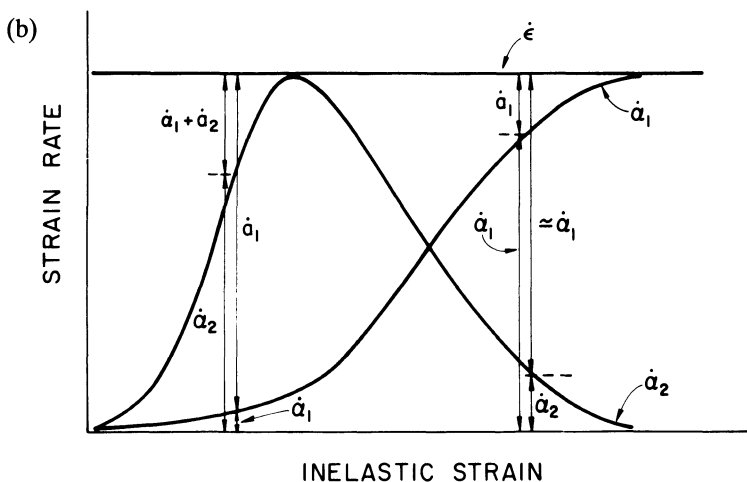


Fig. 5. (b) Strain rates corresponding to the stress-strain curve shown in (a); note that  $\dot{\epsilon} = \dot{a}_1 + \dot{a}_2 = \dot{a}_1 + \dot{a}_2 + \dot{a}_2$ ; after  $\dot{a}_2(\max) = \dot{\epsilon}$  the anelastic strain rate  $\dot{a} \approx 0$ .

The operation of the extended model can be illustrated by the response of a sample initially without any internal stress or stored strain, during a loading, unloading and reversed loading sequence. When the sample is first loaded, dislocation sources between the barriers will be activated and dislocations will start to move forming dislocation pile-ups against the barriers. Dislocation motion, in the absence of any leakage through barriers, contributes only to anelastic strain in the  $a_1$  and  $a_2$  elements. When the applied stress and therefore the internal stress of the pile-ups against the barriers increases, leakage of dislocations through the weak barriers will occur first, resulting in microplastic strain (the  $\dot{\alpha}_2$  element). Dislocation motion over the weak barriers will contribute to the formation of long-range pile-ups against the strong barriers. Finally, as the applied stress is sufficiently increased, leakage of dislocations will occur through strong barriers resulting in macroplastic strain (the  $\dot{\alpha}_1$  element). During unloading the pile-ups are reduced by continued leakage in the forward direction until the back stress becomes larger than the applied stress. When this occurs, dislocations will begin to move backwards (a negative 'effective' stress,  $\sigma - \sigma_{a1} - \sigma_{a2}$ ) contributing to dislocation pile-ups in the opposite direction. At some point during unloading when effective stress (mainly the difference between the applied stress and the back stress of the long-range pile-ups) becomes sufficiently large, we can have leakage of dislocations in the reverse direction (the  $\dot{\alpha}_2$  element). Upon load reversal the applied stress will add to the back stress of the long-range pile-ups, resulting in enhanced microplasticity in the reverse direction. As reverse loading continues, dislocations will move from one side of the zone to the other, sampling the weak barriers and contributing to the formation of the long-range pile-ups against strong barriers, but this time at the opposite side of the zone. Thus, upon load reversal, the residual long-range back stress developed during prior loading will contribute to premature yielding and produce what is known as the Bauschinger effect. The behavior of the model in the microplastic region is illustrated in Fig. 5 which shows schematically the development of different stress and strain rate components during a constant strain rate uniaxial tensile test.

### **3.4. An Extension of the State Variable Description to Grain Boundary Sliding**

an extended deformation model that incorporates the contribution of grain boundary sliding (GBS) can be constructed based on an idea

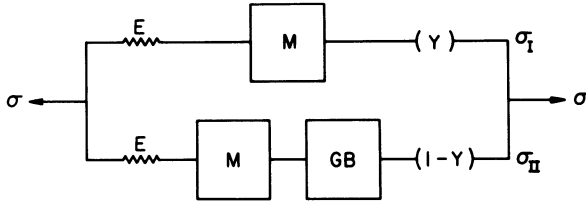


Fig. 6. A rheological diagram of the grain boundary sliding model.

originally proposed by Hart.<sup>20</sup> A schematic representation of the model is shown in Fig. 6, which differs from the one suggested by Hart in the addition of the elastic elements required by the elastic accommodation. In the model, the grain matrix branch (I) operates in parallel with a grain boundary sliding branch (II) consisting of a grain matrix element and a grain boundary element in series. If the proportion of pure grain matrix behavior is denoted by  $Y$ , the constraint equations for overall stress and strain rate become

$$\sigma = Y\sigma_I + (1 - Y)\sigma_{II} \quad (26)$$

$$\dot{\epsilon}_{\text{total}} = \frac{\dot{\sigma}_I}{E} + \dot{\epsilon}_I = \frac{\dot{\sigma}_{II}}{E} + \dot{\epsilon}_{II} + \dot{\epsilon}_g \quad (27)$$

where  $\sigma$  is the applied stress,  $\sigma_I$  and  $\sigma_{II}$  are the stresses and  $\dot{\epsilon}_I$  and  $\dot{\epsilon}_{II}$  are the non-elastic strain rates of grain matrix elements in the upper and lower branches, respectively, and  $\dot{\epsilon}_g$  is the grain boundary sliding rate. The model predicts a sigmoidal  $\log \sigma$  versus  $\log \dot{\epsilon}$  response at a constant plastic state. The contribution of grain boundary sliding is significant only within a certain strain rate range. As discussed previously, above this range grain boundaries are essentially rigid compared with the grain matrix and the flow of the latter dominates. Below this range, grain boundaries are able to slide with very small resistance and the accommodation processes in the grain matrix become rate-limiting. The proportionality factor  $Y$ , which can be viewed as a stress reduction factor, measures the difference in stress between the two limiting behaviors:  $\log Y = \Delta \log \sigma$ . The model reduces to the basic grain matrix deformation model, if no grain boundary shear occurs. The choice and the representation of the grain boundary element have been subject to some uncertainty. For example, Hart<sup>5</sup> has taken the GB element to be an anelastic spring in series with a Newtonian friction element. Because the anelasticity of

the boundary itself is probably very small, the grain boundary element has also often been taken to be a one-component element.<sup>10</sup> In the previous section, it was suggested that, when the segment of grain boundary (Fig. 3) is represented by the grain boundary element, it should exhibit a significant grain matrix character. Thus, two possibilities for the flow equation of the grain boundary element exist:

$$\ln(\sigma_g^*/\sigma_{II}) = (\dot{\epsilon}_g^*/\dot{\epsilon}_g)^{\lambda_g} \quad (28)$$

$$\dot{\epsilon}_g = \dot{a}_g^* \sigma_{II}^{M_g} \quad (29)$$

where the parameters  $\sigma_g^*$ ,  $\dot{\epsilon}_g^*$  and  $\dot{a}_g^*$  have the same meaning as the corresponding parameters of the grain matrix elements, and  $\lambda_g$  and  $M_g$  are material parameters. Even though the definite form of the grain boundary flow law is yet to be determined, experience has shown that both of the two above forms can be used successfully for simulation purposes.

#### 4. THE TYPE OF DATA UTILIZED IN DETERMINING THE MATERIAL PARAMETERS

The demonstration and the application of the present state variable approach require the determination of the various constitutive equations and related material parameters by experiment. In general it has been found that a combination of load relaxation and constant displacement rate tension-compression tests coupled with accurate strain measurement, good temperature control and high-speed digital data acquisition is quite effective. Recent work on stress dip experiments has shown the potential for generating similar type of constant hardness data as the load relaxation test.<sup>14,27</sup>

The key method for establishing the state variable flow equations has been the load relaxation experiment. This experiment allows the determination of the stress-non-elastic strain rate relation of a material at an essentially constant structural state, covering a wide range of strain rates within a short experimental time. The experimental technique involved in the load relaxation test is discussed in detail elsewhere.<sup>9,28,29</sup> Load relaxation testing is usually used in the determination of the value of  $\lambda$ ,  $M$ ,  $f$ ,  $Q$ ,  $m$  and  $\dot{a}$  for Hart's model as well as  $\lambda_2$ ,  $f_2$  and  $m_2$  for the extended model, and  $Y$  for the GBS model. The state variables, such as  $\dot{\epsilon}^*$  and  $\sigma^*$ , are also evaluated based on the

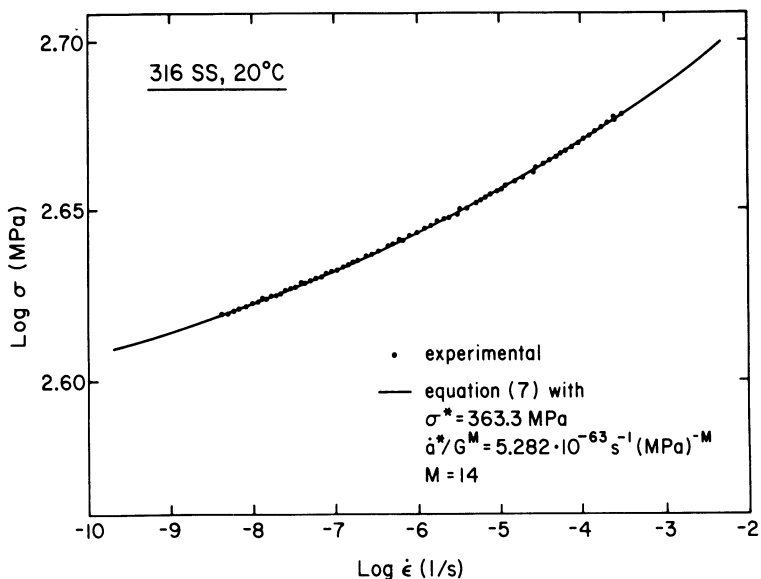


**Fig. 7.** Typical results of load relaxation tests in different flow regimes shown with the proper model fit. (a) Friction stress controlled relaxation ( $\sigma_a \approx \sigma^*$ ).

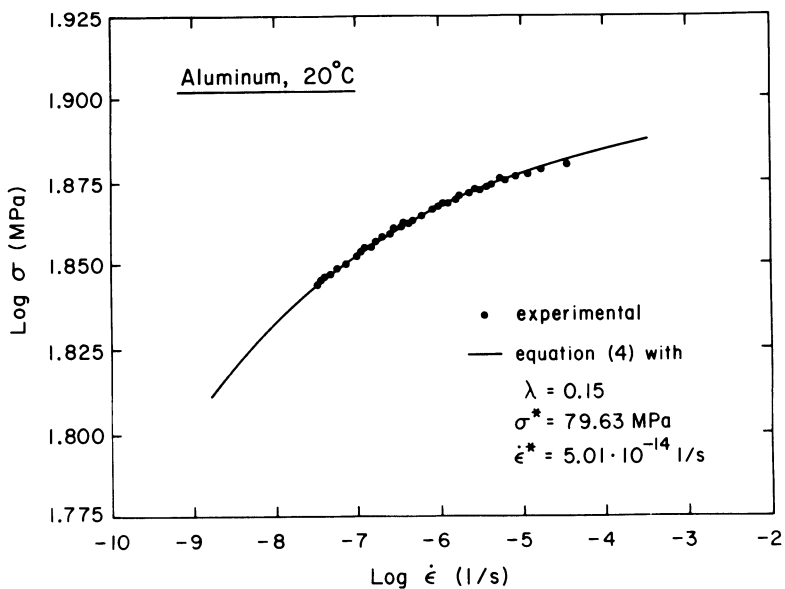


**Fig. 7.** (b) Internal stress controlled relaxation ( $\sigma_f \ll \sigma_a$ ).

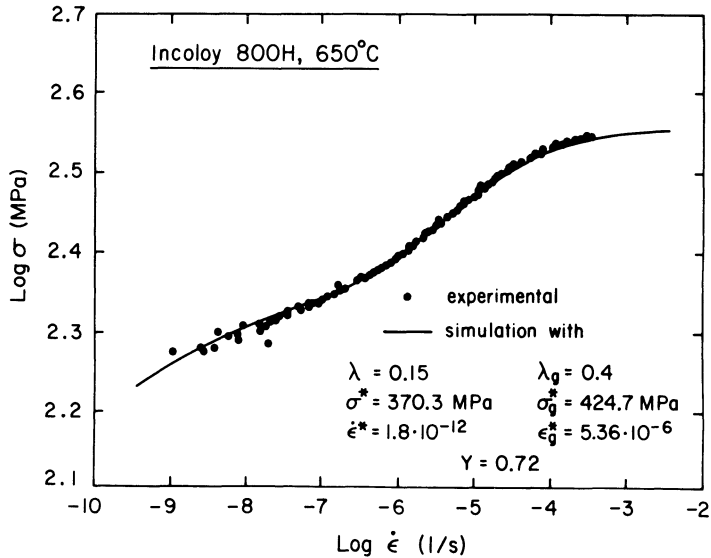
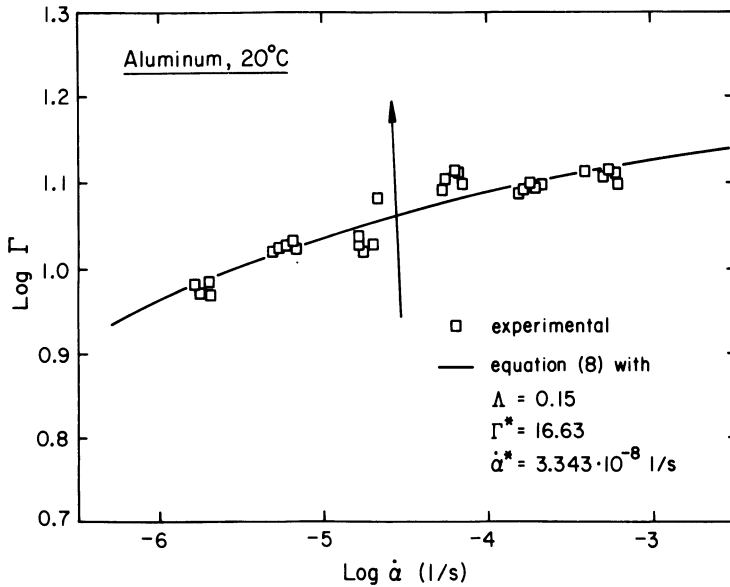


Fig. 7. (c) Internal stress and grain boundary sliding controlled relaxation.

load relaxation data. Typical results from load relaxation tests which exhibit friction stress, internal stress and GB sliding controlled behavior are shown together with the model fit in Fig. 7 (a, b and c, respectively).

Extensive use has been made also of the conventional constant displacement rate experiment.<sup>8,15,23,30</sup> This type of test has been utilized for determining the work-hardening parameters as well as the anelastic moduli for Hart's model and the extended grain matrix model. Figure 8(a) shows the relation between the work-hardening coefficient ( $\Gamma$ ) and the plastic strain rate ( $\dot{\alpha}$ ) in aluminum as deduced from constant displacement rate tests together with the model fit (eqn (8)), and Fig. 8(b) shows a cyclic loop, which has been modeled by using the extension of the basic model. The stress concentration factor  $Y$  for the GBS model can also be measured in a constant displacement rate test.<sup>11</sup>

A recent analysis of the results of a stress dip experiment has suggested the usefulness of this type of experimental method for producing the constant hardness stress-non-elastic strain rate data and transient deformation data.<sup>14</sup> This is especially true at high temperatures, where the effects of thermally induced structural changes impose



**Fig. 8. (a)** Strain rate dependence of the absolute work-hardening coefficient in aluminum at a constant plastic state; shown is a master curve, which has been constructed by translating the data of different plastic states given in reference 23 onto the curve for which  $\sigma^*$  is 38.3 MPa.

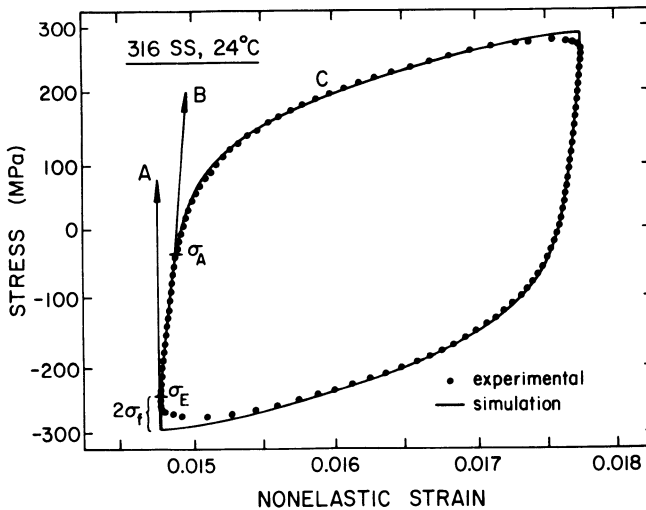


**Fig. 8. (b)** Stress–non-elastic strain data for type 316 stainless steel obtained in a constant displacement rate tension–compression cycle with crosshead speed of 0.5 mm/min; the solid line represents simulation by using the model shown in Fig. 4(b);<sup>8</sup>  $\sigma_E$  is the onset of elastic deformation and  $\sigma_A$  is the onset of microplastic deformation.

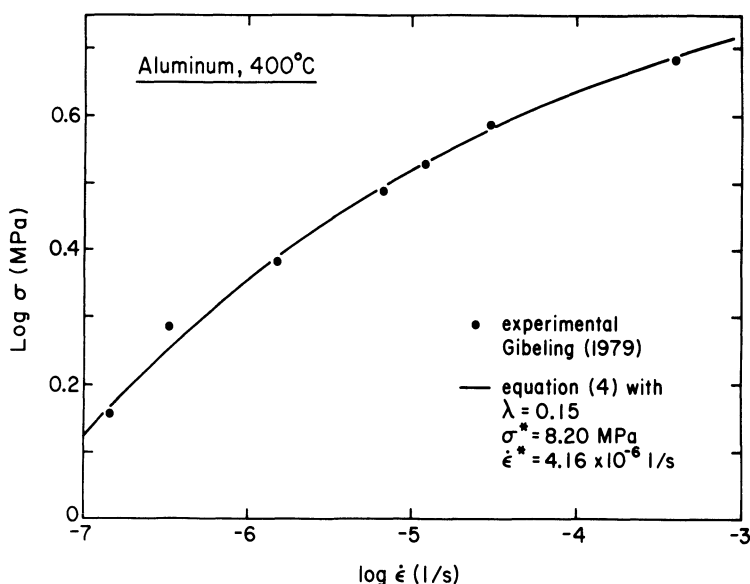


**Fig. 9.** Stress vs. isostructural strain rate obtained in stress dip tests for aluminum by Gibeling;<sup>27</sup> the solid curve is based on eqn (4).<sup>14</sup>

a severe limitation to the applicability of the data from load relaxation experiments. Figure 9 shows an example of stress–strain rate data obtained at 400°C in stress dip tests for aluminum together with the fit by eqn (4).

A detailed description of the methods used for obtaining the material parameters for the state variable approach, by using results of tensile and load relaxation tests, is given in Appendix 1.

## 5. MATERIALS TESTED

The present state variable approach has been applied and tested in a variety of materials. The bulk of these investigations has been aimed to test the concept of a mechanical equation of state and to determine the values of the parameters for the basic grain matrix model. Metals and alloys investigated have included aluminum,<sup>3,15</sup> lead,<sup>31</sup> nickel,<sup>26,32,33</sup> niobium,<sup>34</sup>  $\alpha$ -iron,<sup>34</sup> titanium,<sup>35</sup> TD-nickel,<sup>32</sup> OFHC-copper,<sup>23</sup> 1100 aluminum alloy,<sup>36</sup> type 304 and 316 stainless steels,<sup>12,37–39</sup> Zircaloy-2,<sup>40,41</sup> Zircaloy-4,<sup>41–44</sup> a Cr–Mo–V steel,<sup>45</sup> Incoloy 800H,<sup>46</sup>

and a superplastic superalloy.<sup>47</sup> Among the other materials tested are a metallic glass,<sup>48</sup>  $\text{UO}_2$ ,<sup>49</sup>  $\text{NaCl}$ ,<sup>50,51</sup>  $\text{LiF}$ ,<sup>50</sup>  $\text{KI}$ ,<sup>50</sup>  $\text{AgCl}$ ,<sup>52</sup> and  $\text{NaF}$ .<sup>50</sup> Information on some of the materials for which the data base is largest has been gathered in Tables 1–3.

Experimental work on the transient and grain boundary models has not been as extensive as in the case of the basic grain matrix model. Transient deformation has been studied mainly on aluminum<sup>15</sup> and 316 stainless steel,<sup>8</sup> and grain boundary sliding data have been gathered on nickel,<sup>11</sup> aluminum,<sup>36</sup> 316 type stainless steel,<sup>10</sup> and Incoloy 800H alloy.<sup>46</sup> For these data the reader is referred to the original literature.

## 6. SIMULATIVE AND PREDICTIVE POWERS OF THE STATE VARIABLE APPROACH

The flow equations of the state variable models can be integrated with time along any specified loading path. As an example, a schematic algorithm for uniaxial loading modeled by Hart's original model is described below. Usually consideration of two basic loading types will suffice:

*Creep under constant load.* From the constancy of load it follows that

$$\dot{\sigma} = \sigma \dot{\epsilon} \quad (30)$$

A special case of the above is creep under constant stress, i.e.

$$\dot{\sigma} = 0 \quad (31)$$

*Constant extension/compression rate ( $\dot{x}$ ) test.* The strain rate balance describes the loading path as

$$\dot{\sigma} = E_{\text{eff}}(\dot{x}/l - \dot{\epsilon}) \quad (32)$$

where  $l$  is the inelastic length of the specimen and  $E_{\text{eff}}$  stands for the effective modulus of the loading train and specimen. Note that the load relaxation test is specified by  $\dot{x} = 0$ . A special case is testing under constant non-elastic strain rate where  $\dot{\sigma}_f = 0$ , whence by the relation (2)

$$\dot{\sigma} = \dot{\sigma}_a \quad (33)$$

A more general loading case may often be approximated by a piecewise collection of the above conditions.

### 6.1. Schematic Description of the Flow Chart

A schematic and simplified numerical integration routine detailed elsewhere<sup>12,53</sup> is described below.

- (0) Initialize program
  - give material constants and technological parameters
  - give the initial values of internal state variables  $\sigma^*$ ,  $\sigma_a$  and the non-elastic strain  $\epsilon$  at start
  - specify loading type and give the initial applied stress  $\sigma$
- (1) Calculate rates
  - calculate strain rates  $\dot{\epsilon}$ ,  $\dot{\alpha}$  and  $\dot{a}$  by using relations (1), (4) and (7)
  - calculate stress rates  $\dot{\sigma}^*$ ,  $\dot{\sigma}_a$  and  $\dot{\sigma}$  by using relations (3), (6) and an appropriate loading condition of (30)–(33)
- (2) Integrate stress variables and non-elastic strain
  - determine the time increment to be used (to be considered below in detail)
  - calculate new values of the primary stress variables and inelastic strain (new value = old value + rate  $\times$  time increment)
  - all the other variables can now be calculated based on this basic set
  - go to (1) to calculate new rates

The time increment ( $\Delta t$ ) is generally selected by optimizing the mutually contradictory requirements of fast integration and high accuracy. The Euler strategy accomplishes this in a most simple fashion, while yielding practically the same effectiveness as more elaborate methods.<sup>12,53</sup> In this method, the new values of state variables are predicted by using the present and previous rates of the variables in question; if the predictions differ by more than a predetermined limit (e.g. 0.1%) the time step will be decreased, and if they agree to better than another predetermined limit (e.g. 0.01%) the time step will accordingly be increased.

To implement the integration scheme described above a computer code written in Basic language is given in Appendix 2. Any piecewise sequence of creep and tensile/compressive loadings can be specified as

**TABLE 1**  
Parameters for the Friction Element

Material	Temperature (°C)	$M$	$\mu$	$\dot{a}^*$ (1/s)	$\mathcal{M}$ (GPa)	Ref.	Comments
316 SS	RT	$18.5 \pm 3.5$	0.093			34	Sol. ann. (1100°C) Gupta and Li method <sup>22</sup>
316 SS	RT		0.14			80	Sol. ann. (1025°C)
316 SS	RT		0.6			80	Cold-worked (20%)
316 SS	RT		0.13	181.0 <sup>a</sup>		38	Sol. ann. (1200°C)
	150			120.7 <sup>a</sup>			<sup>a</sup> $G\dot{a}^{*-M}$ (MPa s <sup>-M</sup> ) $M = 1/\mu$
	200			95.7 <sup>a</sup>			
	300			53.1 <sup>a</sup>			
	400			23.6 <sup>a</sup>			
	500			3.5 <sup>a</sup>			
316 SS	RT	$14.1 \pm 0.8$		$1 \times 10^{37}$ $-3 \times 10^{33}$		39	Sol. ann. (1200°C) $\epsilon = 1-30\%$
304 SS	RT	15.3	0.101			34	Sol. ann. (1100°C) Gupta and Li method <sup>22</sup>
	RT	$15.5 \pm 1.7$	0.130				Sol. ann. (1100°C) + prestrained (5%) + ann. (850°C)
304 SS	RT	7.8 <sup>b</sup>		$1.6 \times 10^{22}$	100.7	12	Stabil.; <sup>b</sup> Based on scaling $\epsilon = 1.5-4.3\%$

	100	7.8 <sup>b</sup>				99.3	$\epsilon = 5.7-9.6\%$
	200	7.8 <sup>b</sup>		$1.0 \times 10^{23}$		97.2	$\epsilon = 9.9-12.1\%$
	300	7.8 <sup>b</sup>		$2.4 \times 10^{24}$		93.4	$\epsilon = 10.3-13.2\%$
	400	7.8 <sup>b</sup>		$1.8 \times 10^{24}$		91.0	$\epsilon = 15.4-17.1\%$
	500	7.8 <sup>b</sup>		$6.9 \times 10^{24}$		83.1	$\epsilon = 12.6-14.4\%$
Zircaloy-2	200		0.125	$1.6 \times 10^{28}$	616	40	$\epsilon = 0.3-4.9\%$
Zircaloy-2	375	7.8 <sup>c</sup>		$5-9.5 \times 10^{26}$	221	81	$\epsilon = 1-6\%$
Zircaloy-4	375	7.8 <sup>d</sup>		$1.9 \times 10^{36}$	221	81	<sup>c</sup> Selected $\epsilon = 1-8\%$
Zircaloy-4	200	8		272.7 <sup>e</sup>		42	<sup>d</sup> Selected <sup>e</sup> $G\dot{\epsilon}^{*M}$ (MPa s <sup>-M</sup> ) $\epsilon = 3.8-7.5\%$
	300	8		116.4 <sup>e</sup>			$\epsilon = 6.3-11.5\%$
	350	8		64.3			$\epsilon = 6.8-8.7\%$
	400	8		16.1			$\epsilon = 5.1-7.0\%$
Niobium (99.999%)	RT	8.8 ± 1.5	0.14			34	Gupta and Li method <sup>22</sup>
Niobium (99.9%)	RT	6.6 ± 0.5	0.12			34	Gupta and Li method <sup>22</sup>
$\alpha$ -Iron (decarb.)	RT	2.9 ± 0.7	0.83			34	Gupta and Li method <sup>22</sup>
Nickel 200	RT	11			8.46 ± 0.2	26	Tension-torsion test
LiF	RT	5.0	0.2			50	

**TABLE 2**  
Parameters for the Plastic Element

Material	Temperature (°C)	<i>m</i>	<i>λ</i>	$f \exp(-Q/RT)$ (1/s)	Ref.	Comments
Zircaloy-2	375	5.73	0.15	496 <sup>a</sup>	81	<sup>a</sup> Depends on $\dot{\epsilon}$ $\dot{\epsilon} = 5 \times 10^{-3} \text{ min}^{-1}$ $\dot{\epsilon} = 5 \times 10^{-4} \text{ min}^{-1}$ $\dot{\epsilon} = 5 \times 10^{-5} \text{ min}^{-1}$ $\dot{\epsilon} = 5 \times 10^{-4} \text{ min}^{-1}$
Zircaloy-4	375	3.25	0.15	313	81	Stress-relieved
Zircaloy-4	400	1.02	0.28	132 1.52 $6 \times 10^{-13} \times G^m$	43	at 500°C; tested in bending
	400	2.70	0.096	$1.94 \times 10^{-13} \times G^m$	43	Cold-worked; tested in bending
1100 Al	250	5	0.11	$5.62 \times 10^{-6} \times G^m$	36	$Q = 33.5 \text{ kcal/mol}$
Aluminum (99.99%)	RT	7.53– 8.41 <sup>b</sup>	0.15	$6.12 \times 10^{-49} \times G^m$ $-1.70 \times 10^{-43} \times G^{m_2}$	15	<sup>b</sup> Depends on grain size
	100	4.79	0.15	$1.60 \times 10^{-30} \times G^m$		
	170	1.31	0.15	$3.57 \times 10^{-15} \times G^m$		
Aluminum (99.9995%)	RT	4.38	0.15	$1.16 \times 10^{-28} \times G^m$	15	

Aluminum (99.995%)	RT	4.6 ± 0.25	3
Lead (comm. pur.)	RT	3.85 ± 0.5	31
Cr-Mo-V steel	538	not a const.	45 <sup>c</sup> Or lower
UO	1400	18.5	49 Grain size = 8 μm
	1500	9.4	Grain size = 31 μm
	1700	7.9	Grain size = 31 μm
AgCl (nom. pur.)	RT	1.73	52 [100] single crystal; compr. As above + γ-irradiated
	RT	1.40	0.2
NaCl (opt. pur.)	RT	5.3	51 As above
LiF (opt. pur.)	200	5.0	50 [100] single crystal; compr.
KI (high pur.)	RT	5.0	50 As above

**TABLE 3**  
Parameters for the Work-hardening Equation

Material	Temperature (°C)	$A(\beta)$ (MPa)	$B(\delta)$	$\sigma_0^*$ (MPa)	$\dot{\alpha}^*$ (1/s)	$\Lambda$	Ref.	Comments
316 SS	RT	1034	1	124			23	Sol. ann. (1200°C) $\epsilon = 1-20\%$
Aluminum (comm. pur.)	RT	80	3.5	0	$7 \times 10^{-8a}$	0.15 <sup>b</sup>	23	$\epsilon = 1-12\%$ <sup>a</sup> Approx. const. <sup>b</sup> Or higher
Copper (OFHC)	RT	570	1.6	0	$10^{-6}-10^{-13c}$	0.15	23	$\epsilon = 1-22\%$ <sup>c</sup> Depends on $\sigma^*$
304 SS	RT	1450	1.33				12	Stabilized $\epsilon = 0-5\%$
	300	1300	1.33					$\epsilon = 0-5\%$
	400	1230	1.33					$\epsilon = 0-5\%$
	500	1180	1.33					$\epsilon = 0-5\%$
Aluminum (99.99%)	RT	88.3	3.4				15	$\epsilon = 0-5\%$
Aluminum (99.9995%)	RT	103.4	2.8				15	
Zircaloy-2	375	359	5.55				81	
Zircaloy-4	375	556	56.3				81	

a loading path. Numerical problems in integration may arise; particularly in tensile loading at relatively high strain rates, when  $\sigma_a$  approaches  $\sigma^*$ ,<sup>12,53-55</sup> or near steady-state deformation, when  $\dot{\alpha} = 0$ .<sup>56</sup> Means to deal with the integration problems are discussed in the references cited above; an example is provided in the computer code given in Appendix 2 (lines 2020 to 2060).

A corresponding computer code written in Fortran language, and including 'viscoplastic' approximation to offset the difficulties in integration, can be found from reference 12. More sophisticated computer programs for the cases when microplasticity or grain boundary sliding has to be accounted for have been developed at Cornell University, from where they can be obtained. Large and general multi-purpose computer codes for solving multiaxial stress-strain histories in structural members by the application of FEM and BEM are currently being developed and tested at Cornell. These codes have been applied to several metal-forming problems of technological interest as described below.

## 6.2. Simulations

With a sufficient number of adjustable parameters it is possible, of course, to simulate any desired data of interest. However, in the present state variable approach the number of model parameters has been limited to a practical minimum; moreover, each parameter has more or less distinct physical significance.

Simulation of the data used to generate the model parameters reproduces the original deformation behavior to a high degree of accuracy. As an example, Fig. 7(a-c) shows the experimentally determined points of load relaxation behavior of three different materials, with the simulated behavior indicated by the solid curves. Figure 7(a) depicts the load relaxation behavior of 316 SS at room temperature, which represents a relatively low homologous temperature for stainless steel, while Fig. 7(b) displays the high homologous temperature behavior of pure aluminum at room temperature. Figure 7(c) gives an example of grain boundary sliding intervening in the grain matrix load relaxation in Incoloy 800H at 650°C.<sup>45</sup> Figure 8(a) gives the simulated and observed dependence of the absolute work-hardening coefficient  $\Gamma$  of aluminum on the strain rate at room temperature; the data are from a recent study on work-hardening properties of aluminum, copper and 316 SS.<sup>23</sup> Cyclic loops in the microplastic deformation regime, as shown in Fig. 8(b) with the

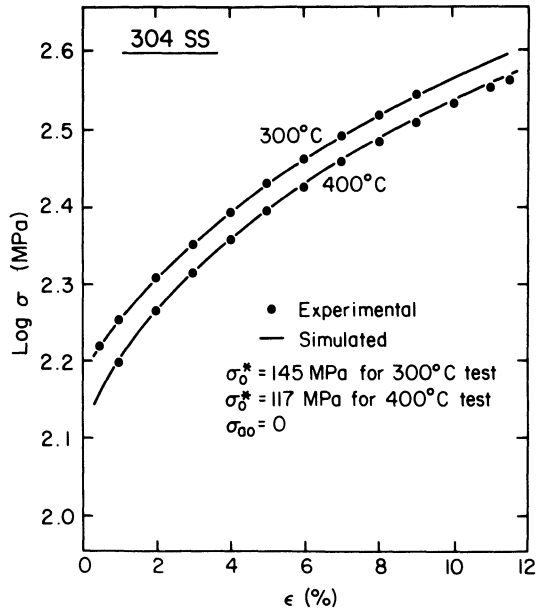


**Fig. 10.** Measured and simulated constant extension rate tensile test curves for stabilized type 304 stainless steel at 300°C and 400°C.<sup>12</sup>

experimental points and the simulated behavior indicated, may advantageously be used for the determination of the anelastic properties of the material, 316 SS in this case, as discussed in Appendix 1. A comprehensive account on tensile test simulations of nickel and 304 SS can be found in reference 12; Fig. 10 here reproduces the observed and simulated results for a tensile test on 304 SS at 300°C and 400°C.

The boundary between simulation and prediction appears somewhat ill-defined. What now is counted as simulation could be considered as a prediction from another point of view, e.g. when some model parameters are obtained by independent means. Further, many predictions to be discussed below are rather qualitative than quantitative in nature, the important point being that the model is able to predict deformation phenomena that were not in mind when constructing the model.

### 6.3. Predictions

Because the model parameters are determined by tensile and relaxation testing, modeling of creep behavior can genuinely be counted as

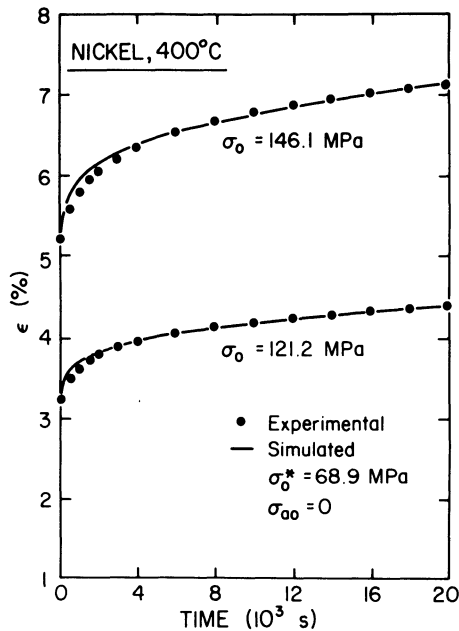


**Fig. 11.** Measured and simulated constant load creep curves for annealed nickel at 400°C;  $\sigma_0$  is the initial stress level.<sup>12</sup>

prediction. A comprehensive account of creep predictions for 304 SS and nickel at several temperatures and under a variety of loads is given in reference 12, from which Fig. 11 displays an example of constant load creep curves on nickel at 400°C. Some other creep predictions as compared to actual tests may be found elsewhere.<sup>57</sup>

The models are capable also of predicting the transients in load relaxation and creep testing. Figure 12 depicts an anelastic/microplastic reloading transient in repeated load relaxation tests,<sup>13</sup> while Fig. 13 shows the back-flow behavior in creep recovery experiments.<sup>14</sup> Particularly important is that the basic Hart model predicts that, after a stress dip during a steady state, a new isostructural strain rate at the reduced stress level is determined by the flow equation (4) in the absence of structural recovery. This prediction has recently been confirmed on several metals at several temperatures.<sup>14</sup>

Hart's basic model in its triaxial form has been extensively applied to the study of a variety of metal-forming problems by using FEM or BEM computer codes for the structural elements. By using the Hart

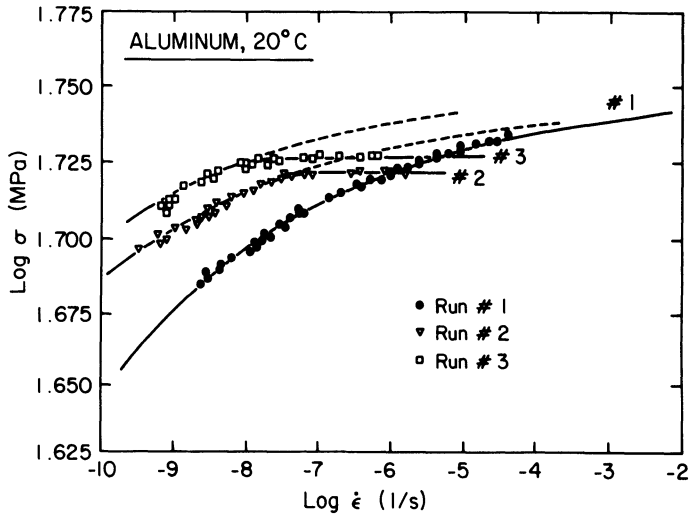


**Fig. 12.** Experimental and simulated stress relaxation runs in commercially pure aluminum after 4.5% of plastic strain: 1, after the initial plastic loading; 2 and 3, after elastic/anelastic reloadings to a stress level below the initial one in the first relaxation.<sup>13</sup>

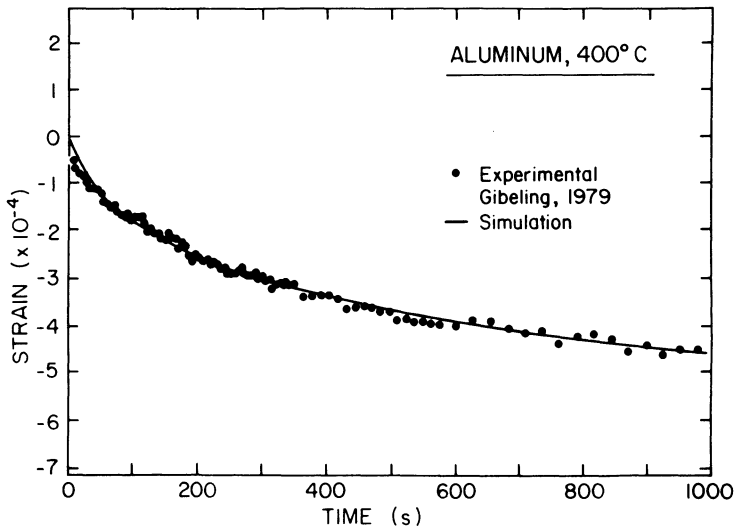


**Fig. 13.** Measured<sup>27</sup> and simulated<sup>14</sup> strain vs. time behavior in a creep recovery test of aluminum.

model a complete stress and deformation history can be determined even in very large strain applications, as contrasted to the usual rigid-plastic approaches.<sup>58</sup> Particularly, the knowledge of residual stresses, obtained by using Hart's model, may be of crucial importance, because these localize the plastic flow and thus increase the danger of crack initiation and growth.

As of now, a large number of general plane stress and plane strain problems have been analyzed, including studies of stress concentrations in geometric discontinuities of plates<sup>58</sup> and a modeling of extrusion in very nearly actual conditions.<sup>59</sup> Some further studies include analysis of the torsion deformation of prismatic shafts of different shapes<sup>60</sup> and bending of plates of arbitrary shape and by using a variety of boundary conditions.<sup>61</sup> These calculations have been able to predict the essential features of the experimental observations very satisfactorily, where comparisons with experiment have been possible.

The state variable model has been tentatively applied in the field of practical engineering, particularly in the nuclear power generating industry, with promising results.<sup>25,57,62,63,64</sup> For engineering applications, however, it may be difficult to use the full models shown in Figs 4 and 6. On the other hand, often some branch of the model can be neglected in comparison with the others, and effective values of material parameters may be used to compensate the resulting inaccuracy in the possibly limited temperature and/or strain rate range of interest. For example, an effective value of the exponent  $\lambda$  in eqn (4) may take some grain boundary sliding into account in addition to grain matrix deformation. Similarly, an effective modulus in eqn (3) may be used to describe grain boundary anelasticity in addition to the matrix anelasticity at elevated temperatures.

An analysis of non-elastic deformation of thin-walled cladding tubes of 20 cold-worked 316 SS under a variety of thermal and mechanical loads at elevated temperatures has been described.<sup>25</sup> The temperature range of the experiment was such that thermal recovery and recrystallization had to be accounted for by the  $\mathcal{R}$  term in eqn (6). The yield stress of the tube material is shown as a function of time at different temperatures in Fig. 14, where it is seen that at 649°C thermal recovery occurred as a function of time, while at higher temperatures recrystallization dominated. Since the yield stress at moderate strain rates at high homologous temperatures is a good approximation for  $\sigma^*$ , the data of Fig. 14 can be used to construct an empirical relation for  $\mathcal{R}(\sigma^*, T)$  for modeling purposes. Of particular interest are the

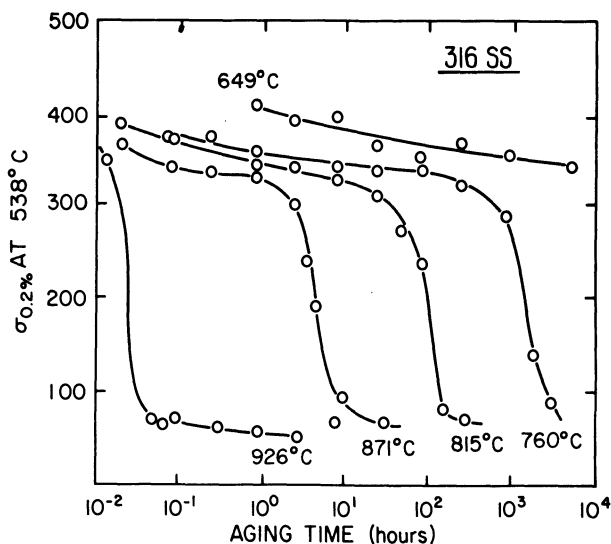


**Fig. 14.** Yield stress vs. time at several temperatures for 20% cold-worked type 316 stainless steel.<sup>25</sup>

data shown in Fig. 15 obtained in a rapid temperature transient experiment, while keeping the internal pressure of the tube constant. The low-strain portion of the data is indicative of anelastic deformation while the high-strain portion reflects the effect of plastic deformation.

The present state variable approach has also been applied to estimate the irradiation effects on materials parameters, and both the flux and the fluence effects have been considered.<sup>57,64,65</sup> However, these studies, as well as some mentioned above, have given qualitative rather than quantitative predictions, because either the initial conditions are not known accurately enough or the behavior depends critically on the values of material parameters, known only to a limited accuracy from load relaxation and tensile testing, or both.

A further example of this kind of qualitative prediction is the axial elongation that accompanies torsion, owing to the rotation of crystallites.<sup>26,66</sup> After adjusting the anelastic modulus the fit to the experimental data was remarkably good.

As a final engineering application, the prediction of creep rupture times based on eqn (4) may turn out to be of significant technological

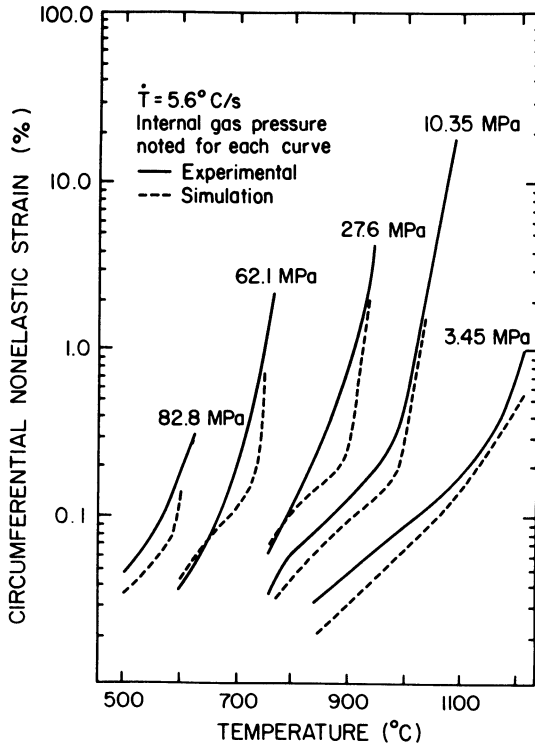


**Fig. 15.** Measured and simulated behavior of thin-walled tubes in a temperature change experiment at several internal gas pressures.<sup>25</sup>

importance.<sup>67-69</sup> By estimating that the plastic strain rate is given by the rupture strain divided by the rupture time, or  $\dot{\alpha} = \alpha_r/t_r$ , it is seen that eqn (4) connects rupture time to the applied stress and temperature (through  $\dot{\epsilon}^*$ ), if the rupture strain can be considered as a constant. Because rupture of engineering interest usually occurs as a result of extensive grain boundary cavitation, which accumulates monotonously with strain owing to grain boundary sliding, it can be argued that the amount of cavitation, leading to rupture, corresponds to a certain straining. The experimental results on 2-25Cr-1Mo steels seem to confirm this expectation.<sup>68</sup>

Finally, it should be noted that the predictive powers of the present state variable approach remain to be fully explored.

## 7. DISCUSSION

The state variable approach described in this paper represents a unified description of a variety of deformation phenomena in a wide temperature regime. As discussed above, it has been successfully used to model such phenomena as tensile deformation, load relaxation, cyclic loops and creep behavior, as well as transients in load relaxation and creep tests that had traditionally been held separate. In the following, some most important general capabilities of the model are discussed and some limitations of the model will be considered. Finally, the discussion addresses possible extensions to cover an even wider range of deformation or deformation-related phenomena.

### 7.1. The Components of the Flow Stress

The two components of flow stress ( $\sigma_a$  and  $\sigma_f$ ) in the present state variable formulation can both be seen to depend on temperature and strain rate. The hardness parameter  $\sigma^*$ , however, can be viewed as a temperature independent parameter when normalized by the shear modulus, even though the evolution of the hardness may be thermally activated. The athermal limit of the internal stress is realized at low temperatures or at high strain rates. When the internal stress approaches the hardness of the barrier structure  $\sigma^*$ , the barrier penetration occurs mechanically without any essential thermal activation; the hardness is therefore related to the mechanical threshold stress used by Kocks.<sup>70</sup>

The other component of the flow stress, the friction stress  $\sigma_f$ , according to eqn (7) is represented by

$$\sigma_f/G = \dot{a}^{*-1/M} \dot{\epsilon}^{1/M} \quad (34)$$

The significance of the rate parameter  $\dot{a}^*$  may be traced by comparing the phenomenological equation (7) to that proposed by Li and co-workers on physical grounds.<sup>22</sup> The parameter  $\dot{a}^*$  can be interpreted as consisting of two components: (i) the number of mobile dislocations, and (ii) the mobility of these dislocations. An increasing strain rate and decreasing temperature thus tend to cause an increase in the friction stress.

The internal stress component of the flow stress,  $\sigma_a$ , can be viewed through eqn (4) as a product of an athermal hardness  $\sigma^*$  and a temperature and strain rate sensitive part such that

$$\sigma_a = \sigma^* \exp[-(\dot{\epsilon}^*/\dot{\alpha})^\lambda] \quad (35)$$

where the temperature and structure dependence of the rate parameter is given by eqn (5). The mechanisms responsible for the reduction of  $\sigma_a$  with increasing temperature or decreasing strain rate evidently involve such thermally assisted processes as cross-slip and intersection of dislocations and climb. It is experimentally found that the activation energy in eqn (5) at higher temperatures closely corresponds to the activation energy for self-diffusion,<sup>36,38</sup> suggesting the importance of vacancy motion as a rate-controlling mechanism. The above processes are intimately connected to dynamic recovery processes, here to be understood in a strict sense, i.e. as processes which can take place only with simultaneously occurring deformation. Of course, at higher temperatures  $\sigma_a$  can change, and  $\sigma^*$  correspondingly decrease, due to intervening static recovery, proceeding with time.

The flow stress component  $\sigma_a$  was depicted in Fig. 2 as a function of the strain rate. Actually, the temperature can be traded for strain rate according to eqns (4) and (5). By using the notion of an effective strain rate defined as

$$\dot{\epsilon}_{\text{eff}} = \dot{\epsilon} \exp(Q/RT) \quad (36)$$

the physically equivalent combinations of  $(T, \dot{\epsilon})$  can be found. With the aid of this the internal stress part of Fig. 2 can be converted from strain rate dependence of stress into temperature dependence of stress. In fact, plotting  $\sigma_a$  as a function of  $\ln \dot{\epsilon}$  and  $1/T$  produces essentially identical results, apart from a constant scale factor. It is thus seen that the state variable theory reproduces the commonly accepted temperature dependence of the flow stress when friction effects are absent as, for example, in high-temperature creep.

So the whole of Fig. 2 will retain the same general shape irrespective of the change of the argument from  $\ln \dot{\epsilon}$  to  $1/T$ . Strictly, this applies for pure metals only. Owing to strain aging and related effects in the presence of solutes,  $\dot{a}^*$  may actually decrease with increasing temperature. This effect may result in a very pronounced 'athermal' plateau for the flow stress as a function of temperature.

## 7.2. Work-hardening

The evolution of the hardness parameter  $\sigma^*$  with deformation is described by the work-hardening function given by eqn (8). Similarly to another work-hardening theory<sup>71</sup> it separates the athermal and thermal contributions of work-hardening from each other. However,

in the present state variable approach, it is possible to determine them both experimentally.<sup>23</sup> If the form of the work-hardening relation given by eqn (8) turns out to have general applicability it would have several important implications. First, it shows that the strain rate independent part of the work-hardening coefficient is not necessarily constant (i.e. generally  $B \neq 1$  in eqn (9)<sup>23</sup>), suggesting that essentially mechanical annihilation of dislocations occurs at high  $\sigma^*$  levels. Secondly, the strain dependent part of work-hardening occurs in the same temperature range where the strain rate dependence of the internal stress is strong and both the absolute work-hardening coefficient and the flow stress are related to the strain rate at a given plastic state and temperature in the same functional form (eqns (4) and (8)). This latter correspondence suggests that the same leakage processes of dislocations through barriers are involved in plastic flow ( $\dot{\alpha}$ ) and in dynamic recovery which governs the rate dependence of  $\Gamma$ .

An athermal work-hardening ( $\Gamma^*$ ) occurs in the region where the strain rates are high or the temperature is low, which corresponds to  $\dot{\alpha} \gg \dot{\alpha}^*$  in eqn (8). This is the temperature region where glide friction is dominating the temperature dependence of flow stress, i.e. at temperatures below the 'athermal' plateau. In certain materials, such as for example stainless steels, this region may extend well above room temperature at ordinary strain rates ( $\sim 10^{-3}$  l/s). The thermally activated reduction in the absolute work-hardening rate at high temperatures and low strain rates is viewed as a result of the operation of dynamic recovery processes during deformation as discussed above.

It is reasonable to take the view that the empirical relation on the athermal work-hardening in a polycrystalline solid (eqn (9)) should generally be applicable to  $\Gamma^*$ . However, the theoretical development of strain rate dependence of  $\Gamma$  (eqn (8)) will have to proceed in parallel with that for the flow equation for the plastic element (eqn (4)).

### 7.3. Limitations of the Present State Variable Approach

The state variable theory addresses essentially homogeneous non-elastic deformation of a single-phase isotropic crystalline solid, and the experimental work performed thus far falls mainly in this category. Based on the evidence described above, the validity of the state variable approach serves as a test for the existence of homogeneous deformation. Because of the very nature of the state variable theory, it seems that such local plastic instabilities as discontinuous yielding will

be difficult if not impossible to treat. However, the other constraints mentioned above may be relaxed to a certain extent.

Experimental work with amorphous solids<sup>48</sup> has given some promise as to possible extension of the modeling capability beyond crystalline materials. A generalization for a case of crystalline anisotropy has been described by Hart.<sup>5</sup> The present model may also be capable of dealing with some multiphase effects, provided that the contribution of the other phase to the mechanical properties is not too strong. A softer, matrix embedded phase may be considered as represented by the microplastic element, while inclusions harder than the matrix mainly enhance anelasticity and strain hardening by the production of the geometrically necessary dislocations to offset the compatibility strains.

Larger quantities of another phase might be dealt with in analogy to the GBS model, Fig. 6. A soft phase in a hard matrix could readily be modeled by replacing the 'grain boundary phase' of Fig. 3 by the matrix element of the soft phase. Reinforcement of the matrix by a harder phase could be modeled by the same GBS model, but now the hard phase would take the part of the former grain matrix, while the matrix itself would play the role of the former soft phase or grain boundary phase. A more general way to model multiphase effects would be to use a parallel or series model or some combination of these, of which the GBS model is but one example.

#### 7.4. Future Developments

Rate effects of deformation, particularly those due to solutes, constitute a key area where theoretical development is required. The rate effects are most likely to be seen first in the rate parameter  $\dot{a}^*$ , describing the density of mobile dislocations and their ability to move. For example, some strain aging effects during load relaxation might be modeled by time (or rate) dependent changes in  $\dot{a}^*$ . There are some indications also that the stress exponent  $M$  may be sensitive to solute effects.<sup>22</sup> Gilman has suggested that a large  $M$  is connected to dislocation generation by overcoming point defects, while small  $M$  is associated with the nucleation of dislocation segments resisted mainly by the Peierls potential besides the line tension.<sup>72</sup> The possibility of including some strain aging effects in the model is presently being investigated.

Another subject which is not yet described by the model is that of cyclic softening. According to the microplastic state variable descrip-

tion, the Bauschinger effect arises solely from residual stresses assisting back-flow. However, it is a widely recognized fact that during cyclic loading and creep fatigue interaction there arises real structural softening, as evidenced, for example, by the enhanced creep rate after partial unloading during creep.<sup>73,74</sup> From a micromechanical point of view it appears quite reasonable that formerly forward moving dislocations may during back-flow partially annihilate structural dislocations, which were effective barriers for the forward but not the backward flow. Because of the permanent nature of the structural softening, as seen e.g. in creep acceleration, it is evident that the hardness  $\sigma^*$  must decrease during back-flow. This feature can be modeled by a suitable change of the evolution law, eqn (8). Thus, although  $\sigma^*$  remains as an isotropic parameter, its evolution would depend on the direction of straining with respect to the internal stress state.

The role of grain boundary sliding in non-elastic deformation involves two types of problems. The first problem concerns the compatibility between grain boundary sliding and grain matrix deformation. This question has been addressed in a series of theoretical papers.<sup>21,75,76</sup> They all predict about the same value of the stress reduction factor  $Y$ , which was recently confirmed experimentally.<sup>11,36,77</sup> The second problem concerns the flow properties of the grain boundary itself. For the segment of grain boundary in Fig. 3, the flow properties should contain significant grain matrix characteristics as represented by eqns (4) and (7). The experimental problem in deciding between these alternatives lies in the fact that the grain boundary flow properties are reflected only by the transition region or the 'knee' in Fig. 7(c). Moreover, in several materials no clear transition region can be seen, possibly because the transition is very gradual owing to the distributions in grain size and grain boundary properties, which both affect the location of the transition.

Grain boundary sliding is known to be a dominating mechanism in superplasticity,<sup>78</sup> and it may be that in superplastic conditions grain boundary sliding might be observed so detached from the grain matrix properties that the form of the grain boundary law can be decided. Grain boundary sliding studies are continuing in this direction.

In the temperature region where the contribution of grain boundary sliding is important, the microstructure is easily altered by static recovery. Thus the stress-strain rate data generally will reflect to some extent thermally induced structural changes which often mask the flow

characteristics of the grain boundary. Experimental techniques such as the stress dip test should be able to minimize this type of problem and should be used to obtain grain boundary flow data.

## REFERENCES

1. A. M. Freudenthal, *The Inelastic Behavior of Engineering Materials and Structures*, J. Wiley and Sons, New York, 1950.
2. E. W. Hart, *Acta Metall.*, **18**, (1970) 599–610.
3. E. W. Hart and H. D. Solomon, *Acta Metall.*, **21** (1973) 295–307.
4. E. W. Hart, C.-Y. Li, H. Yamada and G. L. Wire, in *Constitutive Equations in Plasticity*, ed. A. S. Argon, MIT Press, Cambridge, Mass., 1975, pp. 149–97.
5. E. W. Hart, *J. Eng. Mater. Technol.*, **98** (1976) 193–202.
6. C.-Y. Li, in *Metallurgical Treatises*, ed. J. K. Tien and G. F. Elliott, TMS-AIME, Warrendale, Pennsylvania, 1981, pp. 469–85.
7. M. S. Jackson, G. W. Cho, P. Alexopoulos and C.-Y. Li, *J. Eng. Mater. Technol.*, **103** (1981) 314–25.
8. P. Alexopoulos, Ph.D. Thesis, Cornell University, Ithaca, New York, 1981.
9. P. Alexopoulos, R. L. Keusseyan, G. L. Wire and C.-Y. Li, in *Mechanical Testing for Deformation Model Development*, ed. R. W. Rohde and J. C. Swearingen, American Society for Testing and Materials, ASTM STP 765, 1982, pp. 148–84.
10. F. H. Huang, H. Yamada and C.-Y. Li, in *Characterization of Materials for Service at Elevated Temperatures*, ed. G. V. Smith, Series MPC-7, ASME, 1978, pp. 83–94.
11. R. L. Keusseyan, Ph.D. Thesis, Cornell University, Ithaca, New York, 1985.
12. V. Kumar, S. Mukherjee, F. H. Huang and C.-Y. Li, *Deformation in Type 304 Austenitic Stainless Steel*, Electric Power Research Institute, Report No. EPRI NP-1276, 1979.
13. M. A. Korhonen and C.-Y. Li, *Scripta Metall.*, **15** (1982) 951–5.
14. M. A. Korhonen, J. C. Gibeling and C.-Y. Li, *J. Mat. Sci. Engng*, **74** (1985) 179–88.
15. C.-W. Cho, Ph.D. Thesis, Cornell University, Ithaca, New York, 1980.
16. W. D. Nix and B. Ilschner, in *Strength of Metals and Alloys*, Proc. ICSMA5, Vol. 3, ed. P. Haasen, V. Gerold and Y. Kosterz, Pergamon Press, New York, 1980, pp. 1503–30.
17. W. D. Nix, J. C. Gibeling and K. P. Fuchs, in *Mechanical Testing for Deformation Model Development*, ASTM STP 765, ed. R. W. Rohde and J. C. Swearingen, American Society for Metals and Testing, 1982, pp. 301–21.
18. H. Mughrabi, *Acta Metall.*, **31** (1983) 1367.
19. C. Zener, *Elasticity and Anelasticity of Metals*, University of Chicago Press, 1948.

20. E. W. Hart, *Acta Metall.*, **15** (1967) 1545–9.
21. F. Ghahremani, *Int. J. Sol. Struct.*, **16** (1980) 825–45.
22. I. Gupta and J. C. M. Li, *Metall. Trans.*, **1** (1970) 2323–30.
23. M. A. Korhonen, S.-P. Hannula and C.-Y. Li, *Metall. Trans. A*, **16A** (1985) 411–20.
24. H. Yamada, *Scripta Metall.*, **11** (1977) 321–5.
25. G. L. Wire, D. R. Duncan, N. S. Cannon, G. D. Johnson, P. S. Alexopoulos, S. Mukherjee and C.-Y. Li, *J. Eng. Mat. Tech.*, **103** (1981) 305–13.
26. E. W. Hart and Y.-W. Chang, in *Novel Techniques in Metal Deformation Testing*, ed. R. H. Wagoner, The Metallurgical Society of AIME, Warrendale, Pennsylvania, 1983, pp. 253–63.
27. J. C. Gibeling, Ph.D. Thesis, Stanford University, California, 1979.
28. D. Lee and E. W. Hart, *Metall. Trans.*, **2** (1971) 1245–8.
29. E. W. Hart, in *Stress Relaxation Testing*, ASTM STP 676, ed. A. Fox, American Society for Testing and Materials, 1979, pp. 5–20.
30. G. L. Wire, F. V. Ellis and C.-Y. Li, *Acta Metall.*, **24** (1976) 677–85.
31. G. L. Wire, H. Yamada and C.-Y. Li, *Acta Metall.*, **22** (1974) 505–12.
32. H. Yamada and C.-Y. Li, in *Proceedings of John E. Dorn Symposium*, Oct. 1972, Cleveland, Ohio, ed. J. C. M. Li and A. K. Mukherjee, ASM, Metals Park, Ohio, 1975.
33. S.-J. Chao, M.S. Thesis, Cornell University, Ithaca, New York, 1976.
34. H. Yamada and C.-Y. Li, *Acta Metall.*, **22** (1974) 249–53.
35. F. V. Ellis and C.-Y. Li, *Scripta Metal.*, **8** (1974) 739–42.
36. F. V. Ellis, G. L. Wire and C.-Y. Li, *J. Eng. Mat. Technol.*, **97** (1975) 338–42.
37. H. Yamada and C.-Y. Li, *Metall. Trans.*, **4** (1973) 2133–6.
38. F.H. Huang, F.V. Ellis and C.-Y. Li, *Metall. Trans.*, **A8** (1977) 699–704.
39. S.-P. Hannula and C.-Y. Li, *Scripta Metall.*, **18** (1984) 225–9.
40. H. Suzuki, T. Okubo and H. Ishizaka, *J. Nucl. Sci. Technol.*, **19** (1982) 133–44.
41. R. L. Keusseyan, J. Wanagel, H. Ocken, J. T. A. Roberts and C.-Y. Li, *J. Nucl. Mat.*, **98** (1981) 86–97.
42. F. H. Huang, G. P. Sabol, S. G. McDonald and C.-Y. Li, *J. Nucl. Mat.*, **79** (1979) 214–26.
43. F. Povolo and M. Higa, *J. Nucl. Mat.*, **91** (1980) 189–99.
44. F. Povolo and A. J. Marzocca, *J. Nucl. Mat.*, **98** (1981) 322–8.
45. D. A. Woodford, *Metall. Trans.*, **A6** (1975) 1693–7.
46. H. Wilson, M.S. Thesis, Cornell University, Ithaca, New York, 1985.
47. D. A. Woodford, *Metall. Trans.*, **A7** (1976) 1244–6.
48. T. D. Hadnagy, D. J. Krenitsky, D. G. Ast and C.-Y. Li, *Scripta Metall.*, **12** (1978) 45–8.
49. J. T. A. Roberts, *Acta Metall.*, **22** (1974) 873–8.
50. I. Lerner, S.-W. Chiang and D. L. Kohlstedt, *Acta Metall.*, **27** (1979) 1187–96.
51. I. Lerner and D. L. Kohlstedt, *J. Amer. Ceram. Soc.*, **64** (1981) 105–8.
52. I. Lerner and D. L. Kohlstedt, *Acta Metall.*, **30** (1982) 225–33.

53. V. Kumar, M. Morjaria and S. Mukherjee, *J. Eng. Mat. Technol.* **102** (1980) 92–6.
54. C.-Y. Hui, *Int. J. Sol. Struct.*, **21** (1985) 411–21.
55. V. Banthia and S. Mukherjee, An improved time integration scheme for stiff constitutive models of inelastic deformation, *ASME, J. Eng. Mat. Tech.*, **107** (1985) 282–5.
56. M. A. Korhonen and C.-Y. Li, Numerical integration problems of some stiff constitutive models of inelastic deformation, unpublished work.
57. E. W. Hart and C.-Y. Li, in *Zirconium in the Nuclear Industry*, ASTM STP 633, ed. A. L. Lowe Jr. and G. W. Parry, American Society for Testing and Materials, 1977, pp. 315–25.
58. S. Mukherjee and A. Chandra, in *Developments in Boundary Element Methods-3*, ed. P. K. Banerjee and S. Mukherjee, Elsevier Applied Science Publishers, London, 1984, pp. 27–58.
59. A. Chandra and S. Mukherjee, *Int. J. Numer. Methods Eng.*, **20** (1984) 1613–28.
60. S. Mukherjee and M. A. Morjaria, *Int. J. Numer. Methods Eng.*, **17** (1981) 1576–88.
61. M. A. Morjaria and S. Mukherjee, *ASME J. Appl. Mech.*, **47** (1980) 291–6.
62. S. Mukherjee, S. D. Harkness and C.-Y. Li, *J. Nucl. Mat.*, **85/86** (1979) 183–7.
63. M. Morjaria and S. Mukherjee, *Int. J. Numer. Methods Eng.*, **17** (1981) 909–21.
64. F. Nolfi and C.-Y. Li, *Nucl. Technol.*, **38** (1978) 405–14.
65. H. Yamada, in *Proc. Symp. Metal Physics of Stainless Steels*, Feb. 26 to March 2, 1978, Denver, Colorado.
66. E. W. Hart, *Int. J. Sol. Struct.*, **18** (1982) 1031–42.
67. G. D. Johnson, J. L. Straalsund and G. L. Wire, *Mat. Sci. Eng.*, **28** (1977) 69–75.
68. L.-X. Li, R. L. Keusseyan, J. Wanagel and C.-Y. Li, A correlation between stress-to-rupture data and load relaxation data of 2 1/4 Cr – 1 Mo steels, DOE Report ER 12038/5, Cornell University, Ithaca, New York, 1980.
69. H. Wilson, H. Suzuki and C.-Y. Li, in *Proc. Symp. Fracture, Interactions of Microstructure, Mechanisms, and Mechanics*, Feb 27–29, 1984, Los Angeles California, ed. J. M. Wells and J. D. Landes, TMS-AIME, Warrendale, Pennsylvania, 1984, pp. 419–33.
70. U. F. Kocks, in *Advances in Metal Deformation: Phenomena and Mechanisms*, Chapter 3, Cornell University, 1976.
71. H. Mecking and U. F. Kocks, *Acta Metall.*, **29** (1981) 1865–75.
72. J. J. Gilman, *J. Appl. Phys.*, **36** (1965) 3195–206.
73. D. K. Sherby and M. Meshii, *Metall. Trans.*, **A6** (1975) 349–58.
74. J. T. Evans and R. M. Parkins, *Acta Metall.*, **24** (1976) 511–5.
75. F. W. Crossman and M. F. Ashby, *Acta Metall.*, **23** (1975) 425–40.
76. B. Budiansky and R. J. O'Connell, *Int. J. Sol. Struct.*, **12** (1970) 81–97.
77. M. A. Korhonen, R. L. Keusseyan, L.-X. Li and C.-Y. Li, in *Novel*

- Techniques in Metal Deformation Testing*, ed. R. H. Wagoner, Metallurgical Society of AIME, Warrendale, Pennsylvania, pp. 275–84.
78. K. A. Padmanabhan and G. J. Davies, *Superplasticity*, Springer, Berlin-Heidelberg-New York, 1980.
79. P. S. Alexopoulos, C. W. Cho, C. P. Chu and C.-Y. Li, *Acta Metall.*, **29** (1981) 569–77.
80. J. F. Thomas and F. L. Yaggee, *Metall. Trans.*, **A6** (1975) 1835–7.
81. H. Suzuki and T. Okubo, in *ASTM STP 824*, ed. D. G. Franklin and R. B. Adamson, American Society for Testing and Materials, 1984, pp. 157–75.

## APPENDIX 1: PROCEDURE FOR OBTAINING MATERIAL PARAMETERS

In the following, the determinations of the parameters for the different elements of the models are discussed separately. For the characterization of the elements appearing in the models it is advisable to select experimental conditions, where the element of interest appears at its purest or at least is the rate-controlling factor. For example, for the study of anelastic properties it is required that there is essentially no plastic flow, or for the study of the friction element that the flow behavior is governed by dislocation glide. In the case where the plastic and friction elements cannot be separated, a nonlinear data correlation procedure has to be applied which is described elsewhere.<sup>38</sup>

### A.1. Anelastic Elements

The anelastic modulus  $\mathcal{M} = \mathcal{M}_1 + \mathcal{M}_2$  can be found from a tensile test at a constant displacement rate. The initial portion of the stress–strain curve shows a transition from the slope  $E$  to  $(1/E + 1/\mathcal{M})^{-1}$ , corresponding to a saturation of the anelastic element, if the strain rate is sufficiently low. A test for the non-occurrence of microplastic and plastic flow is that, in unloading and subsequent reloading, the hysteresis loop obtained must remain closed.<sup>8,9,79</sup>

An alternative way is to determine  $\mathcal{M}$  from fully reversed tension–compression loops in the microplastic deformation region. Figure 8(b) shows the total stress as a function of non-elastic strain during such a loop. A two-stage transition after a stress rate reversal can be seen, first from elastic to anelastic and then from anelastic to microplastic. In the example shown, however, the first transition is difficult to discern because of the low value of  $\sigma_f$  and the rounding of the corners of the curve due to machine effects. As above,  $\mathcal{M}$  can be found from

the slope of the curve in the anelastic region but before any essential microplastic yielding.

In an essential absence of microplastic hardening the final slope in the microplastic region reflects the increase of tension in the anelastic spring  $a_1$ , and thus the slope is  $\mathcal{M}_1$ . Another way of deducing this result is to note that the center of the loop corresponds to  $\sigma = \mathcal{M}_1 a_1 = 0$ , while at the maximum anelastic stress before microplastic yield  $\sigma = \sigma_A$ , where  $\sigma_A$  is the anelastic limit. The corresponding total strain can be calculated as

$$\varepsilon_A = \frac{\sigma_A}{E} + \frac{\sigma_A}{\mathcal{M}_1} \quad (\text{A1})$$

if the friction stress can be neglected or remains constant.<sup>8,9</sup>

## A.2. The Friction Element

At low homologous temperatures and/or high strain rates the flow is governed by dislocation glide represented by the friction element. Typical load relaxation data in this deformation regime are shown in Fig. 7(a) for 316 SS at room temperature. Rearranging eqn (7) for the friction element gives

$$\sigma = \sigma_a + G(1/\dot{a}^*)^{1/M} \dot{\varepsilon}^{1/M} \quad (\text{A2})$$

which shows that, if the internal stress can be considered as constant during load relaxation, the measured values  $\sigma$  and  $\dot{\varepsilon}$  yield  $\sigma_a$  and  $\dot{a}^*$  at any fixed value of  $M$ ;  $M$  may be chosen to produce the optimum fit. In the load relaxation test from the macroplastic flow regime governed by local glide friction, the internal stress  $\sigma_a$  remains very close to the barrier strength  $\sigma^*$ , and can thus be considered as constant. An independent test for  $M$  is that  $1/M$  gives the scaling direction  $\mu$  in a logarithmic  $(\sigma, \dot{\varepsilon})$  plot corresponding to different  $\sigma^*$  levels. The rate constant  $\dot{a}^*$  is a measure of local deformation resistance and it remains fairly constant during deformation in a general case. However, strain aging or thermomechanical treatments may give significant effect to it.

In the microplastic deformation regime,  $\sigma_{a2}$  remains close to  $\sigma_2^*$ , and thus  $\sigma_a \approx \sigma_{a1} + \sigma_2^*$ , where  $\sigma_{a1} = \mathcal{M}_1 a_1 = \mathcal{M}_1 \varepsilon$ . With the aid of the relaxation equation

$$\sigma - \sigma_0 = -E_{\text{eff}}(\varepsilon - \varepsilon_0) \quad (\text{A3})$$

shown here in an integrated form, where 0 refers to the start of the

relaxation and  $E_{\text{eff}}$  is the effective modulus, we obtain

$$\sigma = \sigma_{\infty} + \frac{G}{1 + \mathcal{M}_1/E} (1/\dot{a}^*)^{1/M} \dot{\epsilon}^{1/M} \quad (\text{A4})$$

where

$$\sigma_{\infty} = \sigma_{a1,0} + \sigma_2^* + \frac{\sigma_{f,0}}{1 + E/\mathcal{M}_1} \quad (\text{A5})$$

Thus it is seen that, in analogy with the macroplastic case,  $\sigma_2^*$  and  $\dot{a}^*$  can be determined from the ordinate intercept and the slope of eqn (A4).

### A.3. Plastic Elements

At high homologous temperatures and/or low strain rates the flow is governed by plastic elements representing thermally activated deformation, and the glide friction may usually be neglected. Typical load relaxation data representative of this deformation regime are shown in Fig. 7(b). In the absence of anelastic transients (e.g. reference 4), eqn (4) may be written as

$$\ln \sigma \simeq \ln \sigma^* - (\dot{\epsilon}^*)^{\lambda} (1/\dot{\epsilon})^{\lambda} \quad (\text{A6})$$

with  $\sigma \simeq \sigma_a$  and  $\dot{\epsilon} = \dot{a}$ . The values of  $\sigma$  and  $\dot{\epsilon}$  from a load relaxation test thus yield  $\sigma^*$  and  $\dot{\epsilon}^*$  at any fixed exponent  $\lambda$ , and  $\lambda$  may be optimized to give a minimum variance to the scatter of points around the fit. The corresponding scaling relation may be determined by load relaxation tests at different  $\sigma^*$  levels to yield  $D = f \exp(-Q/RT)$  and  $m$  from eqn (5) or

$$\log \dot{\epsilon}^* = \log D + m \log \sigma^* \quad (\text{A7})$$

where  $Q$  is approximately the activation energy for self diffusion. If wished, it can be determined from load relaxation test data at different temperatures.

Corresponding load relaxation tests in microplastic regions ( $\dot{a} \simeq 0$ ) provide the analogous quantities  $\sigma_2^*$ ,  $\dot{\epsilon}_2^*$ ,  $\lambda_2$ ,  $m_2$  and  $D_2 = f_2 \exp(-Q/RT)$  appearing in eqns (24) and (25), once the quantities  $\sigma_{a2}$  and  $\dot{a}_2$  are first determined based on the experimentally observed values of  $\sigma$  and  $\dot{\epsilon}$ . To evaluate the internal stress in soft regions (short-range pile-ups), eqn (21) is written as

$$\sigma_{a2} \simeq \sigma - \mathcal{M}_1 a_1 = \sigma - \mathcal{M}_1 \epsilon \quad (\text{A8})$$

where the friction stress is neglected and a value for  $\sigma_{a1}$  based on eqn (23) is substituted. The difficulty in using the above equation lies in the fact that zero points of the strains  $a_1 = \varepsilon$  are not usually known. One approach is to make use of fully reversed cyclic loops shown in Fig. 8(a), because in the middle of the loop  $\sigma = 0$  and necessarily also  $a_1 = \varepsilon = 0$ , which gives the desired point of reference.<sup>8,9</sup>

To evaluate the microplastic strain rate, eqn (22) is written as

$$\dot{\alpha}_2 = \dot{\varepsilon} - \dot{\sigma}_{a2}/M_2 \quad (\text{A9})$$

where eqn (23b) has been used for  $\dot{a}_2$ .

#### A.4. Evolution of the Plastic Elements

During a particular transient deformation stage, the microplastic strength  $\sigma_2^*$  changes mainly owing to sampling of different barriers for deformation.<sup>8,9</sup> In the long run also the microstructure in soft regions will evolve. Experimental studies seem to indicate that at a constant strain rate the ratio  $\sigma_{a2}/\sigma_2^*$  remains fairly constant;<sup>8</sup> however, the long-time evolution of  $\sigma_2^*$  requires more experimental studies.

The evolution of the macroplastic strength  $\sigma^*$  can be probed in constant extension rate tensile tests. Writing eqn (8) at constant  $\sigma^*$  in the form

$$\ln \Gamma = \ln \Gamma^* - (\dot{\alpha}^*)^{1/\dot{\varepsilon}} \quad (\text{A10})$$

with  $\dot{\varepsilon} \approx \dot{\alpha}$ , it is seen that  $\Gamma^*$ ,  $\dot{\alpha}^*$  and  $\Lambda$  can be found analogously to the analysis of a macroplastic load relaxation curve, eqn (A6); i.e. once  $\Gamma$  has been determined as a function of  $\dot{\varepsilon}$ ,  $\Gamma^*$  and  $\dot{\varepsilon}^*$  can be found from the linear regression coefficients of the fit (A10). Further, the athermal hardening  $\Gamma^*$  as a function of  $\sigma^*$  yields the parameters of eqn (9):  $A$ ,  $B$  and  $\sigma_0^*$ .

#### A.5. The Grain Boundary Element

Stress relaxation tests in the regime where GBS is important are needed for the determination of the stress reduction factor  $Y$  and the properties of the GB element. In the case of an S-shaped relaxation curve, Fig. 7(c),  $Y$  can readily be found as a logarithmic stress difference between the basic grain matrix and combined matrix-grain boundary curves. Owing to the rather limited experimental stress-strain rate range available for the study of the GB element, the form of the GB flow law still remains to be settled. Both proposed flow laws, eqns (28) and (29), are capable of simulating the experimentally

observable behavior with parameters  $(\sigma_g^*, \dot{\epsilon}_g^*, \lambda_g)$  or  $(\dot{a}_g^*, M_g)$  chosen to produce the best fit to experimental data.

## ACKNOWLEDGMENTS

This work is supported by the US Department of Energy through the Materials Science Division. Two of us (M.A.K. and S.-P.H.) also wish to acknowledge the support of Outokumpu Company Foundation in Finland.

## APPENDIX 2: PROGRAM FOR SOLVING BASIC HART'S EQUATIONS. REPRESENTATIVE VALUES ARE FOR ALUMINUM AT ROOM TEMPERATURE

```

0010 PRINT "<27><12>"
0020 PRINT "*****MECHANICAL EQUATION OF STATE/HARTS COMPLETE MODEL*****"
0030 PRINT
0040 DIM F$[13]
0050 DIM S[2],S1[2],S2[2],Z1[2]
0060 DIM E[2],A1[2],A2[2]
0070 CLOSE
0080 INPUT "OUTPUT FILE",F$
0090 OPEN FILE[1,1],F$
0110 REM - ELASTIC & ANELASTIC MODULUS
0120 LET Y=48200
0130 LET Y1=310000
0140 REM - FRICTION STRESS EXPONENT
0150 LET M=7.8
0160 REM - DISLOCATION GLIDE CONSTANT
0170 LET C=2.48E+48
0180 REM - SCALING EXPONENT
0190 LET M1=4.8
0200 REM - LAMDA EXPONENT
0210 LET L1=.15
0215 LET L3=1/L1
0240 REM - MACHINE COMPLIANCE
0250 LET K=.183
0260 REM - WORK HARDENING COEFFICIENTS
0270 LET A3=80
0275 LET B3=3.5
0280 LET E3=3.15E-08
0290 REM - INITIAL GAUGE LENGTH AND AREA
0295 LET L0=25.4
0300 LET A0=11.23
0305 REM - REFERENCE SIG * AND EPOOT *
0310 LET Z1=41.38
0315 LET E1=5.05E-15
0320 LET C1=E1/Z1^M1

```

```

0350 REM      - INITIAL STRESSES
0360 LET      S=37.154
0370 LET      S1=37.105
0380 LET      S2=S-S1
0390 LET      Z1=41.38
0400 REM      - INITIAL STRAINS
0410 LET      E=1.14279E-04
0420 LET      A1=E-S1/Y1
0430 LET      L=L0*EXP(E)
0440 LET      A=A0*L0/L
0450 INPUT    "NUMBER OF LOADING STEPS?", NO
0460 PRINT
0470 PRINT    "RESPOND FOR EACH LOADING STEP:"
0480 PRINT
0490 DIM      T[N0+1],T1[N0],P[N0],U[N0]
0500 FOR      J=1 TO N0
0510 INPUT    "DURATION OF THE LOADING STEPS?", T[J]
0520 LET      T1[J]=9.99999E-25
0530 INPUT    "TYPE OF LOADING:(0) CREEP, (1) TENSILE?", U[J]
0540 INPUT    "LOAD/EXTENSION RATE DURING LOADING STEP?", P[J]
0550 PRINT
0560 NEXT     J
0570 PRINT
0580 REM      - INITIAL TIME
0590 LET      T0=12.2608
0600 REM      - TIME LIMIT
0610 LET      T9=1E+06
0620 REM      - TIME STEP LIMIT
0630 LET      T2=1
0640 REM      - LIMITING RELATIVE ERRORS IN INTEGRATION
0650 LET      D8=.0001
0660 LET      D9 = 001
0670 LET      D7=.01
0680 REM      - LOADING STEP INDEX
0690 LET      N=0
0700 REM      *****START NEW LOADING*****
0710 LET      N=N+1
0720 REM      - INTEGRATION ROUND INDEX
0730 LET      I1=0
0740 REM      - NONCONVERGENCE INDEX
0750 LET      I4=0
0760 REM      - RELATIVE START TIME
0770 LET      T=0
0780 REM      - PRINTOUT TIME
0790 LET      T7=0
0800 REM      - MINIMUM INTERVAL BETWEEN PRINTOUTS
0810 LET      T6=.001
0820 REM      - INITIAL TIME STEP
0830 LET      T1=T1[N]
0840 LET      - VISCOPLASTIC INDEX
0850 LET      V=1
0860 PRINT
0870 IF      U[N]=0 THEN PRINT "*****LOADING STEP ";N;" CREEP*****"
0880 IF      U[N]=1 THEN PRINT "*****LOADING STEP ";N;" TENSILE*****"
0890 PRINT
0900 IF      U[N]=0 THEN LET S=P[N]/A
0910 LET      S0=S
0920 LET      E0=E
0930 IF      U[N]=1 THEN LET X[1]=P[N]
0940 GOSUB   1750

```

```

0950 LET      S[2]=S[1]
0960 LET      S1[2]=S1[1]
0970 LET      S2[2]=S1[1]
0980 LET      E[2]=E[1]
0990 IF      T>=T[N] THEN GOTO 1220
1000 REM      *****EXECUTION OF THE NEXT STEP*****
1010 LET      I1=I1+1
1020 IF      T<T7 THEN GOTO 1190
1030 LET      J=J+1
1040 IF      J=10*INT(J/10) THEN PRINT "<27><12>"
1050 REM      - PRINT RESULTS
1060 PRINT    "*" ; T0+T, S, S1, S2, Z1
1070 PRINT    E, A1, E[1], A1[1], 81[1]/Y1
1080 WRITE    FILE[1], T, S, S[1], 81, S1[1], Z1, Z1[1], E, E[1]
1090 REM      - CONTROL VARIABLES
1100 LET      T4=(T-T8)/(I1-I8)
1110 IF      2*T4>T2 THEN LET T2=2*T2
1120 IF      T4<T2/4 THEN LET T2=T2/2
1130 LET      I8=I1
1140 LET      T8=T
1150 IF      T>.15 THEN LET T6=.01
1160 IF      T>1 THEN LET T6=.1
1170 IF      T>20 THEN LET T6=1
1180 LET      T7=T7+T6
1190 GOSUB    1280
1200 GOSUB    1750
1210 GOTO    0990
1220 REM      *****NEXT LOADING/END*****
1230 LET      T0=T0+T
1240 IF      N<>N0 THEN GOTO 0700
1250 IF      T>=T9 THEN STOP
1260 GOTO    0680
1270 END
1280 REM      *****SUBROUTINE INTEGRATION*****
1290 LET      T3=T[N]-T
1300 IF      T1>T2 THEN LET T1=T2
1310 IF      T1>T3 THEN LET T1=T3
1320 LET      I2=0
1330 LET      D1=ABS(S[1]-S[2])*T1/D7
1340 LET      D2=ABS(S1[1]-S1[2])*T1/D7
1350 LET      D3=ABS(S2[1]-S2[2])*T1/D7
1360 IF      ABS(S)>1 THEN LET D1=D1*D7/ABS(S)
1370 IF      ABS(S1)>1 THEN LET D2=D2*D7/ABS(S1)
1380 IF      ABS(S2)>1 THEN LET D3=D3*D7/ABS(S2)
1390 IF      D1<D2 THEN LET D1=D2
1400 IF      D1<D3 THEN LET D1=D3
1410 REM      - CHOOSE TIME STEP
1420 IF      D1<D9 THEN GOTO 1490
1430 IF      I2<50 THEN GOTO 1690
1440 LET      T1=.5*T1
1450 LET      D1=.5*D1
1460 LET      I2=I2+1
1470 GOTO    1410
1480 REM      - CHECK SIGMA A < SIGMA *
1490 IF      Z1+Z1[1]*T1>ABS(S1+S1[1]*T1) THEN GOTO 1550
1500 IF      I2>50 THEN GOTO 1690
1510 LET      I2=I2+1
1520 LET      T1=.5*T1
1530 GOTO    1490
1540 REM      - CALCULATE NEW VALUES OF THE VARIABLES
1550 LET      S=S+S[1]*T1

```

```

1560 LET S1=S1+S1[1]*T1
1570 LET S2=S2+S2[1]*T1
1580 LET Z2=Z2+Z2[1]*T1
1590 LET E=E+E[1]*T1
1600 LET T=T+T1
1610 IF D1<D8 THEN LET T1=2*T1
1620 REM - SAVE THE PREVIOUS DERIVATIVES
1630 LET S[2]=S[1]
1640 LET S1[2]=S1[1]
1650 LET S2[2]=S2[1]
1660 LET E[2]=E[1]
1670 RETURN
1680 REM - WARNING OF NONCONVERGENT INTEGRATION
1690 PRINT "*****NO CONVERGENCE*****"
1700 IF I4=4 THEN STOP
1710 LET I4=I4+1
1720 LET I2=0
1730 GOTO 1410
1740 END
1750 REM *****SUBROUTINE RATE*****
1760 LET V=1
1770 REM - DEFINITION OF AUXILIARY VARIABLES
1780 LET L=L0*EXP(E)
1790 LET A=A0*L0/L
1800 LET S3=ABS(S1)
1810 IF S3<1E-20 THEN LET S3=1E-20
1820 LET A1=E-S1/Y1
1830 LET E1=C1*(Z1)^M1
1840 LET R1=S3/Z1
1850 IF U[N]=0 THEN LET S=S0*EXP(E-E0)
1860 LET S2=S-S1
1870 REM - STRAIN RATES
1880 LET E[1]=C*(ABS(S2))^M
1890 IF S2<0 THEN LET E[1]=-E[1]
1900 IF I1<>0 THEN LET E[1]=(E[1]+E[2])/2
1910 LET A1[1]=E1/(-LOG(R1))^L3
1920 IF S1<0 THEN LET A1[1]=-A1[1]
1930 LET A2[1]=E[1]-A1[1]
1940 LET R2=A2[1]/A1[1]
1950 LET R3=ABS(Q0/A1[1]-1)
1960 LET R4=ABS(Q1/Z1-1)
1970 LET Q0=A1[1]
1980 LET Q1=Z1
1990 LET Q=-LOG(R1)/L3
2000 LET G=A3*EXP(-(E3/E[1])^L1)/Z1^B3
2010 LET R5=(1-M1*Q)*G*S1/Y1
2020 IF R3>(1/Q-M1)*R4 THEN GOTO 2080
2030 IF R2>.03 THEN GOTO 2080
2040 REM - VISCOPLASTIC BEHAVIOR
2050 LET V=2
2060 LET A1[1]=E[1]/(1+R5)
2070 REM - STRESS DERIVATIVES
2080 LET S[1]=E[1]*S
2090 LET Z1[1]=Z1*G*ABS(A1[1])
2100 LET S1[1]=Y1*(E[1]-A1[1])
2110 LET S2[1]=S[1]-S1[1]
2120 IF U[N]=0 THEN RETURN
2130 LET S[1]=Y*L*(X[1]/L-E[1])/(L+Y*A*K)
2140 LET S2[1]=S[1]-S1[1]
2150 RETURN

```

\*

# 3

## The MATMOD Equations

ALAN K. MILLER

*Department of Materials Science and Engineering, Stanford University,  
California, USA*

### 1. INTRODUCTION

Among the several sets of unified constitutive equations described in this volume, the MATMOD (standing simply for MATerials MODel) equations probably attempt to cover the *broadest* set of phenomena. These are enumerated in Table 1. Like many of the other unified approaches, the MATMOD equations treat most of the phenomena within the categories of ‘creep’ and ‘plasticity’; however, the equations are also designed to predict many aspects of cyclic deformation and, more generally, multiaxial non-proportional straining. The manner in which the equations represent solute drag effects (dynamic strain aging) is unique. This breadth does come at the expense of accuracy, given our present incomplete knowledge of the ‘first principles’ physical laws governing dislocation-controlled straining.

Most of the phenomena in Table 1 can be unequivocally identified with one or more strengthening mechanisms. For example, the Bauschinger effect can be identified with polarized dislocation structures (e.g. pileups) whereas negative strain-rate sensitivity due to dynamic strain aging can clearly be identified with solute drag. In a few cases (such as yield strength plateaus which may be due either to ‘athermal’ obstacles or to solute drag) the governing physical processes are still debatable. Despite such uncertainties, the number of categories of strengthening mechanisms is far less than the number of phenomena to be simulated. For this rather practical reason the MATMOD equations are built around the concept of having a small

**TABLE 1**  
Phenomena Simulated by the MATMOD Constitutive Equations

---

1. 'Plasticity' including:
    - (a) essentially elastic behavior followed by gradual yielding
    - (b) strain-rate sensitivity
    - (c) temperature sensitivity
  2. 'Creep', including:
    - (a) primary creep
    - (b) steady-state creep
    - (c) sinh variation of steady-state creep rate with stress
  3. Cyclic stress-strain behavior, including:
    - (a) Bauschinger effect
    - (b) cyclic hardening and cyclic softening
    - (c) shakedown to a saturated condition of constant stress and strain amplitudes
  4. Recovery:
    - (a) static recovery
    - (b) dynamic recovery
    - (c) effect of stress on recovery
  5. Dynamic strain-aging (solute) effects including:
    - (a) plateau in yield strength vs. temperature
    - (b) negative strain-rate sensitivity
    - (c) interactions with strain hardening
    - (d) effect on creep rate
  6. Complex histories:
    - (a) stress changes
    - (b) strain-rate changes
    - (c) temperature changes
  7. Strain softening effects:
    - (a) unidirectional
    - (b) cyclic
    - (c) multidirectional
  8. Multiaxial deformation:
    - (a) 'yield' surface expansion
    - (b) 'yield' surface translation
    - (c) 'yield' surface distortion
    - (d) anisotropy
  9. Irradiation effects:
    - (a) irradiation hardening
    - (b) irradiation-enhanced creep
  10. Interactions of all the above
-

number of internal (state) variables, each one representing one *category* of physical strengthening mechanisms. By properly designing those equations which govern each internal variable, the overall model can be made to simulate the entire list of phenomena, while still remaining fairly simple mathematically and computationally.

The concept of state variable categories is also necessary in order to make the model as 'correct' as possible scientifically, because in a scientifically correct model there should be a one-to-one correspondence between the internal workings of the model and the internal **physical processes which underlie the macroscopic deformation behavior** being predicted. Thus the presence of several state variables, each representing the action of one group of physical strengthening mechanisms, causes the model to be an approximately valid representation of the governing physical processes.

In this chapter, we will first explore the *types* of equations which are required by the phenomena which we are trying to predict, then discuss in more detail the physical and phenomenological bases for the equations, then describe the development of the specific MATMOD equations, then present simulations and predictions illustrating the equations' capabilities, and then discuss numerical integration methods and calculation of the material-dependent constants.

## 2. DEVELOPMENT OF THE EQUATIONS

### **2.1. General Relations between the Phenomena Addressed and the Types of Equations Required**

#### *2.1.1. History Dependence*

The history dependence of non-elastic deformation includes at least three aspects. First, even under constant boundary conditions (such as constant strain rate or constant stress), *transients* in the response (changes in the flow stress or the creep rate, respectively) reflect the effects of previous straining. Second, under changing boundary conditions (e.g. imposed rapid strain rate or stress changes) the instantaneous response under the *new* conditions reflects the structure induced by straining under the previous conditions. And third, 'creep-plasticity-recovery' interactions occur, again indicating the effect of deformation under one set of conditions upon the subsequent response.

As discussed first by Hart<sup>1</sup> and subsequently by many others, the proper way to deal with the history dependence of the non-elastic strain (hereinafter denoted as  $\epsilon$  for simplicity) response is to make the central equation one for the non-elastic strain *rate* ( $\dot{\epsilon}$ ), and to have  $\dot{\epsilon}$  depend on internal state, or structure, variables  $X$  which are governed by equations for their time rates of change,  $\dot{X}$ . The MATMOD equations adopt this approach. Thus their general form is

$$\dot{\epsilon} = f(\sigma, T, X) \quad (1a)$$

$$\dot{X} = g(\dot{\epsilon}, T, X) \quad (1b)$$

where  $\sigma$  is the applied stress and  $T$  the temperature.

### 2.1.2. *Explicit Temperature Dependence and Creep/Plasticity Unification*

In general, the temperature dependence indicated in eqns (1a) and (1b) may be introduced either by having temperature be an explicit variable in the equations [appearing in Arrhenius-like terms,  $\exp(-Q/kT)$ ], or by having some of the material constants be (empirically) dependent upon temperature. The former approach is far more favorable than the latter for a number of reasons. For example, on scientific grounds, many if not all of the physical processes governing both 'plasticity' and 'creep' are thermally activated, with known activation energies; if temperature is not an explicit variable then much of the scientific information is being ignored. On practical grounds, if the material constants are empirically temperature-dependent, then their values must be determined experimentally at a large number of temperatures within the regime of interest; if the temperature dependence is explicit, then a far smaller number of tests needs to be run. On both scientific and practical grounds, *variable-temperature* histories are treated in a far more logical fashion if the temperature dependence is explicit than if the material constants are temperature-dependent.

Plasticity and creep, at all but very high temperatures where grain boundary sliding or purely diffusional flow can dominate, are accomplished by dislocation glide. Climb may control the rate at which dislocations surmount obstacles between glide events. Despite this common physical basis, the stress sensitivities of the non-elastic strain rate are quite different in the two regimes, being quite large for plasticity but moderate for high-temperature creep. By using the

hyperbolic sine function within the  $\dot{\epsilon}$  and other equations, and by including the temperature dependence explicitly, a single equation with temperature-independent exponents may be used to predict behavior in both regimes, which significantly aids our goal of achieving unification of 'creep' and 'plasticity'.

### 2.1.3. *Steady-state Flow*

Most data on the steady-state strain rate as a function of the steady-state stress (often plotted for various temperatures as a single band in terms of  $\dot{\epsilon}_{ss}/D_{\text{eff}}$  vs.  $\sigma_{ss}/E$ , where  $D_{\text{eff}}$  is the effective diffusion coefficient and  $E$  the elastic modulus) exhibit a sinh-like dependence. Figure 1 shows a particularly good example, for high-purity aluminum.<sup>2</sup> Although small departures of the data from the line predicted by the sinh function leave open to question the exact proper equation, the sinh expression is a good compromise between simplicity and accuracy and has been adopted as the 'true' steady-state behavior. Thus the equations are designed so that, at steady state, they reduce identically to the sinh behavior.

### 2.1.4. *Directional Hardening and Cyclic Deformation*

In a unified approach valid for truly general histories, the current response must be predicted in terms of only the *current* values of the structure variables and the *current* stress (or the current non-elastic strain rate) and temperature. Thus the same set of equations must properly respond, in terms of these variables, to the differences between monotonic and cyclic deformation. For example, the equations must predict that, at a given temperature and magnitude in strain rate, *monotonic* straining leads to a steady-state flow stress which is larger (and an isotropic structure which is stronger) than the saturated value of the peak flow stress (and structure) reached during *cyclic* deformation, as illustrated by the data<sup>3</sup> in Fig. 2. The structure variable which is most obviously different in cyclic compared to monotonic deformation is the back stress. Accordingly, the differences in response can be interpreted in terms of the effects of back stresses on the formation or dissolution of isotropic structures such as cells or subgrains. In the MATMOD equations, the symbol  $R$  ('rest stress') denotes back stresses, and isotropic strengthening is represented by a separate variable called  $F_{\text{def}}$  ('friction stress due to deformation'). Corresponding to this physical picture, in the MATMOD approach the rate of change of  $F_{\text{def}}$  is made dependent on the current value of  $R$ .

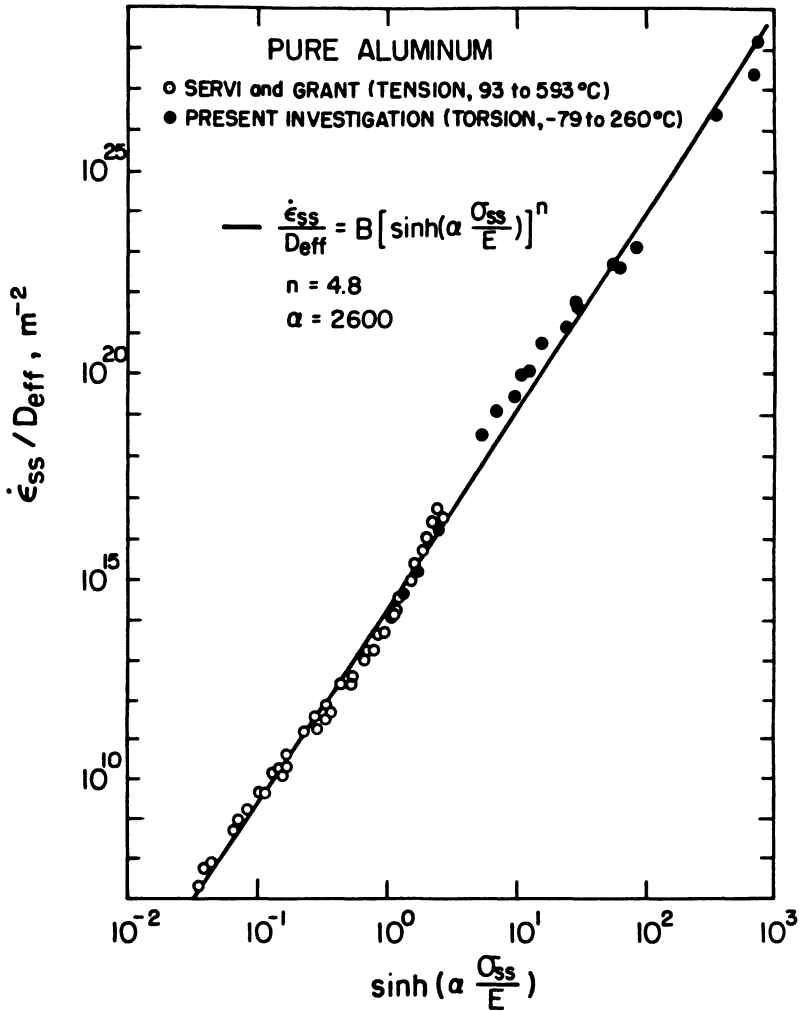


**Fig. 1.** Data on steady-state flow of high-purity aluminum, showing the fit obtained by the use of the hyperbolic sine function. After Luthy *et al.*<sup>2</sup>

This same arrangement is also important for treating strain softening because back stresses (which, when large, cause increases in the isotropic hardening variable) can, once reduced, allow *decreases* in the isotropic strength. Thus the coupling between isotropic and directional hardening in the MATMOD approach is quite useful for predicting mixtures of monotonic and cyclic behavior.

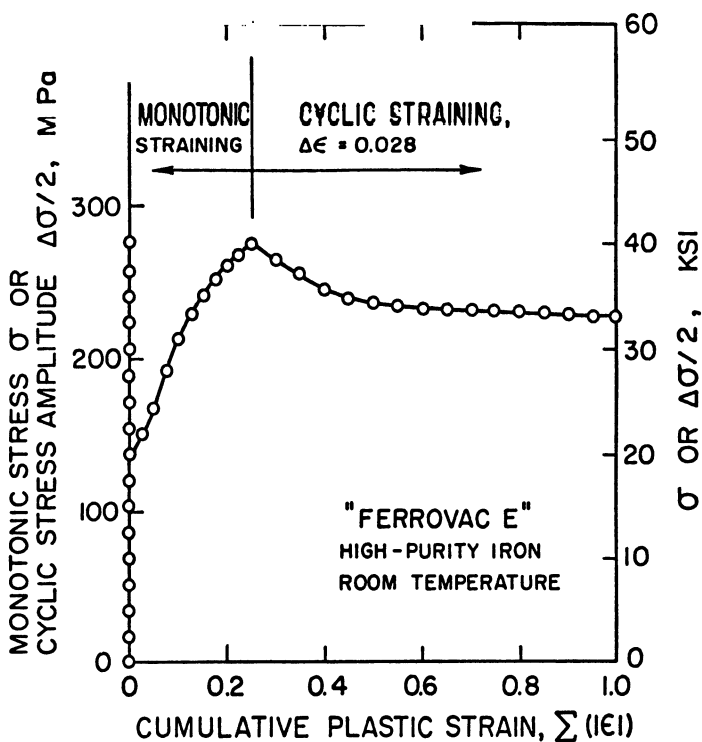


**Fig. 2.** Data showing that monotonic straining results in a higher saturated flow stress than cyclic straining, at the same strain rate and temperature. After Abdel-Raouf and Plumtree.<sup>3</sup>

Furthermore, the same approach proves useful in simulating multi-axial deformation; back stresses are represented in terms of a back stress tensor  $R_{ij}$  while isotropic hardening remains a scalar. The cross-coupling introduced originally to predict cyclic deformation allows the equations to predict the response to non-proportional multiaxial straining.

### 2.1.5. Dynamic Strain Aging

Phenomena such as inverse temperature dependence or negative strain rate sensitivity of the flow stress are observed in solute-strengthened materials; they lead to other phenomena such as serrated yielding and plastic flow concentration. The controlling physical processes involve the drag of solute atmospheres by moving dislocations, with the drag force typically reaching a maximum at *intermediate* temperatures and

strain rates. These processes are represented in the equations by a variable termed  $F_{\text{sol}}$  ('friction stress due to solutes').  $F_{\text{sol}}$  is a non-monotonic function of temperature and non-elastic strain rate, and since solute strengthening is isotropic,  $F_{\text{sol}}$  adds to the variable ( $F_{\text{def}}$ ) which represents strain-induced isotropic work hardening in determining the flow stress. The nature of  $F_{\text{sol}}$  causes a non-monotonic dependence of the flow stress upon temperature in certain regimes (leading to flow stress peaks) and upon strain rate (leading to minima in, or even negative values of, the strain rate sensitivity).

## 2.2. Physical and Phenomenological Bases for the Equations

### 2.2.1. General Approach and the Use of Internal Variables

Like most other unified constitutive equations, the MATMOD approach is based on a mixture of physical mechanisms and phenomenological information; primary emphasis is placed upon those mechanisms and data trends which are generally observed in metals and alloys.

The way in which physical mechanisms are used in constructing unified constitutive equations is worth describing. In 'first principles' models, the basic building blocks are quantitative equations governing specific elementary physical processes, and the variables in those equations are the actual physical entities involved, such as dislocation density, atomic position, local internal stress, etc. These building blocks are assembled (in closed form or by numerical solutions) into models of more complex processes (e.g. creep by climb and glide) but the key feature is that there is still a discrete representation of the actual physical quantities of importance.

In a physical-phenomenological model, it is accepted at the outset that the physical processes governing the behavior to be modeled are too complex to be represented in terms of the actual physical entities. For example, dislocation and cell behavior during *cyclic* deformation are only beginning to be understood. Nevertheless there is enough of an understanding of the physical processes to identify the major physical variables controlling the behavior, and the general manner in which they behave. The key concept is to set up 'state' variables, each of which corresponds to one of the physical variables, and to design the overall *form* of the equations governing these state variables so that the behavior of the state variables under all conditions imitates what we believe to be the behavior of the physical variables under the

same conditions. Thus, as mentioned in Section 1, there is a one-to-one correspondence between the numerical response of the state variables in the physical-phenomenological model and the actual behavior of the internal entities in the real material. This is what distinguishes a physical-phenomenological model from a simple empirical fit to the macroscopic data.

Of course, a complete model requires not only appropriate selection of the state variables and *forms* for the equations linking the variables, but also specific algebraic expressions in the equations. This is where phenomenology comes in; because the behavior and/or materials being modeled are too complex for a 'first principles' derivation of the equations, algebraic expressions are selected which cause the response of the model (in terms of both the externally measured behavior and the behavior of the internal variables) to duplicate the observed responses of real materials under the same conditions. While this aspect of the model development process certainly involves *fitting*, the fact that the expressions which are being fitted to the data govern both the internal variables and the macroscopic response gives the model a degree of physical meaning which is not present in simple empirical equations.

Table 2 summarizes the physical mechanisms represented within the MATMOD equations.

### 2.2.2. Diffusion

It is well established that at high temperatures ( $T > 0.5T_m$ , where  $T_m$  is the absolute melting temperature) steady-state deformation is rate and temperature dependent and that these dependences arise because the fundamental physical processes (e.g. dislocation climb over obstacles) are diffusion-controlled. At intermediate temperatures (e.g.  $0.2T_m < T < 0.5T_m$ ), there is less of a consensus but the available evidence<sup>2</sup> indicates that steady-state deformation is still diffusion-controlled, albeit by dislocation pipe diffusion in this temperature regime compared with lattice self-diffusion at high temperatures. Figure 3 shows data on the activation energy for steady-state deformation of aluminum; it is quite similar to that ( $Q_d$ ) for self-diffusion. Below  $0.2T_m$ , data on the temperature dependence of steady-state deformation are lacking (for experimental reasons, because of the very large strains required to reach steady-state).

Because of the strong reliance on steady-state behavior in shaping the MATMOD equations, it is very convenient to *assume* that the

**TABLE 2**  
Internal Physical Mechanisms Represented within the MATMOD Constitutive Equations

<i>Macroscopic behavior</i>	<i>Internal physical basis</i>	<i>MATMOD variable</i>
Temperature dependence	Diffusion (lattice, pipe)	$\theta', D_{\text{eff}}$
Non-interactive solute strengthening	Cottrell atmospheres (substitutional solutes)	$F_{\text{sol},1}$
Interactive solute strengthening	Vacancy-interstitial pairs	$F_{\text{sol},2}$
Directional work-hardening	Dislocation pileups, bowed segments, curved subgrain boundaries	$R$
Directional recovery	Climb, cross-slip	$R$ (recovery term)
Isotropic work-hardening	Forest dislocations, subgrain boundaries	$F_{\text{def}}$
Isotropic thermal recovery	Dislocation annihilation	$F_{\text{def}}$ (thermal recovery term)
Isotropic strain softening	Glide of 'concave' dislocations	$F_{\text{def}}$ (dynamic recovery term)

temperature dependence of deformation in general is the same as the temperature dependence of steady-state deformation. (This assumption will be justified in Section 2.3.1.) Thus both the strain-rate equation itself and all of the terms in the process equations which do not already contain  $\dot{\epsilon}$  are given a temperature dependence which follows from that of diffusion, i.e.  $\exp(-Q_d/kT)$  ( $k$  is used instead of  $R$  as the symbol for the gas constant, to avoid confusion with the rest stress). This is the origin of the  $\theta'$  factor in the MATMOD  $\dot{\epsilon}$  equation and in the recovery terms of the  $\dot{R}$  and  $\dot{F}_{\text{def}}$  equations. Since the material constants in the MATMOD equations are *not* temperature-dependent, this assumption has a very important practical benefit, namely allowing predictions of the behavior at any desired temperature based on data for other temperatures.

The temperature dependence within the recovery terms of the evolutionary equations represents those physical processes (such as dislocation annihilation and subgrain coarsening) which weaken the obstacles to dislocation motion. The temperature dependence within the strain rate equation represents processes such as thermally

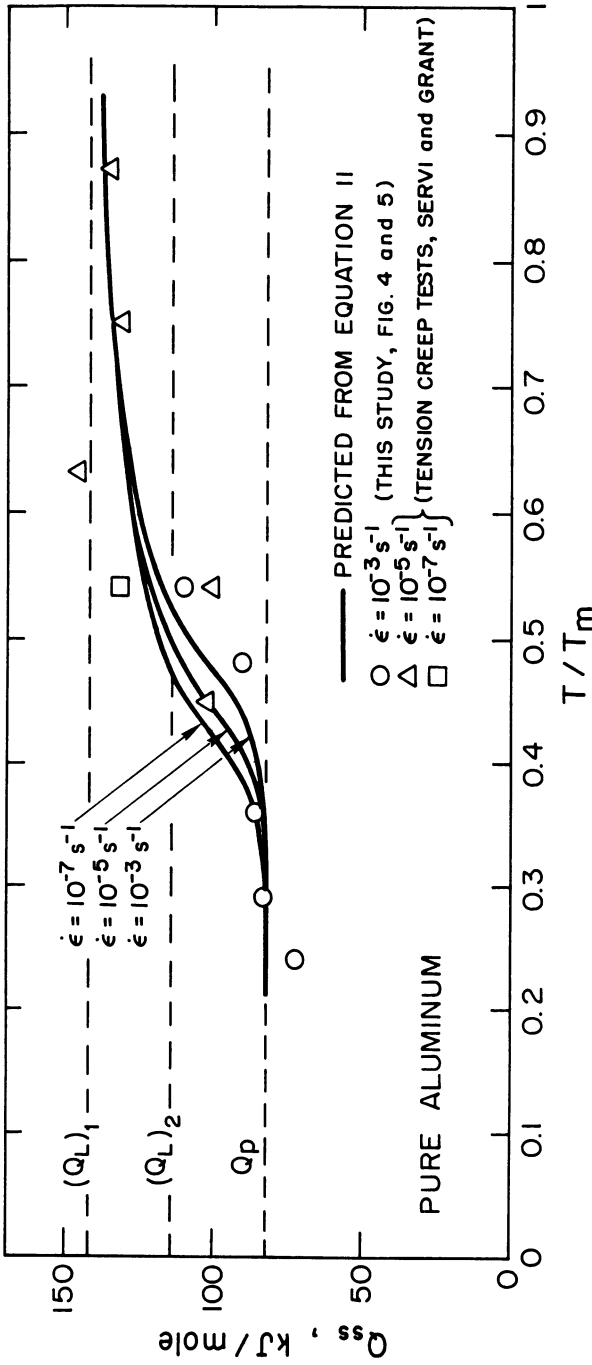


Fig. 3. Data on the activation energy for steady-state flow, showing its similarity to the activation energies for lattice and pipe diffusion. After Luthy *et al.*<sup>2</sup>

activated, viscous drag of dislocations through the (constant) field of obstacles. While it is clear that the former group of processes (recovery) is, in fact, temperature-dependent, the same cannot be said for the latter (straining at constant structure). Certain evidence (such as large changes in flow stress just after temperature changes at constant strain rate, as observed by Dorn *et al.*,<sup>4</sup> and also the classical ‘Cottrell–Stokes ratio’<sup>5</sup> which reflects the changes in flow stress with temperature at constant structure and strain rate) is consistent with an intrinsic temperature dependence of the non-elastic strain rate even at constant structure, as are phenomenological constitutive equations suggested by other authors for both steady-state and constant-structure flow.<sup>6</sup> However, some theoretical treatments hold the intrinsic temperature dependence of the non-elastic strain rate to be relatively small, and prefer to account for the temperature dependence of the observed macroscopic response through recovery terms. (See, for example, Fig. 7 in Chapter 1 of this volume.) Pending experimental resolution of this important question, the presence of  $\theta'$  in the MATMOD  $\dot{\epsilon}$  equation is justified primarily on the practical grounds given above, i.e. simplicity, consistency with much of the experimental evidence, and the useful ability to extrapolate to other temperatures.

$\theta'$  is, then, the factor in the equations which represents lattice and pipe diffusion and their assumed effects both on the non-elastic strain rate at a given structure, and on recovery. In the work of Sherby and colleagues<sup>7</sup> the (additive) effects of lattice and pipe diffusion are expressed as the effective diffusion coefficient  $D_{\text{eff}}$ :

$$D_{\text{eff}} = D_{0,l} \exp(-Q_l/kT) + f_p D_{0,p} \exp(Q_p/kT) \quad (2)$$

where  $f_p$  is the fraction of lattice sites participating in pipe diffusion, and  $Q_l$  and  $Q_p$  are, respectively, the activation energies for lattice and pipe diffusion. There are two reasons why this expression has been converted into the slightly different expression for  $\theta'$  rather than using it directly. (1)  $f_p$  depends on dislocation density and therefore, in general, on previous history, but  $f_p$  has been well defined only for steady-state conditions. Therefore  $D_{\text{eff}}$  is not sufficiently defined for the domain of the more general MATMOD equations, which includes both transient and steady-state behavior. (2) Below  $0.2T_m$  the classic data of Sherby *et al.*<sup>8</sup> indicate a continuing decrease in  $Q_d$  towards zero at 0 K, while  $D_{\text{eff}}$ , being based on steady-state behavior, is undefined below  $0.2T_m$ . While the response measured by Sherby *et al.*<sup>8</sup> below  $0.2T_m$  might well be expected to be a *transient* response, it is

consistent with the rest of the MATMOD approach to assume that it represents the *general* behavior. In accordance with the above,  $\theta'$  in the MATMOD equations has been developed by making a concise mathematical fit to the trend exhibited by the data of Sherby *et al.*,<sup>8</sup> namely assuming that the activation energy for creep,  $Q_c$ , is constant and equal to  $Q_1$  above some transition temperature  $T_t$ , and that, below  $T_t$ ,  $Q_c$  decreases linearly down to zero at 0 K. This is illustrated in Fig. 4.

The definition of  $Q_c$  in any operational sense is  $Q_c = -k \partial(\ln \dot{\epsilon})/\partial(1/T)$ ; by its usage in the equations,  $\dot{\epsilon}$  will be directly proportional to  $\theta'$ , thus  $Q_c = -k \partial(\ln \theta')/\partial(1/T)$ . Integrating this expression<sup>9,10</sup> under the above assumptions concerning  $Q_c$  vs.  $T$ , we obtain the expression for  $\theta'$ :

$$\theta' = \exp\{-Q_1/kT_t[\ln(T_t/T) + 1]\} \quad \text{for } T \leq T_t \quad (3a)$$

and

$$\theta' = \exp(-Q_1/kT) \quad \text{for } T \geq T_t \quad (3b)$$

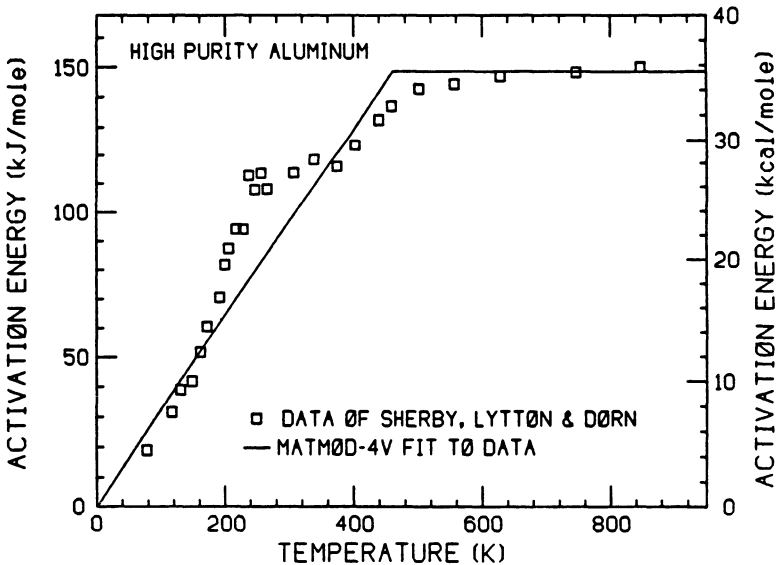


**Fig. 4.** Data<sup>8</sup> on the activation energy for deformation over a wide temperature range, including transient and steady-state behavior; the fit assumed by the MATMOD equations is also shown. After Lowe.<sup>16</sup>

In summary, all of the temperature dependence in the MATMOD equations (other than that of the elastic modulus) is conveyed through  $\theta'$ .

### 2.2.3. *The Role of Internal Structure*

As stated above, the central ('kinetic') equation predicts the non-elastic strain rate,  $\dot{\epsilon}$ , as a function of the current values of stress, temperature (through  $\theta'$ ), and several structure variables. Basically, the choice of this form follows from the belief that the fundamental relationship governing non-elastic deformation is the Orowan equation which predicts the rate of straining in terms of dislocation slip events:

$$\dot{\epsilon} = g\rho_m vb \quad (4)$$

where  $\rho_m$  is the mobile dislocation density,  $v$  is the average dislocation velocity,  $b$  is the Burgers vector, and  $g$  is a geometric factor of order unity. *Structure* enters into both  $\rho_m$  and  $v$ , the former for obvious reasons and the latter because the average dislocation velocity, besides being stress and temperature dependent, will depend on the drag forces exerted by the obstacles through which the dislocations must pass.

Despite the clear physical basis for the above equation, it does not serve well for direct utilization within a general-purpose set of constitutive equations, principally because (1) equations for the dislocation velocity in the presence of many other dislocations (the relevant conditions in technological applications) are not available, and (2) specification of the 'mobile' dislocation density is awkward for conditions involving, for example, changes in straining direction. Nevertheless, the Orowan equation is a useful guide to both the appropriate form for the central strain-rate equation and the fact that it must contain variables to represent the effects of internal structure upon the ease of dislocation motion.

The aspects of a material's internal structure which may affect dislocation motion are numerous. At a rudimentary level, some of these include Peierls forces (due to local energy maxima in between equilibrium positions of a dislocation), grain boundaries, solute atoms, and precipitate and dispersoid particles. For purposes of predicting non-elastic deformation response, all of these may be classified as 'intrinsic' strengthening mechanisms, meaning that they are present without requiring any prior deformation and their effects are not necessarily dependent on the specific history of prior straining. Also,

all of these mechanisms act approximately equally in all directions, i.e. they represent 'isotropic' strengthening mechanisms. For these three reasons this group of strengthening mechanisms has been collected together in terms of one type of structure variable ( $F_{\text{sol}}$ ) in the MATMOD equations.

The major category of strengthening mechanisms not included in the above list is strengthening (or weakening) by other dislocations. This category is inherently different from the others, for two major reasons. First, it is history-dependent, the current dislocation substructure depending on the previous history (including rate, temperature, and direction) of straining. And second, only some aspects of the dislocation substructure strengthen a material *isotropically*; these include the overall forest dislocation density and the average subgrain or cell size. Other aspects of the dislocation substructure strengthen a material *directionally*; for example dislocation pileups are directional because their internal stress fields cause a *decrease* in the average velocity of dislocations moving in the same direction as the dislocation motion which formed the pileup, but would be expected to cause an *increase* in the average velocity of dislocations moving in the opposite direction.

Because of these inherent differences, dislocation substructure is associated with two additional structure variables in the MATMOD equations. The first,  $F_{\text{def}}$  (the 'friction stress due to deformation'), corresponds roughly to the drag stress as defined by Johnson and Gilman<sup>11</sup> and represents isotropically hardening aspects of the dislocation substructure. The other,  $R$  (the 'rest stress', i.e. the applied stress at which  $\dot{\epsilon}_{ij}$  equals zero, or the material is 'at rest'), represents directionally hardening aspects of the substructure such as pileups, bowing, and subgrain wall curvature.

This is the overall physical basis for the use of the three types of structure variables within the equations. Succeeding sections will describe their physical bases in more detail, will develop the specific equations governing each variable, and will describe the correspondences between their behavior and the behavior of their physical counterparts. For now, we have established that the non-elastic strain rate must depend on these three structure variables, in addition to the usual dependence on the current stress and temperature. Thus, eqn (1a) becomes

$$\dot{\epsilon} = f(\sigma, T, F_{\text{sol}}, F_{\text{def}}, R) \quad (5)$$

#### 2.2.4. Isotropic Hardening Mechanisms

As stated above, forest dislocations, subgrains, and dislocation cells are similar in their effects on deformation and therefore in the initial MATMOD equations<sup>9,10</sup> were represented in terms of one structure variable,  $F_{\text{def}}$ . The effect of a density  $\rho$  of forest dislocations is most familiarly represented in terms of the Taylor relation (written in terms of axial quantities instead of the usual shear quantities)

$$\sigma|_{\dot{\epsilon}, T} \propto E\sqrt{\rho} \quad (6)$$

which, when converted to the form generally used in unified constitutive equations, becomes

$$\dot{\epsilon}|_T = f[(\sigma/E)/(\sqrt{\rho})] \quad (7)$$

It is important to note that in eqn (7) the modulus-compensated stress is *divided* by the variable  $\sqrt{\rho}$ . The implication of this dependence is that forest dislocations always strengthen a material, regardless of the direction of straining. This is quite consistent with our concept of forest dislocations as barriers to dislocation motion in *any* direction.

Similarly, the effect of subgrains of an average size  $\lambda$  on the flow stress has been studied<sup>12-14</sup> and expressed by such equations as

$$(\sigma/E)|_{\dot{\epsilon}, T} \propto \lambda^{-1} \quad (8)$$

which becomes

$$\dot{\epsilon}|_T = f[(\sigma/E)/(\lambda^{-1})] \quad (9)$$

Again, the implication of eqns (8) and (9) is that subgrains strengthen a material in *all* directions; this has been demonstrated by experiments in which subgrains are induced by working in torsion but then strengthen the material in compression<sup>14</sup> and is again consistent with our concept of subgrain walls as barriers to the long-range motion of dislocations in any direction.

As stated above, the MATMOD equations attempt to be quite *broad*, not only in terms of number of phenomena predicted but also in the variety of strengthening mechanisms and materials covered and the temperature range which is treated. With respect to the latter points, even a single material (such as austenitic stainless steel) may show a combination of forest dislocation, cell, and subgrain strengthening, the predominant form of isotropic hardening depending on the temperature. Also, at any given temperature (e.g.  $0.4T_m$ ) pure metals exhibit notable subgrain strengthening, while 'class I' solid solution

alloys are dominated by forest dislocation mechanisms of work-hardening. For these reasons, as well as the desire for mathematical simplicity, the initial version of the MATMOD equations<sup>15</sup> lumped these three mechanisms of isotropic hardening into the single structure variable  $F_{\text{def}}$  which, because it represents both  $\sqrt{\rho}$  in eqn (7) and  $\lambda^{-1}$  in eqn (9), must be *divided into*  $\sigma/E$  in determining  $\dot{\epsilon}$ . Hence

$$\dot{\epsilon}|_T = f_1[(\sigma/E)/f_2(F_{\text{def}})] \quad (10)$$

In subsequent refinement of the equations to treat strain softening,<sup>16</sup> it became clear that the behavior of heterogeneous dislocation structures (cells and subgrains) is sufficiently different from the behavior of homogeneously distributed (forest) dislocations that separate structure variables are warranted. The experimental evidence<sup>17</sup> shows that, upon strong changes in the *direction* of straining, cellular structures can dissolve, whereas the overall dislocation density tends to remain constant. Accompanying this cell dissolution is macroscopically observable strain softening which, upon careful experimentation,<sup>18</sup> proves to be a temporary reduction in *isotropic* strength. These data led to the partitioning of  $F_{\text{def}}$  into two separate variables:  $F_{\text{def},\lambda}$  to represent the behavior and effects of heterogeneous dislocation substructures, and  $F_{\text{def},\rho}$  to represent the effects of homogeneously distributed dislocations. Because both of these variables represent isotropic strength, the two are added together in their effect on the non-elastic strain rate:

$$\dot{\epsilon}|_T = f_1[(\sigma/E)/f_2(F_{\text{def},\rho} + F_{\text{def},\lambda})] \quad (11)$$

Separation of isotropic work-hardening into two state variables is also consistent with the work of Kassner *et al.*<sup>19</sup> who found that the strengthening effects of subgrains and forest dislocations could be separately determined and, when this was done, the two contributions appeared to evolve at different *rates*; for example, at 850°C for type 304 stainless steel, forest dislocation hardening built up within the first few percent of strain, whereas subgrain strengthening took tens of percent of strain to manifest itself<sup>20</sup> (see Fig. 5).

Section 2.1 has pointed out that, in addition to the *kinetic* law giving  $\dot{\epsilon}$  as a function of  $\sigma$ ,  $T$ , and current structure, an evolution equation is required for each structure variable. Following the work-hardening-recovery approach first suggested by Cottrell and Aytikin,<sup>21</sup> the differential equation for  $\dot{F}_{\text{def}}$  contains several terms. The first, the

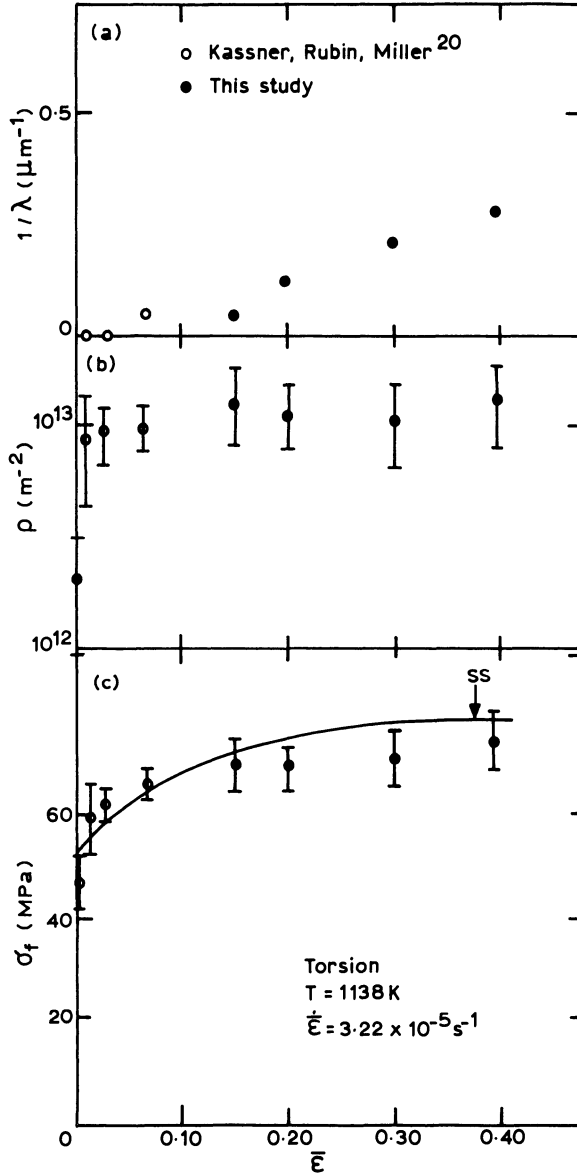


**Fig. 5.** Data on the flow stress vs. strain for type 304 stainless steel, showing that subgrain strengthening and forest dislocation strengthening build up at different rates. After Kassner *et al.*<sup>19</sup>

work-hardening term, represents dislocation multiplication and heterogeneous substructure formation and refinement, all of which are driven by the magnitude of the current non-elastic strain rate, multiplied by a work-hardening coefficient  $H$ . Since large values of  $F_{\text{def}}$  correspond to a strong material, this term is positive; thus the work-hardening term in the  $\dot{F}_{\text{def}}$  equation increases with  $|\dot{\epsilon}|$ . The second term represents dynamic recovery processes such as annihilation by cross-slip of oppositely signed dislocations passing sufficiently near to each other. Since this term is driven by the non-elastic strain rate, it too is proportional to  $|\dot{\epsilon}|$  but is negative and increases in magnitude as  $F_{\text{def}}$  gets larger according to a dynamic recovery function  $d(F_{\text{def}})$ , representing an increasing loss of dislocations by annihilation processes as the dislocations get closer together. The third term represents static recovery processes such as annihilation of oppositely signed dislocations by climb, and coarsening of a subgrain network. These too are negative contributions to  $\dot{F}_{\text{def}}$  which are driven by increasing dislocation density, and thus the third term also depends upon the current value of  $F_{\text{def}}$  according to a static recovery function  $r(F_{\text{def}}, T)$ . However, static recovery is thermally activated instead of being strain activated, and thus the magnitude of the third term increases with  $T$  but does not depend upon  $\dot{\epsilon}$ . Hence, in its skeletal form the  $\dot{F}_{\text{def}}$  equation is

$$\dot{F}_{\text{def}} = H |\dot{\epsilon}| - d(F_{\text{def}}) |\dot{\epsilon}| - r(F_{\text{def}}, T) \quad (12)$$

Since the above-mentioned physical processes pertain to both forest dislocations and heterogeneous substructure, the MATMOD-4V equations contain two equations of the above form, one giving  $\dot{F}_{\text{def},\rho}$  and the other giving  $\dot{F}_{\text{def},\lambda}$ .

### 2.2.5. Directional Hardening Mechanisms

There are a number of mechanisms of directional strain hardening relevant to metals and alloys, including bowing of dislocations between obstacles, pileups at obstacles, curvature of subgrain walls,<sup>22</sup> and elastic mismatch between the different grains of a polycrystal. With all of these mechanisms, some kind of internal stress is created which has directional character. For bowed dislocations, extra energy associated with the extra length of dislocation line creates an internal force tending to straighten the dislocation segment, moving it in the direction opposite to that which created the bowing. In a pileup, the stress fields of nearby similar dislocations act on a dislocation in a

direction which is opposite to the motion of the dislocations which created the pileup. Substantial straining in a given direction creates curved subgrain walls, whose long-range internal stresses (within the subgrain) retard dislocations which are moving in that same direction. Also, grain-to-grain differences in operating slip systems create elastic strains and stresses within each grain which act oppositely to the previous plastic straining. Basically each of the above mechanisms creates an *internal stress* which, although it averages to zero over the volume of concern, slows down dislocations which are moving in a given direction<sup>23</sup> and speeds up dislocations which are moving in the opposite direction. Each of these mechanisms also requires some prior history of straining to create the directional state, which is what distinguishes this 'deformation-induced anisotropy' from the 'intrinsic anisotropy' associated, for example, with the presence of a non-random crystallographic texture.

Hence, the major characteristic which these mechanisms all have in common is that, for a given 'state', they *strengthen* the material in certain subsequent straining directions (generally those in the same direction as the recent previous straining), and *weaken* it for other directions (generally those opposite to the recent history). This macroscopic effect occurs, of course, because the directional internal stresses superpose with the applied stress field to determine the net local stress on any dislocation. Mathematically, the net effect of the internal stress field is best represented in terms of a 'back stress'  $\sigma_b$ ; the linear superposition of the back stresses and the applied stresses leads to the familiar equation form in which the back stress is *subtracted from* the applied stress:

$$\dot{\epsilon}|_T \propto f(\sigma - \sigma_b) \quad (13)$$

Since we are discussing various *directions* of straining which may be characterized by positive or negative values of the internal and external variables, it is appropriate at this time to begin to construct the appropriate mathematical framework. The magnitude of the difference between  $\sigma$  and  $\sigma_b$  is the driving force (sometimes called the 'effective stress') for non-elastic straining, and the direction of straining is determined by the sign of the difference between  $\sigma$  and  $\sigma_b$ . Thus, the conventional form of the equations for uniaxial straining is

$$\dot{\epsilon}|_T = f(|\sigma - \sigma_b|) \text{sgn}(\sigma - \sigma_b) \quad (14)$$

where *sgn* is the *signum* function which equals the algebraic sign of its

argument. The full multiaxial set of constitutive equations (which will be shown below) reduces to eqn (14) for the special case of uniaxial behavior.

In the original MATMOD equations, there was a single variable,  $R$ , which collectively represented as many of the above-mentioned directional hardening mechanisms as might be operating in any given situation;  $R$  was subtracted from  $\sigma/E$  so that it was, in effect, a modulus-compensated back stress. There was no attempt to represent separately the effects of any one of these mechanisms, basically because the knowledge base was (and still is) insufficient to identify each of these mechanisms with some corresponding macroscopic behavior. However, during the above-mentioned equations improvement<sup>16</sup>, aimed at predicting strain softening, it became useful to distinguish between 'long-range back stresses' (probably associated with blockage of dislocations at strong obstacles such as subgrain walls) and 'short-range back stresses' (possibly associated with blockage of dislocations at weaker obstacles such as other individual dislocations). This led to the partitioning of  $R$  into two separate variables,  $R_a$  for short-range and  $R_b$  for long-range back stresses. One specific mechanistic justification for such a partitioning is the observation by Mughrabi<sup>24</sup> that the radii of curvature of dislocations bowed between obstacles fall into a bimodal distribution. Also, measurements by Quesnel and Tsou<sup>25</sup> of the variation of internal stress within strain cycles appear to indicate both a rapidly varying part and a more slowly varying component (Fig. 6). Since both  $R_a$  and  $R_b$  represent internal stresses which oppose the applied stress, their effects are additive. Thus the form of the MATMOD-4V equations<sup>26</sup> which includes these two back stresses as well as the two isotropic hardening variables is

$$\dot{\epsilon}|_T = f_1\{|\sigma/E - (R_a + R_b)|/f_2(F_{def,\rho} + F_{def,\lambda})\} \text{sgn}[\sigma/E - (R_a + R_b)] \quad (15)$$

Again, since  $R_a$  and  $R_b$  are structure variables, they are governed by differential equations giving their time rates of change, and these equations follow the work-hardening-recovery format. In skeletal form, the first term in each equation represents generation of back stresses whose sense (i.e. direction) is similar to the direction of the non-elastic strain which is creating them. Thus this first term is proportional in both magnitude and sign to the current value of  $\dot{\epsilon}$ , with a work-hardening coefficient  $H$  (different in value from the  $H$  in eqn

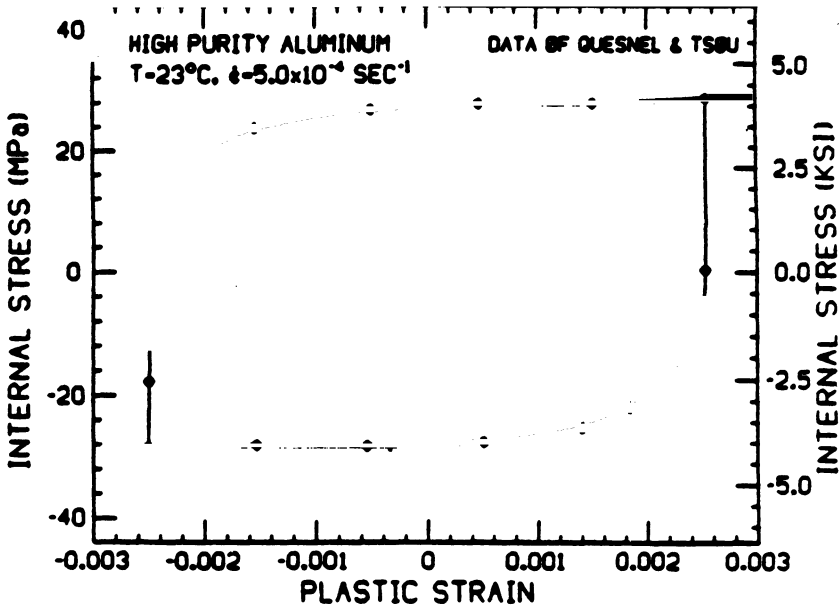


Fig. 6. Data of Quesnel and Tsou<sup>25</sup> on the internal stress measured by stress relaxation probes during cyclic deformation, showing rapid changes in internal stresses just after reversals and slower changes elsewhere.

(12)). The second term represents strain-activated recovery of back stresses. This is driven by the current magnitude of  $\dot{\epsilon}$  and a dynamic recovery function  $d(|R|)$  but pushes  $R$  towards zero; in other words, the direction of this second term is exactly opposite to the current direction of  $R$  itself. The third term represents thermally activated static recovery of back stresses which, like the second term, acts in a direction opposite to the current direction of  $R$  but is driven by a combination of temperature and the current effective value of  $R$ , rather than by  $|\dot{\epsilon}|$ . Hence the form of the equation governing the time rate of change of both back stresses is

$$\dot{R} = H\dot{\epsilon} - d(|R|) |\dot{\epsilon}| R - r(|R|, T)R \quad (16)$$

### 2.2.6. Solute Drag

As mentioned above,  $R$  and  $F_{\text{def}}$  treat strain-induced hardening. Intrinsic strengthening mechanisms are represented by a separate variable,  $F_{\text{sol}}$ . Because these are essentially non-directional in character,  $F_{\text{sol}}$  enters into the strain-rate equation in the same place (the

denominator of the expression governing the strain rate in which  $\sigma/E$  is in the numerator) as  $F_{\text{def}}$ , i.e.

$$\dot{\epsilon}|_T = f[(\sigma/E)/F_{\text{sol}}] \quad (17)$$

turning this equation around to solve for stress gives

$$\sigma|_T = f(\dot{\epsilon})F_{\text{sol}} \quad (18)$$

With this form, that part of  $F_{\text{sol}}$  which corresponds to grain boundary strengthening is consistent with the Hall–Petch equation for the dependence of flow stress upon grain size  $d$ :

$$\sigma|_T = f(\dot{\epsilon})(k_1 + k_2d^{-1/2}) \quad (19)$$

while that part of  $F_{\text{sol}}$  which corresponds to precipitate or dispersoid particles is consistent with the Orowan equation:

$$\sigma|_T = f(\dot{\epsilon})(1/\sqrt{l}) \quad (20)$$

where  $l$  is the mean spacing between particles. A portion (probably quite small) of  $F_{\text{sol}}$  also includes the Peierls stress.

The remaining contributions to  $F_{\text{sol}}$  are associated with solute atoms. These can be subdivided into two categories: general lattice strengthening, and solute drag. The former category simply represents the extra force required to move dislocations through a lattice in which some of the sites are different elements. This portion of  $F_{\text{sol}}$  does not have any remarkable variation with temperature.

The solute drag contribution to  $F_{\text{sol}}$  does have a special variation with temperature, and has been developed to correspond to the concept of Cottrell atmospheres. Substitutional or interstitial atoms whose size is different from that of the solvent can reduce the energy associated with this size mismatch by locating themselves around edge dislocations, larger solutes going to regions of tensile stress and smaller solutes going to regions of compressive stress. Interstitial solute atoms can also join with vacancies to form vacancy–interstitial pairs which, being non-hydrostatic defects, can interact with screw dislocations to exert a drag force. The net drag force on a dislocation increases with both the size of the solute cloud around it and the extra force per solute atom as it is dragged by the moving dislocation. At low temperatures solutes are too immobile to keep up with moving dislocations so the solute cloud is small and the drag force is low. At intermediate temperatures, solutes are more mobile so the solute

cloud can be large and the drag force can be high. At high temperatures, solutes are so mobile (by diffusion) that the extra force required to cause them to move with a dislocation is small again, even though the solute cloud is large. Hence the solute drag force goes through a maximum at intermediate temperature, for a given dislocation velocity (leading to flow stress peaks), and through a maximum at intermediate dislocation velocities, for a given temperature (leading to effects upon the strain-rate sensitivity of the flow stress). In terms of 'first principles' models, this behavior is most familiarly given by the Hirth and Lothe approximation<sup>27</sup> to the Cottrell–Jaswon solute drag formulation, which expresses the solute drag force as a function of temperature and dislocation velocity (Fig. 7).

Since the dislocation velocity varies, roughly, with the non-elastic strain rate and the role of temperature enters through the diffusivity, the solute drag force in the equations can be represented as being dependent upon the diffusion-compensated non-elastic strain rate, i.e.

$$F_{\text{sol}} = f(\dot{\epsilon}/D_{\text{eff}}) \quad (21)$$

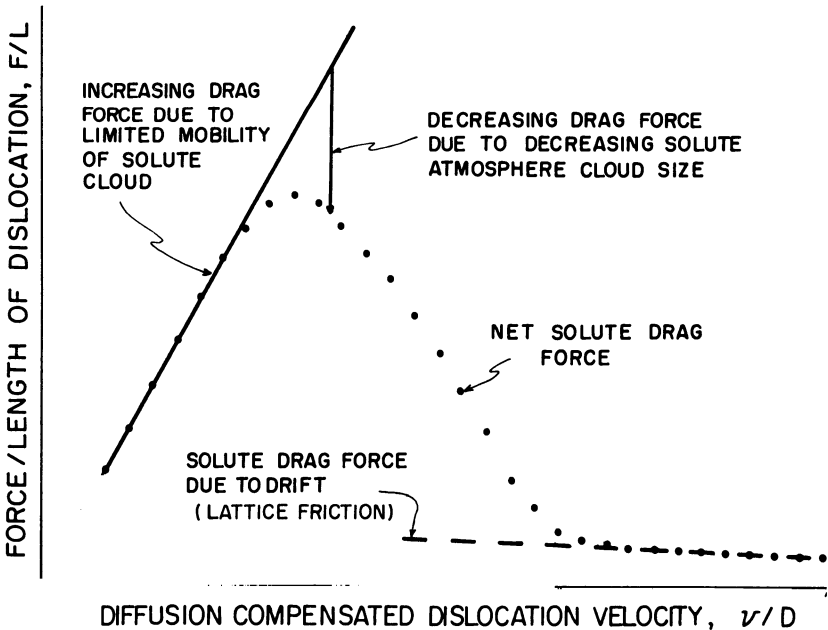


**Fig. 7.** Theoretical solute drag force on a dislocation, showing that the force goes through a maximum at an intermediate diffusion-compensated dislocation velocity. After Hirth and Lothe,<sup>27</sup> as drawn by Schmidt.<sup>29</sup>

where  $f$  will be some non-monotonic function accounting for the fact that  $F_{\text{sol}}$  goes through a peak at an intermediate value of  $\dot{\epsilon}/D_{\text{eff}}$ .

As described already, in the MATMOD equations the effective diffusion coefficient  $D_{\text{eff}}$  is replaced, for mathematical completeness and simplicity, with the temperature-dependent factor  $\theta'$ . Hence, instead of using  $D_{\text{eff}}$  in eqn (21), the variation of the solute drag stress with temperature and strain rate is given in terms of  $\theta'$  by

$$F_{\text{sol}} = f(\dot{\epsilon}/\theta') \quad (22)$$

It is worth noting that the manner in which  $F_{\text{sol}}$  depends upon the other variables is different from that of  $F_{\text{def}}$ ; at any point during a simulation,  $F_{\text{sol}}$  can be calculated directly from eqn (22) as a function of the current temperature and non-elastic strain rate, whereas the value of  $F_{\text{def}}$  is only known through numerical integration of eqn (12) which gives its time rate of change.

In the above equations, solute content has not entered as an explicit variable into the above equation for the solute drag force. Solute content will affect the values of the material constants in the function  $f$  in eqn (22). For the present version of the MATMOD equations this is acceptable because the function  $f$  in eqn (22) is determined by fitting to data on the macroscopic behavior (e.g. yield strength vs. temperature and strain rate) of the alloy being represented so that total solute content does affect  $f$ . Similarly any effects of precipitates, dispersoids, grain boundaries, and Peierls forces will be constant for a given alloy having a given (assumed stable) metallurgical structure, so that these too are accounted for within the function  $f$  through the macroscopic data during the determination of the materials constants. In current research,<sup>28</sup> methods that are more physically based are being developed for predicting  $f$  explicitly from, for example, the solute content and the size and modulus mismatch between solute and solvent atoms.

In their simplest manifestation, the drag forces exerted on dislocations by solutes, precipitates, dispersoids, grain boundaries, and Peierls forces are *additive* to those exerted by forest dislocations and heterogeneous substructure. Thus, ignoring directional hardening for the moment,  $F_{\text{sol}}$  enters into the strain rate equation as

$$\dot{\epsilon} = f_1[(\sigma/E)/f_2(F_{\text{sol}} + F_{\text{def}})] \quad (23)$$

However, in some systems the solutes are more than additive to strain hardening; they are *synergistic* with strain hardening so that if

the material is both in a strain-rate/temperature regime where solute atmospheres can exert considerable drag, and in a strain-hardened state where there is a considerable number of dislocations, then the total solute drag force is quite high. To represent this type of behavior requires a second solute strengthening variable which *multiplies*  $F_{\text{def}}$  instead of adding to it. Thus, in the improved form of the equations developed by Schmidt,<sup>29,30</sup> eqn (23) becomes

$$\dot{\epsilon}|_T = f_1 \{ (\sigma/E) / f_2 [F_{\text{sol},1} + F_{\text{def}}(1 + F_{\text{sol},2})] \} \quad (24)$$

Since  $F_{\text{def}}$  is small at low strains (for an initially annealed material) and large at high strains, the 'yield strength' (e.g. at  $\epsilon = 0.002$ ) is dominated by  $F_{\text{sol},1}$  while the flow stress at high strains is dominated by  $F_{\text{sol},2}$ .

It is worth noting the ongoing research by Henshall<sup>28</sup> who is more critically addressing (with experiments and analysis) the question of whether low-strain flow stress plateaus ought to be modeled 'thermally' through  $F_{\text{sol},1}$  (as above) or 'athermally' through rapidly changing back stresses ( $R_a$  in Section 2.2.5). At the present writing, the latter approach appears to be most correct.

To combine directional hardening, solute strengthening, and isotropic work hardening, we rely on the physical picture in which the dislocation velocity is being set by the local effective stress (applied stress minus local back stress), operating against the total drag stress (solute strengthening plus isotropic work hardening). Considering, for simplicity, only a single  $R$ , a single  $F_{\text{def}}$ , and a single  $F_{\text{sol}}$ , the resulting equation is

$$\dot{\epsilon}|_T = f_1 \{ |\sigma/E - R| / f_2 (F_{\text{def}} + F_{\text{sol}}) \} \text{sgn}[\sigma/E - R] \quad (25)$$

## 2.3. Phenomenological Development of the Specific Equations

### 2.3.1. Strain-rate and $\dot{F}_{\text{def}}$ Equations

Equation (1a), which expresses the non-elastic strain rate as a function of the current stress, temperature, and structure, is the central equation in the set. Ideally, its dependence on temperature and on stress should come from well accepted theoretical information on the constant-structure deformation behavior of metals and alloys. Unfortunately, there are no such well accepted theories at present. As a second choice, experimental data on the temperature and stress dependences at constant structure should be used, but again unfortun-

ately such data do not exist over sufficiently broad regimes in the variables. However, ample data *do* exist on the temperature and stress dependences of steady-state flow. The important early experiments by Sherby *et al.*<sup>8</sup> showed that the activation energy for transient deformation was the same as that for steady-state flow, and that this activation energy depended only on temperature and not on stress or strain, leading to the conclusion<sup>31</sup> that an appropriate form for calculating the creep rate was to multiply the temperature-dependent function by a *separate* function of stress and structure. On the basis of these data, and in the absence of more definitive information, we assume that the temperature dependence in the MATMOD strain-rate equation is the same as that of steady-state flow (which was discussed in Section 2.2.2). Hence

$$\dot{\epsilon} = \theta'(T)f(\sigma/E, F_{\text{def}}, F_{\text{sol}}, R) \quad (26)$$

where  $\theta'$  was defined in eqn (3).

To obtain the remaining dependences in eqn (26), we make further use of the steady-state data. First of all, we consider behavior of pure metals for which, by definition,  $F_{\text{sol}}$  in eqn (25) is 0. Second, many experiments concerned with both steady-state flow and constant structure behavior have shown that the results can be interpreted in terms of isotropic hardening mechanisms such as subgrains. For example, work of Sherby *et al.*<sup>32</sup> shows that, within the power-law regime, at steady-state

$$\dot{\epsilon}_{\text{ss}} \propto (\sigma/E)^5 \quad (27)$$

while at constant subgrain size

$$\dot{\epsilon}|_{\lambda} \propto (\sigma/E)^8 \quad (28)$$

(Exponents in these examples are approximate.)

These two special cases (illustrated in Fig. 8) are readily explained by the more general equation

$$\dot{\epsilon} \propto \lambda^3(\sigma/E)^8 \quad (29)$$

because at steady-state the subgrain size is a unique function of the stress:

$$\lambda_{\text{ss}} \propto (\sigma_{\text{ss}}/E)^{-1} \quad (30)$$

Substitution of eqn (30) into eqn (29) produces the observed

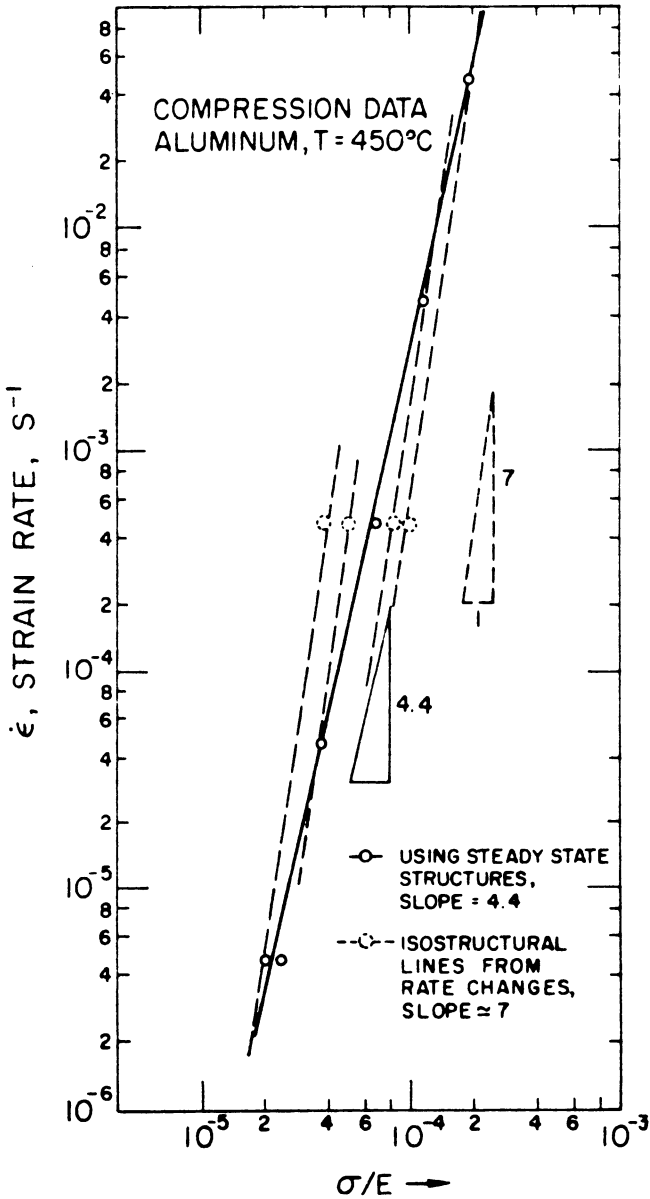


**Fig. 8.** The dependence of the strain rate upon modulus-compensated stress for constant-structure and for steady-state conditions. After Young *et al.*<sup>13</sup>

5-power dependence at steady-state. In other words, it is the systematic variation of subgrain size with the deformation conditions, at steady-state, which causes the steady-state response in terms of  $\dot{\epsilon}$  vs.  $\sigma$  to be different from the constant-structure response.

On the basis of the above data and analysis, we select the *isotropic* hardening variable ( $F_{\text{def}}$ ) in the MATMOD equations as the one which should be most responsible for producing the correct steady-state and constant-structure responses. Accordingly, we defer consideration of the role of back stresses in eqn (26). Recalling that, in calculating the non-elastic strain rate, isotropic hardening effects should be divided into  $\sigma/E$  (Section 2.2.4) and that for both transient and steady-state deformation (i.e. for the general case) the non-elastic strain rate should be expressed as a product of a temperature-dependent term and a stress- and structure-dependent term (as discussed immediately above), we conclude that the proper form for the general strain-rate equation is

$$\dot{\epsilon} = \theta' f_1 [(\sigma/E)/f_2(F_{\text{def}})] \quad (31)$$

As mentioned above, in order to deduce the functions  $f_1$  and  $f_2$  in eqn (31) we must consider steady-state as well as constant-structure responses. Steady-state arises because of a dynamic equilibrium between work-hardening and recovery, causing the rate of change of structure to go to zero ( $\dot{F}_{\text{def}} = 0$ ) even though the material is still undergoing straining. In the initial MATMOD equations, for simplicity only work-hardening and static recovery were considered. This followed from the early work of Cottrell and Aytakin,<sup>21</sup> among others. With only these two terms, for unidirectional deformation eqn (12) becomes

$$\dot{F}_{\text{def}} = H\dot{\epsilon} - r(F_{\text{def}}, T) \quad (32)$$

We have thus deduced what the general form should be of both the strain-rate equation and the equation governing the isotropic hardening variable. To develop the specific functions  $f_1$ ,  $f_2$ , and  $r$  in these equations we adopt an additional constraint; specifically, we force the steady-state behavior of the equations to match the well known phenomenological equation for steady-state deformation first suggested by Garofalo:<sup>33</sup>

$$\dot{\epsilon}_{\text{ss}} = B\theta' [\sinh(A\sigma_{\text{ss}}/E)]^n \quad (33)$$

where we have chosen to express the temperature dependence in

terms of the  $\theta'$  factor discussed previously instead of the  $\exp(-Q/kT)$  used by Garofalo in order that we may encompass a wider range of temperature. In this equation  $n$  is about 5 for most materials and  $A$  and  $B$  are material-dependent constants. This equation is obeyed (closely but perhaps not quite exactly) by a large number of materials; see for example the work by Luthy *et al.*<sup>2</sup> on pure aluminum (Fig. 1) which showed that over 21 orders of magnitude in temperature-compensated strain rate the steady-state behavior agreed well (to within a factor of 3 on strain rate) with the predictions of eqn (33).

We now have four pieces of information concerning the  $\dot{\epsilon}$  and  $\dot{F}_{\text{def}}$  equations (the general form of each equation, the required steady-state behavior at all stresses, and the required constant-structure behavior at low stresses). A pair of equations which satisfies these four constraints is:

$$\dot{\epsilon} = B\theta' \{ \sinh[ ((\sigma/E)/\sqrt{F_{\text{def}}})^{1.5} ] \}^n \quad (34)$$

$$\dot{F}_{\text{def}} = H\dot{\epsilon} - HB\theta' [ \sinh(A^3 F_{\text{def}}^{1.5}) ]^n \quad (35)$$

where  $H$  is an additional constant. For steady-state ( $\dot{F}_{\text{def}} = 0$ ), eqn (35) becomes

$$\dot{\epsilon}_{\text{ss}} = B\theta' [ \sinh(A^3 F_{\text{def,ss}}) ]^n \quad (36)$$

When this is combined with eqn (34), the two equations reduce to eqn (33), thus producing the proper steady-state behavior. For constant  $F_{\text{def}}$  at low stresses, eqn (34) reduces to

$$\dot{\epsilon} \Big|_{T, F_{\text{def}}} \propto (\sigma/E)^{1.5n} \quad (37)$$

which is approximately in agreement with the desired 8-power constant structure behavior (eqn (28)) since  $n$  is about 5.

It is worth noting from eqn (36) that, at steady-state, the variation in  $F_{\text{def}}$  with  $\dot{\epsilon}/\theta'$  is governed by the same sinh function which governs the variation of  $\sigma/E$  with  $\dot{\epsilon}/\theta'$  (eqn (33)). Essentially, we have assumed that the structure varies with temperature-compensated strain rate according to the hyperbolic sine law. More recent and more physically based theories, for example that of Nix and colleagues,<sup>34</sup> explain the transition from power-law to power-law-breakdown behavior as a transition from cell *wall* strengthening to cell *interior* strengthening. Thus the initial MATMOD equations are approximating, in terms of a single relatively complex function (sinh) of a single variable ( $F_{\text{def}}$ ), that behavior which is probably really governed by a combination of *two*

variables (cell wall strength and cell interior strength), possibly involving simpler individual functions.

One additional aspect of the above two equations needs explanation, namely the square root in eqn (34). This is present so that, under constant strain rate conditions, the stress-strain response will be parabolic when isotropic hardening dominates. Such behavior might be expected when the strains are large enough that the buildup of back stresses (kinematic hardening) no longer dominates, but small enough that recovery of isotropic hardening is negligible. Under these conditions,

$$\dot{F}_{\text{def}} \cong H\dot{\epsilon} \quad (38)$$

Integrating eqn (38) over a time interval leads to

$$F_{\text{def}} = F_{\text{def},0} + H\epsilon \quad (39)$$

where  $F_{\text{def},0}$  is the initial value of  $F_{\text{def}}$  at  $\epsilon = 0$ .

Substituting eqn (39) into eqn (34) and rearranging to solve for the flow stress, we obtain

$$\sigma = E(F_{\text{def},0} + H\epsilon)^{1/2} \{ \sinh^{-1} [ (\dot{\epsilon}/B\theta')^{1/n} ] \}^{1/1.5} \quad (40)$$

which indicates that the flow stress will vary parabolically with strain. Such behavior is exhibited by polycrystalline materials (see, for example, the data of Kocks<sup>35</sup> on aluminum, Fig. 9) and in single crystals at fairly large strains (see the data, Fig. 10, and analysis of Bell<sup>36</sup>). Parabolic strain hardening could also be expected from physical arguments if the dislocation density increases linearly with strain and the flow stress varies parabolically with dislocation density according to the Taylor relation

$$\sigma \propto \sqrt{\rho} \quad (41)$$

In the above development of the  $\dot{\epsilon}$  equation and the  $\dot{F}_{\text{def}}$  equation, we have been ignoring back stresses but designing the equations to produce certain behavior (e.g. the proper steady-state response). Of course, as indicated earlier, the full set of equations must contain back stresses in order to treat cyclic deformation and other important related phenomena. In the next section, back stresses will be introduced into the equations in a manner which adds these capabilities while *preserving* the behavior discussed in this section.

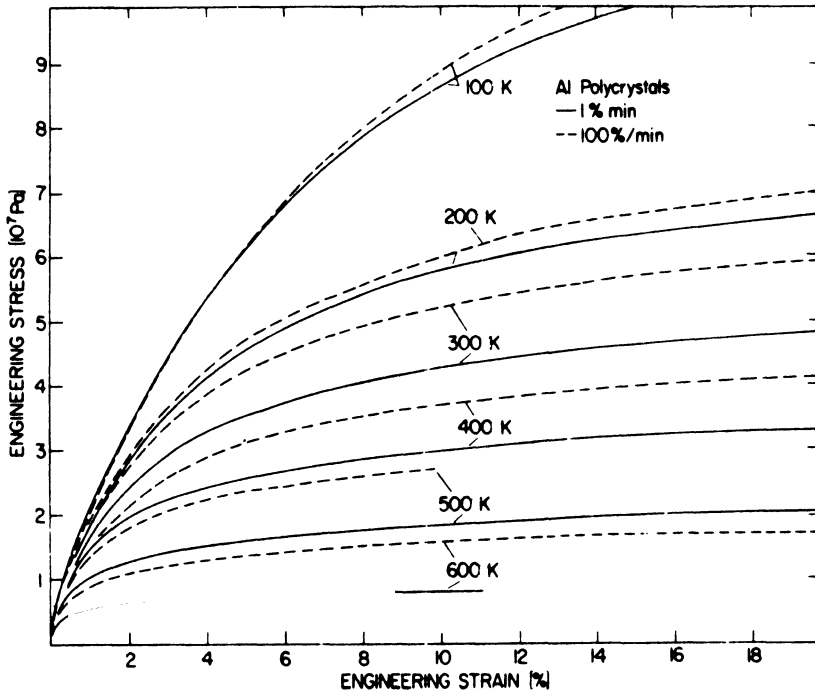


**Fig. 9.** Data on the stress–strain response of polycrystalline aluminum, showing the parabolic hardening obtained at moderately large strains. After Kocks.<sup>35</sup>

### 2.3.3. $\dot{R}$ Equation and Couplings between $R$ and $F_{def}$

Section 2.2.5 has discussed the need for, and proper placement of, the back stress variable ( $R$ ) in the equations, concluding that  $R$  must be *subtracted from*  $\sigma/E$  in the strain rate equation, that the absolute value of  $\sigma/E - R$  must be used to ‘drive’ the non-elastic strain rate, and that the sign of  $\dot{\epsilon}$  must be determined from  $\text{sgn}(\sigma/E - R)$ . Thus eqn (34) becomes

$$\dot{\epsilon} = B\theta' \{ \sinh[ (|\sigma/E - R| / \sqrt{F_{def}})^{1.5} ] \}^n \text{sgn}(\sigma/E - R) \quad (42)$$

Also, since isotropic hardening is a scalar effect ( $F_{def}$  is always positive, like subgrain sizes and dislocation densities), but  $\dot{\epsilon}$  may be positive or negative,  $\dot{\epsilon}$  in eqn (35) is replaced by  $|\dot{\epsilon}|$ .

Just as in the preceding section (in which the  $\dot{F}_{def}$  equation had to be designed correctly in order to be sure that the general strain rate

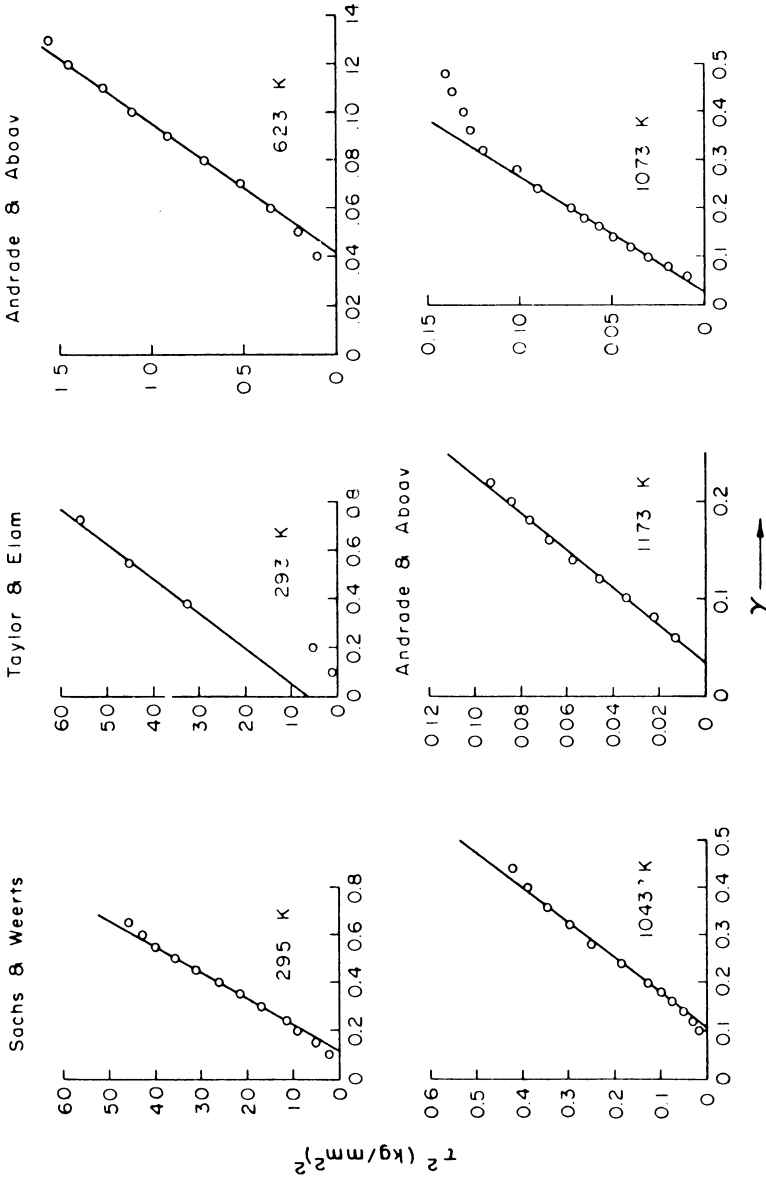
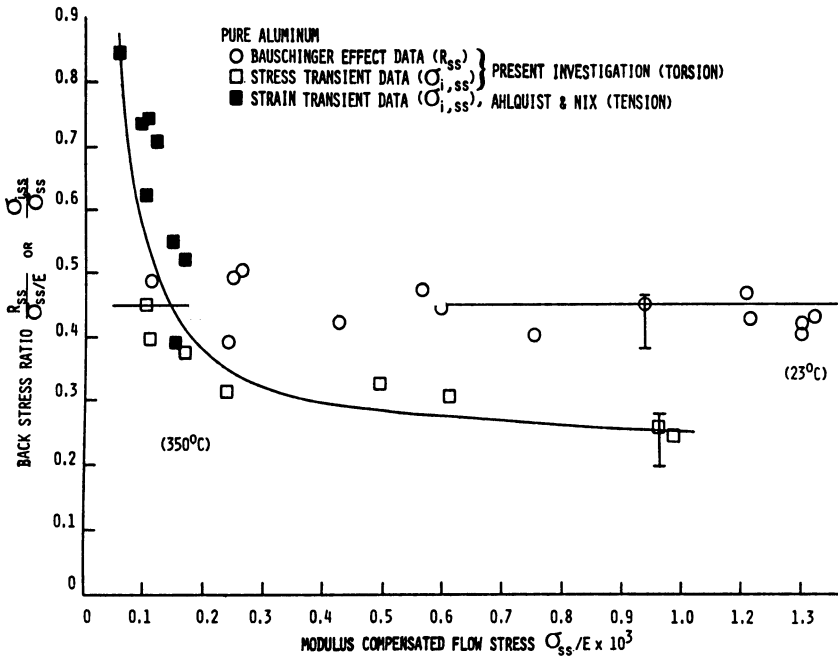


Fig. 10. Data on the stress-strain response of single crystals of copper, showing the parabolic hardening obtained at moderately large strains. After Bell.<sup>36</sup>

equation gave the correct response for the special case of steady-state) the equation governing  $R$  must be designed so that, even when it is present in the strain rate equation, the *steady-state* behavior of the entire system of equations is still in accordance with the Garofalo expression. The way this has been done in the MATMOD equations is to assume that the steady-state value of  $R$  should be directly proportional to the steady-state value of  $\sigma/E$ . This assumption agrees with experimental measurements of back stresses by *some* techniques (such as Ziaai's Bauschinger effect data, over a wide range in temperatures for both aluminum and type 304 stainless steel;<sup>37</sup> see Fig. 11). With other techniques (such as the strain transient dip tests used by Ahlquist and Nix<sup>23</sup> and the stress transient dip test used by Ziaai<sup>38</sup>) the steady-state back stresses have *not* been found to be proportional to the steady-state flow stress, although re-analysis of such data to correct for 'anelastic' effects is currently ongoing by Blum<sup>39</sup> and others.



**Fig. 11.** Data by Ahlquist and Nix<sup>23</sup> and Ziaai<sup>37</sup> on the steady-state back stress as measured by Bauschinger effect tests and by stress and strain transient dip tests. After Ziaai.<sup>37</sup>

The general form of the  $\dot{R}$  equation was discussed in Section 2.2.5. As with  $F_{\text{def}}$ , the initial version of the MATMOD equations considered only work-hardening and static recovery terms in the  $\dot{R}$  equation. To force  $R_{\text{ss}}$  to be proportional to  $\sigma_{\text{ss}}$  it is necessary that the rate of recovery of  $R$  contain a sinh-type dependence on  $R$  itself and that its temperature dependence be the same as that appearing in the  $\dot{\epsilon}$  and  $\dot{F}_{\text{def}}$  equations. Specifically, the equation

$$\dot{R} = H_1 \dot{\epsilon} - H_1 B \theta' [\sinh(A_1 |R|)]^n \text{sgn}(R) \quad (43)$$

produces a steady-state value for  $R$  which, when substituted into eqn (42), causes this equation to reduce to the Garofalo expression. The magnitude of the constant  $A_1$  determines the magnitude of the back stresses at steady state, specifically

$$R_{\text{ss}} = (A/A_1)(\sigma_{\text{ss}}/E) \quad (44)$$

Since, in effect, some of the steady-state strengthening is now being manifest as directional hardening, less is required in the form of isotropic hardening; for this reason  $A^3$  in eqn (35) must be replaced by a new constant  $A_2$  determined from

$$A_2 = [A/(1 - A/A_1)]^3 \quad (45)$$

Equations (35), (42), and (43) constitute a set of equations which will exhibit both kinematic hardening and isotropic hardening and will produce the proper steady-state behavior. However, one major set of effects is not simulated by these equations, namely cyclic hardening, cyclic softening, and cyclic 'saturation' at a stress amplitude which depends on the strain amplitude.

Cyclic hardening and softening are associated, physically, with changes in cell size, subgrain size, and dislocation density (see, for example, the data by Abdel-Raouf and Plumtree<sup>3</sup> associated with Fig. 2, and by Lawrence and Jones<sup>40</sup>). Since these all fall into the isotropic hardening category, one expects their effects to be manifested by changes in  $F_{\text{def}}$  in the equations. As  $F_{\text{def}}$  changes, the flow stress  $\sigma$  will change (at constant strain rate and temperature) according to eqn (42), thus affecting the stress amplitude.

As mentioned above, an important observation in cyclic deformation is that the stress amplitude depends on the strain amplitude. However, the entire concept of state-variable-based constitutive equations prohibits an explicit dependence of any of the variables upon a quantity like strain *amplitude*, because this is an integrated quantity;  $\dot{\epsilon}$ ,

$\dot{R}$  and  $\dot{F}_{\text{def}}$  can only depend on *current* values of the internal and external variables so that the equations will have the generality to treat arbitrary histories of loading. To resolve this dilemma, we can consider the physical nature of cyclic hardening and softening, and in particular the relationship (probably oversimplified but still capturing the essential interdependences) between back stresses and isotropic hardening. As deformation proceeds in a given direction, dislocations are forced against obstacles (building up back stresses) and, as these internal stresses become intense enough, the dislocations will climb and/or cross-slip around the obstacles, producing three-dimensional dislocation substructures (isotropic hardening) in the process. If the deformation is monotonic, large back stresses can be built up, leading to substantial isotropic hardening. When, however, the direction of deformation is changed, dislocations glide back out of their pileups and do not tend to climb or cross-slip until they form pileups consistent with the new direction of straining. If the direction of deformation is *repeatedly* changed (as in cyclic deformation) and the strain range is small, then the pileups never get very intense and there is never much driving force for isotropic hardening. As the strain range increases, the pileup intensity at and near the strain limits increases, and there is more isotropic hardening.

It is worth noting that the oversimplified picture contains some of the same elements as the more rigorously correct picture of cyclic deformation based on persistent slip bands (see, for example, work by Mughrabi and colleagues<sup>41</sup>), in which screw dislocations shuttle back and forth in the bands lying between walls of high dislocation density. When, in one half-cycle, screw dislocations travel in a given direction parallel to the walls, they lay down edge dislocations along the walls, but when the direction of straining is reversed during the next half-cycle, the screw dislocations travel in the opposite direction and can *remove* these edge dislocations from the walls. Thus there is a coupling between directional hardening (associated with dislocation motion in a given direction) and the net amount of isotropic hardening (associated with the wall thickness and/or spacing).

These physical pictures suggest that the proper way to treat cyclic hardening, softening, and saturation is to introduce a cross-coupling between  $R$  and  $F_{\text{def}}$ , making the rate of change of  $F_{\text{def}}$  dependent upon the current value of the back stress  $R$ . The specific version of the  $\dot{F}_{\text{def}}$  equation which embodies this concept<sup>10</sup> is

$$\dot{F}_{\text{def}} = H_2[C_2 + |R| - (A_2/A_1)/F_{\text{def}}^{1.5}]|\dot{\epsilon}| - H_2C_2B\theta'[\sinh(A_2F_{\text{def}}^{1.5})]^n \quad (46)$$

where  $H_2$  replaces  $H$  and  $C_2$  is a new constant. The  $|R|$  term in the work-hardening coefficient represents the manner in which back stresses drive isotropic hardening. The term which follows it produces, in effect, a dynamic equilibrium between  $R$  and  $F_{\text{def}}$  so that, as  $R$  goes through a cycle,  $F_{\text{def}}$  increases (or decreases) until the negative contribution from this term exactly offsets the positive contribution from  $C_2 + |R|$ . With this equation, as the strain range increases, the average value of  $|R|$  during one cycle increases, and thus the value which  $F_{\text{def}}$  takes on at cyclic saturation (meaning  $\dot{F}_{\text{def}} = 0$ , averaged over one cycle) increases. In this manner, the equations simulate the important aspect of the cyclic deformation response in which the extent of isotropic hardening (at saturation) increases with the strain range.

Figure 12 illustrates the behavior of the equations with this addition,

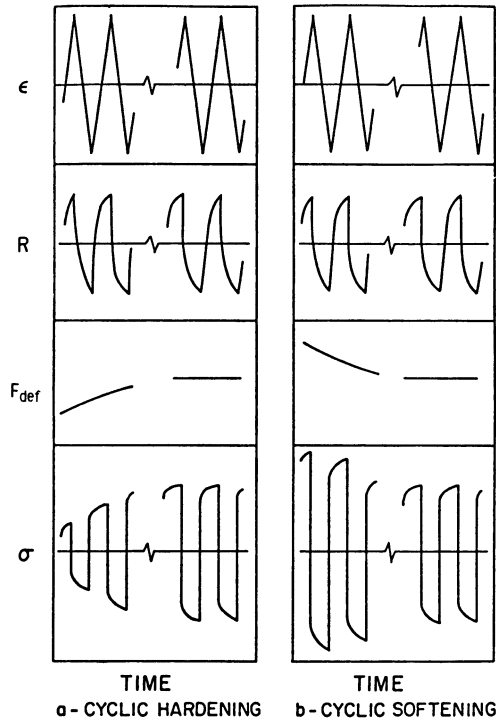


**Fig. 12.** Schematic illustration of the behavior of the MATMOD equations under cyclic deformation, showing how the average amplitude of the back stress ( $R$ ) causes gradual changes in the isotropic hardening variable  $F_{\text{def}}$ , which produce cyclic hardening or cyclic softening. After Miller.<sup>9</sup>

showing how cyclic hardening (or cyclic softening) is simulated if the initial value of  $F_{\text{def}}$  is less than (or greater than, respectively) the saturated value of  $F_{\text{def}}$  which is reached under the imposed strain range, strain rate, and temperature.

The above discussion has focussed on the earlier form of the MATMOD equations which contained only a single back stress,  $R$ , and a single isotropic hardening variable,  $F_{\text{def}}$ . As mentioned above, more recent developments in the form of the MATMOD-4V equations<sup>16,26</sup> refined these concepts and created separate short-range and long-range back stresses ( $R_a$  and  $R_b$  respectively), and separate isotropic hardening variables representing homogeneously distributed dislocations and heterogeneous dislocation substructures ( $F_{\text{def},\rho}$  and  $F_{\text{def},\lambda}$ , respectively). Equation (15) shows how these enter into the strain-rate equation. Since each of these variables represents a category of strain hardening, each of them is governed by a differential equation of the work-hardening/recovery form. Each of these equations contains, in addition to a strain-hardening term and a static recovery term, a dynamic recovery term which is driven by the magnitude of  $\dot{\epsilon}$  instead of by thermal activation. This dynamic recovery term is the key to the ability of the MATMOD-4V equations to treat strain softening. Within the dynamic recovery term for each structure variable ( $X_i$ ) is an 'instability factor' dependent upon the current values of  $X_i$  itself and the current temperature and  $\dot{\epsilon}$ ; this factor is arranged so that, if  $X_i$  is less than the steady-state value of  $X_i$  for the current  $\dot{\epsilon}$  and  $T$ , then straining causes *increases* in  $X_i$ ; however, if  $X_i$  is greater than the steady-state value of  $X_i$  for the current  $\dot{\epsilon}$  and  $T$ , then straining causes *decreases* in  $X_i$ .

Also embodied in the MATMOD-4V equations are several 'structure variable interactions'; one of these is the use of the long-range back stress ( $R_b$ ) as the driving force for heterogeneous substructure isotropic hardening ( $F_{\text{def},\lambda}$ ), as discussed above in connection with the simpler MATMOD equations. Additional interactions include an effect of the homogeneously distributed dislocation density (represented as  $F_{\text{def},\rho}$ ) upon the rate of buildup of short-range back stresses ( $R_a$ ), an effect of the heterogeneous substructure ( $F_{\text{def},\lambda}$ ) upon the rate of buildup of long-range back stresses ( $R_b$ ), and an effect of  $F_{\text{def},\lambda}$  upon the rate of change of  $F_{\text{def},\rho}$ .

The full set of MATMOD-4V equations is shown in Fig. 13a, and the material constants in them (for pure aluminum) are given in Fig. 13b. Further details on their derivation are given elsewhere.<sup>16,26</sup>

$$\begin{aligned} \dot{\epsilon} &= B\theta' \left\{ \sinh \left[ \frac{|\sigma/E - (R_A + R_B)|}{\sqrt{F_{\text{def},\rho} + F_{\text{def},\lambda}}} \right] \right\}^p \text{sgn}[\sigma/E - (R_A + R_B)] \\ \dot{R}_A &= H_2 \left\{ (1 + C_2)\dot{\epsilon} - \frac{A_2 R_A |\dot{\epsilon}| [\sinh^{-1}(|\dot{\epsilon}|/B\theta')^{1/n}]^{p_2-1}}{[A_4 F_{\text{def},\rho}^{p/2(p-1)}]^{p_2}} \right\} \\ &\quad - H_2 C_2 B\theta' [\sinh(A_2 |R_A|)]^n \text{sgn}(R_A) \\ \dot{R}_B &= H_3 \left\{ (1 + C_3)\dot{\epsilon} - \frac{A_3 R_B |\dot{\epsilon}| [\sinh^{-1}(|\dot{\epsilon}|/B\theta')^{1/n}]^{p_3-1}}{[A_5 F_{\text{def},\lambda}^{p/2(p-1)}]^{p_3}} \right\} \\ &\quad - H_3 C_3 B\theta' [\sinh(A_3 |R_B|)]^n \text{sgn}(R_B) \\ \dot{F}_{\text{def},\rho} &= H_4 \left\{ (1 + C_4) - \frac{A_4 F_{\text{def},\rho}^{p/2(p-1)} [\sinh^{-1}(|\dot{\epsilon}|/B\theta')]^{p_4-1}}{[A_5 F_{\text{def},\lambda}^{p/2(p-1)}]^{p_4}} \right\} \\ &\quad \times |\dot{\epsilon}| - H_4 C_4 B\theta' [\sinh(A_4 F_{\text{def},\rho}^{p/2(p-1)})]^n \\ \dot{F}_{\text{def},\lambda} &= H_5 \left\{ C_5 + \frac{A_3 |R_B|}{\sinh^{-1}(|\dot{\epsilon}|/B\theta')^{1/n}} - \left[ \frac{A_5 F_{\text{def},\lambda}^{p/2(p-1)}}{\sin^{-1}(|\dot{\epsilon}|/B\theta')^{1/n}} \right]^{p_5} \right\} \\ &\quad \times |\dot{\epsilon}| - H_5 C_5 B\theta' [\sinh(A_5 F_{\text{def},\lambda}^{p/2(p-1)})]^n \\ \theta' &= \begin{cases} \exp\{- (Q/kT_i)[\ln(T_i/T) + 1]\}, & T \leq T_i \\ \exp(- (Q/kT)), & T > T_i \end{cases} \end{aligned}$$

**Fig. 13a.** The one-dimensional version of the MATMOD-4V equations. After Lowe.<sup>16</sup>

<i>Constant</i>	<i>Value</i>
$Q^*$	35 500 cal/mol
$T_i$	461 K
$B$	$7 \times 10^{10} \text{ s}^{-1}$
$n$	5.0
$p$	2.0
$A_2$	7630
$A_3$	$2.0 \times 10^5$
$A_4$	$1.154 \times 10^8$
$A_5$	$1.000 \times 10^8$
$H_2$	0.3
$H_3$	$1.5 \times 10^{-4}$
$H_4$	$1.0 \times 10^{-7}$
$H_5$	$1.0 \times 10^{-6}$
$C_2$	$2.0 \times 10^{-3}$
$C_3$	$2.0 \times 10^{-3}$
$C_4$	$2.0 \times 10^{-8}$
$C_5$	$2.0 \times 10^{-8}$
$p_2$	0.25
$p_3$	0.10
$p_4$	0.10
$p_5$	0.50

**Fig. 13b.** Material constants for high-purity aluminum for the MATMOD-4V equations. After Lowe.<sup>16</sup>

### 2.3.3. $F_{sol}$ Equations

In Section 2.2.6 the concept of an explicit representation of solute drag forces was introduced. Retaining the manner in which solute strengthening combines with isotropic deformation strengthening (described in connection with eqn (24)) the strain-rate eqn (42) becomes

$$\dot{\epsilon} = B\theta' \{ \sinh[ (|\sigma/E - R| / \sqrt{F_{sol,1} + F_{def}(1 + F_{sol,2})})^{1.5} ] \}^n \operatorname{sgn}(\sigma/E - R) \quad (47)$$

Solute strengthening is dependent upon the temperature-compensated non-elastic strain rate  $\dot{\epsilon}/\theta'$  through the variables  $F_{sol,1}$  (non-interactive solute strengthening) and  $F_{sol,2}$  (interactive, or synergistic, solute strengthening). In both cases, the peak solute drag force occurs at intermediate values of  $\dot{\epsilon}/\theta'$  representing, in rough terms, a 'resonance' between the dislocation velocity and the velocity of diffusion of solute atoms through the solvent.

While various theoretical treatments of the solute drag force exist, none has been shown to have the quantitative accuracy sufficient to predict the actual flow stress behavior of engineering alloys. Also, since  $F_{sol}$ , as used in the MATMOD equations, accounts for *all* intrinsic strengthening mechanisms, some portion of  $F_{sol}$  is due to grain boundaries and any precipitates which are present, so that additional theoretical terms accounting for these would have to be added separately if theoretical expressions specifically pertaining to solute drag were utilized.

In view of the above, the approach taken in the MATMOD equations thus far has been to choose a phenomenologically motivated equation form for the  $F_{sol}$  expressions, and to determine the constants in the equations from the flow stress data itself (e.g. yield strength vs. temperature) on the basis that the data already reflect the collective effects of the entire group of 'intrinsic' strengthening mechanisms. The normal distribution function (from statistics) has been utilized as an expression which goes through a peak at intermediate values of its argument. Thus the cores of the  $F_{sol}$  equations are expressions of the form

$$F_{sol} = F_{sol,max} \exp\{ - [\log(|\dot{\epsilon}|/\theta') - \log(\dot{\epsilon}/\theta')_{max}]^2 / \beta \} \quad (48)$$

where  $F_{sol,max}$  is the peak value of  $F_{sol}$ ,  $\dot{\epsilon}/\theta'_{max}$  is the value of  $|\dot{\epsilon}|/\theta'$  at which  $F_{sol}$  goes through this peak, and  $\beta$  is a third material constant which sets the width of the peak. Since each peak in  $F_{sol}$  is associated

with a particular solute species, the  $F_{\text{sol}}$  equations for an engineering alloy containing multiple solutes are actually a *sum* of terms of the above form.

Recalling the manner in which  $\theta'$  depends upon temperature,  $\dot{\epsilon}/\theta'$  approaches zero as the temperature approaches zero. Hence the contribution to  $F_{\text{sol}}$  from the above normal distribution expression approaches zero as  $\dot{\epsilon}/\theta'$  approaches zero. This is physically meaningful since clouds of solute atoms cannot be sustained at very low temperatures, where the rate of diffusion is too small for the clouds to keep up with the dislocations. However, the intrinsic strength of metals and alloys is decidedly *not* zero at low temperatures, and presumably is set by entities other than solute atmospheres such as individual solute atoms, grain boundaries, and precipitates. To represent the contribution to  $F_{\text{sol}}$  of these other entities, an additional 'baseline' term is added to the  $F_{\text{sol}}$  expression. Reasonable agreement with data is achieved if this baseline term simply contains a linear negative dependence of  $F_{\text{sol}}$  upon  $\log(\dot{\epsilon}/\theta')$ . As an example, the sum of the three terms used in the  $F_{\text{sol}}$  expression for Zircaloy is shown in Fig. 14.

Thus far, it has been assumed that the  $\theta'$  which appears in the  $F_{\text{sol}}$  equation is the same  $\theta'$  which appears in the  $\dot{\epsilon}$ ,  $\dot{R}$ , and  $\dot{F}_{\text{def}}$  equations.

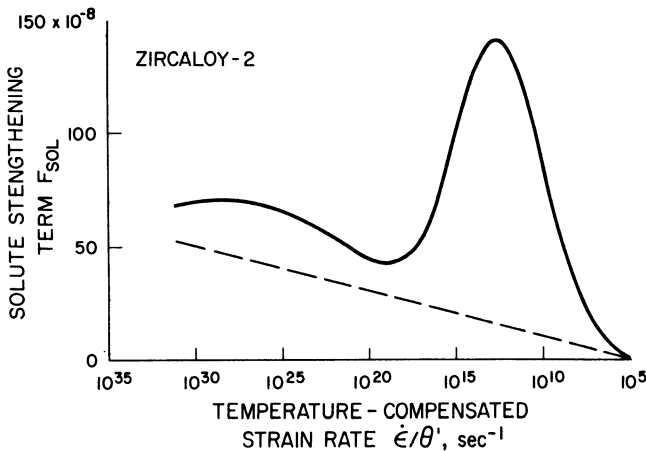


**Fig. 14.** Behavior of the solute strengthening variable  $F_{\text{sol}}$  as a function of temperature-compensated strain rate, showing how  $F_{\text{sol}}$  is composed of a baseline term (dashed line) plus two solute 'peaks' associated with oxygen and hydrogen, respectively.

This is tantamount to assuming that the activation energy for diffusion of solute atoms is the same as the activation energy which controls recovery of back stresses (in the  $\dot{R}$  equation), recovery of isotropic strength (in the  $\dot{F}_{\text{def}}$  equation), and the non-elastic straining process itself (in the  $\dot{\epsilon}$  equation). This assumption was made initially<sup>15</sup> for simplicity, and also because it caused the steady-state flow stress to depend uniquely upon  $\dot{\epsilon}/\theta'$  (in the same manner that, for example, the flow stress of Al–Mg alloys is often correlated against  $\dot{\epsilon}/D$  or some other single function of strain rate and temperature<sup>42</sup>). However, in reality the activation energy within the  $F_{\text{sol}}$  expression (denoted as  $Q_{\text{sol}}$ ) corresponds to diffusion of the solute species in the solvent, whereas the other activation energies (denoted as  $Q_{\text{def}}$ ) are more likely to correspond to self-diffusion of the solvent atoms. Thus in general  $Q_{\text{sol}}$  does not have to equal  $Q_{\text{def}}$ . In fact, it has been shown<sup>43</sup> that, when  $Q_{\text{sol}} \neq Q_{\text{def}}$ , fairly realistic simulations are obtained of the activation energy *peaks* which have been observed in a variety of alloys. Accordingly, in applying<sup>29,30</sup> the MATMOD equations to austenitic stainless steel (type 316), differing values were chosen for  $Q_{\text{def}}$  and for the two activation energies governing  $F_{\text{sol},1}$  and  $F_{\text{sol},2}$  respectively (denoted  $Q_{\text{sol},1}$  and  $Q_{\text{sol},2}$ ). Figure 15a gives the detailed form of the equations as applied to type 316 stainless steel, and Fig. 15b gives the constants in these equations.

Referring back to eqn (47), it will be noted that  $\dot{\epsilon}$  depends upon  $F_{\text{sol},1}$  and  $F_{\text{sol},2}$  but that these depend upon  $\dot{\epsilon}$ . Thus the set of equations is implicit in  $\dot{\epsilon}$ . This necessitates some special attention to the numerical methods used in integrating the equations to generate predictions, as discussed further in Section 4.

Furthermore, the combination of the  $F_{\text{sol}}$  expressions and the basic  $\dot{\epsilon}$  equation can lead to a non-monotonic variation of  $\sigma$  with  $\dot{\epsilon}$ . While this can generate some further numerical difficulties (again treatable using the methods outlined in Section 4), it is physically realistic; local peaks in the flow stress with respect to strain rate<sup>44</sup> and temperature<sup>45</sup> are observed in a variety of materials, and the occurrence of serrated yielding (the Portevin–LeChatelier effect) is readily explained in terms of a non-monotonic dependence of  $\sigma$  upon  $\dot{\epsilon}$ <sup>46</sup> or, alternatively, upon the dislocation velocity.<sup>47</sup> This topic will be further discussed in Section 4.

#### 2.3.4. *Multiaxial Generalization*

The preceding discussions have focussed on the uniaxial version of the equations, for simplicity. All of the concepts utilized, however, are

readily generalized to a full multiaxial set of equations, using only very straightforward assumptions. When this is done, the resulting model contains a mixture of isotropic and kinematic hardening in their full three-dimensional sense. These simulate mixtures of yield surface expansion and yield surface translation. Improvements to the MATMOD equations have recently been made by Helling<sup>48</sup> to treat yield surface *distortion*.

In creating the general multiaxial set of equations, the approach suggested by Rice<sup>49</sup> has been taken, with the following specific implementation.

1. The back stress  $R$  (or, in the more recent MATMOD-4V equations, each of the back stresses  $R_a$  and  $R_b$ ) becomes a back stress tensor  $R_{ij}$  ( $R_{a,ij}$  and  $R_{b,ij}$  in the multiaxial version of MATMOD-4V).

2. The driving force for non-elastic deformation in the strain rate equation ( $|\sigma/E - R|$  in the uniaxial version of the equations) is

$$\begin{aligned}\dot{\epsilon} &= B\theta' \left\{ \sinh \left[ \left( \frac{|\frac{\sigma}{E} - R|}{\sqrt{[F_{\text{sol},1} + F_{\text{def}}(1 + F_{\text{sol},2])}]} \right)^{1.5} \right] \right\}^n \operatorname{sgn} \left( \frac{\sigma}{E} - R \right) \\ \theta' &= \exp(-Q_{\text{id}}/kT) + f \exp(-Q_{\text{cd}}/kT) \\ \dot{R} &= H_1 \exp \left( -H_3 R \operatorname{sgn} \left( \frac{\sigma}{E} - R \right) \right) [\dot{\epsilon} - B\theta' \sinh(A_1 |R|)^n \operatorname{sgn} R] \\ \dot{F}_{\text{def}} &= H_2 \left( C_2 + |R|^{1/1.5} - \left( \frac{A_2}{A_1} \right)^{1/1.5} F_{\text{def}} \right) |\dot{\epsilon}| - H_2 B C_2 \theta' \{ \sinh(A_2 F_{\text{def}}^{1.5}) \}^n \\ F_{\text{sol},1} &= F_{\text{sol},10} + \sum_{i=1}^3 M_i \left\{ \exp \left[ - \left( \frac{\log(|\dot{\epsilon}|/\theta'_{\text{sol},1}) - J_i}{B_i} \right)^2 \right] \right\} \\ \theta'_{\text{sol},1} &= \exp(-Q_{\text{sol},1}/kT) \\ F_{\text{sol},2} &= F_{\text{sol},20} + \sum_{i=1}^2 N_i \left\{ \exp \left[ - \left( \frac{\log(|\dot{\epsilon}|/\theta'_{\text{sol},2}) - K_i}{C_i} \right)^2 \right] \right\} \\ &\quad + F_{\text{sol},30} + O_i \left\{ \exp \left[ - \left( \frac{\log(|\dot{\epsilon}|) - L_i}{D_i} \right)^2 \right] \right\} \\ \theta'_{\text{sol},2} &= \exp(-Q_{\text{sol},2}/kT)\end{aligned}$$

**Fig. 15a.** The one-dimensional version of the MATMOD equations (for Type 313 stainless steel) containing two solute-strengthening variables ( $F_{\text{sol},1}$  and  $F_{\text{sol},2}$ ). After Schmidt and Miller.<sup>30</sup>

$\dot{\epsilon}$ , $\dot{F}_{det}$ , and $\dot{R}$ equation constants	$F_{sol,1}$ constants	$F_{sol,2}$ constants
$B$	$2 \times 10^9 \text{ s}^{-1}$	$38000 \text{ cal/mole}$
$n$	$5$	$4.6$
$Q_{ld}$	$67000 \text{ cal/mole}$	$K_1 = K_2$
$Q_{cd}$	$40000 \text{ cal/mole}$	$F_{sol,20}$
$f$	$4 \times 10^{-7}$	$N_1$
$H_1$	$0.01$	$N_2$
$H_2$	$3 \times 10^{-4}$	$C_1$
$H_3$	$2 \times 10^4$	$C_2$
$A_1$	$11800$	$F_{sol,20}$
$A_2$	$1.4 \times 10^{10}$	$N_1$
$C_2$	$1 \times 10^{-5}$	$N_2$
		$C_1$
		$C_2$
		$F_{sol,30}$
		$L_1$
		$O_1$
		$O_1$
		Note: if $O_1 < 0$ then set $O_1 = 0$
		$D_1$
		$D_1$
		$2$ if $\log  \dot{\epsilon}  < L_1$
		$1.8$ if $\log  \dot{\epsilon}  \geq L_1$
		$2$ if $\log \left( \frac{ \dot{\epsilon} }{\theta'_{sol,1}} \right) > J_1$
		$0.6$ if $\log \left( \frac{ \dot{\epsilon} }{\theta'_{sol,1}} \right) \leq J_1$
		$2$ if $\log \left( \frac{ \dot{\epsilon} }{\theta'_{sol,1}} \right) > J_1$
		$12$ if $\log \left( \frac{ \dot{\epsilon} }{\theta'_{sol,2}} \right) > K_1$
		$8$ if $\log \left( \frac{ \dot{\epsilon} }{\theta'_{sol,2}} \right) \leq K_1$
		$4$ if $\log \left( \frac{ \dot{\epsilon} }{\theta'_{sol,2}} \right) \leq K_1$
		$0$ if $\log \left( \frac{ \dot{\epsilon} }{\theta'_{sol,2}} \right) \leq K_1$
		$10$ if $\log \left( \frac{ \dot{\epsilon} }{\theta'_{sol,2}} \right) \leq K_1$
		$12$ if $\log \left( \frac{ \dot{\epsilon} }{\theta'_{sol,2}} \right) \leq K_1$
		$1$ if $\log \left( \frac{ \dot{\epsilon} }{\theta'_{sol,2}} \right) \leq K_1$
		$2$ if $\log \left( \frac{ \dot{\epsilon} }{\theta'_{sol,2}} \right) \leq K_1$
		$0$ if $\log \left( \frac{ \dot{\epsilon} }{\theta'_{sol,2}} \right) \leq K_1$
		$-9$ if $\log \left( \frac{ \dot{\epsilon} }{\theta'_{sol,2}} \right) \leq K_1$
		$-0.304 \times (T - 273) + 222$ if $T > 811.3 \text{ K}$
		$0.316 \times (T - 273) - 136$ if $T \leq 811.3 \text{ K}$

Fig. 15b. Material constants for type 316 stainless steel for the equations given in Fig. 15a. After Schmidt and Miller.<sup>50</sup>

replaced by a von Mises-like effective stress quantity denoted as  $\overline{\sigma/E - \mathbf{R}}$  which has  $\sigma_{ij}/E - R_{ij}$  as its argument, i.e.

$$\begin{aligned} \overline{\sigma/E - \mathbf{R}} &= (1/\sqrt{2})\{[(\sigma_{xx}/E - R_{xx}) - (\sigma_{yy}/E - R_{yy})]^2 \\ &+ [(\sigma_{yy}/E - R_{yy}) - (\sigma_{zz}/E - R_{zz})]^2 + [(\sigma_{zz}/E - R_{zz}) - (\sigma_{xx}/E - R_{xx})]^2 \\ &+ 6[(\sigma_{xy}/E - R_{xy})^2 + (\sigma_{yz}/E - R_{yz})^2 + (\sigma_{xz}/E - R_{xz})^2]\}^{1/2} \quad (49) \end{aligned}$$

3. The effective multiaxial non-elastic strain rate ( $\bar{\dot{\epsilon}}$ ) is the same function of  $\overline{\sigma/E - \mathbf{R}}$  as the uniaxial non-elastic strain rate  $\dot{\epsilon}$  is of  $|\sigma/E - R|$  (eqn (47)), i.e.

$$\bar{\dot{\epsilon}} = B\theta' \{ \sinh([\overline{(\sigma/E - \mathbf{R})}]/\sqrt{(F_{\text{sol},1} + F_{\text{def}}(1 + F_{\text{sol},2}))^{1.5}})]^n \} \quad (50)$$

4. The *signum* function in the uniaxial version of the equations is replaced by the usual Prandtl-Reuss equation based on the assumption of 'plastic flow normality' or, more exactly for the MATMOD equations in which all 'plastic' strains are time-dependent, the assumption that the current direction of the non-elastic strain rate tensor is normal to the surface of constant  $\overline{\sigma/E - \mathbf{R}}$ . Specifically,

$$\dot{\epsilon}_{ij} = (3/2)(\bar{\dot{\epsilon}}/\overline{\sigma/E - \mathbf{R}})(S_{ij}/E - R_{ij}) \quad (51)$$

where  $S_{ij}$  is the deviatoric part of the stress tensor  $\sigma_{ij}$ .

5.  $F_{\text{def}}$  (and  $F_{\text{def},\rho}$  and  $F_{\text{def},\lambda}$  in the MATMOD-4V equations) remains a scalar.

6. In all of the evolutionary equations,  $|\dot{\epsilon}|$  is replaced by  $\bar{\dot{\epsilon}}$ , and  $|R|$  ( $|R_a|$  and  $|R_b|$  in the MATMOD-4V equations) is replaced by a von Mises-like effective value of  $R$ , defined as

$$\begin{aligned} \bar{R} &= (1/\sqrt{2})[(R_{xx} - R_{yy})^2 + (R_{yy} - R_{zz})^2 + (R_{zz} - R_{xx})^2 \\ &+ 6(R_{xy}^2 + R_{yz}^2 + R_{xz}^2)]^{1/2} \quad (52) \end{aligned}$$

7. The individual equation for  $\dot{R}$  (the two equations for  $\dot{R}_a$  and  $\dot{R}_b$  in the MATMOD-4V equations) becomes a family of equations, one for each component ( $R_{ij}$ ) of the  $R$  tensor.  $\dot{\epsilon}$  in each of these equations is replaced by  $\dot{\epsilon}_{ij}$ , and  $\text{sgn}(R)$  is replaced by  $(3/2)R_{ij}/\bar{R}$ .  $H_1$  in this equation equals  $2/3$  of the  $H_1$  used in the one-dimensional equations, to account for the fact that there are multiple components of  $R$  present.<sup>50</sup>

Based on these principles, a multiaxial generalization of that version of the equations which contains  $F_{\text{sol},1}$  and  $F_{\text{sol},2}$  (but only a single  $R$  and a single  $F_{\text{def}}$ ) has been developed, implemented by Tanaka within the numerically efficient NONSS program<sup>51</sup> (see Section 4), and is

reproduced as Fig. 16. Also, a multiaxial version of the MATMOD-4V equations (without solute effects) has been developed,<sup>16</sup> implemented by Helling *et al.*<sup>52</sup> in a different computer program (based on Gear's method<sup>53</sup>), and is reproduced in Fig. 17.

With the above-described approach, the initial response of an undeformed material ( $R_{ij} = 0$ ) is isotropic, which is a good approximation for most fcc and bcc polycrystalline materials (except perhaps those with very strong textures). For HCP materials, however,

$$\begin{aligned}\dot{\epsilon}_{ij} &= D_{ijkl}^{-1} \dot{\sigma}_{ij} + \dot{\epsilon}_{ij}^N \\ \dot{\epsilon}_{ij}^N &= \frac{3}{2} \frac{\bar{\dot{\epsilon}}^N}{\sigma/E - R} \left( \frac{S_{ij}}{E} - R_{ij} \right) \\ \dot{R}_{ij} &= H_1 \exp \left\{ -H_3 R_{kl} \frac{\dot{\epsilon}_{kl}}{\bar{\dot{\epsilon}}^N} \right\} \left[ \dot{\epsilon}_{ij}^N - (3/2) B \theta' \{ \sinh(A_1 \bar{R}) \}^n \frac{R_{ij}}{\bar{R}} \right] \\ \dot{F}_{\text{def}} &= H_2 \left( C_2 + \bar{R} + \frac{A_2}{A_1} F_{\text{def}}^{1.5} \right) \bar{\dot{\epsilon}}^N - H_2 C_2 B \theta' \{ \sinh(A_2 F_{\text{def}}^{1.5}) \}^n\end{aligned}$$

where

$$\begin{aligned}\bar{\dot{\epsilon}}^N &= B \theta' \left\{ \sinh \left( \frac{\sigma/E - R}{\sqrt{F_{\text{sol},1} + F_{\text{def}}(1 + F_{\text{sol},2})}} \right)^{1.5} \right\}^n \\ F_{\text{sol},1} &= f(\bar{\dot{\epsilon}}^N / \theta'_{\text{sol},1}) \\ F_{\text{sol},2} &= f(\bar{\dot{\epsilon}}^N / \theta'_{\text{sol},2}) \\ \frac{\sigma/E - R}{\bar{R}} &= \sqrt{(3/2)(S_{ij}/E - R_{ij})(S_{ij}/E - R_{ij})} \\ \bar{R} &= \sqrt{(3/2)R_{ij}R_{ij}} \\ S_{ij} &= \sigma_{ij} - (1/3)\delta_{ij}\sigma_{kk}; \quad \delta_{ij} \begin{cases} = 1 & \text{if } i = j \\ = 0 & \text{if } i \neq j \end{cases}\end{aligned}$$

- (1)  $\theta'$ ,  $\theta'_{\text{sol},1}$  and  $\theta'_{\text{sol},2}$  are as defined in Fig. 15a.
- (2) The specific forms of  $F_{\text{sol},1}$  and  $F_{\text{sol},2}$  are defined in Fig. 15a except that  $|\dot{\epsilon}^N|$  is replaced by  $\bar{\dot{\epsilon}}^N$ .
- (3)  $\bar{\dot{\epsilon}}^N$  is the effective non-elastic strain rate which is defined by

$$\bar{\dot{\epsilon}}^N = \sqrt{(2/3)\dot{\epsilon}_{ij}^N \dot{\epsilon}_{ij}^N}$$

- (4) The constant  $H_1$  in these three-dimensional equations is 2/3 of the  $H_1$  in the one-dimensional equations; all other material constants are identical.

**Fig. 16.** Three-dimensional form of the MATMOD equations containing two solute-strengthening variables. After Tanaka.<sup>76</sup>

$$\dot{\epsilon}_i = \frac{(3/2)\bar{\epsilon}}{(\sigma/E) - R} S_i$$

where

$$\begin{aligned} \bar{\epsilon} &= B\theta' \left\{ \sinh \left[ \left( \frac{(\sigma/E) - R}{\sqrt{F_{\text{def},\rho} + F_{\text{def},\lambda}}} \right)^p \right] \right\}^n, \\ \overline{(\sigma/E) - R} &= \{M_{ij}[(\sigma_i/E) - R_i][(\sigma_j/E) - R_j]\}^{1/2}, \\ S_i &= (2/3)M_{ij}[(\sigma_j/E) - R_j], \\ M_{ij} &= \text{anisotropy constants}, \\ R_i &= R_{A_i} + R_{B_i}, \\ \dot{\epsilon}_i &= \text{non-elastic strain rate component}, \\ R_{A_i} &= \text{ith component of } R_A, \\ R_{B_i} &= \text{ith component of } R_B \\ \dot{R}_{A_i} &= H_2 \left\{ (1 + C_2)\dot{\epsilon}_i - \frac{(3/2)A_2R_{A_i}[\sinh^{-1}(|\bar{\epsilon}|/B\theta')^{1/n}]^{p_2-1}\bar{\epsilon}}{[A_4F_{\text{def},\rho}^{p/2(p-1)}]^{p_2}} \right\} \\ &\quad - H_2C_2B\theta'[\sinh(A_2\bar{R}_A)]^n[(3/2)R_{A_i}/\bar{R}_A] \\ \dot{R}_{B_i} &= H_3 \left\{ (1 + C_3)\dot{\epsilon}_i - \frac{(3/2)A_3R_{B_i}[\sinh^{-1}(|\bar{\epsilon}|/B\theta')^{1/n}]^{p_3-1}\bar{\epsilon}}{[A_5F_{\text{def},\lambda}^{p/2(p-1)}]^{p_3}} \right\} \\ &\quad - H_3C_3B\theta'[\sinh(A_3\bar{R}_B)]^n[(3/2)R_{B_i}/\bar{R}_B] \\ \dot{F}_{\text{def},\rho} &= H_4 \left\{ (1 + C_4) - \frac{A_4F_{\text{def},\rho}^{p/2(p-1)}[\sinh^{-1}(\bar{\epsilon}/B\theta')^{1/n}]^{p_4-1}}{[A_5F_{\text{def},\lambda}^{p/2(p-1)}]^{p_4}} \right\} \bar{\epsilon} \\ &\quad - H_4C_4B\theta'[\sinh(A_4F_{\text{def},\rho}^{p/2(p-1)})]^n \\ \dot{F}_{\text{def},\lambda} &= \left\{ H_5C_5 + \frac{A_3R_B}{\sinh^{-1}(\bar{\epsilon}/B\theta')^{1/n}} - \left[ \frac{A_5F_{\text{def},\lambda}^{p/2(p-1)}}{\sinh^{-1}(\bar{\epsilon}/B\theta')^{1/n}} \right]^{p_5} \right\} \bar{\epsilon} \\ &\quad - H_5C_5B\theta'[\sinh(A_5F_{\text{def},\lambda}^{p/2(p-1)})]^n \end{aligned}$$

Fig. 17. Three-dimensional form of the MATMOD-4V equations. After Helling *et al.*<sup>52</sup>

crystallographic texture effects can produce stronger initial anisotropies. An anisotropic version of the MATMOD equations (as applied to Zircaloy) has been developed<sup>54</sup> based on the Hill approach.<sup>55</sup>

### 3. SIMULATIONS AND PREDICTIONS

As used in this work, the term ‘simulations’ refers to comparisons between model calculations and test data in which the data were used

to determine the material constants. Thus 'simulations' are not independent verifications but are simply indications of the categories of behavior which can be treated by the model. The term 'predictions', on the other hand, refers to comparisons in which the data were *not* used in obtaining the material constants and thus successful 'predictions' constitute completely independent verifications of the model. Obviously, convincing demonstrations of predictive capabilities require that the predictions be for cases which are sufficiently different from those in which the material constants were determined.

A comment is necessary concerning the versions of the equations used in these simulations and predictions. The model development process has been an evolutionary one. Thus the application of the model to various materials has involved various versions of the equations, each one being an improvement on the previous version and, in general, retaining its predictive capabilities. Accordingly, there does not exist at present any one large body of predictions made with a single version of the model; however, at various stages, sets of independent predictions have been made to prove the concepts introduced at that stage. Accordingly, this section will be organized according to the materials studied, and reference will be made to the particular equations used for each case.

### **3.1. Aluminum** (emphasizing strain hardening and strain softening behaviors)

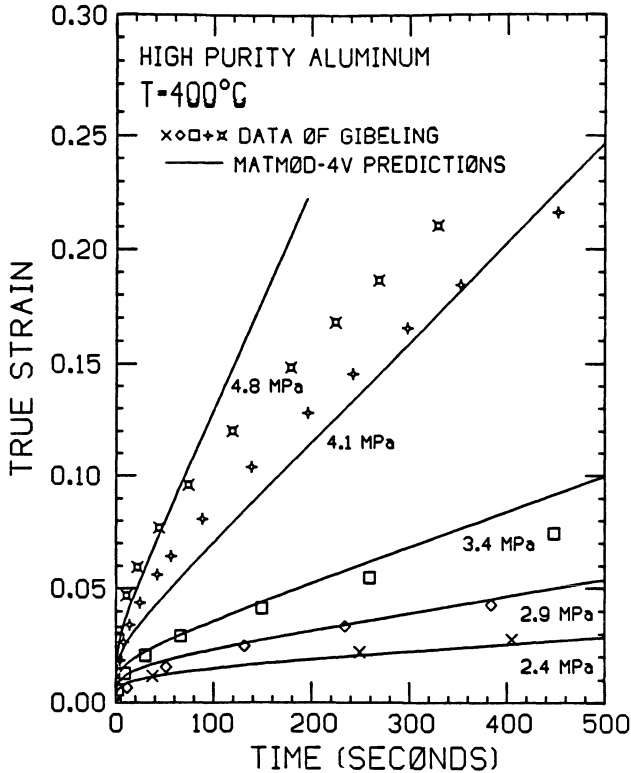
#### *3.1.1. Steady-state and Transient Creep Behavior*

Figure 1 has already shown the way in which the material constants  $Q_1$ ,  $A$ ,  $B$ , and  $n$  can be chosen so that the equations' steady-state creep response agrees with the data. The fit (especially at high stresses) is imperfect, so that some errors in predicted steady-state creep rate can be expected.

Figure 18 shows the full strain-time curves<sup>16</sup> for a few stresses, illustrating the ability of the MATMOD-4V equations independently to predict the transient portion of the creep test response. The results are fairly good.

#### *3.1.2. Strain Hardening under Constant Strain Rate*

Figure 19 compares transient hardening predictions<sup>16</sup> against data for constant strain-rate behavior at a variety of temperatures and strain rates. The overall agreement is far from perfect, but should be



**Fig. 18.** MATMOD-4V predictions for constant-stress creep tests at various stresses, compared against data of Gibeling. After Lowe.<sup>16</sup>

considered encouraging in view of the broad range of temperature being covered and the fact that the temperature and strain-rate dependences are being inferred, in effect, from steady-state creep data and not from data on transients. The poorest results are at low temperature where the data on steady-state behavior are most sparse.

### 3.1.3. Creep-Plasticity Interactions

Figure 20 concerns the transient response to constant-stress loading. Data of Chen *et al.*<sup>56</sup> on the left are compared against independent MATMOD predictions<sup>57</sup> on the right. There are several significant points. First, for simple constant-stress creep of annealed material (curves A), the model predicts approximately the correct total amount of transient creep (obtained by extrapolating the steady-state creep

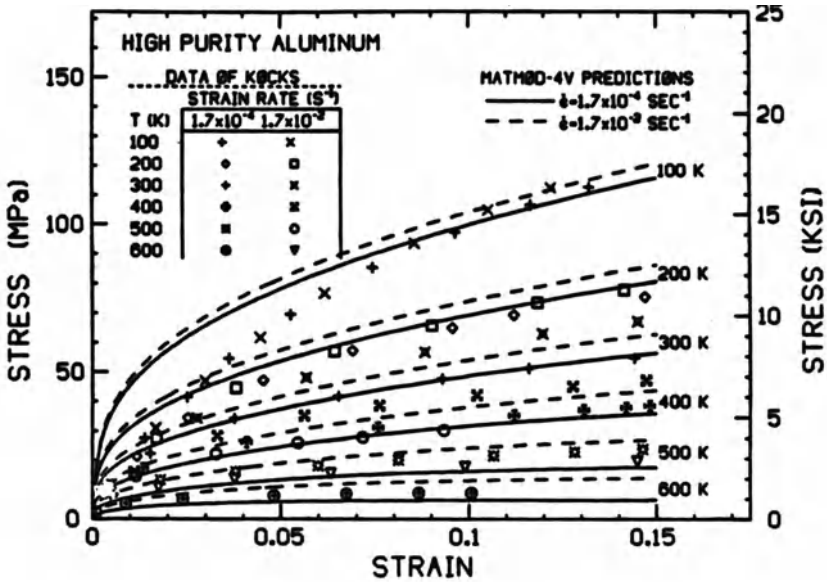


Fig. 19. MATMOD-4V predictions for constant-strain-rate tests at various temperatures and two different strain rates, compared against data of Kocks. After Lowe.<sup>16</sup>

line back to  $t=0$ ); since the principal constant which governs the magnitude of transient creep is the work-hardening coefficient in the  $\dot{F}_{\text{def}}$  equation which is, in turn, obtained by fitting to stress-strain data, this indicates the ability of the model to interrelate 'creep' and 'plasticity' with respect to work-hardening. Second, curves B illustrate the effect of a 5% prestrain (applied under constant-strain-rate conditions and at room temperature) in reducing the amount of subsequent primary creep; this effect is predicted successfully because the prestrain raises  $F_{\text{def}}$  which, in turn, brings it closer to its steady-state value in the creep test so that less transient hardening is required compared to annealed material. Finally, curves C illustrate that, for a 10% prestrain,  $F_{\text{def}}$  is increased to a value which exceeds the steady-state value for the creep test conditions; consequently, during the course of the creep test,  $F_{\text{def}}$  decreases, which causes  $\dot{\epsilon}$  to increase and produces a successful prediction of the inverted primary creep observed in the data.

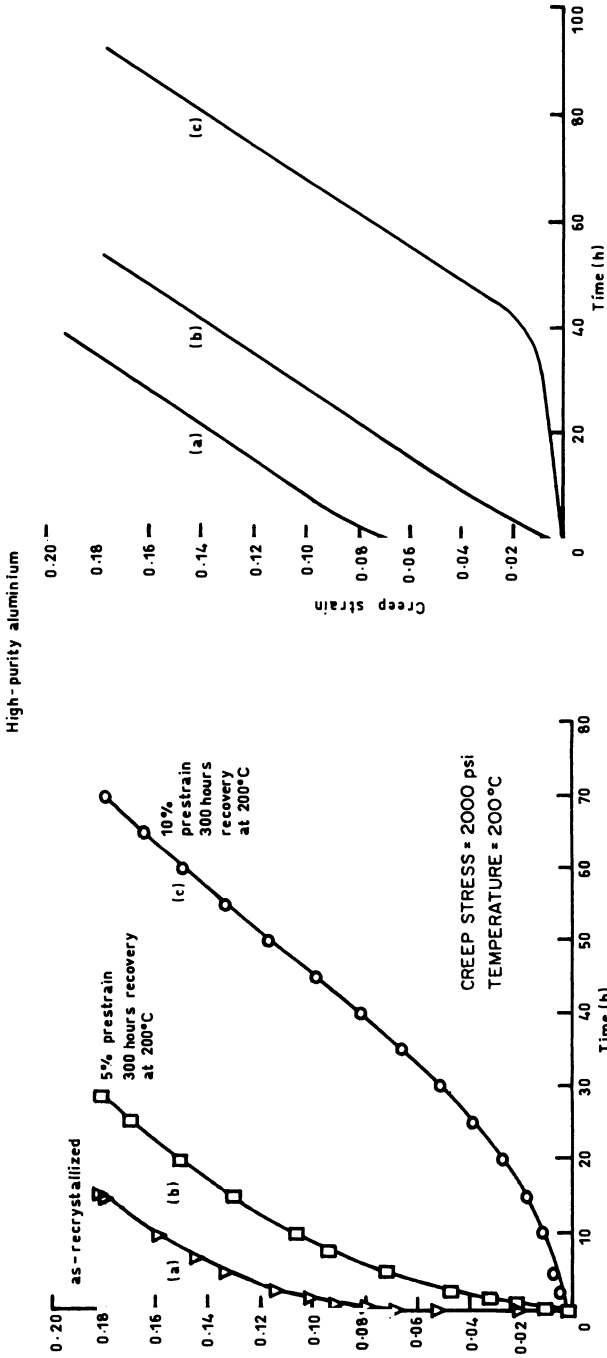


Fig. 20. MATMOD predictions (right) for 'creep-plasticity interaction' (elevated-temperature creep tests following room-temperature prestrain), compared against data (left) of Chen *et al.*<sup>56</sup> After Miller.<sup>57</sup>

### 3.1.4. Stress History Effects

A second example of the equations' capability for treating the effects of previous history on the subsequent deformation response is given in Figs 21 and 22. Figure 21 concerns a stress-increase test, illustrating that after a strain of 16% the creep rate at 27.6 MPa is higher for a specimen previously strained at 13.8 MPa than for one strained at 27.6 MPa. The predictions<sup>15</sup> are in qualitative agreement with the data; the behavior occurs because, at the lower stress, there is more time for recovery (of  $F_{def}$ ) to offset the strain hardening caused by the

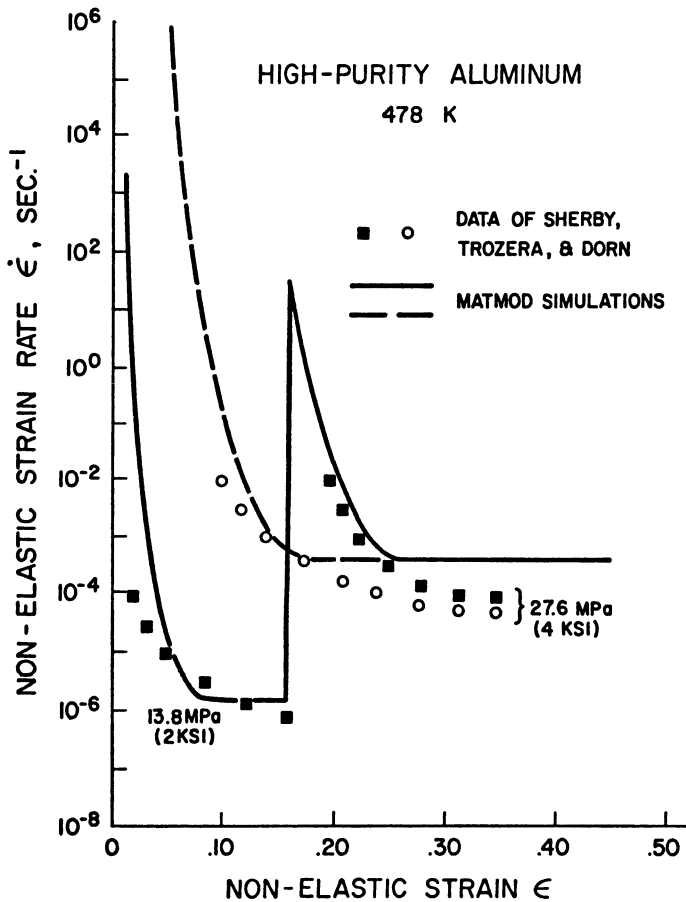
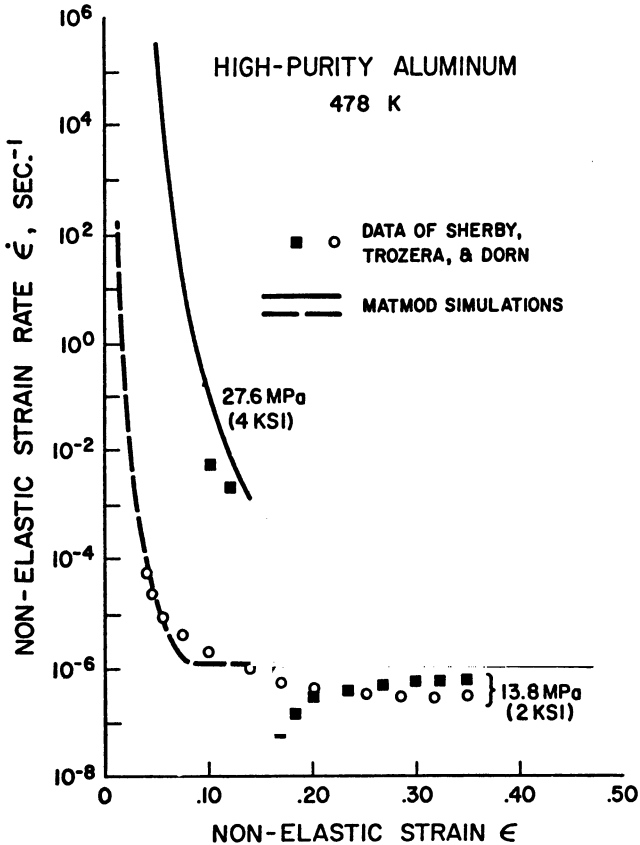


Fig. 21. MATMOD predictions for a stress-increase test, compared against data of Sherby *et al.*<sup>31</sup> After Miller and Sherby.<sup>15</sup>



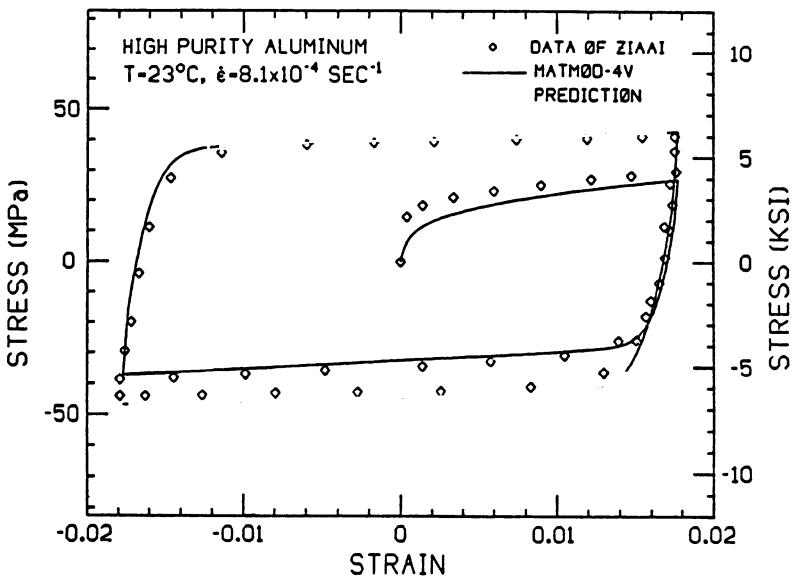
**Fig. 22.** MATMOD predictions for a stress-decrease test, compared against data of Sherby *et al.*<sup>31</sup> After Miller and Sherby.<sup>15</sup>

prestrain; hence at 16% strain the value of  $F_{def}$  is lower after precreep at 13.8 MPa than it is after precreep at 27.6 MPa. After the stress increase, the equations predict approximately the correct rate of renewed transient hardening. Figure 22 shows the converse behavior, for a stress-decrease test. In this case it will be noted that, after the stress decrease, the predicted rate of transient softening is much greater than that in the data; this occurs because, in the equations which were used, only thermally activated (static) recovery was represented. This discrepancy was a strong motivation for the subsequent work in developing the MATMOD-4V equations with their representation of dynamic (strain-activated) recovery.

### 3.1.5. Cyclic Straining

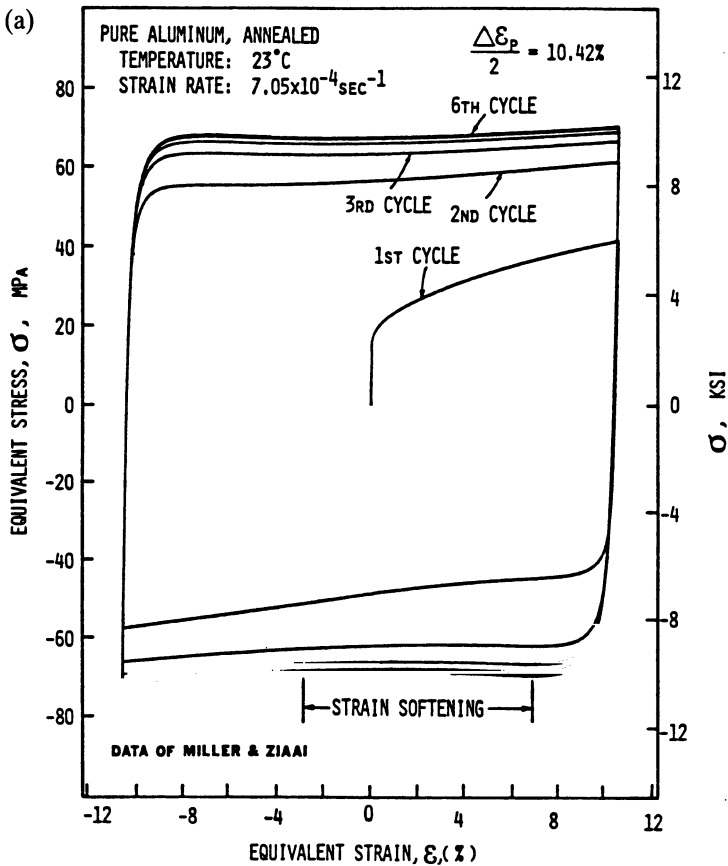
In the early version of the equations, containing only one back stress, the simulated hysteresis loops were quite 'oversquare' compared to data.<sup>10</sup> The MATMOD-4V version<sup>16,26</sup> rectified this, as illustrated in Fig. 23. The rapid changes in the predicted stress shortly after changes in the direction of straining (i.e. within the first few tenths of a percent strain) are associated with rearrangement of the short-range back stress,  $R_a$ , while the slower changes in stress during the rest of each half-cycle are associated with rearrangement of the long-range back stress variable,  $R_b$ . The same figure illustrates the cyclic hardening capability of the equations.

Figure 23 was for a moderate strain range, namely 0.036. Figure 24 compares the MATMOD-4V predictions<sup>26</sup> against data for a much larger strain range, 0.20. In this case, the major feature of both the data and the predictions is the 'directional strain softening' observed shortly after the changes in the straining direction. Experiments by Lowe and Miller<sup>18</sup> demonstrated that this directional strain softening was, in fact, a temporary loss of *isotropic* strength (as opposed to any



**Fig. 23.** MATMOD-4V predictions of the hysteresis loop for pure aluminum (illustrating the gradual curvature produced by the presence of two back stresses) compared against the data of Ziaai.<sup>37</sup> After Lowe and Miller.<sup>26</sup>

unusual behavior of the back stresses). In similar tests accompanied by transmission electron microscopy, Hasegawa<sup>17</sup> demonstrated that such strain softening is due to temporary breakup of the heterogeneous portion of the dislocation substructure. In the MATMOD-4V predictions, the directional strain softening is due to temporary reductions in the value of  $F_{def,\lambda}$ .<sup>16</sup> Thus there is a good correspondence (as there should be) between the behavior of the terms in the model and the behavior of both the external and the internal physical variables.



**Fig. 24.** (a) Data of Ziaai<sup>37</sup> on cyclic response of pure aluminum at high strain ranges, showing local strain softening within each hysteresis loop. After Lowe.<sup>16</sup>

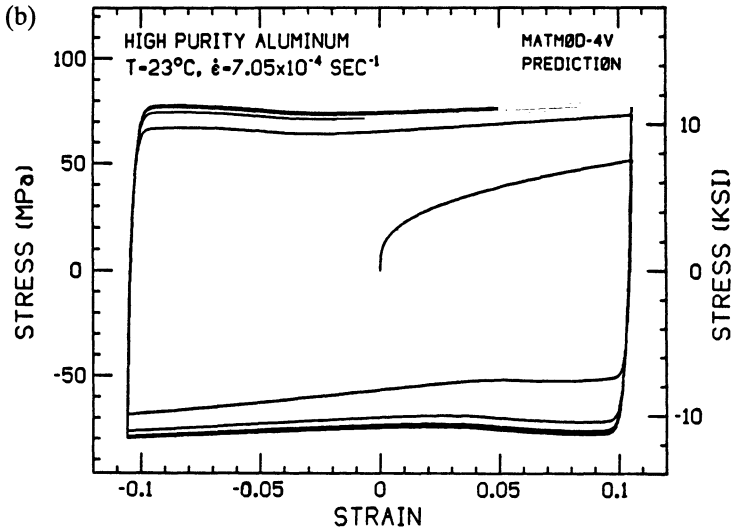


**Fig. 24.** *contd.* (b) MATMOD-4V predictions for the same test as shown in (a). After Lowe.<sup>16</sup>

### 3.1.6. Unidirectional Strain Softening

A subtle phenomenon which has been observed by several investigators is termed 'stress recovery'. Thornton and Cahn<sup>58</sup> observed stress recovery in aluminum, but not in copper, leading to the conclusion that high stacking fault energy and wavy slip encourages stress recovery. Hammad *et al.*<sup>59</sup> observed that, in high-purity aluminum, application of a constant strain rate during recovery at 450°C caused more complete softening than if the material was unstressed. Figure 25 shows these results and compares them against MATMOD-4V predictions.<sup>26</sup> The model shows the same trend (qualitatively) as the data; the model's predictions result from the dynamic recovery terms and instability factors discussed in Section 2.3.2.

### 3.1.7. Effects of Unloading and Reloading

It is well known that, when a material is unloaded after straining, upon reloading it can temporarily act 'weaker' than would be expected from a simple extrapolation of the previous stress-strain response. Alden<sup>60</sup> termed this 'metarecovery' and additional examples of such behavior are found in the work of Lubahn and Felgar<sup>61</sup> and Krempel,<sup>62</sup> among others. Technologically this is thought to be of possible importance in

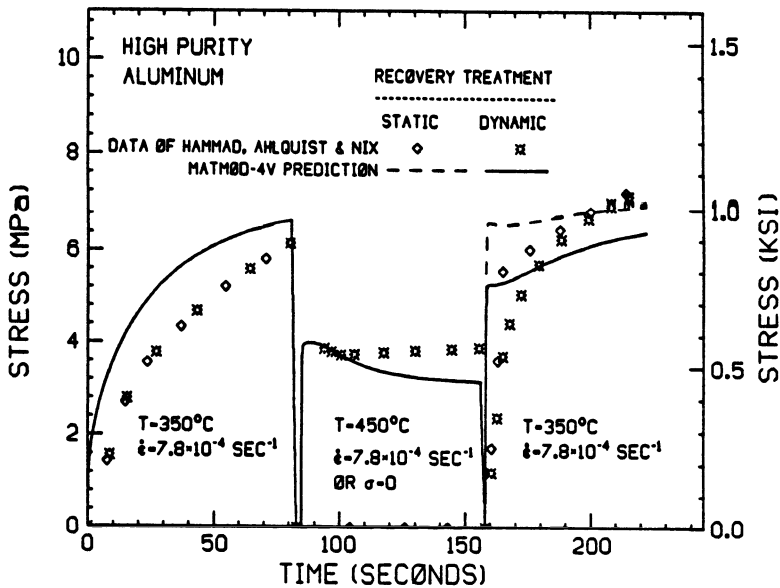
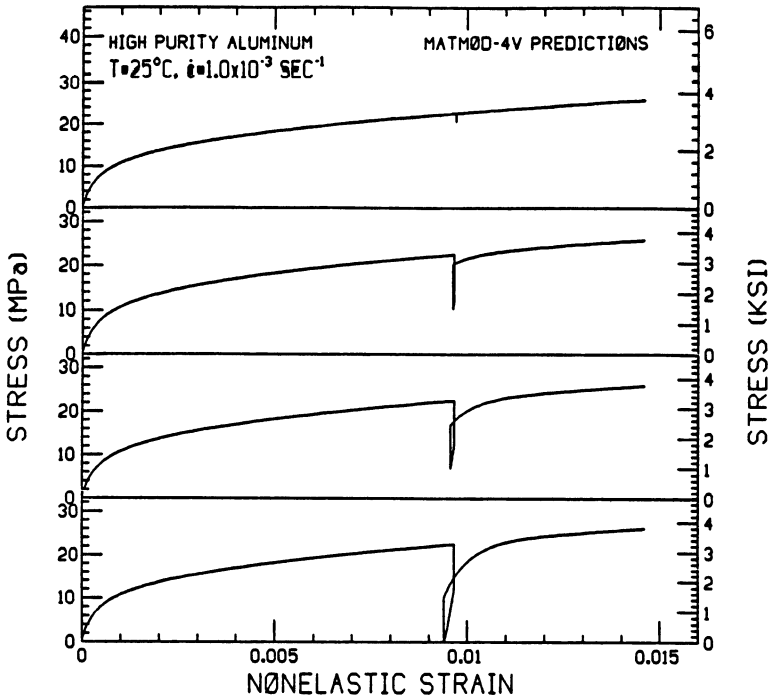


Fig. 25. MATMOD-4V predictions for 'stress-recovery' of pure aluminum (in which concurrent straining accelerates softening) compared against data of Hammad *et al.*<sup>59</sup> After Lowe and Miller.<sup>26</sup>

situations such as stress-corrosion cracking, because the extra strains upon reloading can rupture passivating films and accelerate crack growth.<sup>63</sup> Figure 26 illustrates the behavior of the MATMOD-4V equations for such a situation;<sup>16</sup> metarecovery is, in fact, predicted and is caused by decreases in the short-range back stress  $R_a$  which occur during the unloading process.

### 3.1.8. Multiaxial Directional Strain Softening

As a final example of the equations' capability for predicting strain hardening and strain softening under complex circumstances, Fig. 27 shows the response to multidirectional and unidirectional straining. The equations utilized<sup>52</sup> are a multiaxial generalization of the MATMOD-4V equations, following the approach described in Section 2.3.4, with a minor adjustment in the material constants to allow for the fact that the material tested here was 99% pure aluminum whereas the constants in the MATMOD-4V equations had been worked out for 99.999% pure material. Multidirectional straining (Fig. 27, top) means sequential compression by a given strain amount  $\Delta\epsilon$  along first the



**Fig. 26.** MATMOD-4V predictions for 'metarecovery' transients produced by unloading and reloading. After Lowe.<sup>16</sup>

x-axis, then the y-axis, then the z-axis, then the x-axis, etc. The data of Armstrong *et al.*<sup>64</sup> (Fig. 27, middle) show that the flow stress during multidirectional straining can be substantially lower than during unidirectional straining at the same temperature and strain rate. Transients are observed upon changes from unidirectional to multidirectional straining (and back) which are, essentially, multiaxial cyclic hardening and softening. The equations' predictions<sup>52</sup> (Fig. 27, bottom) behave in essentially the same way because of the cross-coupling between  $R_b$  and  $F_{def,\lambda}$  discussed in Section 2.3.2. Upon changes in straining direction,  $\dot{R}_{b,ij}$  changes direction, temporarily lowering the value of most of the components of  $R_{b,ij}$  and thus of  $\mathbf{R}_b$ . This lowers or makes negative the value of  $\dot{F}_{def,\lambda}$ , and the reduced  $F_{def,\lambda}$  value lowers the flow stress via the kinetic equation.

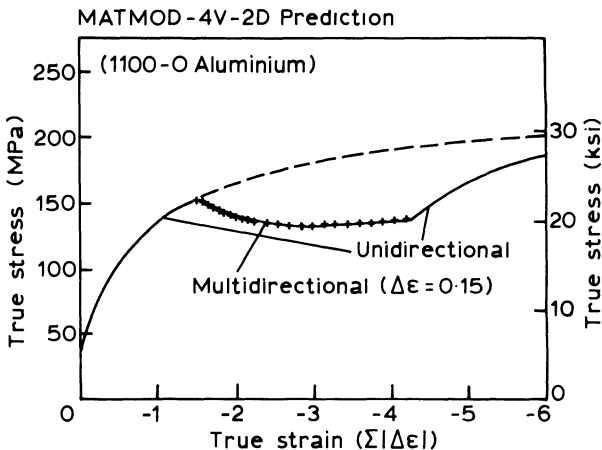
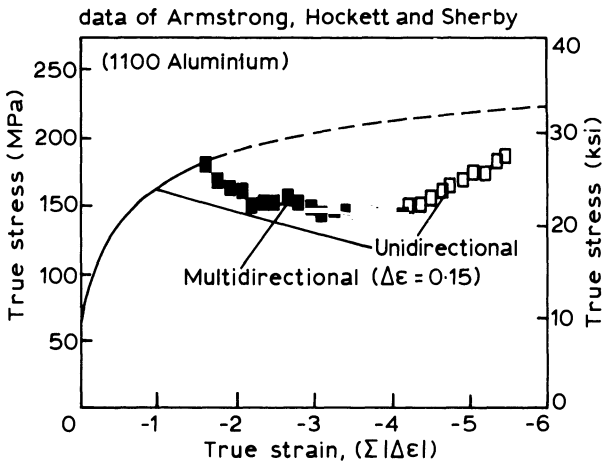
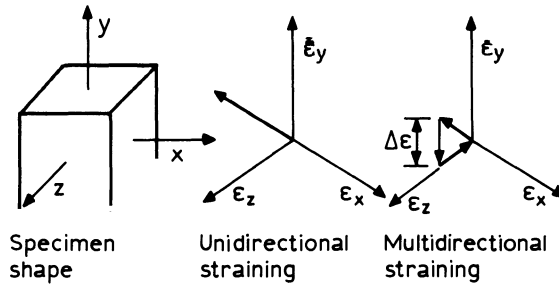


**Fig. 27.** Behavior under multidirectional strain softening. At the top 'unidirectional' and 'multidirectional' tests are defined using the Pi-plane. In the middle, the data of Armstrong *et al.*<sup>64</sup> are shown, illustrating that multidirectional straining reduces the flow stress. At the bottom are MATMOD-4V predictions<sup>52</sup> for the same situations.

### 3.2. Austenitic Stainless Steel (emphasizing solute effects)

#### 3.2.1. Creep Rate vs. Stress and Temperature

For a pure metal (e.g. pure aluminum as shown in Fig. 1), the steady-state creep response is best characterized as 'power law' behavior at low stresses followed by 'power-law breakdown' behavior at high stresses. However, for an alloy, solute strengthening affects the shape of the creep rate vs. stress curve in various ways. Figure 28

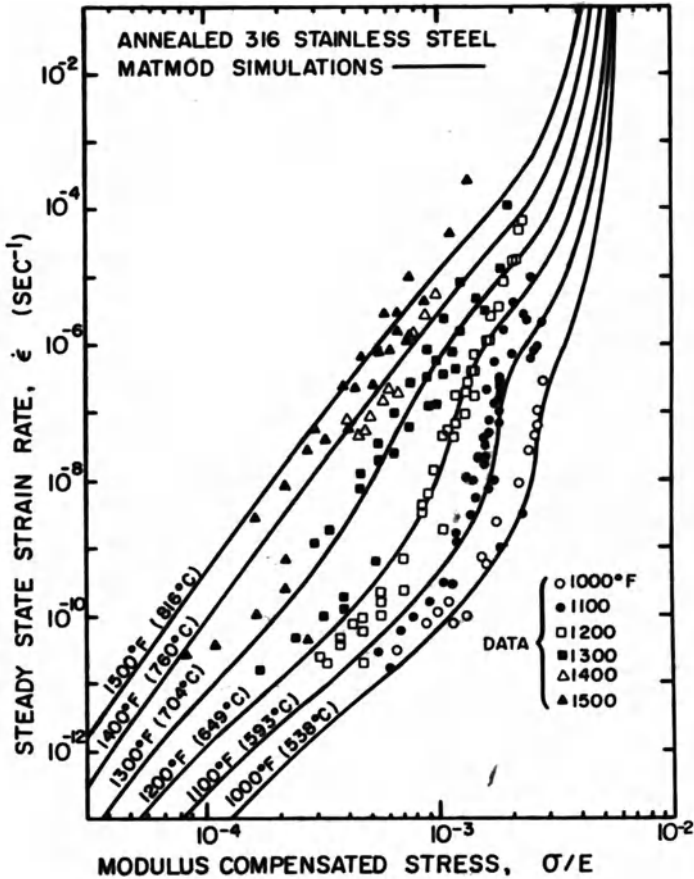


Fig. 28. MATMOD fit to data on the steady-state creep rate of annealed type 316 stainless steel at various stresses and temperatures, illustrating the complex behavior due to solute effects and power-law breakdown. After Schmidt and Miller.<sup>50</sup>

illustrates the capability of the MATMOD equations<sup>30</sup> to fit this more complicated creep behavior (in this case, the steady-state creep rate of annealed type 316 stainless steel) through the use of the  $F_{sol,1}$  and  $F_{sol,2}$  terms discussed in Section 2.2.6. Independent verification of this behavior has been obtained through comparison of predictions against data for the minimum creep rate of 20% cold-worked material.<sup>30</sup>

### 3.2.2. Flow Stress vs. Temperature and Strain

Figure 29 illustrates another capability conferred by the presence of the solute strengthening terms in the model, namely the ability to simulate plateaus and 'humps' (regions of inverse temperature sensitivity) in the flow stress vs. temperature response. In the simulations<sup>30</sup> the plateau, observed at low strains, is associated with  $F_{sol,1}$  because this variable raises the flow stress even at  $F_{def} = 0$ . The 'hump', observed at high strains, is associated with  $F_{sol,2}$  because this

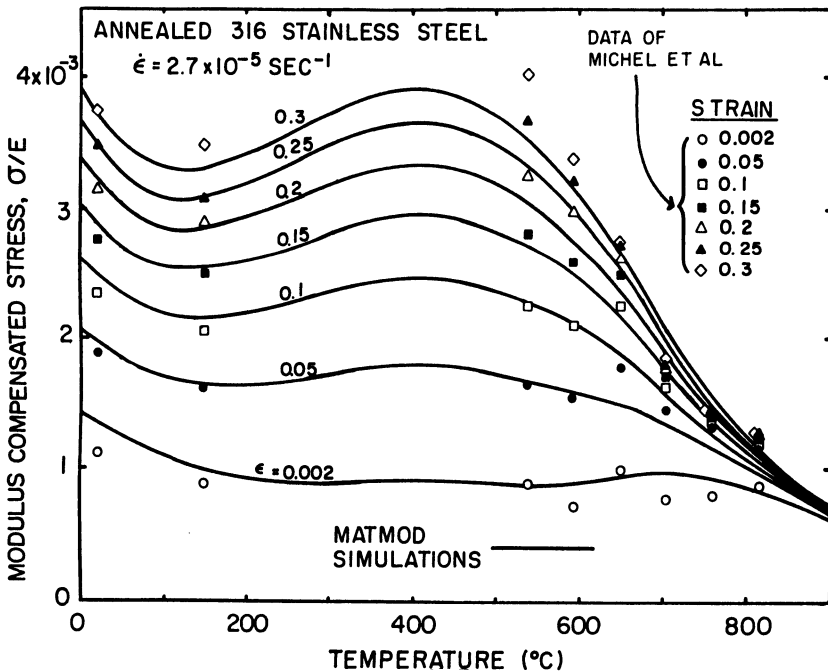


Fig. 29. MATMOD fit to data on the flow stress of annealed type 316 stainless steel at various strains and temperatures, illustrating the complex interaction of solute effects and strain hardening. After Schmidt and Miller.<sup>30</sup>

variable raises the flow stress in the dynamic strain aging regime only when  $F_{\text{def}} \gg 0$ . Although, in the case of the low-strain plateau, alternative explanations are possible (such as 'athermal' behavior due to back stresses<sup>28</sup>), the inverse temperature sensitivity observed in the data at high strains cannot be explained as anything other than a solute atmosphere effect.

### 3.2.3. Cyclic Stress-Strain Behavior

Figure 30 illustrates the capability of the same MATMOD equations<sup>30</sup> to treat cyclic behavior in terms of stress amplitude vs. strain amplitude, for type 316 stainless steel. This result is mostly a 'simulation' in that the data were used to get two of the material constants in the equations.

### 3.2.4. Stress Relaxation

Stress relaxation is, of course, just another manifestation of creep. Figure 31 compares data<sup>65</sup> on stress relaxation after various prestrains against independent MATMOD predictions<sup>30</sup> for the same conditions.

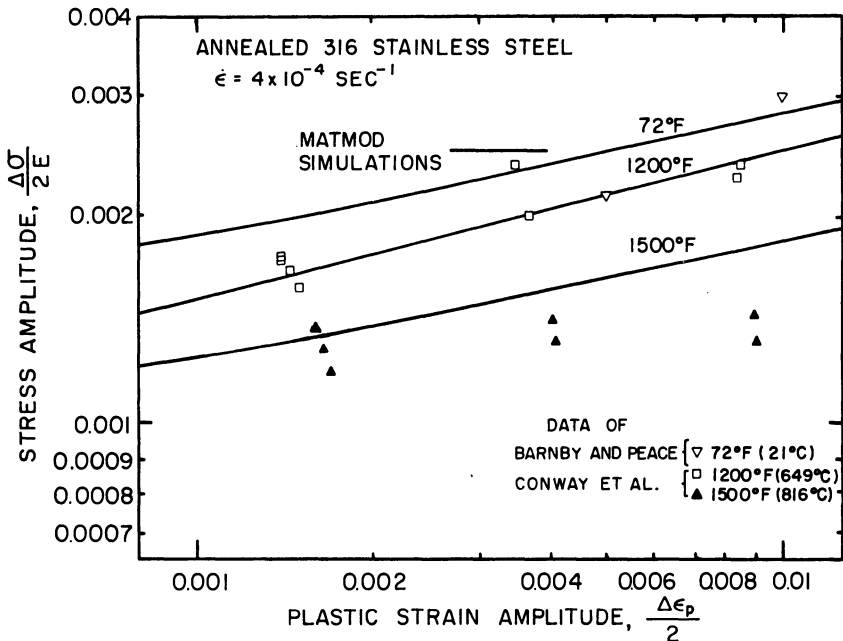
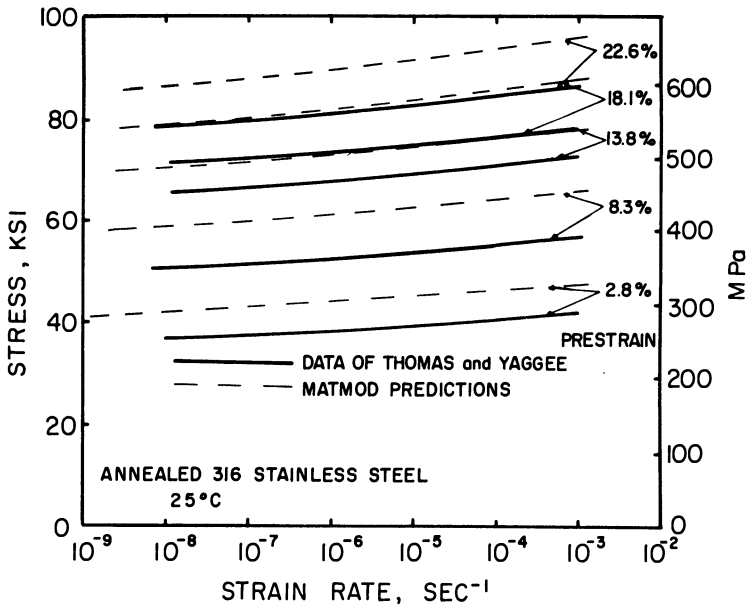


Fig. 30. MATMOD fit to data on the cyclically saturated flow stress amplitude of type 316 stainless steel. After Schmidt and Miller.<sup>30</sup>



**Fig. 31.** MATMOD predictions of room-temperature stress relaxation of type 316 stainless steel after various prestrains, compared against data of Thomas and Yaggee.<sup>65</sup> After Schmidt and Miller.<sup>30</sup>

The shapes and slopes of the curves agree well, and the absolute magnitude of the stress is predicted to within about 10%.

### 3.2.5. Activation Energy Peaks

This is fairly subtle category of behavior which may not be of direct technological relevance, but helps underscore the role of the solute strengthening terms in the equations. Peaks in the activation energy for non-elastic deformation as a function of temperature have been observed in Al-Mg alloys<sup>66</sup> (Fig. 32), in Zircaloy,<sup>67</sup> and in type 304 stainless steel,<sup>68</sup> where the peak is observed to shift to lower temperatures as the strain rate is lowered. Figure 33 shows a series of predictions<sup>43</sup> of the activation energy as a function of temperature and strain rate which show essentially the same behavior. As was mentioned in Section 2.3.3, these activation energy peaks are predicted (at constant  $\sigma/E$ ) only if the activation energy which appears in the  $F_{\text{sol}}$  expressions differs from that which appears in the  $\dot{\epsilon}$  equation.

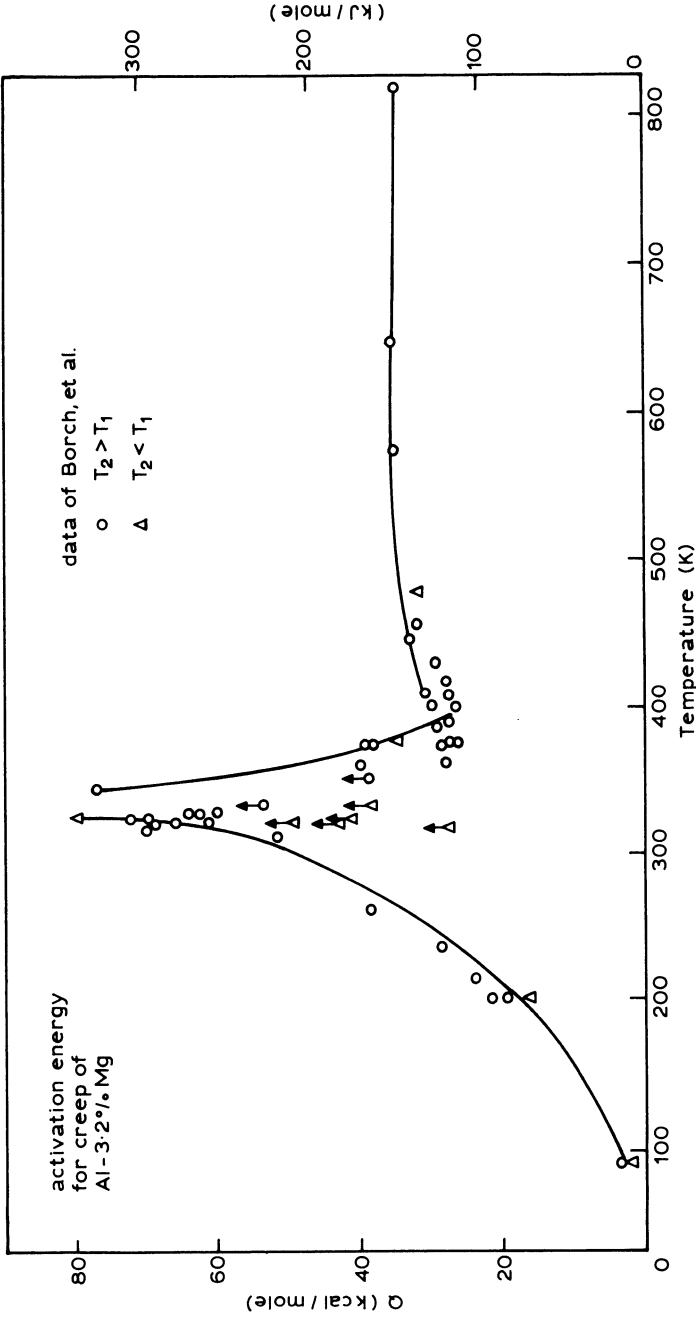


Fig. 32. Peaks in the activation energy for creep of Al-3.2% Mg, as observed by Borch *et al.*<sup>66</sup> After Schmidt *et al.*<sup>43</sup>

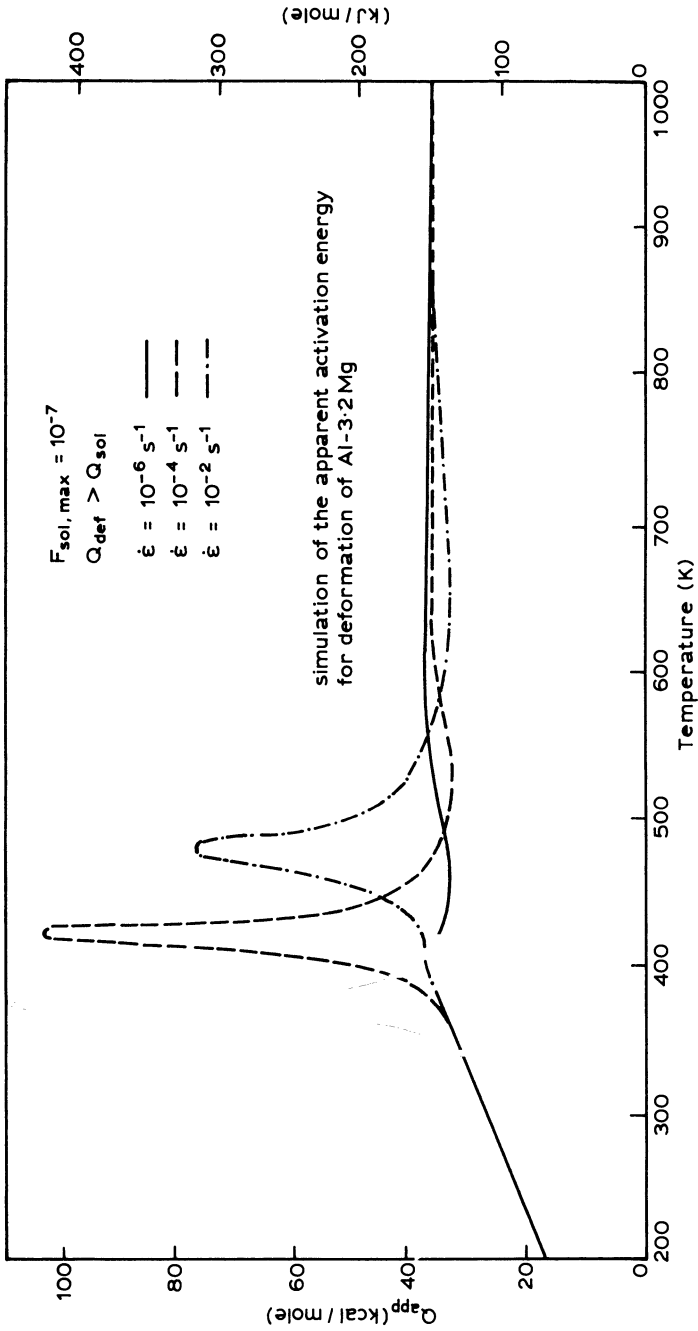


Fig. 33. MATMOD predictions of activation energy peaks at various strain rates. After Schmidt *et al.*<sup>43</sup>

### 3.3. Zircaloy (emphasizing irradiation effects)

The MATMOD-Z equations represent an application of an early version of the model to Zircaloy for nuclear applications; these equations have been incorporated into the BEHAVE-4 LWR fuel rod code.<sup>69</sup> The equations contain only a single back stress, a single isotropic hardening variable, and a single solute strengthening variable, but include additional terms to represent the effects of irradiation. Irradiation *hardening* is treated within the isotropic hardening variable  $F_{\text{def}}$ , by adding a rate term (linearly proportional to the flux) in the  $\dot{F}_{\text{def}}$  equation, i.e.

$$\dot{F}_{\text{def}} = H_2 |\dot{\epsilon}| + H_4 \Phi - f_{\text{recov}}(T, F_{\text{def}}) \quad (53)$$

where  $\Phi$  is the neutron flux and  $H_4$  is a constant. The  $H_4 \Phi$  term can be thought of as being a very oversimplified representation of the rate of accumulation of point defects and point defect clusters due to displacement of atoms out of their normal lattice sites by bombardment. With this mathematical arrangement, a previous history of irradiation ( $\Phi > 0$  for some finite time) increases  $F_{\text{def}}$  which, in turn, increases the subsequent flow stress under any given non-elastic strain rate, thus simulating irradiation hardening. This represents the increased difficulty of dislocation motion through a field of point defects or clusters. For values of  $F_{\text{def}}$  small enough for recovery (see below) to be negligible, the total change in  $F_{\text{def}}$  ( $\int \dot{F}_{\text{def}} dt$ ) will depend only on the accumulated fluence ( $H_4 \int \Phi dt$ ) and not on the flux itself; this is the reason for the one-power dependence of the irradiation hardening term upon  $\Phi$ . Also, under a constant flux, as  $F_{\text{def}}$  increases in accordance with the above equation, the magnitude of the recovery term increases and eventually a dynamic equilibrium is reached at which point  $\dot{F}_{\text{def}}$  goes to zero, thus simulating the saturation of irradiation hardening. The saturated level of  $F_{\text{def}}$  will be independent of its starting value, thus simulating the fact<sup>70,71</sup> that cold-worked, stress-relieved Zircaloy undergoes much less of a strength increase due to irradiation hardening than does fully annealed material (Fig. 34). This behavior is one key reason for choosing to incorporate irradiation hardening within the  $F_{\text{def}}$  term rather than add a separate state variable. (Simplicity is the other key reason.) The higher the temperature, the lower will be the saturated value of  $F_{\text{def}}$  for a given  $\Phi$ . Also, if  $F_{\text{def}}$  has been increased during some period of  $\Phi > 0$  and then the temperature is increased to a sufficiently high level, the recovery term

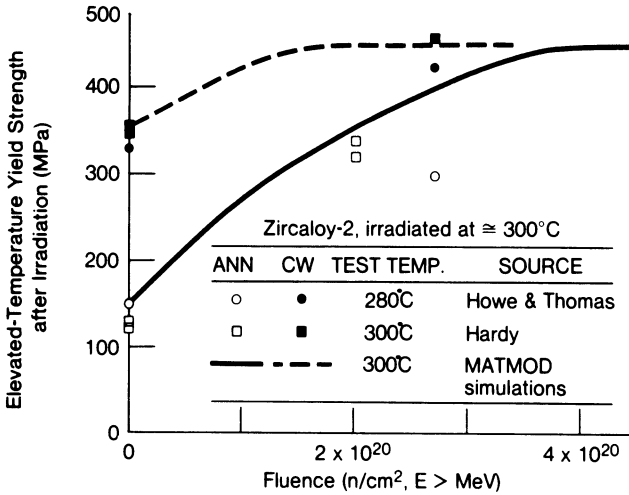


**Fig. 34.** MATMOD-Z predictions of irradiation hardening for annealed and for cold-worked Zircaloy, compared against data of Hardy<sup>71</sup> and of Howe and Thomas.<sup>70</sup> After Oldberg *et al.*<sup>54</sup>

in eqns (46) and (53) causes  $F_{def}$  to decrease, thus automatically simulating the ‘annealing out’ of irradiation hardening (Fig. 35).

One of the deficiencies of the simulations in Fig. 35 is that much of the annealing in the real material is by recrystallization, whereas the equations contain terms to represent only recovery. Work is underway<sup>72</sup> (as applied to HSLA steels) to introduce an explicit recrystallization term into the equations, to obtain improved predictions of both hot working and static recrystallization.

Irradiation-enhanced creep is treated by assuming the existence of two independent processes: ‘thermally activated’ deformation ( $\dot{\epsilon}_{th}$ ) which comprises all of the behavior discussed thus far and represented by  $\dot{\epsilon}$ , and irradiation-activated deformation ( $\dot{\epsilon}_{irr}$ ) which is assumed to depend only on the current stress, flux and temperature. Thus the total non-elastic rate is

$$\dot{\epsilon} = \dot{\epsilon}_{th}(\sigma, T, R, F_{def}, F_{sol}) + \dot{\epsilon}_{irr}(\sigma, \Phi, T) \quad (54)$$

With this arrangement, the differing stress and temperature dependences of irradiation-activated and thermally activated deformation are easily represented (Fig. 36). The specific dependence of  $\dot{\epsilon}_{irr}$  upon

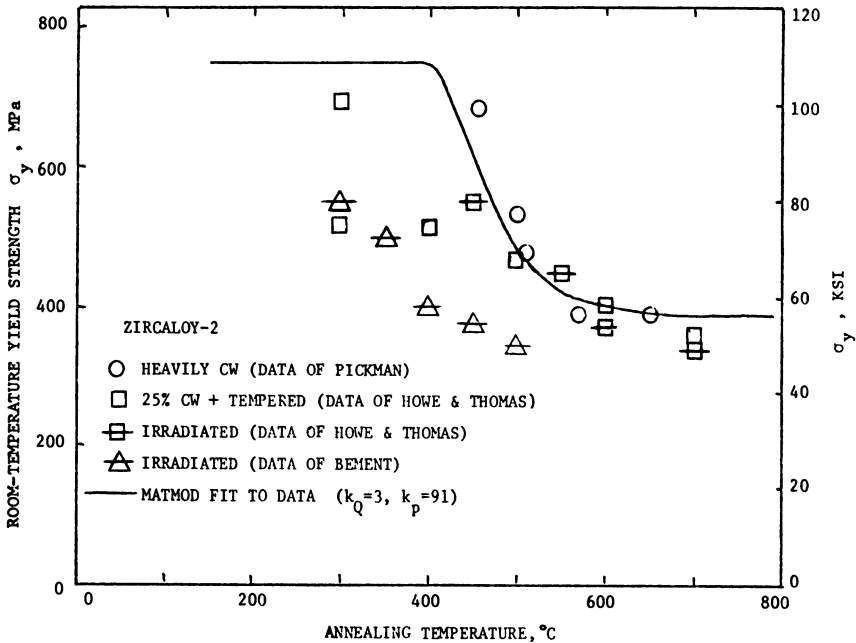


**Fig. 35.** MATMOD-Z predictions of annealing of irradiation hardening for Zircaloy, compared against data from several sources shown. After Miller and Sherby.<sup>50</sup>

stress, flux and temperature is obtainable simply by fitting in-reactor steady-state creep data for the regime where one is convinced that  $\dot{\epsilon}_{irr}$  dominates; for the MATMOD-Z equations the regression analysis of Liu and Bement<sup>73</sup> was adopted. Also, because there are no history-dependent variables in the expression for  $\dot{\epsilon}_{irr}$ , the above equation will predict less transient creep under in-reactor conditions than under out-of-reactor conditions, in agreement with the data. The above approach is undoubtedly an oversimplification of the real details of irradiation-enhanced creep (see, for example, the work of Nichols<sup>74</sup> for a much more complete treatment).

One other example from the work on Zircaloy is instructive, namely the independent prediction of the strain-rate sensitivity ( $m$ ) as a function of temperature (Fig. 37). This reasonably accurate prediction arises from a combination of the solute strengthening and hyperbolic-sine terms in the model. At high temperatures, the flow stress is low, the sinh function is in the power-law regime, and so the strain-rate

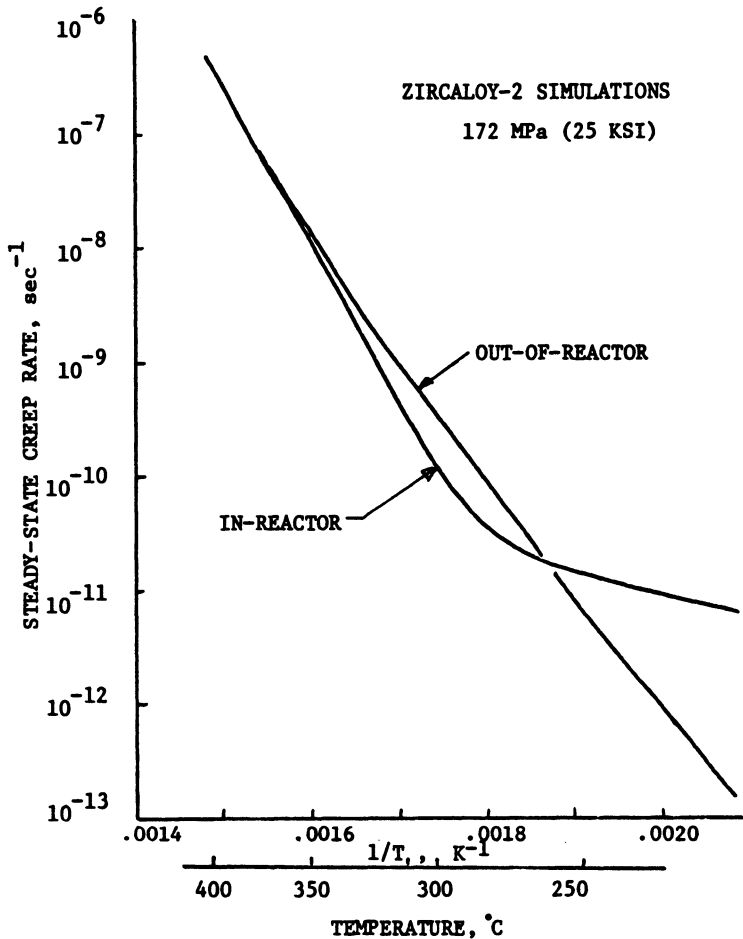


**Fig. 36.** MATMOD-Z predictions comparing in-reactor against out-of-reactor creep rate behavior of Zircaloy; the in-reactor behavior reflects both irradiation-enhanced creep and irradiation hardening. After Miller and Sherby.<sup>50</sup>

sensitivity is typical of power-law creep ( $\dot{\epsilon} \propto \sigma^n$  with  $n$  about 5, or  $\sigma \propto \dot{\epsilon}^m$  with  $m$  about 0.2). At low temperatures, the flow stress is high, the sinh function is in the exponential regime,  $\dot{\epsilon}$  depends very strongly upon  $\sigma$ , and  $m$  is small; this simulates behavior in what is commonly referred to as the 'rate-independent plastic' regime. In the intermediate temperature regime (around 700 K for zirconium alloys containing

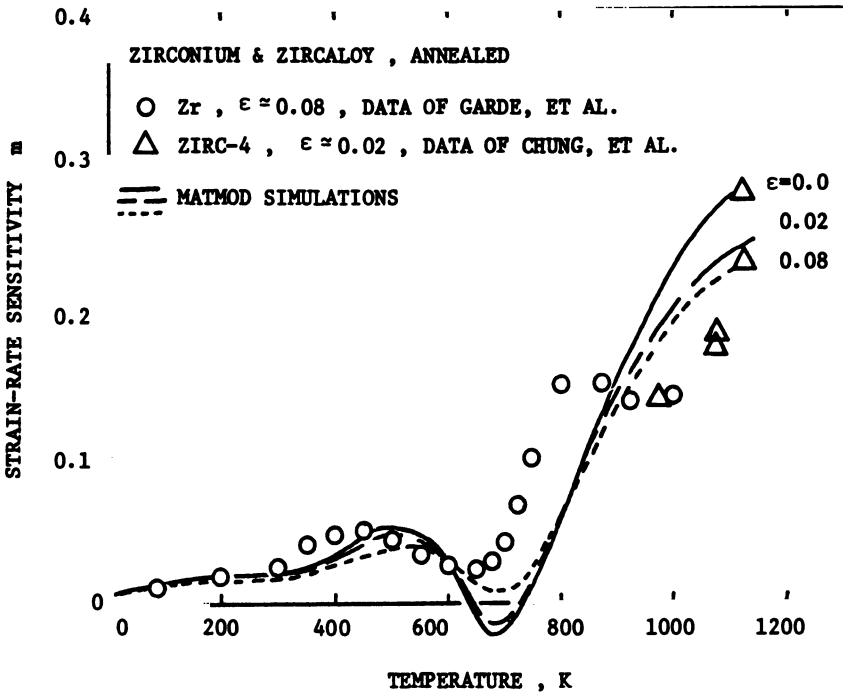


Fig. 37. MATMOD-Z predictions of the strain-rate sensitivity of Zircaloy vs. temperature (illustrating the local minimum value in  $m$  due to solute strengthening) compared against data of Chung *et al.* and of Garde *et al.* After Miller and Sherby.<sup>50</sup>

oxygen interstitials) the solute strengthening terms cause a local minimum in strain-rate sensitivity to be predicted; referring to Section 2.3.3 this occurs because the general tendency for  $\sigma$  to *increase* with increasing strain rate (due to the direct coupling of  $\sigma$  and  $\dot{\epsilon}$  within the  $\dot{\epsilon}$  equation) is offset or even overshadowed within this temperature regime by a local tendency for  $\sigma$  to *decrease* with increasing strain rate (through the  $F_{\text{sol}}$  term, in the domain where  $F_{\text{sol}}$  is decreasing with increasing  $\dot{\epsilon}$ ; see Fig. 14). In steels, this behavior is referred to as the 'blue brittle' regime because the low strain-rate sensitivity causes the post-uniform elongation (which depends on  $m$ ) to be low.

#### 4. NUMERICAL INTEGRATION METHODS

Obviously, the equations discussed herein require numerical integration in order to generate predictions for all but the simplest situations.

Also, numerical integration is required for those portions of the determination of the material constants which involve 'trial and error' comparisons between data and simulations. With modern computing resources this need not be a significant barrier to the use of the equations to predict either the material response by itself, or to the use of the equations as a subroutine within a larger numerical analysis of structural or metal forming behavior. However, attention does need to be given to the numerical methods used in integrating the equations in order to permit reasonably large strain increments and thus keep the computations economical. Because these methods, and their application to the MATMOD equations, have been presented in detail elsewhere, only a summary discussion will be given here.

In common with all other 'unified' constitutive equations, the primary numerical consideration is mathematical 'stiffness' arising from a coupling of the non-elastic ( $\varepsilon$ ) and elastic strains ( $\sigma/E$ ) to calculate the total strain  $\varepsilon_{\text{tot}}$ . For example, assume the total strain rate is specified, and consider prediction of the stress history directly from the compatibility equation

$$\dot{\sigma} = E[\dot{\varepsilon}_{\text{tot}} - \dot{\varepsilon}(\sigma)] \quad (55)$$

Because  $\dot{\varepsilon}$  is a strong function of  $\sigma$ , small numerical or truncation errors in  $\sigma$  are magnified in their effect on  $\dot{\varepsilon}$ ; these feed back as larger errors in  $\sigma$  via the above differential equation for  $\dot{\sigma}$ . Small strain increments are required to get any accuracy at all and to prevent unstable numerical oscillations.

Analogous problems arise in integrating the equations governing the history-dependent state variables  $R$  and  $F_{\text{def}}$ . For example, in the simplest form of the equations  $R$  is governed by a differential equation in which  $\dot{R}$  is calculated as the difference between a work-hardening term and a recovery term which depends on  $R$  itself:

$$\dot{R} = H_1 \dot{\varepsilon} - f_{\text{recov}}(R) \quad (56)$$

If this equation is used directly, then near steady-state the two terms on the right-hand side are nearly equal, so that small errors in  $R$  are magnified; again, small time increments are required for accuracy and numerical stability.

One approach to these difficulties has been to use a numerical method specifically designed for 'stiff' equations, namely the 'Gear method'.<sup>53</sup> Its application to the MATMOD equations is discussed in reference 9; a FORTRAN program which uses this method to

integrate the MATMOD-4V equations (with material constants for pure aluminum) is available.<sup>75</sup>

In the Gear method the governing equations must be expressed as a small number (e.g. 20) of first-order differential equations. This restriction is not a problem if only the behavior at a single material point is to be predicted and either the total strain history or the stress history is known at that point. However, the major purpose for developing improved constitutive equations is as ingredients in improved life prediction or materials processing analyses; in both of these situations heterogeneous stress and strain distributions are generally encountered, and techniques such as the finite element method are used to solve for them. Under such circumstances, one does not know (at any given point in the calculation) either the total strain increment or the stress increment; one only knows the coupling between them expressed as a large set of linear equations representing the structure as a whole. Thus the Gear method is not applicable. A number of researchers have investigated this situation, developing a variety of methods. One of these, developed by Tanaka<sup>76</sup> and available as the NONSS subroutine,<sup>51</sup> has been applied to the MATMOD equations. It contains the equations developed by Schmidt<sup>29,30</sup> but with material constants for mild steel.

In the NONSS method, a Taylor series expansion of the constitutive equations at each point in the problem is used to express them in the form

$$\Delta\sigma_{ij} = D_{ijkl}^* \Delta\varepsilon_{kl}^{\text{tot}} - \Delta\zeta_{ij} \quad (57)$$

where  $D_{ijkl}^*$  and  $\Delta\zeta_{ij}$  are functions of the state variables  $R_{ij}$ ,  $F_{\text{def}}$ , and  $\dot{\varepsilon}_{ij}$  at that temporal and spatial point. The advantage of this method is that the  $D_{ijkl}^*$  term interfaces well to that portion of most finite-element programs which ordinarily receives a 'tangent modulus' term from the constitutive equations governing 'time-independent plasticity', while the  $\Delta\zeta_{ij}$  term interfaces well to that portion of most finite-element programs which ordinarily receives an 'initial strain' term from the constitutive equations governing 'time-dependent creep'. Thus the NONSS method is expected to be convenient for use in most standard finite-element programs which deal with non-elastic material behavior, although this has yet to be demonstrated. At present the NONSS subroutine is being used by Lee and by Obabueki within a model<sup>77</sup> for predicting elevated-temperature fatigue crack initiation and growth which, although not a finite-element program, does represent the

heterogeneous stress and strain fields around a crack using a series of discrete coupled ligaments and thus has many of the same numerical characteristics as finite-element computations. Recent simulation of such stress and strain fields under variable-temperature cycling, showing the manner in which thermal cycling causes high peak tensile stresses, has been done by Tanaka.<sup>78</sup>

One additional problem arises in integrating unified constitutive equations (assuming that the non-elastic strains are coupled to the elastic strains) if the strain-rate sensitivity happens to be negative. Under these conditions multiple values of the non-elastic strain rate are obtainable at a given stress. If the 'standard' numerical techniques are utilized, the program will, essentially, reproduce all of the oscillations in stress which the real material might exhibit as the Portevin–LeChatelier effect (serrated yielding) under the same circumstances. While this would be physically realistic, it is numerically inconvenient. The NONSS subroutine has built into it a 'shortcut' which automatically generates, whenever the strain-rate sensitivity is negative, an approximate smooth solution which permits large strain increments to be taken.

## 5. CALCULATION OF THE MATERIAL CONSTANTS

A major issue in the development of constitutive equations designed to handle the large number of phenomena which metals and alloys exhibit is the balance of complexity against capability. A subset of this issue is the question of how to determine the material constants in

**TABLE 3**  
References for Determination of Material Constants in the MATMOD Constitutive Equations

<i>State variables utilized</i>	<i>Materials studied</i>	<i>References</i>
$R, F_{\text{def}}$	Aluminum	9
	304, 316 Stainless steel	10
	Udimet 700	9
$R, F_{\text{def}}, F_{\text{sol}}$	Zircaloy (including irradi. effects)	50
$R, F_{\text{def}}, F_{\text{sol},1}, F_{\text{sol},2}$	316 Stainless steel	29, 30
$R, F_{\text{def}}, F_{\text{sol},1}, F_{\text{sol},2}$	Zircaloy	79
$R_a, R_b, F_{\text{def},\rho}, f_{\text{def},\lambda}$	Aluminum	16, 26

whatever equations are developed, since in general many of the constants must be deduced from macroscopic test data. As the earlier portions of this chapter indicate, several successive versions of the MATMOD equations have been developed over the past decade. Associated with each has been a specific procedure to determine the material constants. There is insufficient space to reproduce all of these procedures here; rather, they are summarized in Table 3 and the interested reader is referred to the original sources for the details.

## 6. SUMMARY

The origins and capabilities of the MATMOD constitutive equations have been described in detail. Like all of the other 'unified' approaches presented in this volume, these equations predict both 'creep' and 'plasticity' in terms of a single variable, non-elastic strain. By using a 'kinetic' equation to predict the rate of non-elastic straining, and additional 'evolutionary' equations to predict the rates of change of the several 'structure' variables which appear in the kinetic equation, the equations can predict complex history effects in a rational manner. The equations contain three types of structure variables: (1) *isotropic* work hardening,  $F_{\text{def}}$  (representing the effects of forest dislocations and subgrains/cells); (2) *directional*, or 'kinematic', work hardening,  $R$  (representing the effects of pileups, bowed dislocation segments, curved subgrain walls, and grain-to-grain elastic strain differences); and (3) *intrinsic* strengthening,  $F_{\text{sol}}$  (representing the effects of solid solution strengthening, precipitates, and grain boundaries). Irradiation hardening, irradiation-enhanced creep, and textural anisotropy have been included in one version. The MATMOD approach differs from some of the other unified approaches by covering cyclic deformation in greater detail (including strain softening), and also by including temperature as an explicit variable in the equations. The MATMOD approach differs from all of the others by including an explicit representation of solute drag and dynamic strain aging.

A full multiaxial version of the equations has been derived and tested against data. A computationally efficient numerical method for integrating the (multiaxial) equations and interfacing them with finite-element codes has been developed and embedded in the NONSS FORTRAN subroutine.

Various improvements to the equations are currently underway, ranging from yield surface distortion to athermal flow stress plateaus to recrystallization.

### ACKNOWLEDGMENTS

The MATMOD constitutive equations are the product of a number of researchers at Stanford University. Dr. Charles G. Schmidt and Dr. Terry C. Lowe were the principal developers of major versions of the equations focussing on solute strengthening and strain softening, respectively. Dr. Michael E. Kassner, Dr. Ali Ziaai, and Dr. Heinz Luthy conducted experiments and analyses which helped elucidate the controlling mechanisms and dominant phenomenological trends in subgrain/forest dislocation hardening, internal stresses, and steady-state flow, respectively. Dr. Toshimitsu G. Tanaka developed the NONSS subroutine to integrate the equations. Prof. Kenneth D. Challenger assisted in the study of activation energy peaks. Mr. Scott Burton made important contributions to the modeling of precipitation hardening. Messrs. Gregory Henshall, Donald Helling, and Richardson Adebajo assisted earlier work and are carrying out current improvements in the equations.

Discussions over the years with many people have been very helpful in this work. A partial list includes Prof. Oleg D. Sherby, Prof. William D. Nix, Prof. Henry Fuchs, Dr. Raymond Krieg, Dr. Jack Swearengen, Prof. E. W. Hart, Prof. Che-Yu Li, Prof. Sol Bodner, Dr. Siegfried Hecker, Dr. Michael Stout, Dr. Adrian Roberts, Mr. Terry Oldberg, Dr. John H. Gittus, Prof. Erhard Krempl, Dr. Doug Bamann, Dr. Fred Kocks, Dr. Jeffrey Wadsworth, Prof. Franz Kollman, Prof. Tadatsune Okubo, Prof. Michael Bocek, Dr. Fred Nichols, Prof. Glenn Edwards, Prof. Gene Lucas, Prof. Ron Ballinger, Dr. Sam McDonald, and Prof. Terry Langdon.

Financial support for this work has been kindly provided by the Fannie and John Hertz Foundation (early developments, 1973–5), by the Electric Power Research Institute (applications of the equations to Zircaloy, including irradiation effects), by the US Department of Energy, Office of Basic Energy Sciences (improvements to the equations for solute strengthening, strain softening, and their application to austenitic stainless steels), and by the National Science Foundation (numerical integration methods).

## REFERENCES

1. E. W. Hart, A phenomenological theory for plastic deformation of polycrystalline metals, *Acta Metall.*, **18** (1970) 599–610.
2. H. Luthy, A. K. Miller and O. D. Sherby, The stress and temperature dependence of steady-state flow at intermediate temperatures for pure polycrystalline aluminum, *Acta Metall.*, **28** (1979) 169–78.
3. H. Abdel-Raouf and A. Plumtree, On the steady-state cyclic deformation of iron, *Metall. Trans.*, **2** (1971) 1251–4.
4. J. E. Dorn, A. Goldberg and T. E. Tietz, The effect of thermal-mechanical history on the strain hardening of metals, *Trans. AIME*, **180** (1949) 205–24.
5. A. H. Cottrell and R. J. Stokes, Effect of temperature on the plastic properties of aluminum crystals, *Proc. Roy. Soc.*, **A233** (December 1955) 17–34.
6. S. L. Robinson, C. M. Young and O. D. Sherby, Constant structure creep tests and the influence of subgrain size on creep, *J. Mat. Sci.*, **9** (1974) 341–3.
7. O. D. Sherby and C. M. Young, Some factors influencing the strain rate-temperature dependence of the flow stress in polycrystalline solids, in *Symposium on Rate Processes in Plastic Deformation of Materials*, Amer. Soc. for Metals, 1975, pp. 497–541.
8. O. D. Sherby, J. L. Lytton and J. E. Dorn, Activation energies for creep of high-purity aluminum, *Acta Metall.*, **5** (1957) 219–27.
9. A. K. Miller, A unified phenomenological model for monotonic, cyclic, and creep deformation of strongly work-hardening materials, Ph.D. dissertation, Stanford University, Department of Materials Science and Engineering, May 1975.
10. A. K. Miller, An inelastic constitutive model for monotonic, cyclic, and creep deformation. Part I—Equations development and analytical procedures; Part II—Application to type 304 stainless steel, *J. Eng. Mat. Technol.*, **98H** (1976) 97–113.
11. W. G. Johnson and J. J. Gilman, Dislocation velocities, dislocation densities, and plastic flow in lithium fluoride crystals, *J. Appl. Phys.*, **30** (1959) 129–44.
12. D. J. Abson and J. J. Jonas, Substructure strengthening in zirconium and zirconium-tin alloys, *J. Nucl. Mat.*, **42** (1972) 73–85.
13. C. M. Young, S. L. Robinson and O. D. Sherby, Effect of subgrain on the high temperature strength of polycrystalline aluminum as determined by constant strain rate tests, *Acta Metall.*, **23** (1975) 633–9.
14. C. M. Young and O. D. Sherby, Subgrain formation and subgrain-boundary strengthening in iron-based materials, *J. Iron and Steel Inst.*, **211** (1973) 640–7.
15. A. K. Miller and O. D. Sherby, A simplified phenomenological model for non-elastic deformation: Prediction of pure aluminum behavior and incorporation of solute strengthening effects, *Acta Metall.*, **26** (1978) 289–304.

16. T. C. Lowe, New concepts in modeling strain softening, Ph.D. dissertation, Stanford University, Department of Materials Science and Engineering, January 1983.
17. T. Hasegawa, T. Yakou and S. Karashima, Deformation behavior and dislocation structures upon stress reversal in polycrystalline aluminum, *Mat. Sci. Eng.*, **20** (1975) 267-76.
18. T. C. Lowe and A. K. Miller, The nature of directional strain softening, *Scripta Metall.*, **17** (1983) 1177-82.
19. M. E. Kassner, A. K. Miller and O. D. Sherby, The separate roles of subgrains and forest dislocations in the isotropic hardening of type 304 stainless steel, *Metall. Trans.*, **A13** (1982) 1977-85.
20. M. E. Kassner, K. A. Rubin and A. K. Miller, Verification of a microstructurally-based equation for elevated-temperature transient isotropic hardening, *6th Int. Conf. on Strength of Metals and Alloys*, Melbourne, Australia, August 1982, pp. 581-7.
21. A. H. Cottrell and V. Aytekin, The flow of zinc under constant stress, *J. Inst. Metals*, **77** (1950) 389-422.
22. J. C. Gibeling and W. D. Nix, A numerical study of long range internal stresses associated with subgrain boundaries, *Acta Metall.*, **28** (1980) 1743-52.
23. C. N. Ahlquist and W. D. Nix, The measurement of internal stresses during creep of Al and Al-Mg alloys, *Acta Metall.*, **19** (1971) 373-85.
24. H. Mughrabi, Description of the dislocation structure after unidirectional deformation at low temperatures, in *Constitutive Equations in Plasticity*, ed. A. Argon, MIT Press, Cambridge, Mass., 1975, pp. 199-250.
25. D. J. Quesnel and J. C. Tsou, A theory on the shape of saturated hysteresis loops, in *Dislocation Modelling of Physical Systems*, ed. M. F. Ashby, R. Bullough, C. S. Hartley and J. P. Hirth, Pergamon Press, Oxford, 1981, pp. 381-7.
26. T. C. Lowe and A. K. Miller, Improved constitutive equations for modeling strain softening: Part I-Conceptual development; Part II-Predictions for aluminum, *J. Eng. Mat. Techn.*, **106** (1984) 337-48.
27. J. P. Hirth and J. Lothe, *The Theory of Dislocations*, McGraw-Hill, New York 1968.
28. G. Henshall, Development of a physical basis for calculating the MATMOD constants for alloys, in *Internal Variable Based Models for Elevated Temperature Fatigue and Deformation*, ed. A. K. Miller, Annual Progress Report for Dept. of Energy Grant DE-FG03-84ER45119, Stanford University, Dept. Mat. Sci. and Eng., Feb. 1986.
29. C. G. Schmidt, A unified phenomenological model for solute strengthening, deformation strengthening, and their interactions in type 316 stainless steel, Ph.D. dissertation, Stanford University, Department of Materials Science and Engineering, November 1979.
30. C. G. Schmidt and A. K. Miller, A unified phenomenological model for non-elastic deformation of type 316 stainless steel: Part I-Derivation of the model; Part II-Fitting and predictive capabilities, *Res Mech.*, **3** (1981) 109-29, 175-93.

31. O. D. Sherby, T. A. Trozera and J. E. Dorn, The effects of creep stress history at high temperatures on the creep of aluminum alloys, *Proc. ASTM*, **56** (1956) 1–16.
32. O. D. Sherby, R. H. Klundt and A. K. Miller, Flow stress, subgrain size and subgrain stability at elevated temperatures, *Metall. Trans.*, **A8** (1977) 843–50.
33. F. Garofalo *et al.*, Strain-time, rate-stress, and rate-temperature relations during large deformations in creep, *Joint Int. Conf. on Creep*, London, 1963, pp. 1-31–1-39.
34. W. D. Nix and J. C. Gibeling, Mechanisms of time-dependent flow and fracture of metals, in *ASM Mat. Sci. Seminar on Flow and Fracture at Elevated Temperatures*, ed. R. Raj, ASM, Metals Park, Ohio, 1985, p. 1.
35. U. F. Kocks, Laws for work-hardening and low temperature creep, *J. Eng. Mat. Tech.*, **98H** (1976) 76–85.
36. J. F. Bell, A generalized large deformation behaviour for face-centered cubic solids—high purity copper, *Phil. Mag.*, **10** (1964) 107–25; A generalized large deformation behavior for face-centered cubic solids: nickel, aluminum, gold, silver and lead, *Phil. Mag.*, **11** (1965) 1135–55.
37. A. A. Ziaai-Moayyed, Back stresses in monotonic and cyclic deformation: transient and steady state behavior, Ph.D. dissertation, Stanford University, Department of Materials Science and Engineering, March 1981.
38. A. K. Miller and A. A. Ziaai-Moayyed, Some critical experimental tests of the MATMOD equations with respect to directional hardening and cyclic deformation, in *ASTM STP-765*, 1982, pp. 202–22.
39. W. Blum, University of Erlangen (Germany), private communication.
40. F. V. Lawrence, Jr. and R. C. Jones, The formation of cell structures in fatigued iron crystals, *Metall. Trans.*, **1** (1970) 367–76.
41. H. Mughrabi, F. Ackermann and K. Herz, Persistent slipbands in fatigued face-centered and body-centered cubic metals, in *Fatigue Mechanisms*, Proc. ASTM-NBS-NSF Symp., Kansas City, Missouri, May 1978, ed. J. T. Fong, ASTM-STP 675, 1979, pp. 69–105.
42. K. L. Murty, F. A. Mohamed and J. E. Dorn, Viscous glide, dislocation climb and Newtonian viscous deformation mechanisms of high temperature creep in Al-3Mg, *Acta Metall.*, **20** (1972) 1009–18.
43. C. G. Schmidt, A. A. Ziaai-Moayyed, A. K. Miller and K. D. Challenger, The simulation of peaks in the temperature dependence of the activation energy for deformation of solute strengthened materials, *Res Mech.*, **12** (1984) 87–110.
44. M. J. Manjoine, Influence of rate of strain and temperature on yield stresses of mild steel, *J. Appl. Mech.*, in *Trans. ASME*, **66** (1944) A-211–A-218.
45. D. J. Michel, J. Motteff and A. J. Lovell, Substructure of type 316 stainless steel deformed in slow tension at temperatures between 21°C and 816°C, *Acta Metall.*, **21** (1973) 1269.
46. S. F. Gates, An analysis of a numerical model for the Portevin–LeChatelier effect, M.Sc. Thesis, University of Wyoming, Department of Mechanical Engineering, July 1975.

47. S. R. Bodner, The mechanics of repeated discontinuous yielding of metals, *Mat. Sci. Eng.*, **2** (1967) 213–23.
48. D. Helling, Multiaxial constitutive equations, in *Internal Variable Based Models for Elevated Temperature Fatigue and Deformation*, ed. A. K. Miller, Annual Progress Report for Dept. of Energy Grant DE-FG03-84ER45119, Stanford University, Dept. of Mat. Sci. and Eng., Feb. 1986.
49. J. R. Rice, On the structure of stress-strain relations for time-dependent plastic deformation in metals, *Trans. ASME*, **37-E** (1970) 728–37.
50. A. K. Miller and O. D. Sherby, Development of the materials code, MATMOD (Constitutive equations for zircaloy), final report NP-567 to Electric Power Research Institute, Dec. 1977.
51. T. G. Tanaka and A. K. Miller, NONSS (numerical integration of unified constitutive equations), FORTRAN program S83-36, available from Software Distribution Center, Office of Technology Licensing, 105 Encina Hall, Stanford, California 94305.
52. D. E. Helling, R. O. Adebajo, T. G. Tanaka and A. K. Miller, Predicting some complex multiaxial deformation effects using a unified constitutive model, in *Proc. Symp. Computer Modelling of Fabrication Process and Constitutive Behavior of Metals*, Ottawa, May 1986, ed. J. J. M. Too.
53. C. W. Gear, The automatic integration of ordinary differential equations, *Comm. ACM*, **14** (1971) 176–9.
54. S. Oldberg, Jr., A. K. Miller and G. E. Lucas, Advances in understanding and predicting inelastic deformation in zircaloy, in *Zirconium in the Nuclear Industry*, ASTM STP-681, 1979, pp. 291–302.
55. R. Hill, *The Mathematical Theory of Plasticity*, Oxford Univ. Press., London, 1950.
56. P. W. Chen, C. T. Young and J. L. Lytton, Effect of dislocation substructure on the primary creep behavior of aluminum at elevated temperatures, in *Rate Processes in Plastic Deformation of Materials*, ASM, 1975, pp. 605–28.
57. A. K. Miller, Constitutive equations for predicting non-elastic deformation (and fracture) under complex loading, in *Fracture: Interactions of Microstructure, Mechanisms and Mechanics*, ed. J. M. Wells and J. D. Landes, Met. Soc. AIME, 1984, pp. 29–48.
58. P. H. Thornton and R. W. Cahn, The recovery and recrystallization of copper and aluminum under stress, *J. Inst. Metals*, **89** (1961–2) 455–63.
59. F. H. Hammad, C. N. Ahlquist and W. D. Nix, High temperature work softening yield point phenomena in polycrystalline aluminum, *Metall. Trans.*, **1** (1970) 2179–83.
60. T. H. Alden, The mechanism of ‘metarecovery’ and its role in temperature dependent plastic flow, *Metall. Trans.*, **4** (1973) 1047–57.
61. J. D. Lubahn and R. P. Felgar, *Plasticity and Creep of Metals*, Wiley, New York, 1961, pp. 486.
62. E. Krempl, Room temperature rate sensitivity, creep, and relaxation of type 304 stainless steel, Report RPI CS 78-5, Dept. of Mechanical Eng.,

- Aeronautical Eng. and Mechanics, Rensselaer Polytechnic Institute, Troy, New York 12181.
63. Y. S. Garud and T. L. Gerber, Development of an engineering model for predicting IGSCC damage, particularly in type 304 stainless steel in BWR water environments, EPRI Topical Report NP-2808-LD, February 1983.
  64. P. E. Armstrong, J. E. Hockett and O. D. Sherby, Large strain multidirectional deformation of 1100 aluminum at 300K, *J. Mech. Phys. Solids*, **30** (1982) 37-58.
  65. J. F. Thomas, Jr. and F. L. Yaggee, Stress relaxation in solution annealed and 20 pct cold-worked type 316 stainless steel, *Metall. Trans.*, **A6** (1975) 1835-7.
  66. N. R. Borch, L. A. Shepard and J. E. Dorn, Activation energies for creep of an alpha solid solution of magnesium in aluminum, *Trans. ASM*, **52** (1960) 494.
  67. V. Fidleris, The effect of texture and strain aging on creep of Zircaloy-2, in *Applications Related Phenomena for Zirconium and its Alloys*, ASTM-STP 458, 1969, pp. 1-17.
  68. K. D. Challenger, unpublished research at Stanford University, 1978.
  69. R. Stuart, S. Oldberg, Jr., D. Stevenson and E. Rumble, BEHAVE-4 light water reactor fuel rod analysis code, EPRI Topical Report NP-892, August 1978.
  70. L. M. Howe and W. R. Thomas, *J. Nucl. Mat.*, **2** (1960) 248.
  71. D. G. Hardy, in *Irradiation Effects on Structure Alloys for Nuclear Reactor Applications*, ASTM STP 484, American Society for Testing and Materials, 1970, p. 215.
  72. R. Adebajo and A. K. Miller, Development of a model to predict elevated-temperature deformation behavior of steels under complex histories and strain paths, current research at Stanford University under project 65-476 sponsored by American Iron and Steel Institute.
  73. Y. Yung Liu and A. L. Bement, A regression approach for Zircaloy-2 in-reactor creep constitutive equations, 4th Int. Conf. on Structural Mechanics in Reactor Technology, San Francisco, 1977, paper C3/3.
  74. F. A. Nichols, Theory of the creep of zircaloy during neutron irradiation, *J. Nucl. Mat.*, **30** (1969) 249-70.
  75. T. C. Lowe and A. K. Miller, MAT4V (constitutive equations for nonelastic deformation, including strain softening), FORTRAN program S83-35, available from Software Distribution Center, Office of Technology Licensing, 105 Encina Hall, Stanford, California 94305.
  76. T. G. Tanaka, A unified numerical method for integrating stiff time-dependent constitutive equations for elastic/viscoplastic deformation of metals and alloys, Ph.D. dissertation, Stanford University Dept. of Materials Science and Eng., 1983.
  77. A. K. Miller, A. Obabueki and C. H. Lee, Predicting the special growth rates of small fatigue cracks using a unified model, *Second Int. Conf. Small Fatigue Cracks*, Santa Barbara, Calif., Jan. 9, 1985.
  78. T. G. Tanaka and A. K. Miller, Some predictions of the stress and strain behavior near crack tips under thermal fatigue conditions, Stanford

University report under program on Solar Central Receiver Deformation and Fracture Modelling (Sandia National Laboratories, sponsor), April 1986.

79. A. K. Miller, Some improvements in the 'MATMOD-Z' constitutive equations for non-elastic deformation of Zircaloy, Stanford University, Dept. of Materials Science and Eng., Report SU-DMS-82-T-1, prepared for Electric Power Research Institute, Palo Alto, California, Contract RP-700-3.

# 4

## The Mechanical Equation of State

J. H. GITTUS

*Safety and Reliability Directorate, United Kingdom Atomic Energy  
Authority, Warrington, UK*

The mechanical equation of state (MEOS) must relate to the full strain and stress tensor and it must predict not only the steady-state creep contribution (if any) but also the transient creep which follows every change in the stress system. In this chapter we indicate the progress that is being made to arrive at such an equation and the resultant equation that has been developed.

### 1. YIELD CRITERIA

If the axes of a three-dimensional graph are marked with the values of the principal stresses, then we expect to be able to connect points in this 'principal stress space' at which the combined effects of the three stresses will cause yielding to occur. The surface through such points is the yield surface. In materials whose yield stress is independent of hydrostatic compression (metals and ceramics approximate to this requirement) the yield surface will have symmetry (providing the material is isotropic) about the line  $\sigma_1 = \sigma_2 = \sigma_3$  because on this line the stress is *purely* hydrostatic and so points on the line are as far away from the yield surface as they can be.

#### 1.1. Von Mises Yield Criterion

The von Mises criterion implies that yielding commences when the (recoverable) elastic energy of distortion reaches a critical value,<sup>1</sup> and

it can be written in the alternative forms

$$2J'_2 = \sigma'_{ij}\sigma'_{ij} = \sigma_1'^2 + \sigma_2'^2 + \sigma_3'^2 = 2k^2 \quad (1)$$

$$(\sigma_1 - \sigma_2)^2 + (\sigma_2 - \sigma_3)^2 + (\sigma_3 - \sigma_1)^2 = 6k^2 = 6\tau_y^2 = 9\tau_{\text{oct}}^2 \quad (2)$$

$$(\sigma_x - \sigma_y)^2 + (\sigma_y - \sigma_z)^2 + (\sigma_z - \sigma_x)^2 + 6(\tau_{yz}^2 + \tau_{zx}^2 + \tau_{xy}^2) = 6k^2 \quad (3)$$

where  $\tau_y$  is the shear stress for flow in pure shear and  $\tau_{\text{oct}}$  is the octahedral shear stress;  $k$  is a parameter which depends on the amount of prestrain in a strain-hardening material.

### 1.2. Other Yield Criteria

Tresca proposed that yield would occur when the resolved shear stress on any plane in the material reached a critical value:

$$\sigma_1 - \sigma_3 = 2\tau_T \quad (4)$$

where  $\sigma_1 > \sigma_2 > \sigma_3$ . If we draw a plane diagram representing the intersection of the yield surface with the plane  $\sigma_1 + \sigma_2 + \sigma_3 = 0$  (the  $\Pi$  plane) then the resultant curve will be a circle for the von Mises yield criterion and a regular hexagon for the Tresca yield criterion.

The Mohr–Coulomb yield criterion embodies this kind of thinking. It specifies that yielding will occur when the shear stress on any plane in the material reaches a critical value which varies linearly with  $\sigma_n$ , the stress normal to that plane.  $\mu_c$  is termed the coefficient of internal friction, in the following equation for the critical shear stress at which yielding will occur:

$$\tau_c = \tau_c^0 - \mu_c \sigma_n \quad (5)$$

The Tresca yield surface is a hexagonal prism in principal stress space. If we allow the yield condition to be a function of the hydrostatic pressure then the surface becomes a hexagonal cone.

We can apply the same hypothesis to the von Mises yield criterion by making the value of  $\tau_y$  a function of the hydrostatic pressure,  $P$ :

$$\tau_y = \tau_y^0 + \mu_m P \quad (6)$$

Here the constant  $\tau_y^0$  is the yield stress in pure shear, for then the hydrostatic component,  $-P$ , of the stress tensor is zero. The yield surface in principal stress space is now a right circular cone.

### 1.3. Yield Criteria Applicable to Polymers

It is valuable to pause here and review some instructive findings on the yield of polymers. Bowden and Jukes<sup>2</sup> found that the pressure-

modified von Mises criterion best described the behaviour of poly(methyl methacrylate) whilst a modified Tresca criterion was best for polystyrene. These authors say that for any homogeneous deformation it is in general not necessary or possible to define a shear plane. The concept of a shear plane may be introduced as a 'theoretical convenience' as is done in the Tresca yield criterion. The three realistic combinations to which they are led by this argument are the modified von Mises yield criterion, the Mohr-Coulomb criterion and the modified Tresca criterion. In all of these criteria the compressive and tensile yield stresses are predicted to be different.

Caddell *et al.*<sup>4</sup> have explored pressure-dependent yield criteria for polymers following the work of Raghava *et al.*<sup>3</sup> They conclude that, as the mean of the stress state becomes more compressive (or as the pressure condition becomes more pronounced), the criterion suggested by Raghava *et al.*<sup>3</sup> seems to provide a better correlation with experimental results than does the form of the pressure-dependent von Mises criterion used by other workers. Polymers exhibit a broad spectrum of yield behaviour which superficially is distinct from that of metals. However, when we come to consider time-dependent deformation we shall find some interesting similarities between polymer behaviour and metallic creep.

#### **1.4. Yield Criteria Applicable to Metals**

The von Mises yield criterion has been found to be in good agreement with the results of experiment for many ductile metals.<sup>1</sup> The failure of Tresca's criterion to give a good representation for materials such as iron, copper and nickel is due to the experimentally observed importance of the principal stress of intermediate value. The problem of formulating theoretical explanations of this fact has occupied a number of people and can scarcely be said to be entirely disposed of even today.

Supposing that we know the influence of stress, temperature and structure upon the kinetics of slip by the movement of dislocations in an individual crystal within a polycrystal, we may attempt to predict the yield behaviour of the polycrystal. Taylor<sup>5</sup> and Bishop and Hill<sup>6</sup> considered a single-phase polycrystal and neglected elastic strains (rigid-plastic model). They further supposed that each individual grain sustains the macroscopic strain of the entire aggregate. Rice<sup>7</sup> has considered an extension of this analysis to the general time-dependent case. He preserves the assumption that each grain sustains the same strain. These analyses show that the flow stress of a fcc polycrystal

loaded in simple tension is approximately three times the corresponding shear strength on its (111)/(110) slip systems (assumed equal for all). Lin<sup>8</sup> has further extended this approach to the elastic-plastic case by assuming that the total strain is constant in each grain.

The yield surface defined by the work of Bishop and Hill is quite close to the von Mises yield surface. We shall see below that it is possible to deduce the form of the von Mises yield surface from a model of dislocation creep.

## 2. MECHANICAL EQUATION OF STATE FOR DISLOCATION CREEP UNDER MULTIAXIAL STRESSES

The multiaxial creep of a material can generally be represented by an extension of the yield surface ideas presented above. This is not surprising for, as we have remarked, the yielding behaviour is (at least algebraically) merely an extreme case of creep at high stress sensitivity. We shall show in fact that not only the non-recoverable component of strain but also the recoverable component can be handled using the yield surface concept.

### 2.1. Some Anticipated Features of the MEOS

The form of the plastic stress-strain equations for the full stress tensor can best be introduced by considering the rigid-plastic material first, when the Levy-Mises equations are the relevant relationships:

$$d\varepsilon_{ij} = \sigma'_{ij} d\lambda \quad (7)$$

where  $\lambda$  is a scalar factor of proportionality and  $\sigma'_{ij}$  is the deviatoric part of the stress tensor. Despite the similarity between eqn (7) and Newton's law of viscous flow, Hill<sup>1</sup> warns us to guard against the use of this 'facile analogy'.

For the rigid-plastic material we have the additional relationship

$$\sigma'_{ij}\sigma'_{ij} = 2\sigma_y^2/3 = 2k^2 \quad (8)$$

where  $k^2$  was defined in eqn (1) above. We shall deal with the implications of these relations to the time-dependent (creep) case when we come to them, below.

Consider now the time-dependent idealisation for which a definite elastic range (interior of the current yield surface) exists at each stage of the deformation history.<sup>9</sup> The essential content of the theory of

time-independent plasticity is then expressed by the maximum plastic work inequality

$$(\sigma_{ij} - \sigma_{ij}^0) d\varepsilon_{ij} \geq 0 \quad (9)$$

Here  $d\varepsilon_{ij}$  is a plastic strain increment under a stress  $\sigma$  on the current yield surface and  $\sigma^0$  is any other stress state lying either within or on the yield surface. This inequality leads to (a) normality of the plastic strain increments to the yield surface at smooth points, and (b) the requirement for convex yield surfaces. The expression (9) is the key element expressing the validity of certain limit theorems associated with the non-strain-hardening idealisation, uniqueness, and the variational theorems.

Consider the counterpart of the inequality (9), for the time-dependent case, of course. How does the current creep rate depend on the current stress? Rice<sup>9</sup> has considered this and has arrived at

$$(\sigma_{ij}^A - \sigma_{ij}^B) \dot{\varepsilon}_{ij}(\sigma^A) \geq 0 \quad (10)$$

In eqn (10)  $\sigma^B$  is a stress state chosen to lie on or within the surface  $\Omega(\sigma) = \text{constant}$ , passing through the point  $\sigma^A$ . Here  $\Omega(\sigma)$  is a potential function of stress which has a value for each slipped state and whose derivatives with respect to stress yield the components of the creep strain rate tensor. Evidently  $\Omega(\sigma^B) \leq \Omega(\sigma^A)$ .

The problem of describing the response of a monocrystal to an arbitrary stress system and relating this to the response of a polycrystal has been examined by Zarka for the case in which deformation occurs by the movement of dislocations.<sup>10,11</sup> He remarks that work in this area can generally be divided into two categories: that in which phenomenological relations, valid for a few experiments, are developed, and the parallel work in which the different processes leading to deformation are described atomistically. In his work an endeavour is made to link these two approaches. To this end he first develops a mathematical theory of the behaviour of a monocrystal which is based on the fundamental hypotheses that the plastic deformation is a function of the stresses, the temperature and the density of dislocations and of point defects. The dislocation density changes at a rate which depends on its instantaneous value and upon the temperature, the orientation of the monocrystal, and the stress tensor.

## 2.2. Anelasticity: The Delayed Elastic Strain Diagram

Following any change in applied stress, there are two recoverable strains. One occurs instantaneously and is the *elastic* strain. The other

is time-dependent or *delayed* (here termed the delayed elastic strain). The potential magnitude of the delayed elastic strain in any direction in deviatoric stress space will be represented by the distance, from the origin, of points lying on a surface. For an unstressed, annealed isotropic specimen (i.e.  $\sigma'_{ij} = 0, t \rightarrow \infty$ ), this surface will be a spherical shell with its centre at the origin. A point S can be located having the principal external deviatoric stresses  $(\sigma'_1, \sigma'_2, \sigma'_3)$  as co-ordinates. It is noted that  $(OS)^2 = 2J'_2$ ;  $J'_2$  is the second deviatoric external stress tensor invariant<sup>1</sup> and S lies on the von Mises circle.<sup>12</sup> Let OS cut the spherical shell at  $S_1$  and  $S_2$  (Fig. 1).

When the external stress tensor  $\sigma_{ij}$  has been operating for a finite period of time it will have produced delayed elastic strain due to the bow of some dislocations. Position a point  $S'_1$  on OS such that  $S_1S'_1$  is proportionate to this component of delayed elastic strain.

In the fully annealed, unstressed specimen, then, the principal delayed elastic strains are all equal (and equal to zero) and are given by

$$\bar{\xi}_1 = \bar{\chi}_2 - \bar{\chi}_1 \text{ (etc.)} \quad (11)$$

where  $\bar{\chi}_2$  and  $\bar{\chi}_1$  are the  $\chi$  co-ordinates of the points at which the  $\chi$  axis (i.e. the axis of one of the principal deviatoric external stresses) cuts the spherical shell.

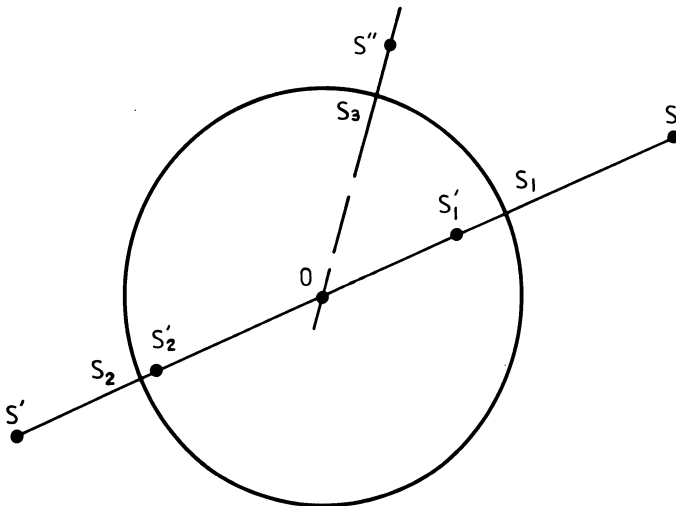


Fig. 1. Section through delayed elastic strain diagram.

If we can determine the surface into which the spherical shell has been transformed by the action of a finite stress system (such as S), then the intercepts made by this new surface should, via eqn (11), define the new values of the three principal delayed elastic strains.

*Theorem: If a Sphere's Centre Lies on the Plane  $x + y + z = 0$ , then the Algebraic Sum of the Co-ordinates of Its Intercepts with Orthogonal Axes is Zero*

The equation of the sphere with radius  $r$  and centre C ( $x_c, y_c, z_c$ ) is

$$(x - x_c)^2 + (y - y_c)^2 + (z - z_c)^2 = r^2 \quad (12)$$

Let its centre be a distance  $R$  from the origin (O) of co-ordinates and let  $L$ ,  $M$  and  $N$  be the direction cosines of OC. Then the equation of OC is

$$x_c/L = y_c/M = z_c/N = R \quad (13)$$

The sphere intersects the  $x$ -axis at

$$y = z = 0 \quad (14)$$

Substituting eqns (13) and (14) into eqn (12) we obtain a quadratic equation in  $x$  whose roots ( $x_2$  and  $x_1$ ) are the co-ordinates of the intercepts which the sphere makes with the  $x$ -axis:

$$x^2 - 2xLR + (R^2 - r^2) = 0 \quad (15)$$

Solving eqn (15) we obtain

$$x_1 + x_2 = 2LR$$

whilst similarly

$$y_1 + y_2 = 2MR \quad (16)$$

$$z_1 + z_2 = 2NR$$

But  $x_c + y_c + z_c = 0$  and so

$$L + M + N = 0$$

Hence from eqn (16):

$$x_1 + x_2 + y_1 + y_2 + z_1 + z_2 = 0 \quad (17)$$

QED

Also, as

$$x_1 + x_2 = \bar{x}_1 - \bar{x}_2 \quad (18)$$

$$\therefore (\bar{x}_1 - \bar{x}_2) + (\bar{y}_1 - \bar{y}_2) + (\bar{z}_1 - \bar{z}_2) = 0 \quad (19)$$

*The Levy–Mises and Volume-conservation Criteria for the Equilibrium Case*

Let a stress  $\sigma_{ij}$  act for  $t \rightarrow \infty$  producing a limiting strain:

$$\xi_L (= S_1 S'_1 - S'_2 S_2) = 2R \quad (20)$$

By our argument about its symmetry, the sphere's centre now lies on OS, a line in the plane  $\sigma'_1 + \sigma'_2 + \sigma'_3 = 0$ .

From eqns (16), (18) and (20):

$$\xi_i = \bar{x}_1 - \bar{x}_2 = x_1 + x_2 = 2LR = L\xi_L$$

Similarly

$$\xi_2 = M\xi_L \quad (21)$$

$$\xi_3 = N\xi_L$$

Now

$$L = \frac{\sigma'_1}{\sqrt{(2J'_2)}} \text{ etc.} \quad (22)$$

From eqns (21) and (22):

$$\frac{\xi_1}{\sigma'_1} = \frac{\xi_2}{\sigma'_2} = \frac{\xi_3}{\sigma'_3} \cdot \frac{\xi_1}{\sqrt{(2J'_2)}} \quad (23)$$

Equations (23) are the Levy–Mises relationships.

From eqns (19) and (21):

$$\xi_1 + \xi_2 + \xi_3 = 0 \quad (24)$$

Equation (24) shows that volume is conserved during straining.

*The Approach to Equilibrium*

If we change the stress state from  $S'$  to  $S''$  then the sphere's centre will move from  $C_1$ , its present position (not necessarily an equilibrium position, for the time spent at  $S'$  may have been finite), towards  $C_2$ , the equilibrium position which would be attained if the new stress state,  $S''$ , prevailed for  $t \rightarrow \infty$ .

The theorem shows that if the sphere's centre  $C$ , during its movement from  $C_1$  towards  $C_2$ , remains in the plane  $\sigma'_1 + \sigma'_2 + \sigma'_3 = 0$  (a plane containing  $OC_1$  and  $OC_2$ ), then volume will be conserved at all times during its transit, i.e. eqn (24) will apply.

Consider now a specimen whose delayed elasticity diagram is that shown in Fig. 2, a sphere whose centre  $C$  has been displaced a distance  $R$  ( $=OC = 2\xi$ ) from the origin of co-ordinates  $O$ , by the prior operation of a stress system. The internal stress ( $\sigma_1$ ) due to dislocation curvature is proportionate to the strain due to dislocation curvature (Mott;<sup>13</sup> Friedel<sup>14</sup>). The delayed elastic creep rate will be a function of the stress acting to cause dislocation bowing.

Then the locus of new stress states ( $S$ ) that produce the same magnitude of effective delayed elastic creep rate will (Fig. 2) be a circle lying in the plane  $J'_1 = 0$ , concentric with the sphere and of radius  $CS = \sqrt{(2J_2(\sigma'_{ni}))}$  where  $J_2(\sigma'_{ni})$  is the second invariant of the deviatoric net stress tensor:

$$i = 1, 2, 3: \sigma'_{ni} = \sigma'_i - \sigma'_{li} \quad (25)$$

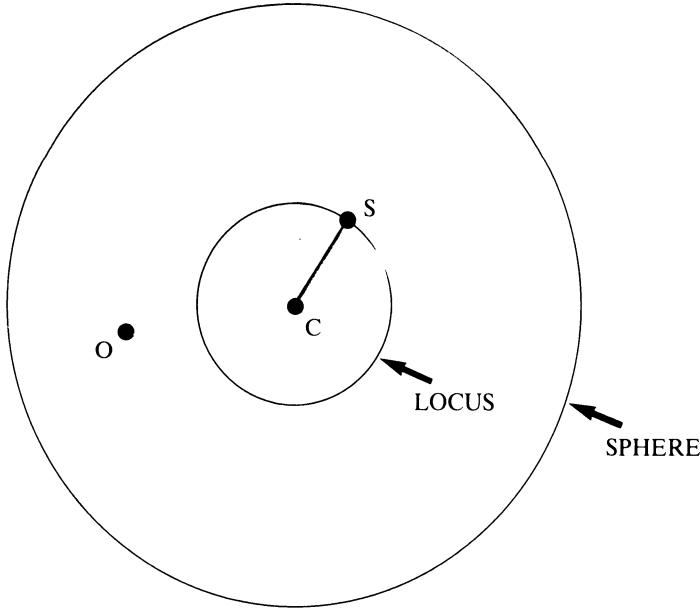


**Fig. 2.** Delayed elasticity sphere and the locus of equivalent stress states in the plane  $J'_1 = 0$ .

where

$$\sigma'_{ii} = (2/3)E'_m \xi_i \quad (26)$$

$E'_m$  is the equivalent, for delayed elasticity, of Young's modulus. Hence

$$\dot{\xi}_i = \sigma'_{ni} \dot{\lambda} \quad (27)$$

where

$$\dot{\lambda} = \frac{f[J_2(\sigma'_{ni}), T]}{\sqrt{(2J_2(\sigma'_{ni}))}} \quad (28)$$

The function  $f$  links the effective delayed elastic strain rate with net stress and temperature. It can be determined experimentally by measuring the instantaneous creep rate in uniaxial tension for a fully annealed material ( $\sigma_1 = 0$ ) at  $t = 0$ . in such cases  $\xi_1 \sqrt{3} = f[\sigma_1/\sqrt{3}, T]$ , a relationship which enables  $f$  to be evaluated by curve fitting techniques.

#### *Dilation, $E'$ and $\nu'$*

The elastic equations relating principal elastic strains ( $\varepsilon_{e1}, \varepsilon_{e2}, \varepsilon_{e3}$ ) with stress, Young's modulus ( $E$ ) and Poisson's ratio ( $\nu$ ) are

$$\begin{Bmatrix} \varepsilon_{e1} \\ \varepsilon_{e2} \\ \varepsilon_{e3} \end{Bmatrix} = \frac{1}{E} \begin{bmatrix} 1 & -\nu & -\nu \\ -\nu & 1 & -\nu \\ -\nu & -\nu & 1 \end{bmatrix} \begin{Bmatrix} \sigma_1 \\ \sigma_2 \\ \sigma_3 \end{Bmatrix} \quad (29)$$

whilst the delayed elastic equilibrium equations are

$$\begin{Bmatrix} \xi_1 \\ \xi_2 \\ \xi_3 \end{Bmatrix} = \frac{1}{E'} \begin{bmatrix} 1 & -\nu' & -\nu' \\ -\nu' & 1 & -\nu' \\ -\nu' & -\nu' & 1 \end{bmatrix} \begin{Bmatrix} \sigma_1 \\ \sigma_2 \\ \sigma_3 \end{Bmatrix} \quad (30)$$

where, from eqn (23):

$$\nu' = 1/2 \quad (31)$$

and

$$E' = \frac{3\sqrt{(J'_2/2)}}{\xi_L} \quad (32)$$

The analogy between delayed elasticity and elasticity would lead us to expect some similarity between  $\nu$  and  $\nu'$ . In particular, if  $\nu'$  (like  $\nu$ ) is

less than 0.5, then dilational strains will occur, superimposed upon the conservative strains with which this section has so far been concerned.

*If the Delayed Elastic Strain is Due to Recoil of Obstacle Dislocations*

If the internal stress (which tends to return the dislocations to their zero stress rest positions when the external stress is removed) is mainly due to the forces exerted by the dislocations on one another and not to the bowing-induced self-stress, then

$$S_1 S'_1 = l_a(1 - \bar{\rho}) \quad (33)$$

where  $\bar{\rho}$  is the mobile dislocation density and  $l_a$  is a characteristic parameter of dimension length when  $S$  is the external stress vector. Evidently

$$OS'_1 = \bar{\rho} \quad (34)$$

Similarly the mobile dislocation density would be  $OS'_2 = \bar{\rho}_c$  if we suddenly rotated the stress vector to  $S'$ , i.e. (in the uniaxial case) changed the stress from tensile to compressive. We now have a method of reading off the value of the mobile dislocation density for any arbitrary direction of the applied stress vector. For example, if it changes from  $OS$  to  $OS''$  (Fig. 1) then the length of the intercept which it makes ( $OS_3$ ) is the new value of the mobile dislocation density.

So we have

$$S_2 S'_2 = l_a(1 - \bar{\rho}_c) \quad (35)$$

and at the limit, when a given stress vector has been acting for infinite time, the delayed elastic strain will move to

$$\xi_L = l_a(1 - \bar{\rho}_L) \quad (36)$$

where  $\bar{\rho}_L$  is the normalised density of the dislocations that are mobile under compressive stressing and  $\bar{\rho}_L$  is the limiting value of the mobile dislocation density under the prevailing conditions of stress and temperature. We use eqn (36) with eqns (30) and (32) to calculate the delayed elastic strain tensor for this case.

### 2.3. Non-recoverable Strain

If the mobile dislocation density,  $\rho$  ( $\text{m}^{-2}$ ), represents those of the dislocations that are gliding at any instant, then

$$\dot{\epsilon} = gb\rho v \quad (37)$$

In eqn (37)  $\dot{\epsilon}$  is the creep rate,  $v$  is the mean velocity of the  $\rho$  gliding dislocations and  $b$  is the Burgers vector;  $g$  is a constant of order unity.

As the dislocations glide they encounter obstacles such as grain boundaries, precipitate particles and other dislocations which halt them and in this way reduce  $\rho$ . Some of the dislocations so immobilised can escape from the obstacles and resume their glide. This process of remobilisation tends to raise  $\rho$ , so also does the operation of dislocation sources. During a brief period of time  $dt$ , then, the mobile dislocation density will change by a small amount  $d\rho$  whose magnitude will depend on the rates of immobilisation and remobilisation.

Observations on the behaviour of dislocations in stressed lithium fluoride led Johnston and Gilman<sup>15</sup> to conclude that

$$\dot{\rho}_A = -i\rho + S_g \quad (38)$$

where  $i$  is the frequency with which gliding dislocations encounter barriers that halt them and  $S_g$  is the rate at which new dislocations are generated by sources.

Consider two orthogonal, intersecting slip systems, (1) and (3), having mobile dislocation densities  $\rho_1$  and  $\rho_2$ . If the dislocations are moving at absolute velocities  $V_1$  and  $V_2$  then their relative velocity is

$$\sqrt{(V_1^2 + V_2^2)} \quad (39)$$

and the flux of system (1) dislocations relative to system (3) dislocations is

$$\rho_1 \sqrt{(V_1^2 + V_2^2)} \quad (40)$$

Hence the rate at which system (1) dislocations immobilise system (3) dislocations (and are themselves immobilised in the process) is proportionate to

$$\rho_2 [\rho_1 \sqrt{(V_1^2 + V_2^2)}] \quad (41)$$

If the initial mobile dislocation density, before immobilisation commenced, was  $\rho_0$  on both system (1) and system (3) then, since the rate of subsequent immobilisation is the same for both systems,  $\rho_1 = \rho_2$  ( $=\rho$ , say) at all times.

Note that the rate of immobilisation of system (3) dislocations does not depend merely upon their velocity; it is just as much influenced by the velocity of system (1) dislocations (and vice versa). The material has a natural tendency to remain isotropic, with

$$i \propto \rho \sqrt{(V_1^2 + V_2^2)}$$

i.e. (using eqn (37))

$$i \propto \sqrt{(\dot{S}_1^2 + \dot{S}_2^2)} \quad (42)$$

where  $\dot{S}_1$  and  $\dot{S}_2$  are the shear strain rates.

This then is the train of reasoning which was advanced by Johnston and Gilman<sup>15</sup> to explain their experimental finding, for lithium fluoride, that

$$i \propto \dot{\epsilon} \quad (43)$$

where  $\dot{\epsilon}$  is the tensile strain rate. They also found that

$$S_g \propto \dot{\epsilon} \quad (44)$$

Equation (42) reduces to eqn (43) for a specimen subjected to uniaxial tension, whilst for triaxial stressing

$$i \propto \sqrt{(\dot{S}_1^2 + \dot{S}_2^2 + \dot{S}_3^2)} \quad (45)$$

which may be written

$$i \propto \dot{\epsilon}_v \quad (46)$$

where

$$\dot{\epsilon}_v = (\sqrt{2}/3)\sqrt{[(\dot{\epsilon}_1 - \dot{\epsilon}_2)^2 + (\dot{\epsilon}_1 - \dot{\epsilon}_3)^2 + (\dot{\epsilon}_2 - \dot{\epsilon}_3)^2]} \quad (47)$$

In eqn (47),  $\dot{\epsilon}_1$  etc. are the principal strain rates.

Now, in the development of the uniaxial MEOS,<sup>16</sup> it was found that a good representation of experimental data, valid for stresses that were varied (during the creep experiment) in both sign and magnitude, was produced when the steady-state creep rate,  $\dot{\epsilon}_s$ , was substituted for the instantaneous creep rate ( $\dot{\epsilon}$ ) in eqns (43) and (44). So for the multiaxial case

$$i \propto \dot{\epsilon}_{vs}$$

$$S_g \propto \dot{\epsilon}_{vs}$$

and substituting these expressions into eqn (38):

$$\rho_A = -\lambda \dot{\epsilon}_{vs} (\rho - \rho_\infty) \quad (48)$$

where

$$\dot{\epsilon}_{vs} = (\sqrt{2}/3)\sqrt{[(\dot{\epsilon}_{1s} - \dot{\epsilon}_{2s})^2 + (\dot{\epsilon}_{1s} - \dot{\epsilon}_{3s})^2 + (\dot{\epsilon}_{2s} - \dot{\epsilon}_{3s})^2]} \quad (49)$$

In eqn (48)  $\lambda$  and  $\rho_\infty$  are the two materials constants which relate  $i$  and  $S_g$  to  $\dot{\epsilon}_{vs}$ ;  $\rho_\infty$  is the lower asymptote towards which  $\rho$  falls. When

$\rho = \rho_\infty$ , the rate at which dislocations immobilise one another becomes equal to the rate at which new mobile dislocations are generated by source operation (i.e.  $i\rho = S_g$ ).

Turning to the rate of thermally activated re-mobilisation, the hypothesis which was used in the uniaxial equations will be retained, and so

$$\dot{\rho}_1 = \gamma(\rho_0 - \rho) \quad (50)$$

Here  $\rho_0$  is the upper asymptote of the mobile dislocation density and

$$\gamma = \exp(E' - Q/RT) \quad (51)$$

where  $E'$  and  $Q$  are constants; the earlier work revealed, as would be expected, that  $Q$  commonly equals the activation energy for self-diffusion. Thermally activated recovery is not, however, the only potential re-mobilisation process; the earlier work showed that stress reversal can be equally effective and this mechanism will be generalised to the multiaxial case in the next section.

#### 2.4. Remobilisation by Stress Reversal

Figure 3 shows that the average behaviour, under a tensile stress ( $+\sigma$ ), of a dislocation at 'c' is identical with that of a dislocation at 'b';

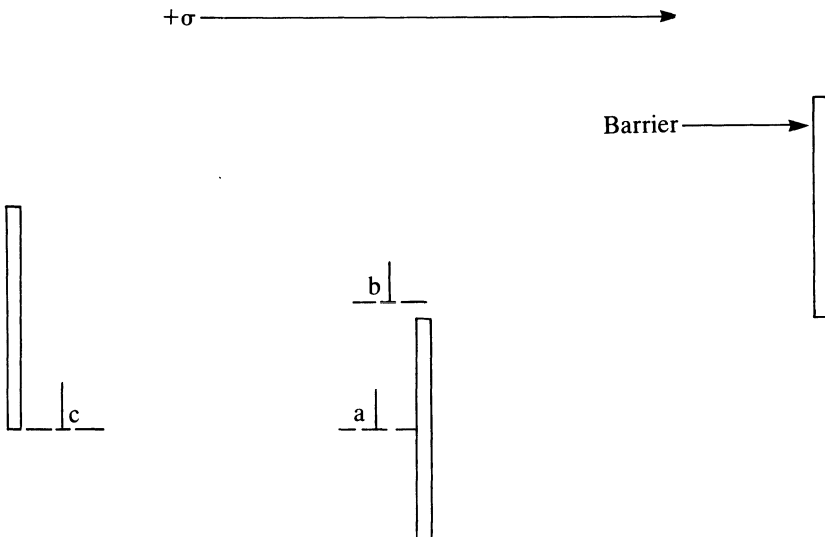


**Fig. 3.** Remobilisation of a dislocation (a) by either climb (to position b) or reversed glide (to position c).<sup>18</sup>

both will glide the mean distance between adjacent barriers. The model specifies that remobilisation by climb from 'a' to 'b' occurs by the recovery process of eqn (50) and at a rate  $\gamma$ . Remobilisation by glide from 'a' to 'c' can be accomplished by temporarily reversing the stress; if it is reversed for a period of time  $dt$ , then a fraction  $i dt$  of the  $(\rho_0 - \rho)$  dislocations that had become immobilised at 'a' will glide back to 'c'.

The total rate at which dislocations are rendered 'tension-mobile' by climb and glide under a compressive stress is therefore

$$(i + \gamma)(\rho_0 - \rho) \quad (52)$$

## 2.5. Multiaxial Strain Rates and the Dislocation Velocity

We wish to arrive at the form of a function,  $f$ , linking the velocity,  $v$ , of dislocations on a specific shear system with the shear stress causing that motion. As before, the axes are chosen to coincide with the directions of the three principal stresses. Then, from eqn (37), for one of the principal shear planes

$$\dot{\epsilon}_1 - \dot{\epsilon}_2 = b\rho \cdot f(\sigma_1 - \sigma_2) \quad (53)$$

or, more generally

$$\frac{1}{b\rho} \begin{bmatrix} 1 & -1 & 0 \\ 0 & 1 & -1 \\ -1 & 0 & 1 \end{bmatrix} \begin{Bmatrix} \dot{\epsilon}_1 \\ \dot{\epsilon}_2 \\ \dot{\epsilon}_3 \end{Bmatrix} = \begin{bmatrix} 1 & -1 & 0 \\ 0 & 1 & -1 \\ -1 & 0 & 1 \end{bmatrix} \cdot f \begin{Bmatrix} \sigma_1 \\ \sigma_2 \\ \sigma_3 \end{Bmatrix} \quad (54)$$

whilst, for the octahedral shear plane

$$\dot{\epsilon}_v = b\rho \cdot f\{(\sqrt{2}/3)\sqrt{[(\sigma_1 - \sigma_2)^2 + (\sigma_1 - \sigma_3)^2 + (\sigma_2 - \sigma_3)^2]}\} \quad (55)$$

Eliminating  $\dot{\epsilon}_{1,2,3}$  between eqns (47) and (54) gives an alternative equation for  $\dot{\epsilon}$ :

$$\dot{\epsilon}_v = (\sqrt{2}/3)b\rho\sqrt{\{[f(\sigma_1 - \sigma_2)]^2 + [f(\sigma_1 - \sigma_3)]^2 + [f(\sigma_2 - \sigma_3)]^2\}} \quad (56)$$

The most general form of function  $f$  that satisfies both eqn (55) and eqn (56) is

$$f(\sigma_1 - \sigma_2) = (\sigma_1 - \sigma_2)\Phi \quad (57)$$

and similar expressions for  $\sigma_1, \sigma_3$  and  $\sigma_2, \sigma_3$ . In eqn (57),  $\Phi$  is some function of the temperature and stress system which must be a constant independent of time and strain.

Equations (54), (56) and (57) may be combined to yield

$$\frac{1}{2} \begin{Bmatrix} \dot{\epsilon}_1 \\ \dot{\epsilon}_2 \\ \dot{\epsilon}_3 \end{Bmatrix} \div \begin{bmatrix} 1 & -\frac{1}{2} & -\frac{1}{2} \\ -\frac{1}{2} & 1 & -\frac{1}{2} \\ -\frac{1}{2} & -\frac{1}{2} & 1 \end{bmatrix} \begin{Bmatrix} \sigma_1 \\ \sigma_2 \\ \sigma_3 \end{Bmatrix} = \frac{\dot{\epsilon}_v}{\sigma_v} = b\rho\Phi \quad (58)$$

where

$$\sigma_v = (\sqrt{2/3})\sqrt{[(\sigma_1 - \sigma_2)^2 + (\sigma_1 - \sigma_3)^2 + (\sigma_2 - \sigma_3)^2]} \quad (59)$$

Some deductions about  $\rho\Phi$  are possible; thus dislocation creep is insensitive to hydrostatic stress and so  $\rho\Phi$  must be a function of the deviatoric stress tensor. The predicted creep rates must not depend upon the choice of axes and so  $\rho\Phi$  must be a function of the deviatoric stress tensor invariants,  $J'_2$  and  $J'_3$ . In eqn (58), the sign of  $\dot{\epsilon}_v/\sigma_v$  is independent of the signs of  $\sigma_{1,2,3}$ ; therefore the sign of  $\rho\Phi$  must be independent of the signs of  $\sigma_{1,2,3}$  and so  $\rho\Phi$  must be independent of (or an even function of) the third deviatoric stress tensor invariant,  $J'_3$ . It can be any function of  $J'_2$  (i.e. of  $\sigma_v$ ).

Experiments support these conclusions, for they generally reveal that

$$\dot{\epsilon}_{vs} = \sigma_v^n \exp(E_a - Q/RT) \quad (60)$$

where  $E_a$  and  $n$  (typically  $n = 2$  to  $8$ ) are materials constants.

Substituting eqn (60) into eqn (58) gives

$$\sigma_v^{n-1} \exp(E_a - Q/RT) = b\rho_L\Phi \quad (61)$$

which provides experimental verification of our inference that  $\rho\Phi$  (here represented by the specific value,  $\rho_L\Phi$ , which it attains when steady-state creep is reached and  $\dot{\epsilon}_v = \dot{\epsilon}_{vs}$ ) should be a function of  $\sigma_v$  (i.e. of  $J'_2$ ) and  $T$ .

## 2.6. The Strain–Time Equation

Divide time into a succession of periods (durations  $t_1, t_2, \dots, t_m$ ) during each of which the stresses and temperatures are held constant at values which would eventually produce steady-state principal creep rates of

$$\begin{aligned} m = 1: & \quad \dot{\epsilon}_{1s1} \quad \dot{\epsilon}_{2s1} \quad \dot{\epsilon}_{3s1} \\ m = 2: & \quad \dot{\epsilon}_{1s2} \quad \dot{\epsilon}_{2s2} \quad \dot{\epsilon}_{3s2} \\ & \quad \vdots \\ m = m: & \quad \dot{\epsilon}_{1sm} \quad \dot{\epsilon}_{2sm} \quad \dot{\epsilon}_{3sm} \end{aligned}$$

The limiting value,  $\rho_{Lm}$ , of the mobile dislocation density is derived by solving eqns (48) and (50) for  $\dot{\rho} = 0$ :

$$\dot{\rho} = -\rho(\lambda\dot{\epsilon}_{vsm} + \gamma_m) + \lambda\dot{\epsilon}_{vsm}\rho_\infty + \gamma_m\rho_0 \quad (62)$$

and so, when  $\dot{\rho} = 0$ :

$$\bar{\rho}_{Lm} = (\lambda\dot{\epsilon}_{vsm}\bar{\rho}_\infty + \gamma_m)/\mu_m \quad (63)$$

where

$$\left. \begin{aligned} \bar{\rho}_{Lm} &= \rho_{Lm}/\rho_0; \bar{\rho}_\infty = \rho_\infty/\rho_0 \\ \mu_m &= \lambda\dot{\epsilon}_{vsm} + \gamma_m \end{aligned} \right\} \quad (64)$$

Substituting eqn (63) back into eqn (62) yields

$$\dot{\bar{\rho}} = -(\bar{\rho} - \bar{\rho}_{Lm}) \cdot \mu_m \quad (65)$$

Equation (65) is now integrated to define the value which  $\bar{\rho}$  ( $=\rho/\rho_0$ ) attains after time  $t$  ( $0 < t \leq t_m$ ) during the  $m$ th period:

$$\bar{\rho} = (\bar{\rho}_{Fim} - \bar{\rho}_{Lm})\exp(-\mu_m t) + \bar{\rho}_{Lm} \quad (66)$$

In eqn (66),  $\bar{\rho}_{Fim}$  and  $\bar{\rho}_{Lm}$  are, respectively, the initial value and the asymptote of  $\bar{\rho}$ . The subscript *Fim* stands for 'forward-mobile, initial dislocation density for period  $m$ '. The forward direction is the direction of straining and the forward-mobile dislocations are those whose glide, under the applied stress, causes creep. At the end of period  $m$  the forward-mobile dislocation density will have fallen to the value  $\rho_{Fem}$  (*Fem* = Forward-mobile dislocation density at end of period  $m$ ) given by eqn (66) with  $t = t_m$ . That is

$$\bar{\rho}_{Fem} = (\bar{\rho}_{Fim} - \bar{\rho}_{Lm})\exp(-\mu_m t_m) + \bar{\rho}_{Lm} \quad (67)$$

From eqn (66) the strain-time integral can be formed for, from eqn (58):

$$n = 1, 2, 3: \frac{\dot{\epsilon}_{nm}}{\bar{\rho}} = \frac{\dot{\epsilon}_{nsm}}{\bar{\rho}_{Lm}} \quad (68)$$

In eqn (68),  $\dot{\epsilon}_{nm}$  is the instantaneous strain rate along principal direction  $n$  during the  $m$ th period, so

$$n = 1, 2, 3: \epsilon_{nm} = \int \dot{\epsilon}_{nm} dt$$

i.e.

$$n = 1, 2, 3: \epsilon_{nm} = \frac{\dot{\epsilon}_{nsm}}{\bar{\rho}_{Lm}} \int_{\bar{\rho}_{Fim}}^{\bar{\rho}} \bar{\rho} dt \quad (69)$$

where, from eqn (58):

$$n = 1, 2, 3: \dot{\epsilon}_{nsm} = \sigma'_{nm} \dot{\epsilon}_{vsm} / \sigma_{vm} \quad (70)$$

with

$$\sigma'_{nm} = \sigma_{nm} - (\sigma_{1m} + \sigma_{2m} + \sigma_{3m})/3 \quad (71)$$

Substituting eqn (66) into eqn (69) and integrating:

$$n = 1, 2, 3: \epsilon_{nm} = \frac{\dot{\epsilon}_{nsm}}{\mu_m} \left[ \frac{\bar{\rho}_{Fim}}{\bar{\rho}_{Lm}} - 1 \right] (1 - \exp(-\mu_m t_m)) + \dot{\epsilon}_{nsm} t_m \quad (72)$$

In the uniaxial equations previously developed, the effect of tensile straining on both the tension-mobile and compression-mobile dislocation densities was calculated. The counterpart of this computation, for the multiaxial equations, is the calculation of the effects of forward straining on both the forward-mobile and reverse-mobile dislocation densities. Equation (67) gives the former; the latter may be derived by integrating eqn (52):

$$\begin{aligned} \dot{\rho}_R &= (i_m + \gamma_m)(\rho_0 - \rho_R) \\ &= (\lambda \dot{\epsilon}_{vsm} + \gamma_m)(\rho_0 - \rho_R) \end{aligned}$$

so that

$$\bar{\rho}_{Rim} = (\bar{\rho}_{Rim} - 1) \exp(-\mu_m t_m) + 1 \quad (73)$$

Subscript *Rem* stands for 'Reverse-mobile dislocation density at the end of period *m*'; subscript *Rim* indicates the initial value.

Now, the uniaxial equations recognised that, when the stress changed from tension to compression, the compression-mobile dislocation density dictated the subsequent strain rate. In the multiaxial equations, then, the influence of a specific shear system on the mean mobile dislocation density is altered when slip on that system changes direction:

$$n = 1, 2, 3: \text{If signum } \dot{\epsilon}_{ns(m+1)} = \text{signum } \dot{\epsilon}_{nsm} \text{ then } \delta_n = 1$$

$$\text{If signum } \dot{\epsilon}_{ns(m+1)} \neq \text{signum } \dot{\epsilon}_{nsm} \text{ then } \delta_n = 0$$

Let

$$\delta = (\delta_1 + \delta_2 + \delta_3)/3 \quad (74)$$

then

$$\bar{\rho}_{Fi(m+1)} = \bar{\rho}_{Fem} \delta + \bar{\rho}_{Rem} (1 - \delta) \quad (75)$$

**TABLE 1**  
Computer Program that Solves the Multiaxial MEOS for Anelastic plus Plastic Strains

---

*Algorithm*

---

```

REAL LASTE (3),LASTEDOTS(3)
DIMENSION SFAC(3),ANT",ALAN"
DIMENSION EDOTS(3), SIG",EPS",IDELTA"
TOTIM=1M=0
INPUT,AN,EA,EPRIME,Q,LAMBDA, ROINF, ROFI, RORI, AL
REAL MU
STAR:IM=IM+1
INPUT,SIG(1),SIG(2),SIG(3),T,TIME
IF(TIME)DONE,ALONG,ALONG
ALONG:SIGV=0.3333*1.414*SQRT(SIG(1) - SIG(2))**2+(SIG(1)
+ - SIG(3))**2+(SIG(2) - SIG(3))**2)
GAMMA=EXP(EPRIME - Q/2T)
EDOTVS=SIGV**AN*EXP(EA - Q/2T)
IDEL=0
DO ONE,N=1,3
SFAC(N)=(SIG(N) - (SIG(1)+SIG(2)+SIG(3))/3)/SIGV
EDOTS(N)=(SIG(N) - (SIG(1)+SIG(2)+SIG(3))/3)*EDOTVS/SIGV
ONE:
MU=LAMBDA*EDOTVS + GAMMA
ROL=(LAMBDA*EDOTVS*ROINF + GAMMA)/MU
ALIM=AL*(1 - ROL)
IF(IM - 2)D,E,E
E:IDEL=0
DO C,N=1,3
J=SIGN(1,EDOTS(N))-SIGN(1,LASTEDOTS(N))
IF(J)A,B,A
A:IDELTA(N)=0:GOTO C
B:IDELTA(N)=1
C:IDEL=IDEL+IDELTA(N)
DEL=IDEL;DEL=DEL/3
ROFI=ROFE*DEL+RORE*(1-DEL)
RORI=RORE*DEL+RORE*(1-DEL)
D:DO THREE,M=1,10
TIM=TIME*M/10
DO TWO,N=1,3
ANT(N)=(ALAN(N) - ALIM*SFAC(N))*EXP(- MU*TIM)+ALIM*SFAC(N)
FAC=(ROFI/ROL - 1)*(1 - EXP(- MU*TIM))/MU+TIM
TWO:EPS(N)=EDOTS(N)*FAC+LASTE(N)+ANT(N)
TOTIM=TOTIM+TIME/10
PRINT,TOTIM,EPS(1),EPS(2),EPS(3)
THREE:
DO FOUR,N=1,3
ALAN(N)=ANT(N)
LASTEDOTS(N)=EDOTS(N)
FOUR:LASTE(N)=EDOTS(N)*FAC+LASTE(N)
ROFE=(ROFI - ROL)*EXP(- MU*TIME)+ROL
RORE=(RORI - 1)*EXP(- MU*TIME)+1
GOTO STAR
DONE:

```

---

**TABLE 2**  
**MEOS Parameters for Stainless Steel (Input for the Algorithm)**

<i>Parameter</i>	$\eta$	$E_a$	$E^{-1}$	$Q$	$\lambda$	$\rho_x$	$\rho_{F\pi}$	$\rho_{R\pi}$	$I_a$
Algorithmic name	AN	EA	EPRIME	Q	LAMBDA	ROINF	ROFI	RORI	AL
Experimental value	2.3529	20.1137	18.2	$6 \times 10^4$	8460	0.113	1.0	1.0	0.001
Theoretical value	3.0 (eqn (60))	18-20 (eqn (60))	19.5	$6.5 \times 10^4$	3876	0	1.0	1.0	0.00129

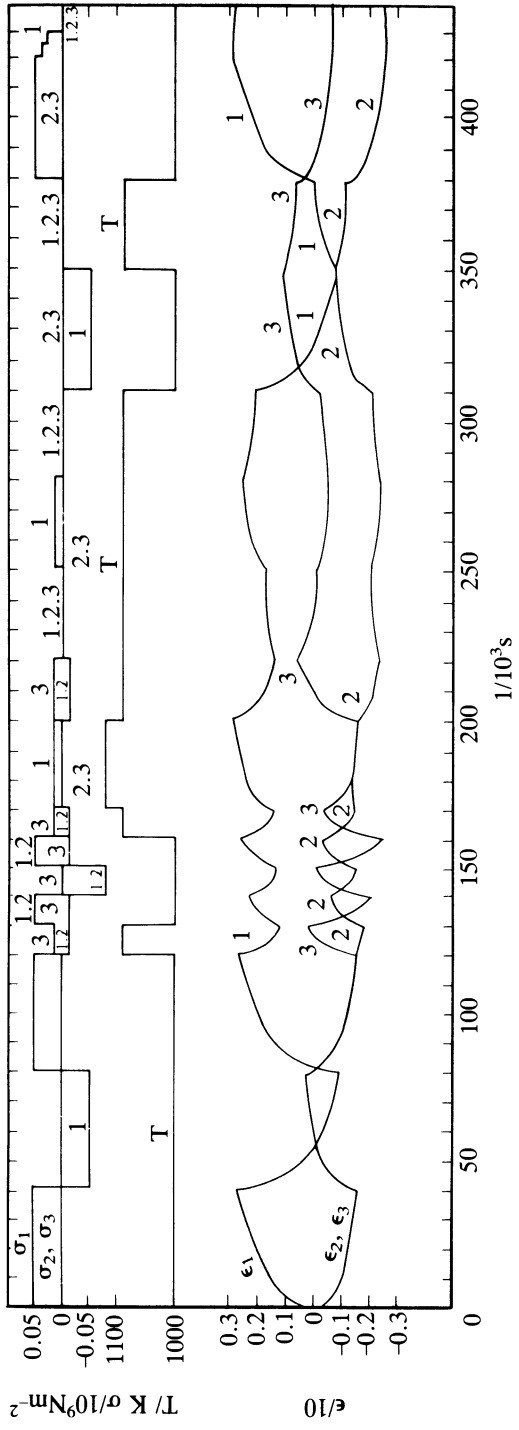


**Fig. 4.** Stress ( $\sigma$ ), temperature ( $T$ ) and creep strain ( $\epsilon$ ) versus time ( $t$ ),  $t/10^3$  s.

and

$$\bar{\rho}_{\text{Ri}(m+1)} = \bar{\rho}_{\text{Rem}}\delta + \bar{\rho}_{\text{Fem}}(1 - \delta) \quad (76)$$

Equations (75) and (76) reduce to those previously derived when the stress is uniaxial.

Finally

$$n = 1, 2, 3: \epsilon_n = \sum_{(m)} \epsilon_{nm} \quad (77)$$

In eqn (77), the values of  $\epsilon_{nm}$  are those given by successive solutions of eqn (72).

Clough and Simmons have developed a theory of multiaxial plasticity based on integral dislocation dynamics.<sup>17</sup> They remark that their theory may be considered as complementary to that of Gittus,<sup>18</sup> described in this section.

## 2.7. Computer Program that Solves the MEOS

Table 1 is an algorithm written in the high-level computer language FORTRAN which solves the equations of Sections 2.2 to 2.6 and so calculates the sum of the delayed elastic and the non-recoverable strains. Table 2 gives the input parameter values that best fit the experimental creep data for 20Cr–25Ni–Nb stainless steel. For comparison it also gives theoretical values of these parameters. An example of the output of the computer program is provided by Fig. 4 in which the results predicted for arbitrary sequences of stresses and temperatures are illustrated. Here the experimental values of the parameters (Table 2) have been used and there is good agreement with the results of variable stress (including stress reversal) experiments.

## REFERENCES

1. R. Hill, *The Mathematical Theory of Plasticity*, Oxford Univ. Press, London, 1950.
2. P. B. Bowden and J. A. Jukes, *J. Mat. Sci.*, **7** (1972) 52–63.
3. R. Raghava, R. M. Caddell and G. S. Y. Yeh, *J. Mat. Sci.*, **8** (1973) 225–32.
4. R. M. Caddell, R. S. Raghava and A. G. Atkins, *Mat. Sci. Eng.*, **13** (1974) 113–20.
5. G. I. Taylor, *J. Inst. Metals*, **62** (1938) 307.

6. J. F. W. Bishop and R. Hill, *Phil. Mag.*, **42** (1951) 414, 1298.
7. J. R. Rice, USAEC Contract AT(11-1)-3084, Technical Report No. 18, Brown University, Providence, Rhode Island, USA, 1973.
8. T. H. Lin, *J. Mech. Phys. Solids*, **5** (1957) 143.
9. J. R. Rice, *ASME J. Appl. Mech.*, **37** (1970) 728–37.
10. J. Zarka, Constitutive laws of metals in plasticity and viscoplasticity, lectures presented at the Royal Institute of Technology Stockholm, Sweden, April 1973.
11. J. Zarka, Concerning the viscoplasticity of metals, Ecole Polytechnique, Laboratoire de Mécanique des Solides, 17 rue Descartes, Paris 5, 1973.
12. R. von Mises, *Göttinger Nachrichten, Math.-Phys.* (1913) 528.
13. N. F. Mott, *Phil. Mag.*, **43** (1952) 1151.
14. J. Friedel, *Phil. Mag.*, **44** (1953) 444.
15. W. G. Johnston and J. J. Gilman, *J. Appl. Phys.*, **30** (1959) 129.
16. W. Whitney and R. D. Andrews, *J. Polymer Sci., C*, **16** (1967) 2981.
17. R. B. Clough and J. A. Simmons, *Acta Metall.*, **22** (1974) 513.
18. J. H. Gittus, *Phil. Mag.*, **21** (1970) 495; **23** (1971) 1281; **24** (1971) 1423.

# A Physically Based Internal Variable Model for Rate Dependent Plasticity

R. D. KRIEG, J. C. SWEARENGEN and W. B. JONES

*Advanced Systems Division, Sandia National Laboratories,  
Albuquerque, New Mexico, USA*

## 1. INTRODUCTION

In 1978 Krieg *et al.* published a 'unified creep-plasticity' model for rate-dependent deformation of metals, incorporating a power-law relationship between inelastic strain rate, applied stress, and instantaneous value of two internal variables.<sup>1</sup> The internal variables were permitted to evolve by a Bailey-Orowan process, including strain hardening and recovery. Hardening was taken to be linear and to increase the internal variables rather than the flow stress directly; recovery was treated as thermal (as opposed to dynamic strain-activated) only, where the kinetics were derived from dislocation mechanics for the process in question. The physical basis was established because (a) the power-law flow rule was taken to be a mathematically convenient approximation to rate-process theory at fixed microstructural state, (b) linear strain hardening in polycrystals is usually viewed as an aggregate manifestation of the linear (stage II) hardening behavior of fcc single crystals oriented initially for single slip and in the absence of dynamic recovery,<sup>2,3</sup> and (c) the recovery kinetics were derived from dislocation models. The value of physical bases follows, of course, from the confidence (indeed the meaning) that is given to extrapolation of the relationship beyond the range of measured data. No theoretical justification was offered for the assumption that descriptions of dislocation processes could be used for continuum descriptions of the deformation of polycrystalline

aggregates. Such justification is being developed, however, in the work of Asaro and Needleman.<sup>4</sup>

In addition to the physical basis claimed, a second supposed virtue of the 'KSR model'<sup>1</sup> was its comparative simplicity. Fewer material parameters were incorporated than in other unified creep-plasticity models in the literature at that time,<sup>5-7</sup> and thus the experimental task was simplified. In support of their approach the present authors have appealed to the principle of diminishing returns, or 'Occam's Razor'.<sup>8,9</sup> In adding ever more parameters to their relationships to capture wider variants of material behavior, modelers may satisfy the materials scientists but increase the burden for the computational and experimental communities.

The KSR model, as presented in 1978, was incomplete because its predictive capabilities were evaluated only for the specialized case of purely kinematic behavior. Furthermore, the model produced a sharp yield behavior, leading to parallelogram shaped hysteresis loops upon cyclic deformation. This problem was also encountered by Miller<sup>5</sup> and could be a result of either underprediction of hardening or overprediction of recovery in the evolutionary functions. We are not aware of evidence that strain hardening (in the absence of any recovery) should be less than linear; therefore, it follows that the squareness is produced by underprediction of the rate of recovery at smaller strains.

The purpose of the present work is to update the original KSR model to overcome the above limitations while retaining its major virtues. In what follows we add isotropic behavior by admitting evolution of the 'drag stress' in the KSR model, and identifying the drag stress with mean free slip distance of dislocations. The kinetics of the evolution are determined directly from microstructural information, namely, transmission electron microscopy measurements of the change in dislocation cell size during plastic deformation. Incorporation of drag-stress evolution may induce rounding of the first quarter cycle of the stress-strain loop, but unless some complex 'un-knitting' function is introduced for unloading behavior, the drag stress saturates and does not provide rounding on subsequent cycles. Therefore, we address the squareness problem pragmatically by modifying the back-stress recovery function, rather than by adding another adjustable parameter.

Improving the goodness-of-fit of any model to the experimental data always presents a dilemma. There are three basic strategies available

to the model developer in this task:

- (i) Add more adjustable parameters to the basic constitutive model.
- (ii) Modify the evolutionary equations which describe the current value of each material parameter of the model.
- (iii) Change the functional form of the constitutive model while leaving the number of adjustable parameters the same.

All of these strategies have been used in model development. The earliest motivating factor in the choice of strategy revolved around the question of whether the resultant equations could be solved reasonably. Of increasing recent interest has been the desire to develop models which have a solid basis in deformation mechanisms. This has become an issue since these models are being applied to the long-time (10 to 1000 years) behavior of structures.<sup>10</sup> This extrapolation many orders of magnitude beyond experimental verification requires a physical basis for the models. These two goals of computational economy and high resolution are in some conflict. The necessity of posing models in differential form, and the need to eliminate strain as a variable from the constitutive equation, has been well established.<sup>9,11</sup> Unfortunately, the simplest and most straightforward expressions for deformation by dislocation motion are very difficult to integrate.<sup>12</sup>

These issues have, to-date, dominated concerns in improving constitutive models. In this work we add a third concern in choosing a strategy for model development. For all models, the final equations are examined to define the specific mechanical tests which must be conducted to determine each of the materials parameters unambiguously. Clearly, these tests should be minimal in number and straightforward in execution. A model which requires too large a number of different tests to characterize a material can only find limited utilization as a design tool. The mechanical tests must also be reasonable to execute and produce data which can be clearly interpreted. At each point in the development of a constitutive model, the requisite mechanical tests for material characterization must be examined.

Each deformation model currently extant has a unique profile of strengths and weaknesses *vis-à-vis* these issues. Certainly modeling of creep and plasticity is inherently strewn with significant challenges. Nevertheless, each model must first be evaluated as to whether or not

it is fatally flawed in any single consideration. Next, each step in model development must be examined using a cost-benefit type of evaluation. Such an approach will be followed in this work.

## 2. THE GENERAL PROBLEM

A rate-dependent plasticity model can be formulated in many ways. Krieg<sup>12</sup> showed in 1977 that the models available at that time could be cast in terms of a 'skeletal model' and general behavior classified as isotropic or kinematic. Various hardening and recovery functions used by different authors were then identified. It is also instructive to look at the general behavior of various models. We consider two very simple cases; the first is a linear kinematic hardening model (using the nomenclature of Krieg<sup>12</sup>), and the second is a non-linear kinematic hardening model.

### 2.1. Linear Model

The simplest kinematic hardening model is a linear one where all the 'functions' are constants. Uniaxial (or scalar) models are used here for clarity. The descriptive equations are

$$\dot{\sigma} = E(\dot{\epsilon} - \dot{\epsilon}_p) \quad (1)$$

$$\dot{\alpha} = A\dot{\epsilon}_p - B\alpha \quad (2)$$

$$\dot{\epsilon}_p = C(\sigma - \alpha) \quad (3)$$

where  $\sigma$  is the external stress,  $\alpha$  is the back stress,  $\dot{\epsilon}$  is the external strain rate,  $\dot{\epsilon}_p$  is the inelastic strain rate,  $E$  is the elastic modulus, and  $A$ ,  $B$ ,  $C$  are material constants.

The plastic strain rate can be eliminated by substituting eqn (3) into eqns (1) and (2) to give

$$\dot{\sigma} = E\dot{\epsilon} - EC(\sigma - \alpha) \quad (4)$$

$$\dot{\alpha} = AC\sigma - (B + AC)\alpha \quad (5)$$

These two first-order simultaneous differential equations can be replaced by a single second-order differential equation by eliminating the back stress. This is accomplished by differentiating eqn (4) and substituting eqn (5) for  $\dot{\alpha}$  and eqn (4) for  $\dot{\sigma}$ . The result is

$$\ddot{\sigma} = E\ddot{\epsilon} - EC\{[E\dot{\epsilon} - EC(\sigma - \alpha)] - [AC\sigma - (B + AC)\alpha]\}$$

Equation (4) is solved for  $\alpha$  and substituted to yield the final equation

$$\ddot{\sigma} + [CE + (B + AC)]\dot{\sigma} + [ECB]\sigma = E\ddot{\epsilon} + [E(B + AC)]\dot{\epsilon} \quad (6)$$

There is a good deal to be learned from this differential equation. First, we note that only directly measurable quantities are used as variables, viz. the stress, the strain, and time derivatives of these quantities. The back stress  $\alpha$  and plastic strain rate may be calculated from the measurable variables but cannot be measured directly and are not present in eqn (6). The second thing we note is that only the *combinations* of constants in the brackets can be determined by observing the behavior of eqn (6). In this case, if the four bracketed quantities are determined, then this information can be used to find  $A$ ,  $B$ ,  $C$ , and  $E$  uniquely. A third observation is that if constants are to be determined from strain controlled tests, i.e. if  $\dot{\epsilon}$  and  $\ddot{\epsilon}$  are specified, then the equation is harmonic in stress. In this case it is an overdamped harmonic equation where the homogeneous solution for stress is the sum of two decaying exponentials in time. On the other hand, for stress controlled tests where the left side of eqn (6) is known, then we are left with a first-order equation in strain rate. The homogeneous solution is a single decaying exponential of strain rate in time. Because of the simple nature of eqn (6), we can devise a set of tests to determine the constants.

The first test would be a creep test. The stress is suddenly raised to  $\sigma_0$  and held fixed. If  $r$  is the strain rate then eqn (6) is written

$$\dot{r} + (B + AC)r = CB\sigma_0 \quad (7)$$

which has the solution

$$r = \left( r_0 - \frac{CB\sigma_0}{B + AC} \right) \exp[-(B + AC)t] + \frac{CB\sigma_0}{B + AC} \quad (8)$$

Primary creep is described by the sum of the terms and steady creep by the second term alone. Note that steady creep can be used to find  $CB(B + AC)^{-1}$ . This quantity can be subtracted from the primary creep and the result plotted on semilog coordinates; the slope would be  $-(B + AC)$ . Note that, for this linear case, testing at various stress levels produces no new information. We have found  $(B + AC)$  and  $BC$  from a single creep test.

The second test would be a stress ramp test where  $\dot{\sigma}$  is held constant starting from  $\sigma = 0$ . This is also a stress controlled test and is described

by eqn (7) where the right side is replaced with  $R[C + (B + AC)E^{-1} + CBt]$  where  $R$  is the stress rate. The strain rate in this case is given by

$$r = X + ECB(B + AC)^{-1}t + (R/E - X)\exp[-(B + AC)t] \quad (9)$$

where  $X = 1 + EAC^2(B + AC)^{-2}$ . The useful information from this test is the initial condition ( $t = 0$ ) where we find  $r_0 = R/E$  or  $\dot{\sigma} = E\dot{\epsilon}_0$  which is commonly used to find the elastic modulus. Note that eqn (9) contains only groups of terms which were already determined in the creep test. Furthermore, other stress-rate controlled tests will produce no new information.

Stress relaxation provides a simple strain controlled test ( $\dot{\epsilon} = \ddot{\epsilon} = 0$ ). The right side of eqn (6) is set to zero for this case, which leaves a homogeneous second-order ordinary differential equation where the solution takes the form

$$\sigma = D_1 \exp(-\beta_1 t) + D_2 \exp(-\beta_2 t)$$

This relation is substituted into the differential equation to find the decay constants. Initial conditions  $\sigma_0$  and  $\dot{\sigma}_0$  are used to find  $D_1$  and  $D_2$ . The result is

$$\sigma = \frac{\dot{\sigma}_0 + (\phi + \psi)\sigma_0}{2\psi} \exp[-(\phi - \psi)t] - \frac{\dot{\sigma}_0 + (\phi - \psi)\sigma_0}{2\psi} \exp[-(\phi + \psi)t] \quad (10)$$

where

$$2\phi = B + C(A + E) \quad (11)$$

$$\psi = (\phi^2 - ECB)^{1/2} \quad (12)$$

From eqns (10)–(12) we note that it is difficult to determine any of the groups of terms. The sum of two decaying exponentials is difficult to separate at early times, but if  $\phi$  and  $\psi$  are comparable in size then one decays more quickly. The first term in eqn (10) has the greatest amplitude and the longest decay so it would dominate at long times. The resulting straight line on semilog coordinates would produce the slope  $-(\phi - \psi)$ . This slope is roughly

$$\phi - \psi \cong ECB/(B + AC + CE) \quad (13)$$

so that a new combination of terms appears. It is likely that the quantities  $A$ ,  $B$ ,  $C$ , and  $E$  could then be found.

An *ad hoc* approximation which is sometimes made<sup>6,11</sup> is that a stress relaxation test is a constant structure test, i.e. during the test  $\alpha$  is constant. This is argued on micromechanical grounds. It is instructive to examine the consequences of this approximation. Equation (6) is then invalid since eqn (2) is assumed to be inactive. Equations (1) and (3) are combined to give a new differential equation for stress relaxation ( $\dot{\epsilon} = 0$ ):

$$\dot{\sigma} + EC\sigma = EC\alpha_0 \quad (14)$$

which has the solution

$$\sigma = \alpha_0 + (\sigma_0 - \alpha_0)\exp(-ECt) \quad (15)$$

This demonstrates a simple decay with a single exponent. The difference between the solutions given by eqns (10) and (15) could be considerable. For early times neither would plot as a straight line on semilog coordinates, but eqn (15) approaches  $\sigma = \alpha_0$  in the limit whereas eqn (10) decays to zero in the limit. More importantly, one component in eqn (10) decays to zero on a much shorter time scale than the other. Equation (13) is the exponent which corresponds to that of eqn (15) since they are equal for  $B \gg C(A + E)$ . Thus eqn (15) must be used with care since it would indicate incorrect results for short times and long times.

At this point we must step back from these results to gain perspective. The first postulate was of a simple linear material [eqns (1), (2), and (3)]. Assuming that all material behavior follows the resulting differential equation, then the mechanical tests must be designed accordingly. Second, the standard test methods were found not to yield the material constants in a simple manner, with the exception of Young's modulus. Specifically, stress controlled tests alone would not be sufficient to define the material constants. Furthermore, *ad hoc* micromechanical assumptions which step around the basic descriptive equations can lead to inconsistencies. In the next section we consider a non-linear model where the fitting process is even more involved and our observations are not as crisp.

## 2.2. Non-Linear Model

A more realistic model can be written

$$\dot{\sigma} = E(\dot{\epsilon} - \dot{\epsilon}_p) \quad (16)$$

$$\dot{\alpha} = A\dot{\epsilon}_p - B\alpha^3 \quad (17)$$

$$\dot{\epsilon}_p = C(\sigma - \alpha)^5 \quad (18)$$

with the symbols as previously defined except that  $A$ ,  $B$ , and  $C$  are new constants. In the same manner as before, a single second-order differential equation can be derived as

$$\ddot{\sigma} = E\ddot{\epsilon} - 5\sqrt[5]{EC}(E\dot{\epsilon} - \dot{\sigma})^{4/5}[-A\dot{\epsilon} + (1 + A/E)\dot{\sigma} + B(\sigma - \sqrt[5]{(1/C)(\dot{\epsilon} - \dot{\sigma}/E)})^3] \quad (19)$$

This equation is obviously non-linear and its closed-form solution is beyond reach. Nevertheless there are some conclusions which may be drawn from eqn (19). The first is that there are more groups of parameters than for the linear case of eqn (6). Determination of each parameter through some combination of tests is almost guaranteed. A second point is that we cannot separate controlled strain and controlled stress tests as clearly. The third very important observation is that steady creep tests are a much richer source of information than in the linear case. The elastic modulus would be found as in the linear case. Steady creep (where  $\ddot{\epsilon} = 0$ ,  $\ddot{\sigma} = 0$ ,  $\dot{\sigma} = 0$ ) is now described by

$$\sigma_{\infty} = \sqrt[3]{A\dot{\epsilon}/B} + \sqrt[5]{\dot{\epsilon}/C} \quad (20)$$

Since strain rate enters with two different powers, the coefficients  $C$  and  $A/B$  can be determined from steady creep tests. (A second incidental observation is that the curve of  $\log \dot{\epsilon}$  vs.  $\log \sigma$  is concave downward; this result is not particularly useful *per se*.)

In this non-linear case, the expressions describing creep and stress relaxation are both very non-linear differential equations, given respectively by the following two expressions:

$$\dot{\epsilon} = 5(C\dot{\epsilon}^4)^{0.2}\{-A\dot{\epsilon} + B[\sigma_0 - (\dot{\epsilon}/C)^{0.2}]^3\} \quad (21)$$

$$\ddot{\sigma} = 5(CE)^{0.2}(-\dot{\sigma})^{0.8}\{(1 + A/E)\dot{\sigma} + B[\sigma - (-\dot{\sigma}/CE)^{0.2}]^3\} \quad (22)$$

Neither of these equations can be solved in closed form; accordingly, in order to determine the parameters one must resort to curve matching. Even this less than precise method is not simple. One must use the quantities  $E$ ,  $C$ , and  $A/B$  as found from the fast load and steady creep tests. Then these are used together with a guess for  $A$  and either eqn (21) or (22) integrated numerically to find  $\dot{\epsilon}(t)$  or  $\sigma(t)$ , respectively. The results are compared with data. This is repeated until the best value of  $A$  is determined.

The foregoing discussion illustrates that inclusion of any non-linear material response greatly complicates the process of determining the material parameters and solving the general equation. The principle

established in the preceding sections is problematic to the materials scientist who would say that deformation is mechanistically non-linear and complex and, thus, constitutive models should be also. The challenge is to embody physical reality in a model but still keep its form simple enough to maintain potential usefulness as an analytical tool for engineering materials.

The unified creep–plasticity model proposed by Krieg *et al.*<sup>1</sup> is a candidate for improvement under these guidelines. In the following sections, we seek to maintain a physical basis to the model while improving its ability to predict material behavior.

### 3. PROPOSED NEW MODEL

#### 3.1. The Kinematic Internal Variable

A ‘back stress’ term was incorporated in the KSR model to permit description of material response to unloading, including the Bauschinger effect.† Possible microstructural bases for the observed responses to unloading and reversed loading included bowing of individual dislocations, bowing of dislocation ‘groups’ such as cell or subgrain walls, or ‘runback’ of dislocation pileups.<sup>9</sup> The time dependent or rate dependent nature of the response was incorporated with the flow law and the evolutionary function for the back stress. In this approach, the dislocations are assumed to move in a viscous medium; back stress increases linearly with plastic strain and decreases due to thermal recovery. The original evolutionary form is retained as a classical Bailey–Orowan form where  $\alpha$  increases linearly with plastic strain and decreases due to ‘leakage’, i.e. relaxation of stresses due to escape of dislocations from tangles or piled up groups of dislocations. Linear hardening of the internal variable is in accord with observations of behavior in stage II of single crystals and larger-grained polycrystals.<sup>2,3</sup>

It seems likely that dynamic (strain dependent) recovery will have to

† Kwai-Chan *et al.*<sup>13</sup> have pointed out that Bauschinger-like behavior can be produced by incorporating appropriate evolutionary behavior into the drag stress variable, so that a back stress is not required. We believe that the heterogeneous microstructure associated with the drag stress is too stable to recover, upon unloading, with the kinetics required for the observed response to (for example) stress drop tests.<sup>14</sup> Therefore, even though the mathematics may be made to produce unloading effects without back stress, physical reality requires incorporating back stress in the model.

be added to the evolution of  $\alpha$  before the model will be fully capable of describing the rounded yield behavior. Our definition of dynamic recovery, in this regard, is any strain-activated process which causes the hardening of the internal variable to be less than linear. The functional form for the evolution of  $\alpha$  is the same as established for the KSR model<sup>1</sup> and is based on a recovery process dominated by dislocation climb (rather than cross slip). The back stress is assumed to be independent of the isotropic internal variable, consistent with the idea that back stress should depend upon strain and barrier strength rather than the distance separating the barriers.

### 3.2. The Isotropic Internal Variable

Isotropic hardening is assumed to derive from strain-induced reductions in mean free slip distance. The slip distance is the diameter to which a dislocation loop expands before being stopped. This concept is embodied in the literature of work hardening of fcc and bcc single crystals and polycrystals wherein the flow stress is determined by grain size or subgrain size.<sup>2,3</sup>

A phenomenological relationship of widespread acceptance in this regard is the Hall–Petch equation. There is ample evidence for a  $-1/2$  exponent in the yield stress versus grain size relationship, but the exponent changes as the grain size becomes large and the slip length becomes limited by dislocation cells or subgrains rather than grain boundaries. A further problem for us is that the Hall–Petch relationship does not include strain or strain rate as variables, i.e. it predicts the flow stress for a given microstructural state.

Thompson<sup>2</sup> addressed the problem of grain-size dependent hardening by admitting the heterogeneity of plastic deformation associated with grain boundaries. He pointed out that the Taylor work hardening theory assumes infinite grain size (i.e. uniform slip throughout the grains, on five independent slip systems), and thus cannot explain grain size dependence of strength. Thompson introduced Ashby's analysis of plastically non-homogeneous deformation and developed the relationship

$$\sigma = \sigma_0 + (1 - \lambda/d)(K_1/\lambda) + (\lambda/d)(K_2/\sqrt{d}) \quad (23)$$

where the mean free slip length  $\lambda$  is regarded as a function of both strain and grain size,  $K_2$  is the Hall–Petch slope for yielding, and  $K_1$  is a constant proportional to the saturation flow stress at large strain.

Equation (23) reduces to the Hall–Petch equation at small strain and to  $1/\lambda$  at large strain, in accord with observations incorporating dislocation cell structures.

The ‘operational’ problem with equation (23) is that  $\lambda$  is a function, so that a major aspect of the behavior is left unquantified; but the function does correspond to an experimentally measurable quantity, the slip length. Plots of  $\lambda$  versus  $\varepsilon$  are available in the literature for several metals and alloys; the example of pure aluminum from the work of Swann<sup>15</sup> and Kelly<sup>16</sup> is given in Fig. 1. There are three obstacles, however, to direct use of eqn (23) as an isotropic evolutionary function. First, it is a rate independent function, applicable for an instantaneous value of grain size  $d$  and at the strain rate and temperature of the test. Second, because no back stress is included, it is only applicable under conditions of forward loading. Third, it includes the effects of simultaneous work hardening and recovery without separately considering those processes. It is known, for example, that the mechanism of recovery changes from cross slip to climb as temperature approaches  $T_m/2$ .

Svensson<sup>17</sup> sought to generalize the approach of Thompson<sup>2</sup> by including hardening and recovery processes in cell-forming metals. He combined the general dislocation hardening relationship

$$\sigma = \sigma_0 + \alpha\mu b\sqrt{\rho} \quad (24)$$

(where  $\sigma_0$  is the friction stress,  $\mu$  is the shear modulus,  $b$  is the Burgers vector,  $\rho$  is the dislocation density, and  $\alpha$  is a constant) with an evolutionary function for dislocation density of the form

$$d\rho/d\varepsilon = U - \Omega\rho \quad (25)$$

where  $U = m/b\lambda$  is the hardening factor,  $m$  is the Taylor orientation factor, and  $\Omega(\dot{\varepsilon}, T)$  is the dynamic recovery rate factor. Both  $\Omega$  and  $\lambda$  are experimentally derived quantities.

Svensson also addressed the problem of strength directionality at larger strains due to development of non-equiaxed dislocation cell shape. He showed that the appropriate  $\lambda$  is measured on the intersecting plane which yields the smallest value for  $\lambda$ . Of course, this procedure would apply to any subsequent change in the direction of applied stress with respect to the first loading, but it would not work for stress reversals, in that it would not produce a Bauschinger effect. In the isotropic model, enhanced flow upon stress reversal could only be produced by some instability of the subgrain structure, e.g.

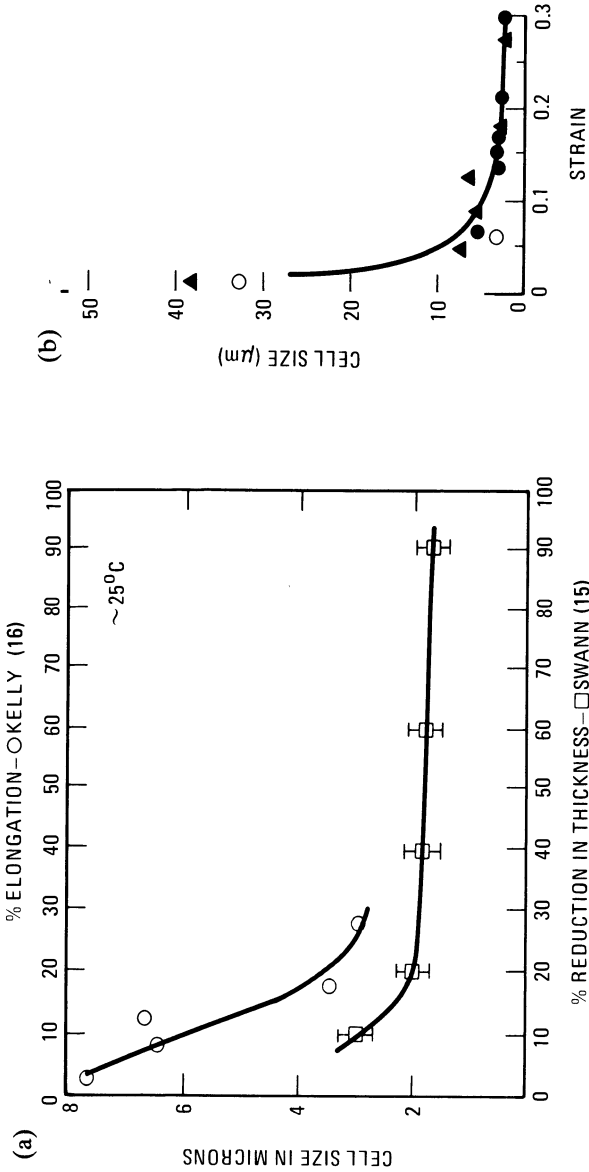


**Fig. 1.** (a) The dislocation cell size in aluminum as a function of deformation at room temperature (after Swann<sup>14</sup> and Kelly<sup>15</sup>). (b) The variation of cell size with plastic strain for three specimens of aluminum at room temperature; the curve represents Kelly's relation  $t = a/\epsilon_p + c$ .

'un-knitting'. In our model, therefore, Bauschinger effect behavior is determined entirely from the kinematic variable. For this work we choose to sidestep most of the 'operational' difficulties associated with eqns (23) and (24) by incorporating  $\lambda$  directly into the kinematic function, rather than indirectly through the drag stress. This is an entirely pragmatic choice that substitutes a physically observable variable for a mechanical one.

Several functional forms have been proposed relating the scalar  $\lambda$  to a scalar measure of the plastic strain.<sup>2,15,16</sup> For high purity aluminum, Kelly<sup>16</sup> recommends the functional form  $\lambda = A + B/\varepsilon_p$ . From our perspective this is not desirable because  $\lambda(\varepsilon_p = 0)$  cannot be evaluated and in fact does not fit his data well. We pose instead the alternative function (where  $\varepsilon_p$  is effective plastic strain)

$$\lambda = A_0 + B \exp(-\beta\varepsilon_p) \quad (26)$$

with  $A_0 = 2.4$ ,  $B = 21.1$ , and  $\beta = 18.7$  as a best fit to the data of Fig. 1(b). Consistent with the foregoing assumption, the data of Fig. 1 include both hardening and dynamic recovery effects, so that the evolution rate of  $\lambda$  must be

$$\dot{\lambda} = -\beta(\lambda - A_0)\dot{\varepsilon}_p \quad (27)$$

or

$$\dot{\lambda} = -\beta\dot{\varepsilon}_p\lambda + (\beta A_0)\dot{\varepsilon}_p \quad (28)$$

i.e. evolution of  $\lambda$  is the result of competition between strain hardening and dynamic recovery. Strictly speaking, of course, eqns (26)–(28) hold only for the plastic strain rate used in the test, and the strain rate in Kelly's work<sup>16</sup> was not treated as a variable (or reported). The authors are not aware of any systematic study on the evolution of cell size as a function of strain rate. It is known that  $\lambda$  is a strong function of temperature but a rather weak function of stress (or plastic strain).<sup>18–21</sup> Under steady conditions  $\dot{\lambda} = 0$  in eqn (27), which can be satisfied only for  $\lambda_{ss} = A_0$ . In accord with experimental observations we let

$$A_0 \propto (G/\sigma)\exp(-Q/kT)$$

Dynamic recovery is absent only when test temperature is very low ( $T/T_m < 0.3$ ). In fact, grouping of dislocations into cells or subgrains is a manifestation of dynamic recovery.<sup>18</sup> Once formed, however, cells and subgrains are stable and resistant to thermal recovery. The work

of Beck *et al.*,<sup>22</sup> as reviewed by McQueen,<sup>18</sup> shows that subgrains in pure aluminum deformed at room temperature do not increase in size for annealing times as long as  $10^4$  s at temperatures below about 200°C. Hence, for the model in its present state of development, applied only to description of the ambient-temperature response of pure aluminum,  $\lambda$  can be taken as independent of annealing time. In other words, no thermal recovery term is incorporated into the  $\lambda$  evolution function.

### 3.3. Final Equations for the Model

Evolutionary equations for the back stress and the mean free slip length have been presented in the previous two sections as eqns (17) and (27). In this section we present the form of the plastic strain rate and assemble the equations into a mathematically complete description. The stress and strain can be decomposed into bulk and deviatoric components:

$$\sigma_{ij} = S_{ij} + \sigma_m \delta_{ij} \quad (29)$$

where  $S_{ij}$  are the tensor components of the deviatoric stress (positive in tension),  $\sigma_m$  is the mean stress  $= (1/3)(\sigma_{11} + \sigma_{22} + \sigma_{33})$ ,

$$\delta_{ij} = \begin{cases} 1, & i = j \\ 0, & i \neq j \end{cases}$$

A similar decomposition of the strain rate is made:

$$\dot{\epsilon}_{ij} = \dot{\epsilon}_{ij} + (1/3)\delta_{ij}\dot{\epsilon}_v \quad (30)$$

There is some concern in the applied mechanics community regarding the proper formulation of large strain plasticity theories. We follow the approach of Dienes<sup>23</sup> who shows that  $\sigma_{ij}$  and  $\dot{\epsilon}_{ij}$  should be defined as the Cauchy stress and the stretching or rate of deformation tensors, respectively. The Green–McInnis stress flux  $\overset{\nabla}{\sigma}$  is defined as

$$\overset{\nabla}{\sigma}_{ij} = \dot{\sigma}_{ij} - \omega_{ik}\sigma_{kj} - \sigma_{ik}\omega_{kj} \quad (31)$$

where

$$\omega_{ij} = \dot{R}_{ik}R_{jk}$$

and the rotation  $R_{ij}$  comes from the polar decomposition of the deformation gradient,  $F_{ij} = R_{ij}V_{jk}$  and  $V_{jk}$  is symmetric. For most tests (torsion is a notable exception) in the laboratory, rotations are zero so that the stress flux is the stress rate. Although  $\dot{\epsilon}_{ij}$  is the stretching

tensor we will refer to it as the 'strain rate' to aid our intuition and interpretation.

We restrict our formulation to disallow microcrack or microvoid nucleation and growth and radiation damage. We further restrict our attention to elastic bulk behavior, which is generally true for metals. The bulk behavior is then

$$\sigma_m = K \varepsilon_v \quad (32)$$

where  $K$  is the elastic bulk modulus, and  $\varepsilon_v$  is the volumetric strain =  $\varepsilon_{11} + \varepsilon_{22} + \varepsilon_{33}$ .

The relation between deviatoric stress and deviatoric strain is of course the topic of this paper. The effect of mean stress on the deviatoric behavior is being ignored. Spitzig and Richmond<sup>24</sup> have shown that the yield stress does indeed increase with increasing compression (increasing  $|\sigma_m|$ ) for several metals. They have further speculated that this is true of metals in general and that, to a first approximation, the yield stress varies linearly with mean stress and decreases to zero at a mean stress of roughly  $E/10$  where  $E$  is Young's modulus. Because time dependent behavior would probably also be affected to second order by mean stress, it is ignored here.

The deviatoric strain rate is decomposed into elastic and inelastic parts:

$$\dot{\varepsilon}_{ij} = (\dot{\varepsilon}_e)_{ij} + (\dot{\varepsilon}_p)_{ij} \quad (33)$$

and the elastic part stated in terms of the stress flux. The rearranged result is

$$\dot{S}_{ij} = 2G(\dot{\varepsilon}_{ij} - (\dot{\varepsilon}_p)_{ij}) \quad (34)$$

where  $G$  is the elastic shear modulus.

The kinetic relationship for inelastic strain rate is assumed to be of the form

$$(\dot{\varepsilon}_p)_{ij} = A_2 \lambda^m \exp(-Q/RT) [\sinh(A_1 \xi)]^p (\xi_{ij}/\xi) \quad (35)$$

where  $A_1$ ,  $A_2$ ,  $m$ ,  $Q$ ,  $p$  are material constants,  $\xi = |\xi_{ij}| = \sqrt{\xi_{ij} \xi_{ij}}$ ,  $\xi_{ij}$  is the effective stress =  $S_{ij} - \alpha_{ij}$ ,  $T$  is the absolute temperature,  $R$  is the gas constant. In this expression it appears that we have implied that the yield/creep surface is a von Mises surface. Since a unified creep-plasticity model has no explicit yield surface, this is not a particularly useful observation.

The sinh function in eqn (35) is capable of describing kinetic data over a wider range of stress and temperature than the original power-law formulation;<sup>1</sup> its use has been argued by Miller.<sup>5</sup> Incorporation of  $\lambda$  directly instead of by a drag stress as in KSR has the distinct advantage of using a potentially measurable quantity as the isotropic variable, as discussed earlier. As inelastic strain is accumulated,  $\lambda$  decreases, hardening the material, and decreasing  $\dot{\epsilon}_p$ . This implies a positive value for  $m$ .

The complete constitutive formulation can now be stated as

$$\dot{\Sigma}_{ij} = 2G(\dot{\epsilon}_{ij} - (\dot{\epsilon}_p)_{ij}) \quad (36)$$

$$(\dot{\epsilon}_p)_{ij} = A_2 \lambda^m \exp(-Q/RT) [\sinh(A_1 \xi)]^p (\xi_{ij}/\xi) \quad (37)$$

$$\dot{\alpha}_{ij} = A_5 (\dot{\epsilon}_p)_{ij} - A_4 [\exp(A_3 \alpha^2/RT) - 1] \alpha \alpha_{ij} \quad (38)$$

$$\dot{\lambda} = -\beta(\lambda - A_0) \dot{\epsilon}_p \quad (39)$$

where

$$\dot{\epsilon}_p = \sqrt{(2/3)(\dot{\epsilon}_p)_{ij}(\dot{\epsilon}_p)_{ij}} \quad (40)$$

### 3.4. Determination of Constants

In a preceding section we discussed the general behaviors of a linear and a non-linear model. We noted that internal variables cannot be observed directly and hence are of no value in determination of material constants. The external observables are the only parameters which can be of aid. For the two models presented the external observables were stress and strain with time as the dependent variable. All sorts of tests can be devised for those models but they will always fall into two general categories: controlled strain tests and controlled stress tests. For the linear case we found the controlled stress tests resulted in a strain rate which was a simple exponential in time plus a particular solution depending upon the stress history. For a strain controlled test the stress was always the sum of two exponentials, plus a particular solution specified by the strain history imposed.

For the model specified in eqns (36)–(40) we have a somewhat different situation. Now there are three external observables: stress, strain and mean free slip length (assuming that  $\lambda$  can be observed optically or perhaps by X-rays). There is a possibility here of controlling two of the three observables in order to simplify data reduction. In particular, we see that eqn (39) can be integrated directly

to give the result

$$\lambda = A_0 + (\lambda_0 - A_0)\exp(-\beta\varepsilon_p) \quad (41)$$

Operationally, a tensile test is interrupted periodically and  $\lambda$  is measured to yield the constants  $A_0$  and  $\beta$  where  $\lambda_0$  is the initial value. Thus it is no more difficult to devise material tests for the combined isotropic-kinematic model than if the isotropic hardening were not present.

Consider a test procedure for finding the remaining constants in the equation set (36)–(38). The elastic shear modulus  $G$  could be determined with rapid unloading tests and also checked with ultrasonic shear wave velocity tests. Since  $A_0$ ,  $\beta$ , and  $\lambda_0$  were determined independently above, only the six constants  $A_1, A_2, \dots, A_5$ , and  $m$  remain to be determined. We choose a fixed temperature and rewrite the equations in terms of uniaxial stress variables as

$$\dot{\sigma} = E(\dot{\varepsilon} - \dot{\varepsilon}_p) \quad (42)$$

$$\dot{\varepsilon}_p = C_2\lambda^m[\sinh(C_1\xi)]^p \operatorname{sgn} \xi \quad (43)$$

$$\dot{\alpha} = C_5\dot{\varepsilon}_p - C_4[\exp(C_3\alpha^2) - 1]|\alpha| \alpha \quad (44)$$

Equation (41) for  $\lambda$  would also be part of the set. The  $C_i$  values in eqns (36)–(40) are related to the  $A_i$  values in eqns (42)–(44) in a simple manner.

The first test would be a stress dip–stress rise sequence to find  $C_1$ . The hyperbolic sine function in eqn (43) was chosen because it has the desired exponential behavior for large values of the argument but becomes nearly linear for  $\xi$  near zero. The experiment is conducted such that  $\xi$  is large, so that

$$\begin{aligned} [\sinh C_1\xi]^p &= \frac{1}{2}p[\exp(C_1\xi) - \exp(-C_1\xi)]^p \\ &\cong \frac{1}{2}p \exp(C_1p\xi) \end{aligned} \quad (45)$$

The stress dip test is performed (Fig. 2) as a creep test at  $\sigma_T$  (and  $\alpha_T$  and  $\lambda_T$ ) which is suddenly changed to another stress  $\sigma_B$  (and  $\alpha_B$  and  $\lambda_B$ ) and the plastic strain rates  $\dot{\varepsilon}_{pT}$  and  $\dot{\varepsilon}_{pB}$  are measured. Equation (43) is applied for the two conditions and ratioed.

If the stress change is made very quickly then  $\alpha_B = \alpha_T$  from eqn (44) since little time passed (this approximation can be verified after the constants  $C_3, C_4, C_5$  are determined). We also have  $\lambda_B = \lambda_T$  from eqn (41) since no plastic strain accumulated during the stress change.

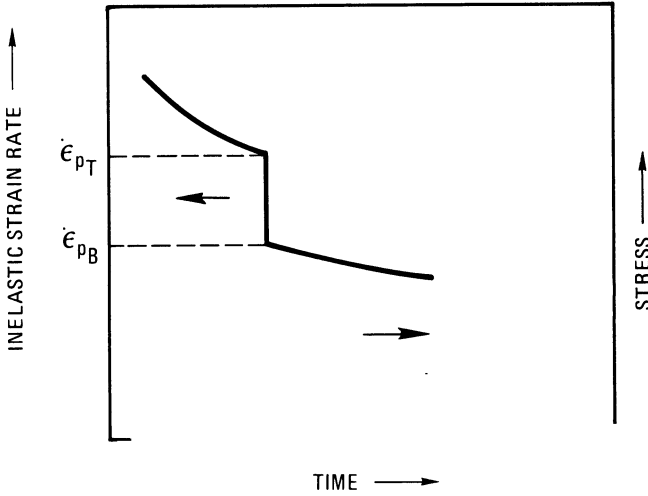


Fig. 2. The stress dip test; stress controlled experiment for  $C_1$ .

These observations are used to give the ratio

$$\frac{\dot{\epsilon}_{pT}}{\dot{\epsilon}_{pB}} = \left[ \frac{\sinh C_1(\sigma_T - \alpha)}{\sinh C_1(\sigma_B - \alpha)} \right]^p$$

Equation (45) can be applied if  $\xi_T$  and  $\xi_B$  are large. The result is simply

$$\dot{\epsilon}_{pT}/\dot{\epsilon}_{pB} = \exp C_1 p(\sigma_T - \sigma_B)$$

or

$$C_1 p = \frac{\ln(\dot{\epsilon}_{pT}/\dot{\epsilon}_{pB})}{\sigma_T - \sigma_B} \tag{46}$$

This same equation could be applied for either a stress dip or a stress rise; both might be done and the average  $C_1 p$  found. Note in particular that the value of the back stress was not required.

The test is then repeated for a low stress level where power law creep takes place. In that case the hyperbolic sine function is approximately

$$[\sinh C_1 \xi]^p \cong (C_1 \xi)^p$$

A stress dip test is again performed, now at a lower stress level than before, but similar conditions of  $\alpha_B = \alpha_T$  and  $\lambda_B = \lambda_T$  again hold at the

top and bottom of the dip. The ratio of strain rates is

$$\frac{\dot{\epsilon}_{pT}}{\dot{\epsilon}_{pB}} = \frac{(C_1 \xi_T)^p \operatorname{sgn} \xi_T}{(C_1 \xi_B)^p \operatorname{sgn} \xi_B} = \frac{\operatorname{sgn} \xi_T}{\operatorname{sgn} \xi_B} \left( \frac{\xi_T}{\xi_B} \right)^p$$

This is solved for the exponent as

$$p = \frac{\ln|\dot{\epsilon}_{pT}/\dot{\epsilon}_{pB}|}{\ln|(\sigma_T - \alpha_T)/(\sigma_B - \alpha_B)|} \quad (47)$$

The values of strain rate and stress are easily measured quantities but the back stress is more difficult to determine accurately. The conventional approach is to achieve steady state creep at  $\dot{\epsilon}_{pT}$  and drop the stress by various amounts until  $\dot{\epsilon}_{pB}$  is zero. The externally applied stress should be the back stress both before and immediately after the stress dip. All quantities on the right side of eqn (47) are known so that  $p$  can be determined.

An alternative method of determining the back stress is to perform at least two dip tests where the lower stress values are above  $\alpha$ . The strain rates after the dip are still positive and easily measured. Then the conditions before and immediately after the dips are plotted on log strain rate versus log effective stress where a value of the back stress is simply guessed. This is shown in Fig. 3 for three guessed values of  $\alpha$ . If eqn (37) is to hold in the power-law region, the data should plot as a straight line when the correct value of  $\alpha$  is used (pictured as  $\alpha_2$  in Fig. 3). A low value of  $\alpha$  (pictured as  $\alpha_1$ ) would produce a concave downward curve and a high value would produce a concave upward curve. The slope of the line produced with the correct  $\alpha$  would be  $p$  as given in eqn (47).

The third test requires that the back stress be determined, as shown in Fig. 4. The condition  $\dot{\epsilon}_p = 0$  is imposed by controlling either  $\dot{\sigma}$  or  $\dot{\epsilon}$  such that  $\dot{\sigma} = E\dot{\epsilon}$ . From eqn (43) we note that  $\dot{\epsilon}_p = 0$  if and only if  $\xi = 0$  or  $\alpha_1 = \sigma_1$ . The cell size  $\lambda_1$  is also determined or evaluated from eqn (41) at that time. Now the stress magnitude is suddenly raised to  $\sigma_2$ ,  $\dot{\epsilon}_{p2}$  observed, and as in the stress dip test we note that  $\alpha_2 = \alpha_1 = \sigma_1$  and  $\lambda_2 = \lambda_1$ . Equation (43) can be written as

$$\dot{\epsilon}_{p2} = C_2 \lambda_2^m [\sinh C_1 (\sigma_2 - \sigma_1)]^p \quad (48)$$

where all the entries are known except  $C_2$  and  $m$ . At point 3 in Fig. 4 we again choose  $\dot{\epsilon}_1$  or  $\dot{\sigma}$  such that  $\dot{\epsilon}_p = 0$  and this condition is maintained to allow  $\alpha$  to drop somewhat. Again during this time  $\xi = 0$

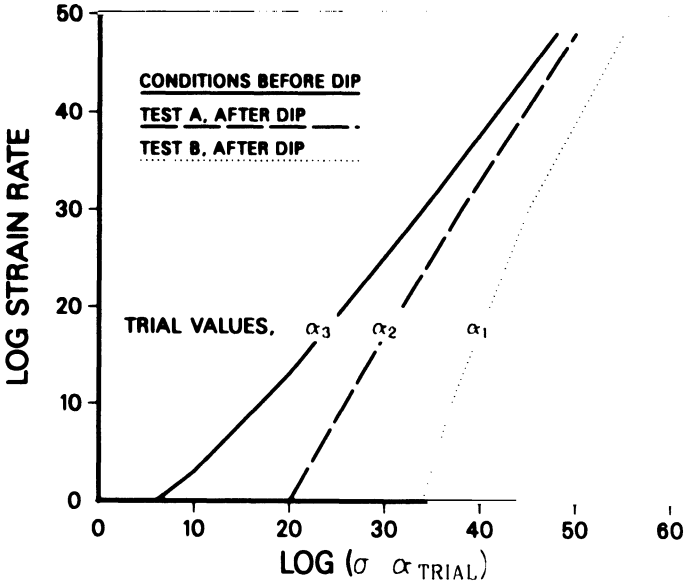


**Fig. 3.** Data for two or more dip tests at low stress levels where power-law creep takes place, plotted using assumed values of  $\alpha$ ; the data plot as a straight line with the correct  $\alpha$ ; the sought stress power is the slope of that line.

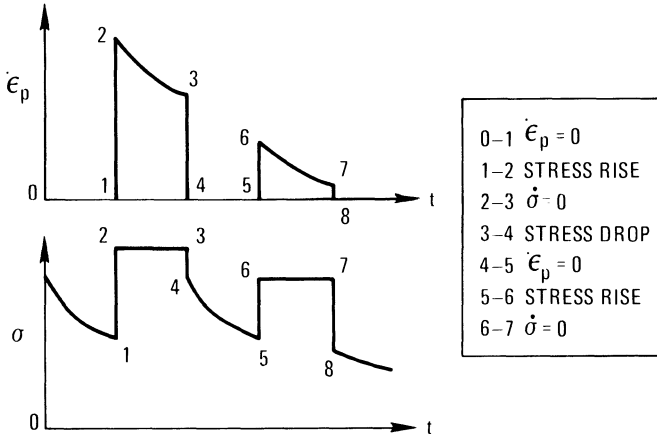


**Fig. 4.** Sequence of controlled events leading to determination of back stress and the constants  $C_2$  to  $C_5$ , and  $m$ .

from eqn (43) so that the external stress is the back stress and in particular  $\alpha_5 = \sigma_5$ . The cell size is measured at state 5 or determined from eqn (41). Now the stress is suddenly raised to  $\sigma_6$  and fixed, and the plastic strain rate  $\dot{\epsilon}_{p6}$  measured. As before, we note that  $\alpha_6 = \alpha_5 = \sigma_5$  and  $\lambda_6 = \lambda_5$ . Equation (43) is written for state 6 as

$$\dot{\epsilon}_{p6} = C_2 \lambda_5^m [\sinh C_1(\sigma_6 - \sigma_5)]^p \tag{49}$$

the ratio  $\dot{\epsilon}_{p2}/\dot{\epsilon}_{p6}$  is found from eqns (48) and (49) to give

$$\frac{\dot{\epsilon}_{p2}}{\dot{\epsilon}_{p6}} = \left(\frac{\lambda_2}{\lambda_5}\right)^m \left[\frac{\sinh C_1(\sigma_2 - \sigma_1)}{\sinh C_1(\sigma_6 - \sigma_5)}\right]^p$$

This is solved for  $m$  to give

$$m = \frac{\ln(\dot{\epsilon}_{p2}/\dot{\epsilon}_{p6}) - \ln\left[\frac{\sinh C_1(\sigma_2 - \sigma_1)}{\sinh C_1(\sigma_6 - \sigma_5)}\right]^p}{\ln(\lambda_2/\lambda_5)} \tag{50}$$

This value for  $m$  can now be used in eqn (48) or (49) to give

$$C_2 = \frac{\dot{\epsilon}_{p6}}{\lambda_5^m [\sinh C_1(\sigma_6 - \sigma_5)]^p} \tag{51}$$

The third test involves steady creep. From experimental observation, an empirical expression can be written for the steady creep strain rate as a function of the externally applied stress. This relation can

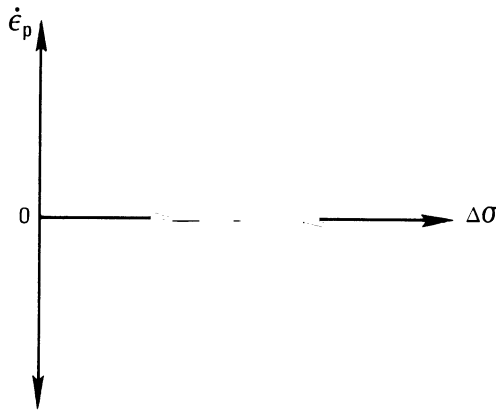


**Fig. 5.** General trend of inelastic strain response vs. stress drops of various magnitudes from steady creep.

then be used to find the steady creep back stress. Equation (43) is solved for the steady back stress as

$$\alpha_{ss} = \sigma - \frac{1}{C_1} \operatorname{arc} \sinh \left( \frac{\dot{\epsilon}_{ss}}{C_2 \lambda^m} \right)^{1/p} \quad (52)$$

where cell size  $\lambda$  must also be measured for steady creep at the various stress levels to be used here. The steady condition  $\dot{\alpha} = 0$  is applied to eqn (44) to give

$$0 = \dot{\epsilon}_{ss} - (C_4/C_5) \alpha_{ss}^2 [\exp C_3 \alpha_{ss}^2 - 1] \quad (53)$$

Thus, at a given  $\sigma$  we can find  $\dot{\epsilon}_{ss}$  and  $\alpha_{ss}$ . The two constants  $C_4/C_5$  and  $C_3$  are then found by fitting  $\dot{\epsilon}_{ss}$  versus  $\alpha_{ss}^2$  in a 'best' manner using eqn (53).

The last test actually involves no new experiment but simply takes advantage of data from the creep hold phase 2-3 of the second step depicted in Fig. 4. The values of the back stress are known at points 2 and 3 to be  $\alpha_2 = \alpha_1 = \sigma_1$  and  $\alpha_3 = \alpha_4 = \sigma_4$  and  $\dot{\epsilon}_p$  is measured throughout the step 2-3 so that we can write eqn (44) as

$$C_5^{-1} \dot{\alpha} = \dot{\epsilon}_p - (C_4/C_5) \alpha^2 [\exp C_3 \alpha^2 - 1] \quad (54)$$

where we have taken advantage of knowing that  $\alpha_3 > \alpha_2$ .

The constants  $C_3$  and  $C_4/C_5$  in eqn (54) are known from the third step, the function  $\dot{\epsilon}_p(t)$  has been measured over the time  $t_2$  to  $t_3$ , and the initial value  $\alpha_2$  is known. A value of  $C_5$  is assumed and eqn (54) numerically integrated from  $t_2$  to  $t_3$  to find the end state  $\alpha_3^*$ . This is compared with the known  $\alpha_3$ . If  $\alpha_3 \neq \alpha_3^*$  then  $C_5$  is changed and the process repeated. The value of  $C_5$  which satisfies  $\alpha_3 = \alpha_3^*$  is the solution to eqn (54).

### 3.5. Problems with Parameter Determination

This test series could, in principle, be used to determine all of the necessary constants. The only assumption made was that a steady state creep state existed in the material. Unexamined to this point in the discussion has been the conduct of the mechanical tests, i.e. can the tests actually be carried out in the laboratory?

Mechanical tests conducted in the laboratory generally fall into two categories: tests to determine properties and tests to compare with model predictions. The requirements for accuracy and precision are

much less demanding for the latter than for the former. The material parameters used in this or any model must be precisely and unambiguously determined. Experiments which are difficult to perform and results which are difficult to analyse unambiguously will not produce satisfactory material parameters. Both the stress dip/rise test and the constant plastic strain rate test fall into this category.

The stress dip/rise test has been used for a number of years as a probe of microstructural state, particularly as a proposed measure of back stress.<sup>25</sup> The difficulties in conducting the test and interpreting the data have been discussed in earlier papers.<sup>14,26</sup> A critical point in conducting stress dip tests is the resolution of  $\dot{\epsilon} = 0$ . In fact, a zero strain rate is defined as a rate lower than a discernible change in the strain signal. This is a function of the noise level on the strain signal, the precision of temperature control, and the duration of the observation. Since the stress dip test is intended to be a constant internal structure test, the duration of observation must be short. All of these contribute to a band of strain rate between about  $\pm 10^{-5} \text{ s}^{-1}$  which is operationally a 'zero strain rate' band. The data collected from these tests generally have the form shown in Fig. 5. The very shallow cross-over near zero strain rate cannot be unambiguously interpolated to estimate the  $\Delta\sigma$  value at which  $\dot{\epsilon} = 0$ . This is discussed in more detail elsewhere.<sup>26</sup>

The proposed test at a constant plastic strain (the 0–1 and 4–5 segments of Fig. 4) has not been examined previously. The first difficulty arises from the fact that the direct measurements available in servo-controlled testing are load and total elongation; all other quantities must be derived. The plastic strain must be calculated and up-dated at high frequency during the test and the total strain adjusted to maintain constant plastic strain. The value of plastic strain depends on the cross-sectional area and the value chosen for Young's modulus. For any unloading, these values very strongly affect the calculated plastic strain. Especially problematic is the difficulty in maintaining test machine control during elastic unloading under these conditions. At all points in the unloading, the plastic strain is constant and the control algorithms have difficulty knowing whether to unload or to reload, and at what rate to do either. Machine control software has been developed to mitigate these difficulties to some extent, but the test cannot be cleanly controlled in a manner that closely follows the concept as shown in Fig. 4. Metals with higher flow stresses are more amenable to the conduct of this test than very soft metals, i.e. 1100

aluminum can be reasonably tested while annealed pure aluminum cannot.

Continued refinement in test technique and data analysis for both tests will allow some increased confidence; however, it should be emphasized that the inherent difficulties in these approaches make them poor tests for establishing material parameters. In spite of a reasonably clean mathematical description of a test series for determination of constants, the practical aspects of the material behavior are not conducive to conducting clean experiments.

#### 4. BEHAVIOR OF THE MODEL

There are some basic properties of the new model which can be illustrated by reference to eqns (41)–(44). The first observation is that mean free slip length  $\lambda$  is not determined from force or stress measurements, so that it is only an indirect indication of isotropic hardening. We feel that this weak point in the choice of a state variable is overshadowed by the advantage that it can be directly and independently observed and because it is closely related to isotropic hardening. It allows more freedom in the difficult task of designing a test series for determination of constants. The actual choice of the form of eqn (39) is not completely satisfactory at this point since it includes no thermal recovery term. The equation would mathematically admit secondary creep only if  $\lambda = A_0$ . More data are needed to resolve this issue.

The behavior during secondary creep is illustrated by evaluating the model under conditions of  $\ddot{\alpha} = 0$ ,  $\dot{\sigma} = 0$ , and  $\dot{\lambda} = 0$ . Equations (36)–(39) can be particularized to these steady state conditions at a fixed temperature and the strain rate eliminated to give a non-dimensional equation of the form

$$y(e^y - 1) = C(\sinh A_1 \xi)^p$$

where  $y$  is proportional to the square of the back stress. The case where  $p = 3$  and  $C = 1$  has been evaluated in order to illustrate the basic behavior of the model. The stress is related to  $\xi$  and  $y$  as

$$A_1 \sigma = A_1 \xi + \sqrt{C_2 y}$$

and the ratio of the back stress to the external stress is

$$\alpha/\sigma = (1 + \sqrt{C_2 y})^{-1}$$

The back stress ratio is plotted against the external stress in Fig. 6 for several values of  $C_2$ . This figure shows that our model predicts that the ratio  $\alpha/\sigma$  decreases with increasing external stress. This behavior is in qualitative agreement with early measurements using the strain-transient dip test on polycrystalline aluminum<sup>25</sup> and Al-Zn<sup>27</sup> which seemed to indicate a value for this ratio of 0.8 at low stress and 0.5 at higher stresses. These data for Al-Zn have been re-examined by Blum and Finkel,<sup>28</sup> who have shown that this ratio may more correctly be approximately constant at 0.5 over the experimental stress range from 20 to 70 MPa. As shown in Fig. 6, our model predicts a monotonic decreasing back stress ratio which is roughly constant over the practical experimental range of external stress. It should also be noted that more careful experimental measurement and interpretation are needed to establish the back stress behavior more exactly.

The new model has both isotropic and kinematic terms and has the usual attributes of such a model. A Bauschinger effect is inherent and, depending upon the cycle limits, cyclic straining will produce stress loops which grow in size. The growth will slow as predicted by eqn

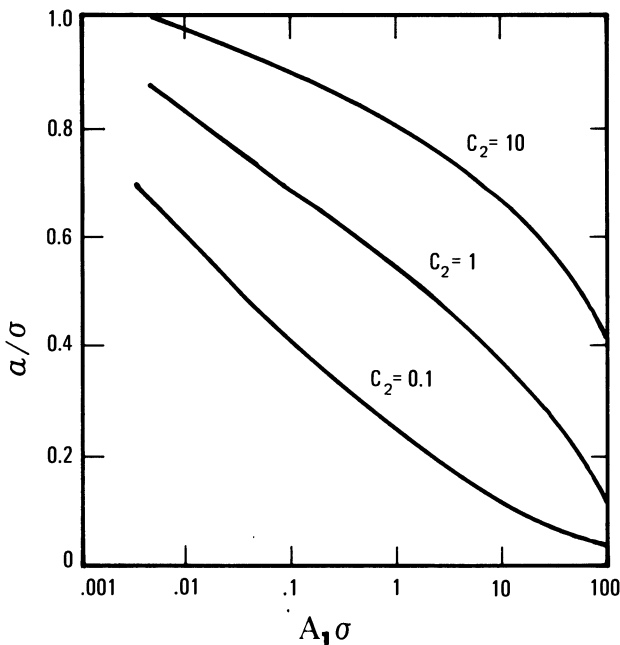


**Fig. 6.** Model predictions for back stress ratio *vs.* dimensionless external stress under isothermal conditions.

(41) and will appear to saturate when

$$A_0 \gg (\lambda - A_0) \exp(-\beta \epsilon_p)$$

Further ramifications of the assumptions made in the model and its predictions are relegated to a subsequent report.

### ACKNOWLEDGMENT

This work was sponsored by the US Department of Energy under contract DE-AC04-DP00789. Sandia National Laboratories is a US Department of Energy facility.

### REFERENCES

1. R. D. Krieg, J. C. Swearngen and R. W. Rohde, in *Inelastic Behavior of Pressure Vessel and Piping Components*, ed. T. Y. Chang and E. Krempl, ASME, New York, 1978, p. 15.
2. A. W. Thompson, in *Work Hardening in Tension and Fatigue*, ed. A. W. Thompson, AIME, New York, 1977, p. 89.
3. J. C. Swearngen, T. C. Lowe and J. Lipkin, in *Annual Reviews of Materials Science*, ed. R. A. Huggins, Annual Reviews, Inc., Palo Alto, California, p. 249.
4. R. J. Asaro and A. Needleman, Brown University Research Report, May 1984.
5. A. K. Miller, *ASME J. Eng. Mat. Techn.*, **96** (1976) 97.
6. E. W. Hart, *ASME J. Eng. Mat. Techn.*, **98** (1976) 193.
7. S. R. Bodner and Y. Partom, *ASME J. Appl. Mech.*, **42** (1975) 385.
8. R. W. Rohde and J. C. Swearngen, in *Mechanical Testing for Deformation Model Development*, ed. R. W. Rohde and J. C. Swearngen, ASTM STP 765, 1982, p. 469.
9. J. C. Swearngen and J. H. Holbrook, *Res. Mech.*, **13** (1985) 93.
10. R. D. Krieg, in *Mechanical Testing for Deformation Model Development*, ed. R. W. Rohde and J. C. Swearngen, ASTM STP 765, 1982, p. 139.
11. E. W. Hart, *Acta Metall.*, **18** (1970) 599.
12. R. D. Krieg, *Proc. 4th Conf. Structural Mechanics in Reactor Technology*, Paper No. M6/4, 1977.
13. K. S. Chan, S. R. Bodner, K. P. Walker and U. S. Lindholm, *Second Symp. on Nonlinear Constitutive Relations for High-Temp Applications*, Cleveland, Ohio, June 1984.
14. W. B. Jones, R. W. Rohde and J. C. Swearngen, in *Mechanical Testing for Deformation Model Development*, ed. R. W. Rhode and J. C. Swearngen, ASTM STP 765, 1982, p. 102.

15. P. R. Swann, in *Electron Microscopy and Strength of Crystals*, ed. G. Thomas and J. Washburn, Interscience, New York, 1963, p. 131.
16. A. Kelly, *Acta Cryst.*, **7** (1954) 554.
17. T. Svensson, Plasticity of metals: stress, strain, and structure, Research Inst. of National Defence (Sweden) FOA, Report C 20467-D4, Sept. 1982.
18. H. McQueen, *Metall. Trans.*, **A8** (1977) 807.
19. M. R. Staker and D. L. Holt, *Acta Metall.*, **20** (1972) 569.
20. E. U. Lee, H. H. Kranzlein and E. E. Underwood, *Mat. Sci. Eng.*, **7** (1971) 348.
21. O. D. Sherby, R. H. Klundt and A. K. Miller, *Metall. Trans.*, **A8** (1971) 843.
22. P. A. Beck, B. G. Ricketts and A. Kelly, *Trans TMS-AIME*, **215** (1959) 949.
23. J. K. Dienes, *Acta Mech.*, **32** (1979) 217.
24. W. A. Spitzig and O. Richmond, *Acta Metall.*, **32** (1984) 457.
25. C. N. Ahlquist and W. D. Nix, *Acta Metall.*, **19** (1971) 373.
26. W. B. Jones and R. W. Rohde, in *Novel Techniques in Metal Deformation Testing*, ed. R. H. Wagoner, TMS-AIME, New York, 1983, p. 373.
27. G. Konig and W. Blum, *Acta Metall.*, **25** (1977) 1531.
28. W. Blum and A. Finkel, *Acta Metall.*, **30** (1982) 1705.

# 6

## Review of a Unified Elastic–Viscoplastic Theory

S. R. BODNER

*Department of Mechanical Engineering, Technion—Israel Institute of  
Technology, Haifa, Israel*

### 1. INTRODUCTION

Although inelastic response of solid materials at low stress levels has been observed and measured for over a century and a half (an account of the early work is given by Bell<sup>1</sup>), engineering thinking on material behavior has been dominated by the considerable success of the classical elastic and plastic theories. In contrast, the work on ‘dislocation dynamics’ in the 1950s and early 1960s by Johnston and Gilman<sup>2,3</sup> and by Hahn<sup>4</sup> and others was based on the concept of considering both elastic and plastic deformations to be generally non-zero at all stages of loading. Those formulations were one-dimensional and restricted to simple loading histories such as uniaxial extension and creep. One of the main interests in those studies was to obtain the form of the equations and the material constants from measurements of microstructural quantities.

Some of the physical ideas behind ‘dislocation dynamics’ were adopted by Bodner and Partom in their multi-dimensional formulation of elastic–viscoplastic constitutive equations without a specified yield criterion. The first publication on the equations and their relation to the work on ‘dislocation dynamics’ and to the more classical theories of viscoplasticity appeared in 1968.<sup>5</sup> The overall approach was to develop an elastic–viscoplastic model motivated and guided by physical and phenomenological considerations, and based on the principles of continuum mechanics. It was also the intention to include the more important manifestations of inelastic behavior in the same set of

equations, e.g. strain rate dependent plastic flow, creep, stress relaxation. Such equations are currently referred to as 'unified'.

Non-requirement of a yield criterion also eliminates the need to specify loading and unloading conditions, and the same equations can be directly used for all loading and unloading histories. The 'unified' theory therefore parallels and couples both elasticity and plasticity theories so they do not have separate domains of applicability determined by a stress amplitude and loading/unloading conditions.

Inelastic behavior of solids is exceedingly complex and many aspects of the physics of polycrystalline solids are far from understood. The material model was intended to be as simple as possible consistent with the essential physics, the requirements of continuum mechanics, and overall thermodynamic constraints. On that basis, the material constants that appear in the equations can generally be given physical or phenomenological interpretations, which facilitates their determination from test results. An objective of the formulation was to enable the material constants to be obtained from standard tests such as uniaxial stress-strain and creep.

One of the first papers on the subject<sup>6</sup> considered large deformations for the case of no hardening, and applied the equations to the inflation of a thick-walled spherical shell. The power law and simple exponential law used in examples in reference 6 for the stress dependence of the inelastic strain rate component were combined in later work to a slightly more complicated exponential function [eqn (8), following]. Elimination of a completely elastic domain requires that the inelastic deformation rate function be almost zero at low stresses. The exponential function used in the subsequent work for the plastic strain rate seems to give the necessary properties at both low stresses and also at very high strain rates.

At the present state of development, the equations can provide for a number of important characteristics of strain rate dependent inelastic deformation: isotropic and directional hardening leading to cyclic stress-strain relations with cyclic hardening or softening, additional hardening due to non-proportional loading, thermal recovery of both isotropic and directional hardening, temperature and pressure dependence, and isotropic and directional damage development. The equations have been used to model a number of metals over a wide range of temperatures and strain rates; details are given in a subsequent section. They have been applied to problems of creep crack growth, metal matrix composites, and dynamic plastic structural

deformations and wave propagation. These applications are also described in a subsequent section.

## 2. CONSTITUTIVE EQUATIONS

### 2.1. Basic Equations

Only the case of small strains (less than about 5%) is discussed here. A large deformation theory with work hardening is presently under development. The total strain rate  $\dot{\epsilon}_{ij}$  is assumed to be decomposable into elastic and plastic components:

$$\dot{\epsilon}_{ij} = \dot{\epsilon}_{ij}^e + \dot{\epsilon}_{ij}^p \quad (1)$$

where the elastic component is given by the time derivative of Hooke's law:

$$\dot{\epsilon}_{ij}^e = (\dot{\sigma}_{ij}/2\mu) - \lambda \dot{\sigma}_{kk} \delta_{ij} / [2\mu(3\lambda + 2\mu)] \quad (2)$$

In eqn (2),  $\lambda$  and  $\mu$  are the Lamé constants of the material and  $\delta_{ij}$  is the Kronecker delta. For the inelastic strain rate component, the isotropic form of the Prandtl-Reuss flow law is assumed to be applicable even, as an approximation, under loading conditions generating directional hardening. That equation is

$$\dot{\epsilon}_{ij}^p = \dot{e}_{ij}^p = \lambda s_{ij}; \quad \dot{\epsilon}_{kk}^p = 0; \quad \lambda \geq 0 \quad (3)$$

where  $\dot{e}_{ij}^p$  and  $s_{ij}$  are the deviatoric plastic strain rate and stress. Equation (3) indicates plastic incompressibility and non-reversibility of the inelastic strains without change in sign of the deviatoric stress.

A full treatment of directional hardening effects would require use of the anisotropic form of the flow law:<sup>7,8</sup>

$$\dot{\epsilon}_{ij}^p = \lambda_{ijkl} s_{kl} \quad (4)$$

where, from symmetry and reciprocity conditions,

$$\lambda_{ijkl} = \lambda_{jikl} = \lambda_{ijlk} = \lambda_{klij} \quad (5)$$

and, for incompressibility,

$$\lambda_{iikl} = \lambda_{ijkk} = 0 \quad (6)$$

Directional hardening would be represented as a second-order tensor in the fourth-order tensor coefficient  $\lambda_{ijkl}$ .

Equation (4) is complicated to use in engineering analyses and an

approximate method of treating directional hardening is to include a scalar effective value of that parameter in the scalar coefficient  $\lambda$  of the isotropic flow law (3). That equation could then be considered as 'incrementally isotropic' since  $\lambda$  would depend on the loading history and the current stress state at each stage of the loading history. A parameter taken to represent directional hardening in yield surface theories, the 'back stress' or 'kinematic' hardening variable, is not used in the equations under discussion.

Although certain response characteristics cannot be represented by eqn (3), they are considered to be of secondary importance in structural analyses. For example, eqn (3) does not admit the class of inelastic deformations that are geometrically reversible with energy losses, the 'anelastic' deformations. These can be provided, if required, by an additional term in the flow law or by re-defining the expression for stress. Equation (3) states that the plastic strain rate and deviatoric stress vectors are coaxial, which does not hold consequent to a rapid change in stress direction. The loss of coaxiality is a transient effect and would not be expected to have a significant influence on the stresses and strains.

Squaring eqn (3) leads to

$$D_2^p = \lambda^2 J_2 \quad (7)$$

where  $D_2^p$  and  $J_2$  are the strain rate and deviatoric stress invariants. The relation governing inelastic deformations is the 'kinetic equation',  $D_2^p = F(J_2)$ , and the particular function chosen is

$$D_2^p = D_0^2 \exp[-(Z^2/3J_2)^n] \quad (8)$$

In eqn (8),  $D_0$  is the limiting strain rate in shear,  $n$  is a material constant, and  $Z$  is interpreted as a load history dependent parameter that represents the hardened state of the material with respect to resistance to plastic flow. Another load history variable,  $\omega$ , could be introduced to indicate damage development in a continuum sense where damage is the deterioration in the ability of a material to support stress. With the inclusion of damage, eqn (8) becomes

$$D_2^p = D_0^2 \exp\{-[Z^2(1-\omega)^2/3J_2]^n\} \quad (9)$$

Combining eqns (3), (7) and (8) for the one-dimensional stress case gives

$$\dot{\epsilon}_{11}^p = \frac{2}{\sqrt{3}} \left( \frac{\sigma_{11}}{|\sigma_{11}|} \right) D_0 \exp\left\{ -\frac{1}{2} \left[ \frac{Z}{\sigma_{11}} \right]^{2n} \right\} \quad (10)$$

This equation can be written in the form

$$(\sigma_{11}/Z) = f[(\dot{\epsilon}_{11}^p/D_0), n] \tag{11}$$

which is plotted in Fig. 1 for various values of  $n$ . It is seen that  $n$  controls strain rate sensitivity and also influences the overall level of the flow stress. Various exercises (e.g. references 9 and 10) indicate that  $n$  is temperature dependent and decreases with increasing temperature, giving lower flow stress levels and increased rate sensitivity. Pressure dependence of inelastic flow can be accommodated by taking  $n$  to be an increasing function of pressure. This method provides for pressure sensitive incompressible plastic flow which is in general agreement with test results (e.g. references 11 and 12). It avoids the question of association of strain rates with potential functions because of the parametric nature of the pressure dependence.

Equation (10) has the desirable feature that  $(\dot{\epsilon}_{11}^p/D_0)$  is small, essentially negligible, at low values of  $(\sigma_{11}/Z)$  until a threshold value is

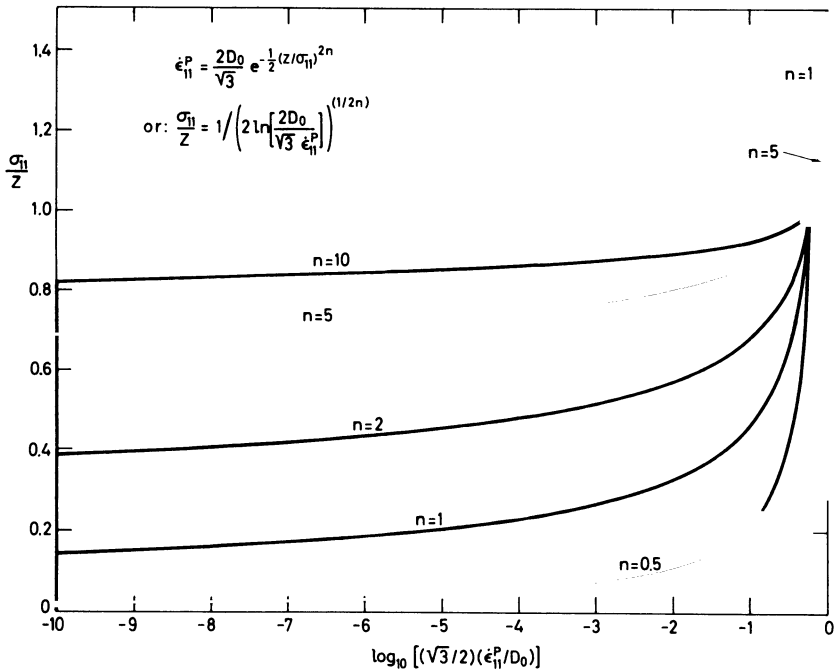


**Fig. 1.** Dependence of the uniaxial flow stress parameter on the strain rate parameter for different values of the strain rate sensitivity constant  $n$ .

reached and it then increases with a slope determined by  $n$ . The flow stress parameter shows a significant increase at  $(\dot{\epsilon}_{11}^p/D_0)$  values larger than about  $10^{-3}$ . Such large increases of flow stresses at strain rates about  $10^5 \text{ s}^{-1}$  have been reported recently (e.g. reference 13); eqn (10) would indicate approximate correspondence with those results if  $D_0$  were about  $10^7 \text{ s}^{-1}$ .

The preceding basic equations were published initially in 1972,<sup>14</sup> again in 1975,<sup>15</sup> and repeated in subsequent work. A factor  $[(n+1)/n]$  appeared in the kinetic equation (8) in the earlier papers. It was introduced to give  $Z$  a particular interpretation but was deleted in more recent work. The damage variable was introduced into the equations in 1981.<sup>16</sup>

## 2.2. Evolution Equations

A useful concept in material modeling is the interpretation of certain parameters in the kinetic equation as load history dependent variables. These parameters are not state quantities in the usual sense since their current values would be load path dependent, but they are presumed to provide relevant information on the material 'state' that is incorporated in the basic response equations. The notion of 'internal state' to describe properties which influence mechanical behavior is described by Onat<sup>17,18</sup> who also outlines general requirements on those variables and their evolution equations. Another factor concerning the internal variables is material stability. Ponter's generalization<sup>19</sup> of Drucker's stability postulate leads to conditions on the hardening variables and their evolution with loading. The stability postulate would not be applicable, however, for softening effects due to continuum damage or adiabatic heating.

In the case of material hardening, i.e. deformation induced resistance to plastic flow, it appears that two variables are the minimum required to represent the principal phenomenological characteristics: a scalar for isotropic hardening and a second-order symmetric tensor for directional hardening. Onat and most investigators choose that tensor to be traceless on the grounds that it is not further reducible. This is not an essential condition and a general second-order symmetric tensor is used in the present case for directional hardening.

On the basis of 'incremental isotropy' of the flow law, the scalar hardening variable  $Z$  in the kinetic equation (8) is taken to consist of isotropic and directional components:

$$Z = Z^I + Z^D \quad (12)$$

The evolution equation proposed for the isotropic hardening component is

$$\dot{Z}^I(t) = m_1[Z_1 - Z^I(t)]\dot{W}_p(t) - A_1 Z_1 \left[ \frac{Z^I(t) - Z_2}{Z_1} \right]^{r_1} \quad (13)$$

with the initial condition,  $Z^I(0) = Z_0$ . In the first term,  $Z_1$  is the limiting (saturation) value of  $Z^I$ ,  $m_1$  is the hardening rate, and  $\dot{W}_p = \sigma_{ij}\dot{\epsilon}_{ij}^p$  is the plastic work rate which is taken as the measure of hardening. The negative part of this first term can be interpreted as 'dynamic recovery' but the form can be motivated by the requirement that  $Z^I$ , and therefore the flow stress, have upper limits. The second term in eqn (13) corresponds to thermal or 'static' recovery of hardening where  $Z_2$  is the stable (minimum) value of  $Z^I$  at a given temperature and  $A_1$  and  $r_1$  are temperature dependent material constants.

Plastic work rate,  $\dot{W}_p$ , was taken as the measure of hardening, because of its physical motivation (with  $Z$  considered to be directly related to the stored energy of cold work) and the relative simplicity of the resulting equations. For example, the use of  $\dot{W}_p$  enables the main features of strain rate jump (and decrement) tests to be reproduced without requiring that  $Z_1$  be a function of strain rate. That would be necessary if the effective plastic strain rate were taken as the hardening measure. An alternative suggestion<sup>20</sup> is to have the hardening measure a functional of strain rate history.

In the absence of thermal recovery of hardening, the response equation for uniaxial stress (10) combined with eqn (13) for  $\dot{Z}$  could be analytically integrated for the case of constant plastic strain rate.<sup>21</sup> That set of equations, however, is not derivable from a closed form potential function as shown by Ponter.<sup>19</sup> However, they are associated with potential functions that include an infinite series, as shown by Kim and Oden.<sup>55</sup>

Inclusion of thermal recovery of hardening is important at high temperatures and enables response characteristics such as secondary creep to be properly predicted. Equations (3), (8) and (13) therefore form a full set of constitutive equations that are applicable for loading histories compatible with isotropic hardening. Applications based on this relatively simple set of equations are described in a subsequent section.

As discussed previously, directional hardening is represented by a second-order symmetric tensor  $\beta_{ij}$ , and a scalar effective value  $Z^D$  is

used as a component of the total hardening parameter  $Z$ , eqn (12), in the kinetic equation (8). That value is defined as

$$Z^D(t) = \beta_{ij}(t)u_{ij}(t) \quad (14)$$

where  $u_{ij}$  are taken to be the direction cosines of the current stress state:

$$u_{ij}(t) = \sigma_{ij}(t)/[\sigma_{kl}(t)\sigma_{kl}(t)]^{1/2} \quad (15)$$

The evolution equation for  $\beta_{ij}(t)$  has the same general form as that for isotropic hardening but has tensorial character:

$$\begin{aligned} \dot{\beta}_{ij}(t) = m_2[Z_3u_{ij}(t) - \beta_{ij}(t)]\dot{W}_p(t) \\ - A_2Z_1\left\{\frac{[\beta_{kl}(t)\beta_{kl}(t)]^{1/2}}{Z_1}\right\}^{r_2}v_{ij}(t) \end{aligned} \quad (16)$$

where

$$v_{ij}(t) = \beta_{ij}(t)/[\beta_{kl}(t)\beta_{kl}(t)]^{1/2} \quad (17)$$

and generally,

$$\beta_{ij}(0) = 0$$

Equation (16) is similar to the expression used by Chaboche<sup>22</sup> for the 'back stress' variable, with the differences that Chaboche takes the effective plastic strain rate instead of  $\dot{W}_p$  as the hardening measure and uses the plastic strain rate rather than the stress for the directional index in the hardening term. An index based on stress avoids the transverse softening effect in the uniaxial stress case and more closely parallels Ziegler's modification of Prager's kinematic hardening rule.

Another characteristic of eqn (16) is that the thermal recovery term has zero as the limit for directional hardening in the fully recovered state. The parameter  $Z_1$  appears in the recovery term only as a non-dimensionalizing factor. As in eqn (13),  $m_2$  is the hardening rate and  $A_2$  and  $r_2$  are temperature dependent material constants.

It is noted that the calculation of effective scalar values  $Z^D$ , eqn (14), corresponds to the method described in earlier papers of associating hardening values to each coordinate and sign direction in stress space.<sup>7,8</sup> The present procedure is neater and requires less storage in numerical work.

Under proportional unidirectional loading,  $u_{ij}$  is constant and  $\beta_{ij}$  would have the same direction in stress space. Equations (14) and (16)

would then reduce to the isotropic hardening format so that  $Z^I$  and  $Z^D$  could be combined to the fully isotropic hardening case but with two different hardening rates. For general loading conditions, both  $Z^I$  and  $Z^D$  must be evaluated at each load increment. Cyclic hardening or softening is controlled by the  $Z^I$  term; cyclic hardening would result for  $Z_0 < Z_1$  and softening for  $Z_0 > Z_1$ . The strain range of cycling does not enter explicitly in the equations but is part of the load control function. In some cases, the stress-strain curve upon stress reversal is too 'square' and a smoothing function can be added for better agreement with test results. A possible smoothing procedure is to make  $m_2$  a function of  $Z^D$ :

$$m_2 = (\bar{m}_2/2)[1 + \exp(-m_3 Z^D)] \quad (18)$$

which would add another material constant  $m_3$ .

A number of experimentalists have observed that non-proportional cyclic loading histories can result in a hardening increment for some materials. This has been physically attributed to the activation of more intersecting slip planes under non-proportional loading conditions. Preliminary observations for some materials suggest that the hardening increment appears primarily as recoverable isotropic hardening. To account for this effect in the constitutive equations, a measure of non-proportionality of loading is introduced by a parameter  $\theta$  defined by either of the following expressions:

$$\theta = \cos^{-1}(v_{ij} \bar{v}_{ij}) \quad (19)$$

$$\theta = \cos^{-1}(u_{ij} \bar{u}_{ij}) \quad (20)$$

where  $u_{ij}$  and  $v_{ij}$  have been defined previously and

$$\bar{v}_{ij} = \dot{\beta}_{ij} / (\dot{\beta}_{kl} \dot{\beta}_{kl})^{1/2} \quad (21)$$

$$\bar{u}_{ij} = \dot{\sigma}_{ij} / (\dot{\sigma}_{kl} \dot{\sigma}_{kl})^{1/2} \quad (22)$$

Time dependence of all these variables is understood. Which of the expressions for  $\theta$ , (19) or (20), is more appropriate is not yet settled. Equation (19) involves the history of previous loading in the construction of the value of  $\beta_{ij}$ , while only the current stress state and its rate of change appear in eqn (20). In a limited number of exercises, both expressions led to almost identical results.

Another load history dependent variable,  $\alpha = \alpha(\theta, \dot{W}_p)$ , is introduced into the evolution equation for  $Z^I$  to provide the additional hardening increment where  $\alpha$  is a growth function of non-zero values

of  $\theta$ . Based on the limited observations described previously, the following modification to the evolution equation for  $Z^I$ , eqn (13), is suggested:

$$\dot{Z}^I(t) = m_1[Z_1 + \alpha(t)Z_3 - Z^I(t)]\dot{W}_p(t) - A_1 Z_1 \left[ \frac{Z^I(t) - Z_2}{Z_1} \right]^n \quad (23)$$

where

$$\dot{\alpha}(t) = m_2[\alpha_1[\sin \theta(t)] - \alpha(t)]\dot{W}_p(t); \quad \alpha(0) = 0 \quad (24)$$

It is seen that  $\alpha$  grows with non-proportional loading history from zero to  $\alpha_1$ . Upon resumed proportional loading,  $\alpha$  would decay to zero and the revised saturation value,  $Z_1 + \alpha Z_3$ , would revert back to  $Z_1$ . If an increase in directional hardening rate under non-proportional loading is observed, a possible method for including this effect would be to modify eqn (18) to

$$m_2 = (\bar{m}_2/2)(1 + \alpha_2 \sin \theta)[1 + \exp(-m_3 Z^D)] \quad (25)$$

where  $\alpha_2$  is the modification constant. For the example of Hastelloy-X at room temperature (Fig. 3),  $\alpha_1 = \alpha_2 = 1$ .

Inclusion of continuum damage,  $\omega$ , in the kinetic equation (9) requires specification of an evolution equation for that variable. Most studies on the subject employ the general form suggested by Kachanov:

$$\dot{\omega} = f_1(\omega)f_2(\sigma) \quad (26)$$

As in the case of hardening, the total scalar damage variable  $\omega$  in eqn (9) is assumed to have isotropic and (effective) directional components:

$$\omega = \omega^I + \omega^D \quad (27)$$

A specific expression suggested for isotropic damage development is

$$\dot{\omega}^I = \frac{p}{H} \left\{ \left[ \ln \left( \frac{1}{\omega^I} \right) \right]^{(p+1)/p} \right\} \omega^I \dot{Q} \quad (28)$$

where  $p$  and  $H$  are material constants and  $\omega^I(0) \sim 0$ . The assumed stress function is

$$\dot{Q} = [A\sigma_{\max}^+ + B\sqrt{3J_2} + CI_1^+]^v \quad (29)$$

where  $\sigma_{\max}^+$  is the maximum tensile principal stress,  $I_1^+$  is the first stress

invariant (positive),  $J_2$  is defined previously, and  $A$ ,  $B$ ,  $C$  and  $\nu$  are material constants, where  $A + B + C = 1$ . Equation (29) is the scalar stress function proposed by Leckie and Hayhurst<sup>23</sup> for damage development under multiaxial stress states.

For the case of constant applied stress, eqn (28) can be integrated to

$$\omega^I = \exp[-(H/Q)^p] \quad (30)$$

which is the same functional form as the kinetic equations (8, 9). It has been shown<sup>24,36</sup> that combination of this evolution equation with the flow, kinetic and hardening evolution equations leads to reasonable agreement with creep test results including tertiary creep.

Directional damage is properly represented by a second-order symmetric tensor  $\omega_{ij}^D$ . An evolution equation similar to eqn (28) can be postulated for  $\omega_{ij}^D$ :

$$\dot{\omega}_{ij}^D = \frac{q}{M} \left\{ \left[ \ln \left( \frac{1}{\omega^D} \right) \right]^{(q+1)/q} \right\} \omega^D \dot{Q} u_{ij} \quad (31)$$

where

$$\omega^D = (\omega_{kl}^D \omega_{kl}^D)^{1/2} \quad (32)$$

and  $q$  and  $M$  are material constants comparable to  $p$  and  $H$ . However, the use of eqn (31) would lead to non-invariance since damage development under compression would have to be suppressed. Alternatively, as suggested by Leckie and Onat,<sup>56</sup> the equation can be transformed to principal axes with the damage increments obtained from the tensile stresses and then referred back to the reference axes. The effective scalar value of  $\omega_{ij}^D$  for use in eqn (27) could then be defined as

$$\omega^D = \omega_{ij}^D u_{ij} \geq 0 \quad (33)$$

A problem with eqn (33) is that reversal of the sign of the applied stress would lead to a negative value of  $\omega^D$  which is unrealistic. Physically, this would mean that the developed damage state is ineffective under the new stress. A possible procedure would be to store such damage states, commence calculation of damage from zero under the new stress condition, and retrieve and examine all previously stored damage states with respect to eqn (33) upon changes in stress to determine the active directional damage component. A more complete discussion on the inclusion of isotropic and directional damage in the constitutive equations appears elsewhere.<sup>36</sup>

Material hardening should have an influence on the damage evolution equation, with increased hardening lowering the damage rate. A more complete general expression than eqn (26) of the evolution equation for damage would be

$$\dot{\omega} = f_1(\omega)f_2(\sigma/Z) \quad (34)$$

where  $Z$  is the hardening variable described previously. To obtain this form, the stress terms in the function  $\dot{Q}$ , eqn (29), should be divided by  $Z$ . This would lead to a fully coupled theory for damage and hardening.

### 2.3. Temperature Dependence

Temperature sensitivity of the flow stress of metals is an essential characteristic of their mechanical behavior. The general effects of a temperature increase are a reduction in the flow stress level and an increase in strain rate sensitivity. The detailed behavior is often complex and certain metallurgical processes such as strain aging and age hardening could complicate the temperature dependence and even lead to reverse effects over some temperature range.

In the case of the particular equations under discussion, the primary influence of temperature on the flow stress can be obtained through the material parameter  $n$  in the kinetic equation (8), i.e.  $n = n(T)$ . For uniaxial stress, eqn (10), the flow stress parameter  $(\sigma_{11}/Z)$  then becomes a function of strain rate and temperature, the flow stress level decreases and rate sensitivity increases as can be seen from the plot in Fig. 1. Alternatively, eqn (10) for  $(\sigma_{11}/Z)$  can be plotted as a function of  $1/n$  for different constant strain rates so that for  $n = n(T)$ , e.g.  $n = a/T$ , the temperature dependence can be readily visualized (Fig. 2). An interesting result of this plot is that the flow stress becomes essentially temperature independent and  $(\sigma_{11}/Z)$  becomes approximately unity at very high strain rates, i.e. as  $\dot{\epsilon}_{11}^p/D_0$  approaches 0.7. The same result applies at very low temperature since  $n$  becomes large as  $T \rightarrow 0$  and  $(\sigma_{11}/Z)$  approaches unity independently of the strain rate. Some experiments have shown that the flow stress does not vary with temperature at very high strain rates<sup>25</sup> and also tends toward rate independence at very low temperature.<sup>34</sup>

The kinetic equation (8) can be expressed in the classical thermal activation form where the activation energy function would be a function of temperature. For the case of setting  $n = C/kT$ , where  $k$  is

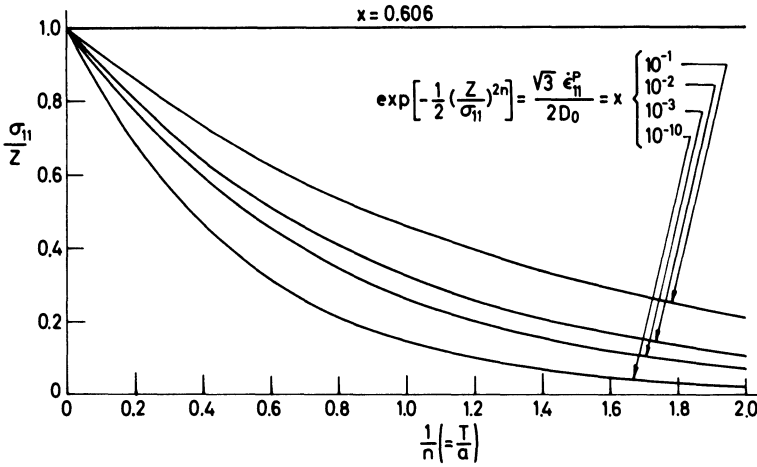


Fig. 2. Dependence of the uniaxial flow stress parameter on the (temperature dependent) strain rate sensitivity constant  $n$  for different values of the strain rate parameter.

Boltzmann's constant, eqn (8) becomes

$$D_2^p = D_0^2 \exp[-(Z^2/3J_2)^{C/kT}] \tag{35}$$

and the corresponding activation energy function is

$$H = kT[Z^2/3J_2]^{C/kT} \tag{36}$$

Activation energy functions can be obtained for alternative forms of the kinetic equation, and the strain rate and temperature dependence of the flow stress can be examined and compared.

In exercises on determining material constants for metals, the primary influence of temperature was found, in fact, to be on the material constant  $n$ . A single general thermo-rheological equation such as holds for many polymers does not seem to be applicable for metals. In a number of cases (e.g. references 9 and 10) the function

$$n = (a/T) + b \tag{37}$$

could serve as a reasonable approximation. In addition to the material constant  $n$ , the quantities  $Z_0$ ,  $Z_2$  and  $A_1$  usually exhibit temperature dependence. In many applications  $Z_0 = Z_2$  since the initial condition is the fully recovered state. Increasing temperature tends to cause a decrease of  $Z_0$  and  $Z_2$  and an increase in  $A_1$  corresponding to an enhanced thermal recovery rate. The constants  $m_1$ ,  $m_2$ ,  $Z_1$ ,  $Z_3$  and  $r_1$

appear to be essentially temperature independent in the various exercises performed to date. To reduce the number of material constants, it is usual to take  $A_2 = A_1$  and  $r_2 = r_1$  in the modeling exercises.

An interesting consequence of the uniaxial response equation (10) with  $n(T)$  given by eqn (37) and  $Z_1$  independent of temperature is that the natural logarithm of the saturation stress at constant plastic strain rate decreases linearly with absolute temperature. This result has been derived<sup>21</sup> and agrees with previous experimental observations.<sup>33</sup>

### 3. INTERPRETATION AND EVALUATION OF MATERIAL CONSTANTS

In the full set of constitutive equations considering isotropic and directional hardening, thermal recovery of hardening, temperature dependence, and isotropic and directional damage development, the number of material constants is large. Nevertheless, the various constants can be obtained in a systematic manner by methods based on physical and phenomenological interpretations of those constants in relation to standard uniaxial tests. This is a mechanistic approach and involves attempting to distinguish kinetic, hardening, recovery and damage effects separately in the experimental data. Overall 'best fitting' of the constants to sets of test data by numerical means is also possible but the results are likely to have more limited predictive capability.

Most practical applications of the constitutive equations involve more specific circumstances. For example, a class of problems concerned with creep crack growth can be treated where the material modeling involves only strain rate dependence, isotropic hardening, and thermal recovery under isothermal conditions. The number of material constants would then be eight:  $D_0$ ,  $n$ ,  $Z_1$ ,  $Z_0$ ,  $Z_2$ ,  $m_1$ ,  $A_1$ ,  $r_1$ . Of these, the constant  $D_0$  can generally be fixed for a strain rate range,  $r_1$  can be set within narrow limits, and also  $Z_0 \sim Z_2$ , so that only the five constants  $n$ ,  $Z_1$ ,  $Z_0$ ,  $m$  and  $A_1$  need to be determined and can be obtained from a few uniaxial stress-strain and creep tests.

The quantity  $D_0$  in the kinetic equation (8) is the maximum value of strain rate in shear, and its physical existence can be argued on the basis of dislocation theory.<sup>57</sup> In particular, there is a bound to the dislocation velocity, namely the sonic speed, and there appears to be a

limit to the dislocation flux—the mobile dislocation density.<sup>26</sup> It then follows from the basic equation of dislocation motion that there would be an upper limit on the plastic strain rate. A terminal value of about  $10^7 \text{ s}^{-1}$  for  $\dot{\epsilon}^p$  seems reasonable from both physical arguments and extrapolated test results,<sup>57</sup> so that  $D_0$  could be set equal to  $10^7 \text{ s}^{-1}$  for use in high strain rate problems, i.e.  $\dot{\epsilon}^p > 10^3 \text{ s}^{-1}$ . This value would indicate the large increase of flow stress at strain rates above  $10^5 \text{ s}^{-1}$  (Fig. 1). For applications at much lower strain rates, the high value of  $D_0$  leads to numerical difficulties and is not required for accurate modeling. The recommendation, therefore, is to set  $D_0 = 10^4 \text{ s}^{-1}$  in modeling for applications in which the maximum strain rates are less than  $10 \text{ s}^{-1}$  (most quasi-static and low rate dynamic problems), and to set  $D_0 = 10^6 \text{ s}^{-1}$  for applications where the strain rates are in the range  $10^1$ – $10^3 \text{ s}^{-1}$ , e.g. wave propagation problems. Further refinement of  $D_0$  is probably not necessary in most applications.

The material constant  $n$  appears to be related to the basic velocity of dislocations in the crystalline lattice and is therefore temperature and pressure dependent. Its value, at a given temperature, can be obtained from the strain rate dependence of the flow stress under conditions where the hardening parameter  $Z$  is constant and thermal recovery effects are not present, e.g. saturated stress values at sufficiently high strain rates. Separate evaluations should be performed at various temperatures and a functional relationship  $n = n(T)$  would be determined empirically. Particular techniques for obtaining  $n$  are described by Merzer,<sup>21,27</sup> by Stouffer<sup>28,29</sup> and by Chan *et al.*<sup>59</sup>

As discussed previously, the parameter  $Z$  is interpreted as a load history dependent variable and the kinetic equation (8) with temperature dependent  $n$  indicates that  $Z$  is the value of the flow stress at zero temperature. As has been shown<sup>58</sup> it follows from dislocation theory that  $Z$  would be related to the total dislocation density  $\rho$  by

$$Z = C_1 \mu b \sqrt{\rho} \quad (38)$$

where  $\mu$  is the shear modulus,  $b$  is the Burgers vector and  $C_1$  is a constant. Since the stored energy of cold work,  $W_s$ , can be expressed as

$$W_s = C_2 \mu b^2 \rho \quad (39)$$

it follows that

$$W_s = C_3 Z^2 / \mu \quad (40)$$

A number of measurements have been made of the variation of  $W_s$  with plastic work,  $W_p$  (e.g. reference 30), and show that  $W_s$  tends toward a saturation value with continued monotonic loading. If the form for  $W_s = W_s(W_p)$  is taken to be

$$\sqrt{W_s} = \sqrt{W_1} - (\sqrt{W_1} - \sqrt{W_0})\exp(-mW_p) \quad (41)$$

it then follows from eqn (40) that

$$\dot{Z} = m(Z_1 - Z)\dot{W}_p \quad (42)$$

which is the proposed evolution equation for isotropic hardening  $Z^I$ , eqn (13), in the absence of thermal recovery. Equation (42) is equivalent to an evolution equation for dislocation density:

$$\dot{\rho} = (k_1\sqrt{\rho} - k_2\rho)\dot{W}_p \quad (43)$$

The negative term in eqn (43) is sometimes referred to as dynamic recovery and is seen to be first-order in  $\rho$ . Possible generalizations of these equations are also discussed in reference 58.

A similar evolution equation in tensorial form was proposed for the directional hardening tensor  $\beta_{ij}$ , eqn (16). The combined isotropic and directional hardening equations,  $Z = Z^I + Z^D$ , eqns (13), (14) and (16), indicate changes under cyclic loading that are in qualitative agreement with some (unpublished) experimental observations<sup>31</sup> on the variation of  $W_s$  with cycling. Part of  $W_s$  alternates with cyclic loading in a manner similar to that predicted by the equations for  $Z^D$ . The analogy between  $W_s$  and the hardness variable  $Z$  gives some further justification for the use of a scalar value of  $Z$  in the isotropic form of the flow law.

Methods for determining the isotropic hardening constants  $Z_1$ ,  $Z_0$  and  $m_1$  are also described by Merzer<sup>21,27</sup> and by Stouffer.<sup>28,29</sup> The analytical integration of the constitutive equations for this case<sup>21</sup> is also helpful in obtaining the constants. For isotropic hardening with thermal recovery of hardening, the recovery constants can be obtained from either creep or relatively slow stress-strain test results under conditions where recovery is significant. Based on metallurgical reasons, it seems that the recovery exponent  $r_1$  can be set to a value between 2 and 3 for most metals, where a few trials can determine the preferred value. Then the recovery coefficient  $A_1$  and the lower hardening limit  $Z_2$  can be evaluated from some creep tests.

Under conditions where directional hardening is important, the full

set of hardening and thermal recovery constants must be determined. This consists of  $Z_1$ ,  $Z_3$ ,  $Z_0 (=Z_2)$ ,  $m_1$ ,  $m_2$ ,  $r_1 (=r_2)$  and  $A_1 (=A_2)$ . A systematic method for doing so based on only uniaxial monotonic stress-strain test results has recently been developed by Chan and co-workers.<sup>32,59</sup> The constants  $m_1$  and  $m_2$  can be obtained from plots of  $\gamma = (d\sigma/dW_p) = (d\sigma/\sigma d\epsilon^p)$  versus  $\sigma$  derived from monotonic stress-strain data in the absence of thermal recovery. Such graphs generally show an approximately bilinear relationship between the coordinates, which indicates that two distinct hardening rates are operative at the lower and higher stress levels. At the higher stresses, the slope of the  $\gamma$  vs.  $\sigma$  graphs is  $m_1$ , while the term  $m_2$  is the applicable slope at the lower stresses. Typical deduced results indicate that the rate of directional hardening  $m_2$  is about 5 to 10 times greater than  $m_1$  which is a known metallurgical observation. Such results had been reported previously<sup>28</sup> for a similar representation of creep test data for René 95, and some difficulty was encountered in modeling that metal based on a fully isotropic hardening formulation. In some of the earlier exercises,<sup>9,35</sup> a variable  $m$  function was introduced to provide better matching to stress-strain data.

The  $\gamma$  vs.  $\sigma$  graph also facilitates determination of the saturation stress which provides values of  $Z_1 + Z_3$  and enables  $n$  to be obtained from the strain rate dependence of that stress. In addition,  $Z_1$  and  $Z_3$  can be obtained once  $Z_0$  is determined from the yield stress of stress-strain curves. If required,  $m_3$ ,  $\alpha_1$  and  $\alpha_2$  are obtained by fitting the relevant response results. Assuming, as before, that the recovery exponent  $r_1 (=r_2)$  is between 2 and 3, an appropriate value can also be deduced from the  $\gamma$  vs.  $\sigma$  plot for operative thermal recovery conditions. Finally, the recovery coefficient  $A_1 (=A_2)$  can be obtained from creep data. A detailed description of this procedure is given elsewhere.<sup>32,59</sup>

The procedures just described for obtaining the material constants are based on using test data for which material damage should be non-existent. Some manifestations of damage are fairly obvious, notably tertiary creep and the reduction in flow stress at large strains in the absence of possible thermal effects. In some instances it may be difficult to distinguish between damage development and thermal softening.

A number of additional material constants arise with the inclusion of continuum damage development in the constitutive equations. For the

simple case of uniaxial creep, the stress function  $\dot{Q}$ , eqn (29), is constant so that  $Q = Kt$  and eqn (30) can be expressed as

$$\omega^1 = \exp[-(H/Kt)^p] \quad (44)$$

and the full damage can be represented by  $\omega^1$ . To fit the constitutive equations to test data in the tertiary creep range when the other material constants are known, it is only necessary to choose appropriate values for  $(H/K)$  and  $p$ . It has been demonstrated<sup>24</sup> that fairly good agreement with creep test results can be obtained by proper choice of those parameters. Additional exercises on modeling isotropic damage are reported in reference 36.

The main problems in obtaining the material constants for damage development arise with multiaxial stress states and changes in the stress direction. For multiaxial loading, the coefficients of the stress terms in the expression for  $\dot{Q}$ , eqn (29), and the exponent  $\nu$  must be evaluated. Then the relative contributions of isotropic and directional damage need to be determined by suitable tests such as changing the loading direction in the range when damage development is operative. Appropriate tests and numerical procedures for the general treatment of continuum damage as a load history dependent variable in constitutive equations have still to be established.

#### 4. MODELING OF METALS

A number of metals and metallic alloys have been modeled by the elastic-viscoplastic constitutive equations described in this article. In some cases, the resulting equations have been used to predict response characteristics for loading histories appreciably different from those used to determine the material constants. In other investigations, the equations were employed in static and dynamic structural analyses and certain computed results could be compared with experimental observations.

The initial modeling exercises were based on isotropic hardening and were later extended to include thermal recovery of hardening. Since the reference tests and intended applications involved low to moderate strain rates, the parameter  $D_0$  was set equal to  $10^4 \text{ s}^{-1}$  in these studies. Some more recent modeling exercises have been concerned with both isotropic and directional hardening and recovery

while others have been directed at material representation at high strain rates.

A few metals in the commercially pure state, namely Ti, Cu and Al, were examined since they are frequently used as specimen materials in laboratory experiments. Also, three high temperature alloys, René 95, IN-100 and Inconel 718, were each modeled at an elevated temperature corresponding to their operational use where thermal recovery effects are significant. A listing of the material constants of these metals and alloys on the basis of isotropic hardening and thermal recovery, when important, is given in Table 1.

A few changes were made in the detailed form of the constitutive equations during their development which altered the precise definition of some of the material constants. It is therefore important to recognize the exact reference equations in using a particular set of constants. For most of the sets listed in Table 1, the kinetic equation contained a multiplying factor  $[(n + 1)/n]$  in the exponential term. That equation would then read

$$D_2^e = D_0^2 \exp\{-(Z^2/3J_2)^n[(n + 1)/n]\} \quad (45)$$

and is referred to as form A in Table 1. The equations discussed in this article are referred to as form B. In some of the earliest exercises (e.g. reference 15) the hardening rate  $m_1$  was divided by  $Z_0$  in the evolution equation for  $Z$ . The constants  $m_1$  listed in Table 1 are based on the current version, eqn (13), but some investigators still use the early definition of  $m_1$  in their work. That definition is dimensionless whereas the current one has dimension 1/stress.

Modeling exercises based on both isotropic and directional hardening and recovery have been carried out recently for three high temperature alloys, Hastelloy-X, B1900 + Hf and Mar-M247. Tests were performed at room temperature and at a number of elevated temperatures, up to 871°C for Hastelloy-X and up to 1093°C for B1900 + Hf and Mar-M247. The overall test program included combined extensional and torsional loading of specimens. Some of these were out-of-phase cyclic tests in which additional hardening effects were observed only for the Hastelloy-X material. A plot of such test results for Hastelloy-X at room temperature and corresponding computational results obtained from the constitutive equations are shown in Fig. 3. The room temperature material constants for these alloys are listed in Table 2 and are based on the equations in this

**TABLE 1**  
 Material Constants of the Reference Constitutive Equations for Various Metals and Metallic Alloys under Conditions of Isotropic Hardening and Thermal Recovery at Low to Moderate Strain Rates

Metal	Ti	Cu	Cu	Al	Al 2024-0	René 95	IN-100	Inconel 718
Temp.	RT	RT	550°C	200°C	RT	650°C	732°C	650°C
Ref.	15	10	27	27	39	28	29, 44	54
Form	A	B	B	B	A	A	A	A
$D_0$ ( $s^{-1}$ )	$10^4$	$10^4$	$10^4$	$10^4$	$10^4$	$10^4$	$10^4$	$10^4$
$n$	1.0	7.5	1.2	1.43	10.0	3.2	0.7	1.17
$Z_0$ (MPa)	1150	63	16	39	90	1680	6300	3130
$Z_1$ (MPa)	1400	250	250	220	200	2200	7000	4140
$Z_2$ (MPa)	N.A.	63	16	31	N.A.	1680	4130	2760
$m_1$ ( $MPa^{-1}$ )	0.087	0.13	2.5	5.0	0.22	0.37	0.37	0.024
$A_1$ ( $s^{-1}$ )	N.A.	N.A.	$4.3 \times 10^{-3}$	$3.4 \times 10^{-3}$	N.A.	5.3	$1.9 \times 10^{-3}$	$1.1 \times 10^{-4}$
$r_1$	N.A.	N.A.	3.6	3.25	N.A.	3.0	2.66	2.86
$\bar{E}$ (GPa)	118	120	~100		73	177	179	165

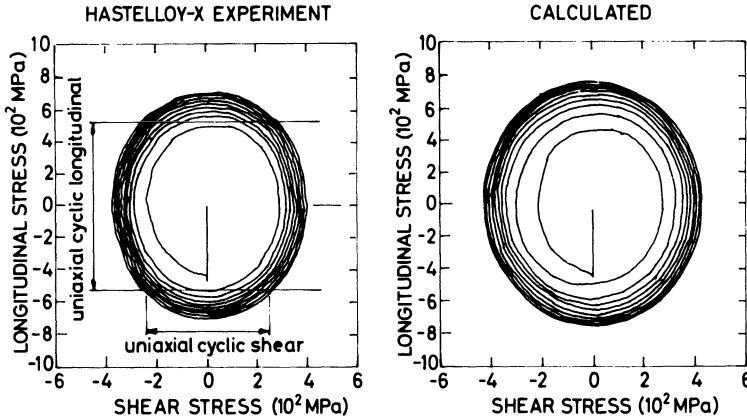


**Fig. 3.** Comparison of experimental and calculated results on the stress response of Hastelloy-X (at room temperature) to  $90^\circ$  out-of-phase longitudinal/shear cyclic straining of  $\pm 1\%$ .

article (form B). Thermal recovery constants are, of course, unimportant at room temperature for these materials.

Reports on the results of an extensive test and modeling program for the B1900 + Hf and Mar-M247 materials are available.<sup>36,37,59</sup> Experimental and modeling studies were performed over a wide range

**TABLE 2**

Material Constants of the Reference Constitutive Equations for Two Special Metallic Alloys (at Room Temperature) under Conditions of Isotropic and Directional Hardening at Low to Moderate Strain Rates

Metal	Hastelloy-X	B1900 + Hf
Temp.	RT	RT
Ref.	37	37
Form	B	B
$D_0$ ( $s^{-1}$ )	$10^4$	$10^4$
$n$	1.0	1.05
$Z_0$ (MPa)	1200	2700
$Z_1$ (MPa)	2000	3000
$Z_2$ (MPa)	1200	2700
$Z_3$ (MPa)	1200	1150
$m_1$ ( $MPa^{-1}$ )	0.02	0.27
$m_2$ ( $MPa^{-1}$ )	0.9	1.52
$m_3$ ( $MPa^{-1}$ )	0.001	0
$E$ (GPa)	207	200

of temperatures and loading histories. One of the conclusions was that the directional hardening material constants obtained from the monotonic straining tests using the procedure of references 32 and 59 led to adequate prediction of the cyclic response characteristics.

Capability for accurate representation of the flow stress at high strain rates was a prime consideration in the development of the constitutive equations. A recent experimental investigation of the high strain rate behavior of five metallic alloys has been reported.<sup>38</sup> The split Hopkinson bar technique of Kolsky was used to generate the basic strain rate data that served to determine the material constants. Constants for three alloys are listed in Table 3 and are based on form A of the equations. Modeling material response for the conditions of monotonic loading at high strain rate requires only the basic rate dependence of plastic flow and isotropic hardening without thermal recovery. It is noted that the value of  $D_0$  for the modeling exercises in reference 38 was set at  $10^8 \text{ s}^{-1}$  which is somewhat above the present recommendation for the high strain rate range.

It is seen in Table 3 that the  $n$  value for the aluminum alloy is 5. This indicates from Fig. 1, that the flow stress would be relatively insensitive to strain rate for strain rates below  $10^4 \text{ s}^{-1}$  for  $D_0 = 10^8 \text{ s}^{-1}$ . To obtain almost complete strain rate independence in modeling some other aluminum alloys at strain rates lower than  $10 \text{ s}^{-1}$ , Aboudi<sup>39</sup> set  $n = 10$  and  $D_0 = 10^4 \text{ s}^{-1}$ . An example, aluminum 2024-0, is given in Table 1.

**TABLE 3**

Material Constants of the Reference Constitutive Equations for Three Metallic Alloys (at Room Temperature) under Conditions of Isotropic Hardening at High Strain Rates

Metal	Steel-1020	HY-100	Al 6061-T6
Temp.	RT	RT	RT
Ref.	38	38	38
Form	A	A	A
$D_0$ ( $\text{s}^{-1}$ )	$10^8$	$10^8$	$10^8$
$n$	4.0	1.2	5.0
$Z_0$ (MPa)	640	2400	450
$Z_1$ (MPa)	930	3550	550
$m_1$ ( $\text{MPa}^{-1}$ )	0.03	0.01	0.12
$E$ (GPa)	203	203	73.9

## 5. APPLICATIONS

The main scope for application of the elastic-viscoplastic constitutive equations is in structural analysis problems involving time dependent inelastic material behavior, multiaxial stress states, and non-simple loading histories. For this purpose, the equations should be adaptable to finite element and finite difference computer programs. A fair amount of effort has been expended in this direction and the equations have been included in a number of commercial and specially developed computer programs. They also have been used as the material representation in the solution of some particular problems involving thermo-mechanical coupling and metal matrix composite materials.

### 5.1. Finite Element Computer Programs

Implementation of the reference constitutive equations in a finite element code was first carried out by Newman *et al.*<sup>40</sup> That paper was concerned with the stress analysis of a reinforced cylindrical shell subjected to external pressure and subsequent unloading from the inelastic range. This was essentially an exercise to demonstrate the use of the equations in a finite element program and to show the effect of time dependent inelastic behavior in a typical structural problem. The computer program of reference 40 was further refined by Zaphir<sup>41,42</sup> who examined the DCB fracture mechanics specimen subjected to loading at different rates and to cycles of loading and unloading. From examination of the stress and strain fields surrounding the (stationary) crack, information was obtained on possible criteria for crack extension and on the residual stresses due to overloading and unloading. These analyses were quasi-static in the sense that inertial effects were not included. Isotropic hardening without thermal recovery was considered in references 40 and 41, while Zaphir<sup>42</sup> included both isotropic and directional hardening in a manner similar to that described in this article.

A research task undertaken at the US Air Force Materials Laboratory, Wright-Patterson Air Force Base, is concerned with determining crack growth rates from measurements of external displacements in high temperature structures subjected to constant and variable loadings. A special finite element computer program was developed by Hinnerichs *et al.*<sup>43</sup> which incorporates the 'unified' elastic-viscoplastic constitutive equations. They applied the program to the center cracked panel specimen and subsequently Smail and Palazotto<sup>44</sup> examined the

compact tensile specimen. The numerical procedure involves extending the length of the crack by breaking nodal points in the finite element model to enable the computed external displacements to match the experimentally observed displacement–time history. Crack growth can thereby be obtained as a function of time from externally measured displacements of the structural component. Strain rates are relatively slow in this application which is essentially one of high temperature creep with varying multiaxial stress states. The material modeling was based on isotropic hardening with thermal recovery of hardening.

A current NASA sponsored research program involves implementing the complete set of constitutive equations described in this article in the MARC finite element computer code. Included are both isotropic and directional hardening and their respective thermal recovery terms. Outlines of the procedures for adopting the constitutive equations to the computer program are described by Lindholm *et al.*<sup>37</sup> and Chan *et al.*<sup>59</sup> The overall objective of the research task is to develop methods to analyze turbine engine hot section components subjected to complicated loading and temperature histories.

Another current research investigation is concerned with dynamic fracture mechanics problems that consider inertial effects and rate dependent inelastic material behavior. The problems are analyzed by a finite element computer program that contains the ‘unified’ elastic–viscoplastic constitutive equations. Both stationary and moving cracks are examined.

## 5.2. Finite Difference Computer Programs

A structural dynamic plasticity problem was analyzed by Sperling and Partom<sup>45</sup> using a finite difference computer program. An advantage of the reference constitutive equations in such problems is that the same equations apply for all conditions of loading and unloading so that a continuous check is not required in the computer program instructions. It has generally been difficult to include both elasticity and strain rate dependent, work-hardening plasticity in dynamic structural analyses. The ‘unified’ constitutive equations (without a yield criterion) appear to be particularly well suited to handling this class of problems.

Other dynamic problems involving inertial effects and time dependent inelastic material behavior were treated by finite difference techniques by Aboudi and Bodner.<sup>46,47</sup> An early version of the

directional hardening formulation was included in the material representation and a number of two-dimensional dynamic problems were solved numerically in reference 46. Bodner and Aboudi<sup>47</sup> calculated the response of a rod of elastic-viscoplastic, work-hardening material subjected to longitudinal impact. This is a classical problem for which a large literature of analytical and experimental investigations exist. The aim in reference 47 was to examine the consequences of the new formulation with respect to the previous studies.

A series of studies on dynamic crack propagation in elastic-viscoplastic, work-hardening materials was carried out by Aboudi and Achenbach (e.g. references 48 and 49). A finite difference procedure was developed to obtain numerical solutions to this class of problems which includes inertial effects. The stress field changes continually with crack advance and exhibits loading and unloading events. It appears that the classical elastic-plastic theory is not well suited to this type of problem while the reference elastic-viscoplastic theory can be implemented in a fairly straightforward manner. The finite difference technique proved to be efficient and a number of interesting results were obtained in these studies, but the current trend is to use finite element methods.

### 5.3. Special Problems

The constitutive equations have served as the material model in a number of particular mechanics problems. Merzer<sup>50</sup> examined adiabatic shear band formation in a cold-rolled steel specimen subjected to a high rate of shearing. This problem involves thermo-mechanical coupling and the material model was based on isotropic hardening and temperature dependence of the parameter  $n$  according to eqn (37). Inclusion of thermal conductivity in the field equations led to results in fairly good agreement with experimental observations. In order to obtain results over the full response range, the parameter  $D_0$  was set equal to  $10^6 \text{ s}^{-1}$  because of the high strain rates in this problem.

A subject of engineering importance is the mechanical behavior of metal matrix composites considering elastic-viscoplastic, work-hardening properties of the individual constituents. Aboudi has developed procedures for calculating the characteristics of such composites for a wide range of internal geometries and material types and for general modes of loading. Most of the examples use the elastic-viscoplastic constitutive equations with isotropic hardening (and no thermal recovery), but directional hardening has been

included in some investigations. Certain exercises consider anisotropic, elastic filaments in an elastic-viscoplastic, work-hardening matrix. A number of papers have been published by Aboudi on this topic (e.g. references 51–53). The ‘constitutive equations’ obtained for the metal matrix composite from the properties of the constituents can be used, in turn, in structural analysis computer programs.

### ACKNOWLEDGMENT

The research program on the development of the ‘unified’ elastic-viscoplastic constitutive equations has been supported by the Air Force Office of Scientific Research (AFSC), through the European Office of Aerospace Research and Development (EOARD), US Air Force. The present paper was prepared under grant AFOSR-84-0042.

### REFERENCES

1. J. F. Bell, *The Experimental Foundations of Solid Mechanics, Encyclopedia of Physics*, Vol. VIa/1, Springer-Verlag, New York, 1973.
2. W. G. Johnston and J. J. Gilman, Dislocation velocities, dislocation densities, and plastic flow in lithium fluoride crystals, *J. Appl. Phys.*, **30** (1959) 129–44.
3. J. J. Gilman, Dislocation mobility in crystals, *J. Appl. Phys.*, **36** (1965) 3195.
4. G. T. Hahn, A model for yielding with special reference to the yield point phenomena of iron and related b.c.c. metals, *Acta Metall.*, **10** (1962) 727–38.
5. S. R. Bodner, Constitutive equations for dynamic material behavior, in *Mechanical Behavior of Materials Under Dynamic Loads*, ed. U. S. Lindholm, Springer-Verlag, New York, 1968, pp. 176–90.
6. S. R. Bodner and Y. Partom, A large deformation elastic-viscoplastic analysis of a thick-walled spherical shell, *ASME J. Appl. Mech.*, **39** (1972) 751–7.
7. D. C. Stouffer and S. R. Bodner, A constitutive model for the deformation induced anisotropic plastic flow of materials, *Int. J. Eng. Sci.*, **17** (1979) 757–64.
8. S. R. Bodner and D. C. Stouffer, Comments on anisotropic plastic flow and incompressibility, *Int. J. Eng. Sci.*, **21** (1983) 211–5.
9. S. R. Bodner and A. Merzer, Viscoplastic constitutive equations for copper with strain rate history and temperature effects, *ASME J. Eng. Mat. Tech.*, **100** (1978) 388–94.
10. A. Merzer and S. R. Bodner, Analytical and computational repre-

- sensation of high rate of straining behavior, in *Mechanical Properties of Materials at High Rates of Strain*, ed. J. Harding, Inst. Physics Conf. Series, No. 47, London, 1979, pp. 142–51.
11. W. A. Spitzig, R. J. Sober and O. Redmond, The effect of hydrostatic pressure on the deformation behavior of maraging and HY-80 steels and its implication for plasticity theory, *Metall. Trans.*, **7A** (1976) 1703–10.
  12. O. Richmond and W. A. Spitzig, Pressure dependence and dilatancy of plastic flow, in *Proc. 15th Int. Congress of Theoretical and Applied Mechanics*, ed. F. P. J. Rimrott and B. Tabarrok, North Holland, New York, 1980.
  13. R. W. Klopp, R. J. Clifton, and T. G. Shawki, Pressure–shear impact and the dynamic viscoplastic response of metals, *Mech. Mater.*, **4** (1985) 375–85.
  14. S. R. Bodner and Y. Partom, Dynamic inelastic properties of materials. Part II. Representation of time dependent properties of metals, *Proc. 8th Congr. Int. Council Aeronautical Sciences (ICAS)*, Amsterdam, 1972.
  15. S. R. Bodner and Y. Partom, Constitutive equations for elastic–viscoplastic strain-hardening materials, *ASME J. Appl. Mech.*, **42** (1975) 385–9.
  16. S. R. Bodner, A procedure for including damage in constitutive equations for elastic-viscoplastic work-hardening materials, *Proc. IUTAM Symp. Physical Nonlinearities in Structural Analysis*, ed. J. Hult and J. Lemaitre, Springer-Verlag, Berlin, 1981, pp. 21–8.
  17. E. T. Onat and F. Fardshisheh, On the state variable representation of mechanical behavior of elastic-plastic solids, *Proc. Symp. Foundations of Plasticity*, P. Noordhoff, Groningen, The Netherlands, 1973, pp. 89–115.
  18. E. T. Onat, Representation of inelastic behavior in the presence of anisotropy and of finite deformations, in *Recent Advances in Creep and Fracture of Engineering Materials and Structures*, ed. B. Wilshire and D. R. J. Owen, Pineridge Press, Swansea, 1982, pp. 231–64.
  19. A. R. S. Ponter, Dynamic behavior of structures composed of strain and work-hardening visco-plastic materials, *Int. J. Solids Struct.*, **16** (1980) 793–806.
  20. H. Ghoneim, S. Matsouka and Y. Chen, Viscoplastic modelling with strain rate history dependence, *ASME J. Appl. Mech.*, **50** (1983) 465–8.
  21. A. Merzer and S. R. Bodner, Analytical formulation of a rate and temperature dependent stress-strain relation, *ASME J. Eng. Mat. Tech.*, **101** (1979) 254–7.
  22. J. L. Chaboche, Viscoplastic constitutive equations for the description of cyclic and anisotropic behaviour of metals, *Bull. Acad. Polon. Sci., Ser. Sci. Techn.*, **25**(1) (1977) 33–42.
  23. F. A. Leckie and D. R. Hayhurst, Constitutive equations for creep rupture, *Acta Metall.*, **25** (1977) 1059–70.
  24. S. R. Bodner, Evolution equations for anisotropic hardening and damage of elastic-viscoplastic materials, in *Plasticity Today: Modelling, Methods and Applications*, ed. A. Sawczuk and G. Bianchi, Elsevier Applied Science, Barking, 1984, pp. 471–82.

25. R. W. Rohde, *Acta Metall.*, **17** (1969) 353.
26. J. M. Kelly and P. P. Gillis, The influence of a limiting dislocation flux on the mechanical response of polycrystalline metals, *Int. J. Solids Struct.* **10** (1974) 45–59.
27. A. M. Merzer, Steady and transient creep behavior based on unified constitutive equations, *ASME J. Eng. Mat. Tech.*, **104** (1982) 18–25.
28. D. C. Stouffer and S. R. Bodner, A relationship between theory and experiment for a state variable constitutive equation, in *Mechanical Testing for Deformation Model Development*, ASTM STP 765, Philadelphia, 1982, pp. 239–50.
29. D. C. Stouffer, A constitutive representation for IN-100, AFWAL-TR-81-4039, Wright–Patterson AFB, Ohio, 1981.
30. M. B. Bever, D. L. Holt and A. L. Titchener, The stored energy of cold work, in *Progress in Materials Science*, ed. B. Chalmers, J. W. Christian and T. B. Massalski, **17** (1973) 1–190.
31. J. D. Morrow, Dept. of Theoretical and Applied Mechanics, Univ. Illinois, Champaign, private communication, 1979.
32. K. S. Chan, S. R. Bodner and U. S. Lindholm, Phenomenological modeling of hardening and thermal recovery in metals, Report on NASA Contract No. NAS 3-23925, Southwest Research Institute, San Antonio, Texas. *ASME J. Eng. Mat. Tech.*, (1986) submitted for publication.
33. U. F. Kocks, Laws for work-hardening and low temperature creep, *ASME J. Eng. Mat. Tech.*, **98** (1976) 76–85.
34. U. S. Lindholm, *High Velocity Deformation of Solids*, ed. K. Kawata and J. Shioiri, Springer-Verlag, Berlin, 1979, pp. 26–35.
35. S. R. Bodner, I. Partom and Y. Partom, Uniaxial cyclic loading of elastic-viscoplastic materials, *ASME J. Appl. Mech.*, **46** (1979) 805–10.
36. S. R. Bodner and K. S. Chan, Modelling of continuum damage for application in elastic-viscoplastic constitutive equations, *J. Eng. Fract. Mech.*, **25** (1986) 705–12.
37. U. S. Lindholm *et al.*, Constitutive modeling for isotropic materials, Second Annual Status Report on NASA Contract No. NAS3-23925, Southwest Research Institute, San Antonio, Texas, also NASA Report CR-174980, 1985.
38. A. M. Rajendran, S. J. Bless and D. S. Dawicke, Evaluation of Bodner–Partom model parameters at high strain rates, *ASME J. Eng. Mat. Tech.*, **108** (1986) 75–80.
39. J. Aboudi, Elastoplasticity theory for porous materials, *Mech. Mater.*, **3** (1984) 81–94.
40. M. Newman, Z. Zaphir and S. R. Bodner, Finite element analysis for time dependent inelastic material behavior, *J. Comput. Struct.*, **6** (1976) 157–62.
41. Z. Zaphir and S. R. Bodner, Implementation of elastic-viscoplastic constitutive equations into ‘NONSAP’ with applications to fracture mechanics, in *Proc. ADINA Conf.*, MIT Report 82448-9, ed. K. J. Bathe, August 1979.
42. Z. Zaphir, Analysis of an elastic-viscoplastic specimen with a crack, Ph.D. thesis, Tel Aviv Univ., 1983.

43. T. Hinnerichs, T. Nicholas and A. Palazotto, A hybrid experimental-numerical procedure for determining creep crack growth rates, *Eng. Fract. Mech.*, **16** (1982) 265–77.
44. J. Smail and A. N. Palazotto, The viscoplastic crack growth behavior of a compact tension specimen using the Bodner–Partom flow law, *Eng. Fract. Mech.*, **19** (1984) 137–58.
45. A. Sperling and Y. Partom, Numerical analysis of large elastic-plastic deformation of beams due to dynamic loading, *Int. J. Solids Struct.*, **13** (1977) 865–76.
46. J. Aboudi and S. R. Bodner, Dynamic response of a slab of elastic-viscoplastic material that exhibits induced plastic anisotropy, *Int. J. Eng. Sci.*, **18** (1980) 801–13.
47. S. R. Bodner and J. Aboudi, Stress wave propagation in rods of elastic-viscoplastic material, *Int. J. Solids Struct.*, **19** (1983) 305–14.
48. J. Aboudi and J. D. Achenbach, Arrest of mode III fast fracture by a transition from elastic to viscoplastic material properties, *J. Appl. Mech.*, **48** (1981) 509–14.
49. J. Aboudi and J. D. Achenbach, Numerical analysis of fast mode-I fracture of a strip of viscoplastic work-hardening material, *Int. J. Fract.*, **21** (1983) 133–47.
50. A. M. Merzer, Modelling of adiabatic shear band development from small imperfections, *J. Mech. Phys. Solids*, **30** (1982) 323–38.
51. J. Aboudi, Effective constitutive equations for fiber-reinforced viscoplastic composites exhibiting anisotropic hardening, *Int. J. Eng. Sci.*, **21** (1983) 1081–96.
52. J. Aboudi, Effective behavior of inelastic fiber-reinforced composites, *Int. J. Eng. Sci.*, **22** (1984) 439–49.
53. J. Aboudi, Elastoplasticity theory for composite materials, *Solid Mech. Arch.*, **11** (1986) 141–83.
54. T. M. Milly and D. H. Allen, A comparative study of nonlinear rate-dependent mechanical constitutive theories for crystalline solids at elevated temperatures, Report API-E-5-82, Virginia Polytechnic Institute and State University, March 1982.
55. S. J. Kim and J. T. Oden, Generalized flow potentials in finite elastoplasticity. II. Examples, *Int. J. Eng. Sci.*, **23** (1985) 515–30.
56. F. A. Leckie and E. T. Onat, Tensorial nature of damage measuring internal variables, in *Proc. IUTAM Symp. Physical Non-linearities in Structural Analysis*, ed. J. Hult and J. Lemaitre, Springer-Verlag, Berlin, 1981, pp. 140–55.
57. S. R. Bodner, Material modeling at high rates of strain. *Proc. Int. Conf. on Impact Loading and Dynamic Behavior of Materials*, Deutsche Gesellschaft für Metallkunde, Oberursel, FRG, 1987.
58. Y. Estrin and H. Mecking, An extension of the Bodner–Partom model of plastic deformation, *Int. J. Plasticity*, **2** (1986) 73–85.
59. K. S. Chan *et al.*, Constitutive modeling for isotropic materials, Third Annual Status Report on NASA Contract NAS 3-23925, Southwest Research Institute, San Antonio, Texas, also NASA Report CR-179522, 1986.

# 7

## Summary and Critique

D. BAMMANN

*Mechanics of Materials Division, Sandia National Laboratories,  
Livermore, California, USA*

and

R. D. KRIEG

*Applied Mechanics Division, Sandia National Laboratories,  
Livermore, California, USA*

### 1. INTRODUCTION

Unified creep–plasticity (UCP) models have many facets. Because there is no clear demarcation between plastic and creeping behavior, a good model should mimic both behaviors and should pass from one behavior to the other in a continuous manner. Furthermore, since plasticity and creep are both caused by similar physical processes, there should be no specific separation of the processes in the constitutive model. It appears that all of the models examined here have accomplished these basic objectives and in that sense qualify as unified creep–plasticity models. But constitutive modeling is multifaceted as stated above. Some authors have made a great effort to model time-dependent monotonic mechanical loading, others cyclic mechanical loading, and others multiaxial or temperature effects. Each author has also identified microstructural processes which he is modeling, and these are not the same in every case.

For these reasons, it is instructive to compare the models side-by-side. That is the intent of this chapter. As stated above, UCP models are multifaceted. They are different ‘things’ to different people. They can therefore be compared and discussed from many aspects. We choose to regard the models as having one ultimate use: as a material descriptor in a structural analysis program to predict stresses and deformations in real structures such as components in power plants. With this restricted end use in mind for the UCP models, the models

can be dissected into three major parts: conceptual model, mathematical representation, and computational implementation. Our comparisons will treat each of these three parts separately. Because of our restricted view of the models ultimately being used in structural analyses, we put great emphasis on the mathematical model and furthermore the multi-axial form of the model. The conceptual models described by the authors are then compared with the behavior which may be deduced from the mathematical equations. It is not enough that the author describe how he wants the model to behave. Everyone has good intentions. The real issue is what behavior the equations describe. A structural computer program knows nothing about the good intentions of any programmer.

The authors of the various chapters have gone to some length to present the microstructural motivation for their models, and for this reason have sometimes presented more variables than are absolutely necessary, have described more than one version of their model, or have stated the equations in a form which is unfamiliar. To facilitate a model comparison, we have in each case chosen one particular version of each model, have eliminated mathematically redundant variables, and have stated each in a differential form. This is identified as the skeletal form.

Krieg, in comparing eight UCP models which were available in 1977 when his study was published,<sup>1</sup> noted that by placing the models into a common framework they could be categorized as isotropic or kinematically hardening models. In the present work the number of models has been reduced to five but the models are more diverse than those considered by Krieg in that early work. For this reason, we have enlarged the definition of our skeletal model somewhat in order to accommodate that diversity. Throughout this chapter we have ignored the effects of temperature and how the various authors treat this behavior. We feel that thermal behavior is important but have omitted a discussion of this for lack of space.

In each case the authors have either explicitly or implicitly separated the behavior into bulk (or volumetric or spherical) behavior and deviatoric (or distortional or shear) behavior. The total strain rate  $\dot{\epsilon}_{ij}$  and total stress  $\sigma_{ij}$  are decomposed into deviatoric parts,  $\dot{\epsilon}'_{ij}$  and  $s_{ij}$ , and volumetric parts,  $\dot{\epsilon}_{kk}$  and  $\sigma_{kk}$ . These are written as

$$\dot{\epsilon}_{ij} = \dot{\epsilon}'_{ij} + \dot{\epsilon}_{kk}\delta_{ij} \quad (1.1)$$

$$\sigma_{ij} = s_{ij} + \sigma_{kk}\delta_{ij} \quad (1.2)$$

where summation convention is used here and throughout the chapter, and  $\delta_{ij}$  is the Kronecker delta. The Latin indices take the values 1, 2, and 3 in all cases. Some of the authors have included volumetric effects through the introduction of damage variables to account for the presence of defects such as voids in addition to the elastic volume change. For this comparison we are interested in only the dislocation related or deviatoric plastic behavior. Hence, if  $K$  is the elastic bulk modulus, then we can write

$$\varepsilon_{kk} = K\sigma_{kk} \quad (1.3)$$

The deviatoric strain rate is further decomposed into an elastic part and an inelastic part (denoted with a superscript p). These expressions are written as

$$\dot{e}_{ij} = \dot{e}_{ij}^e + \dot{e}_{ij}^p$$

where

$$\dot{e}_{ij}^e = s_{ij}/2G$$

and where  $G$  is the elastic shear modulus. These are combined into a single equation and solved for the stress rate:

$$s_{ij} = 2G(\dot{e}_{ij} - \dot{e}_{ij}^p) \quad (1.4)$$

The inelastic strain rate is taken to be of the form

$$\dot{e}_{ij}^p = F\xi_{ij} \quad (1.5)$$

where the tensor  $\xi_{ij}$  is taken by some authors to be  $s_{ij}$  and by others to be  $(s_{ij} - \alpha_{ij})$  where  $\alpha_{ij}$  is the back stress, a state variable for kinematic hardening models. The function  $F$  is taken to be of a different form by the authors of the models. One requirement on the function  $F$  is that the product  $F\xi_{ij}$  must involve all the state variables, either explicitly or implicitly, since changes in the stress are computed from eqn (1.4) which only involves the elastic shear modulus  $G$ , the externally imposed strain rate  $\dot{e}_{ij}$ , and the inelastic strain rate  $\dot{e}_{ij}^p$ . All material behavior must enter through  $\dot{e}_{ij}^p$ .

The remaining equations describing the material are generally evolutionary equations for the state variables. They are of the Bailey–Orowan form of a hardening term minus a recovery term:

$$\dot{\eta}_\phi = \mathbf{H}_\phi(s_{ij}, \eta_1, \eta_2, \dots, \dot{e}_{ij}^p) - \mathbf{G}_\phi(s_{ij}, \eta_1, \eta_2, \dots, \dot{e}_{ij}^p)\eta_\phi \quad (1.6)$$

where any particular state variable,  $\eta_\phi$ , is denoted with a Greek

subscript,  $\phi$ , to distinguish it from the Latin subscripts used to denote tensor components. Bold type is used to denote a tensor character of some order, including possibly zeroth order (a scalar). For a relatively simple form of these models, as noted by Krieg,<sup>1</sup> an evolutionary equation for the back stress would be

$$\dot{\alpha}_{ij} = H_{\alpha} \dot{e}_{ij}^p - G_{\alpha} \alpha_{ij} \quad (1.7)$$

where  $H_{\alpha}$  and  $G_{\alpha}$  are scalar functions of the stress, the strain rate, and the state variables. This would apply for kinematic models. An isotropic model would be described by a scalar equation of the form

$$R = H_R |\dot{e}_{ij}^p| - G_R (R - R_0) \quad (1.8)$$

where  $H_R$  and  $G_R$  are scalar functions of the stress, the strain rate, and the state variables;  $R_0$  is the base or fully recovered state for  $R_0$  (possibly zero) and  $||$  denotes a norm. Usually  $|\dot{e}_{ij}^p|$  is taken to be the effective plastic strain rate.

The reader should note that the simple set of relations given by eqns (1.4), (1.5), (1.7) and (1.8), with  $\xi_{ij} = s_{ij} - \alpha_{ij}$ ,  $F = C/R$ , and with  $C$ ,  $H_{\alpha}$ ,  $H_R$ , and  $R_0$  assuming constant values and  $G_{\alpha}$  and  $G_R$  homogeneous functions of only  $\alpha$  and  $R$ , respectively, will qualitatively predict much of the observed response of crystalline material in a variety of loading conditions. This is shown as follows. Consider the case where  $s_{ij}$  and  $\alpha_{ij}$  are initially zero and  $R$  is initially  $R_0$ . Then, if a stress is applied and held for some time, a transient phase is modeled where  $\alpha_{ij}$  and  $R$  build up to stationary values. We observe that if  $\alpha_{ij}$  and  $(R - R_0)$  are initially zero then initially the recovery terms in eqns (1.7) and (1.8) are zero and the hardening terms (the first terms in the two equations) are dominant. The rates  $\dot{\alpha}_{ij}$  and  $R$  are therefore large and positive. As  $\alpha_{ij}$  and  $R$  grow, the recovery or second terms in the equations become more dominant until the first and second terms become equal and the rates  $\dot{\alpha}_{ij}$  and  $R$  decrease to zero. Steady state values of  $\alpha_{ij}$  and  $R$  are then determined from eqns (1.7) and (1.8) with  $\dot{\alpha}_{ij}$  and  $R$  equal to zero. The values are

$$(\alpha_{ij})_{ss} = \frac{H_{\alpha}}{G_{\alpha}} (\dot{e}_{ij}^p)_{ss} \quad (1.9)$$

$$R_{ss} = R_0 + \frac{H_R}{G_R} |\dot{e}_{ij}^p|_{ss} \quad (1.10)$$

Furthermore, note from eqn (1.4) that if  $s_{ij}$  is held fixed then  $\dot{e}_{ij}^p$  is the

externally applied strain rate,  $\dot{\epsilon}_{ij}$ . For a suddenly applied load then a transient period of high strain rate (primary creep) is followed by a gradual reduction to a steady value as  $\xi_{ij}$  is reduced in eqn (1.5) due to an increase in  $\alpha_{ij}$  to its steady state value. This demonstration of primary creep behavior, as well as the characteristic of representing steady state creep as a state of dynamic equilibrium of balanced hardening and recovery, are thus inherent properties of UCP models. This same behavior will apply to the more general case where the general evolutionary equation (1.6) is used to describe several state variables and the functionals  $\mathbf{H}_\phi$  and  $\mathbf{G}_\phi$  are suitably restricted. In addition to the steady state described by eqns (1.9) and (1.10) for the case of constant stress, models with these types of evolutionary equations predict a similar steady state or 'saturation' stress under constant true strain rate loading conditions. This simply means that in uniaxial stress or tension, for example, the stress will asymptotically approach a constant value consistent with the steady state values in eqns (1.9) and (1.10) and given by the inversion of eqn (1.5) for the stress. The behavior is observed in many materials, at least those in which distortions remain the only mechanism of plastic deformation, and in particular at high temperatures where steady state can be reached before failure occurs.

A second general behavior which may be illustrated concerns unloading. Consider a system in secondary creep where the applied stress is suddenly reduced to zero. If  $F\xi_{ij}$  were a homogeneous function of  $s_{ij}$  then  $\dot{\epsilon}_{ij}^p$  would suddenly become zero also, a behavior which is usually not observed physically. But if  $F\xi_{ij}$  were a homogeneous function of  $(s_{ij} - \alpha_{ij})$  then the plastic strain rate  $\dot{\epsilon}_{ij}^p$  would be non-zero and would be directed in the minus  $\alpha_{ij}$  direction, i.e. opposite to the direction in which the stress was originally applied. This would model anelastic strain recovery. Under this zero load condition, the magnitude of  $\dot{\epsilon}_{ij}^p$  given by eqn (1.5) is usually small so that, in passing from the steady state (where the rates given by eqns (1.7) and (1.8) are zero) to the zero stress state, the second terms on the right sides of eqns (1.7) and (1.8) are dominant. The rates of the state variables are roughly  $\dot{\alpha}_{ij} = -G_\alpha \alpha_{ij}$  and  $\dot{R} = -G_R(R - R_0)$ . These rates would decrease as  $\alpha_{ij}$  and  $(R - R_0)$  decrease. This decrease in  $\alpha_{ij}$  and  $(R - R_0)$  would result in a rate  $\dot{\epsilon}_{ij}^p$  from eqn (1.5) which would reduce in magnitude with time. This strain recovery behavior is thus a general characteristic of UCP models.

General behavior of UCP models, especially concerning tests for

determining material constants for general UCP models, is presented in Chapter 5 (Krieg *et al.*). Some very specific but simple kinematic hardening models are shown to have analytic solutions to some common loading cases.

In the remainder of this chapter we will consider each of the five UCP models in turn. We begin with the model nearest to the skeletal model and proceed to that least like the skeletal model. We do not mean to imply that nearness to the skeletal model correlates with quality of the model (either good or bad). The first models are simply easier to discuss under our ground rules.

The effect of temperature in the models will not be discussed for lack of space, but it is worth noting that in four of the models, namely those of Krieg *et al.*, Miller, Korhonen *et al.* and Gittus (Chapters 5, 3, 2 and 4, respectively) temperature is an explicit variable in the equations, whereas in the other model (that of Bodner, Chapter 6) the basic equations treat isothermal behavior, and effects of temperature are introduced by making the material constants temperature-dependent.

## 2. MODEL BY KRIEG, SWEARENGEN AND JONES

The model by Krieg, Swearngen and Jones is described in mathematical form by their eqns (36)–(40) which are repeated here for convenience:

$$\begin{aligned}
 s_{ij} &= 2G(\dot{e}_{ij} - \dot{e}_{ij}^p) \\
 \dot{e}_{ij}^p &= A_2 \lambda^m \exp(-Q/RT) [\sinh(A_1 \xi)]^p (\xi_{ij}/\xi) \\
 \dot{\alpha}_{ij} &= A_5 \dot{e}_{ij}^p - A_4 [\exp(A_3 \alpha^2/RT) - 1] \alpha \alpha_{ij} \\
 \dot{\lambda} &= -\beta(\lambda - A_0) \dot{e}^p \\
 \dot{e}^p &= \sqrt{(2/3) \dot{e}_{ij}^p \dot{e}_{ij}^p} = (2/3) |\dot{e}_{ij}^p| \\
 \xi_{ij} &= s_{ij} - \alpha_{ij}; \quad \xi = |\xi_{ij}|
 \end{aligned} \tag{2.1}$$

This set of equations is already in the form of the skeletal model. The inelastic strain rate vector is taken to be in the direction of the effective stress,  $\xi_{ij}$ . The model is an isotropic-kinematic hardening model with a scalar state variable,  $\lambda$ , and a tensor state variable,  $\alpha_{ij}$ . Note, however, that the isotropic variable  $\lambda$  decreases as the material strain hardens. Hardening of the kinematic variable is linear in the

inelastic strain rate and is in a direction parallel to the inelastic strain rate. Hardening of the isotropic variable is initially linear in the magnitude of the inelastic strain rate. The hardening is reduced, however, as  $\lambda$  decreases. It saturates at a final level of  $A_0$ . There is no thermal recovery term for the isotropic variable. Recovery of the back stress,  $\alpha_{ij}$ , is in the direction of  $\alpha_{ij}$ .

The equation for the inelastic strain rate contains the stress and all state variables explicitly. It is similar to the expression which has been used for some years by Miller as noted in Section 3. The hyperbolic sine function raised to a power is a convenient form for creep which has been used in conventional creep models. It spans the range between power-law creep and power-law breakdown.

A unique aspect of the model concerns the isotropic hardening variable,  $\lambda$ . The authors have made an effort to identify  $\lambda$  as the mean free slip length, a physically observable quantity which the authors suggest should be characterized independently from the experimentally observed behavior of mechanical stresses and strains. The advantage of that approach is that independent observations can be made so that eqn (2.1d) can be completely characterized without any knowledge of the form of the remainder of the constitutive equations. This approach is somewhat different from the usual approach of merely identifying deformation mechanisms in order to define the form of the equation. In the conventional approach then all constants in the resulting equation are evaluated, not by observing the mechanism but rather by fitting the mechanically observable stress and strain behavior. It is unfortunate that the authors have not demonstrated the viability of the approach they present. It remains to be shown.

One shortfall of the model concerns the form of the equation chosen for  $\lambda$ . In particular, there is only a hardening term, no recovery term. The second problem is that the saturation value for  $\lambda$  is  $A_0$ , chosen by the authors to be a constant. This is possibly too restrictive and  $A_0$  should possibly be made a function of stress. It is also felt that the evolutionary equation for  $\lambda$  should have involved temperature. If the basic approach used by the authors is indeed viable, more work is needed to prove or disprove the need for such thermal terms.

One of the more significant positive aspects of this model is that it is a three-dimensional generally multiaxial formulation. This model was carefully formulated in three dimensions properly accounting for invariance requirements, as opposed to scaling a one-dimensional

model to three dimensions. This enables the model to be used in the analysis of finite deformation problems.

In summary, the model is mathematically concise. It has a unique character in that the physical identification of the cause for isotropic hardening has been carried to an extreme. The authors suggest direct experimental observation of the mean free slip length in order to characterize it, rather than determining the constants in such a way that the observable stress and strain behavior is modeled in a 'best' manner. The approach has definite advantages in characterizing the model, and would open new means of tying the mechanical behavior to more basic physical microstructure. Unfortunately, the authors have stopped short of demonstrating the utility of the process.

### 3. MODEL BY MILLER

Miller's model is presented in two different forms, depending upon the application. In the case where deformation is considered over large ranges in strain rate and solute drag can result in the observed phenomena of negative strain rate sensitivity, the model used is MATMOD2V with solute drag. This model has two internal state variables, one tensor valued kinematic variable,  $R_{ij}$ , and one scalar or isotropic variable,  $F_{\text{def}}$ . The variable  $F_{\text{def}}$  is coupled to the two variables representing the effect of solute atoms on the motion of dislocations,  $F_{\text{sol},1}$  and  $F_{\text{sol},2}$ . These are not independent state variables in that they are functions of the state variables  $\dot{e}_{ij}$  and  $T$ .

The model is consistent with the skeletal structure in that linear deviatoric elastic behavior is assumed. From eqns (M5.46)† and (M5.47)

$$\dot{s}_{ij} = 2G(\dot{e}_{ij} - \dot{e}_{ij}^p) \quad (3.1)$$

where

$$\dot{e}_{ij} = \dot{e}_{ij}^e + \dot{e}_{ij}^p \quad (3.2)$$

The stresses in the model are all scaled with respect to Young's modulus,  $E$ , hence the inelastic flow is assumed to occur in the direction analogous to  $\xi_{ij}$  or

$$\dot{e}_{ij}^p = \lambda \frac{\xi_{ij}}{|\xi_{ij}|} \quad (3.3)$$

† Equation nos. preceded by M refer to the numbers used in Chapter 3 of this volume (by Miller).

where

$$\hat{\xi}_{ij} = \frac{s_{ij}}{E} - R_{ij} \quad (3.4)$$

Then  $\lambda$  is given as

$$\lambda = B\Theta' \left\{ \sinh \left( \frac{|\hat{\xi}|}{f \left( \frac{\lambda}{\Theta'_{\text{sol},1}} \right) + F_{\text{def}} \left[ 1 + f \left( \frac{\lambda}{\Theta'_{\text{sol},2}} \right) \right]} \right)^{1.5} \right\}^n \quad (3.5)$$

and the evolution equations (M5.48) and (M5.49) for  $R_{ij}$  and  $F_{\text{def}}$  become

$$\dot{R}_{ij} = H_i \exp \left\{ -H_3 \frac{R_{kl} \hat{\xi}_{kl}}{|\hat{\xi}_{kl}|} \right\} \left[ \dot{\epsilon}_{ij}^p - \frac{3}{2} B\Theta' \left\{ \sinh(A_1 |R_{ij}|)^n \frac{R_{ij}}{|R_{ij}|} \right\} \right] \quad (3.6)$$

and

$$\dot{F}_{\text{def}} = H_2 \left( C_2 + |R_{ij}| + \frac{A_2}{A_1} F_{\text{def}}^{1.5} \right) |\dot{\epsilon}_{ij}^p| - H_2 C_2 B\Theta' \left\{ \sinh(A_2 F_{\text{def}}^{1.5}) \right\}^n \quad (3.7)$$

Each of these evolution equations includes static as well as dynamic recovery effects. The tensor variable hardens in the direction of inelastic flow and recovers in the direction of the variable as in the skeletal model. For the case of cyclic deformation the kinematic variable  $R_{ij}$  is decomposed into a short-range variable  $R_{ij}^a$  and a long-range variable  $R_{ij}^b$ . The short-range kinematic variable saturates (reaches a steady state) early and allows a more accurate description of the shape of the hysteresis loop upon cyclic loading. This, in conjunction with an analogous decomposition of  $F_{\text{def}}$  into  $F_{\text{def},\rho}$  and  $F_{\text{def},\lambda}$ , allows the prediction of strain softening in cyclic loading. Similar evolution equations are proposed for these variables.

These additional variables allow Miller's model to predict both rapid transient effects as well as long-time phenomena. Through a physically motivated coupling of the internal variables, the model is able to predict cyclic strain softening as well as hardening. This model is the only one included which is capable of describing metastable behavior such as unidirectional strain softening. The structure of the model is strongly influenced by the underlying mechanisms. Unfortunately, this additional predictive capability is a result of additional material parameters which in turn requires a larger number of independent tests in order to determine these parameters. The model suffers the

same numerical stiffness problems associated with implementation into finite element codes, which is also common to the other models.

One very positive aspect of this model is the detail in which underlying physical mechanisms are modeled. Having once determined the parameters of the model for a particular alloy, the effects of material changes such as additional solute content may be included in this model with a limited number of additional tests. This allows the changes in macroscopic response due to composition changes to be determined more easily. This complex model could then possibly be used to determine parameters for a numerically efficient model, thereby decreasing the required number of experiments.

#### 4. MODEL BY BODNER

The Bodner model is based upon an assumption of small strain and an assumption of the additive decomposition of the total strain rate into elastic and plastic parts, consistent with the basic skeletal structure. Bodner also introduces dilatational effects through a damage variable. As stated previously, we are only considering the deviatoric portions of the models in this comparison. Through the additivity of the strain rates along with the assumption of linear elasticity, the constitutive equation for the deviatoric stress,  $s_{ij}$ , can be written

$$\dot{s}_{ij} = 2G(\dot{\epsilon}_{ij} - \dot{\epsilon}_{ij}^p) \quad (4.1)$$

The inelastic flow is assumed in the direction of the deviatoric stress:

$$\dot{\epsilon}_{ij}^p = \gamma \frac{s_{ij}}{\sqrt{s_{ij}s_{ij}}} \quad (4.2)$$

where

$$\gamma = D_0^2 \exp\left(-\left[\frac{Z^2}{3\sqrt{s_{ij}s_{ij}}}\right]^n\right) \quad (4.3)$$

This assumption of directionality is a major difference between this model and the models by Krieg *et al.* and Miller. This is a result of the manner in which Bodner introduces directional hardening without a Prager type kinematic hardening variable. The assumption of the direction of plastic flow leads to the same difficulties as in the case of the Li model for considerations of non-proportional loading. In the

case of proportional loading this assumption is equivalent to an assumption that the plastic flow occurs in the direction of the deviatoric stress minus the back stress for forward loading. When the stress is dropped to zero during simulation of creep, an additional strain rate is required to predict so-called anelastic behavior. This is rather unsatisfying since this response is the result of the reverse flow of dislocations, the same mechanism which causes the forward creep response.

The variable  $Z$  is linearly decomposed into the sum of a directional part  $Z^D$  and an isotropic part  $Z^I$ :

$$Z = Z^D + Z^I \quad (4.4)$$

where

$$Z^D = \beta_{ij} \frac{\sigma_{ij}}{\sqrt{\sigma_{mn}\sigma_{mn}}} \quad (4.5)$$

and where  $\beta_{ij}$  is a directional hardening variable to be described below. Notice that, although Bodner introduces both scalar and tensor valued internal variables into his constitutive model, they are introduced in a rather unique manner. The component of the directional variable in the direction of the total stress is added to the isotropic variable. The evolution equations for the isotropic variable  $Z^I$  and the directional variable  $\beta_{ij}$  follow a hardening minus recovery format as in the skeletal model. The evolution of the isotropic variable is given by eqn (B4.13)<sup>†</sup>

$$\dot{Z}^I = m_1(Z_1 - Z^I)\dot{W}^p - A_1 Z_1 \left( \frac{Z^I - Z_2}{Z_1} \right)^{r_1} \quad (4.6)$$

In this equation  $\dot{W}^p$  is the rate of plastic work,  $Z_1$  is the saturation value for the variable  $Z^I$ ,  $Z_2$  is the minimum value of this variable for a particular temperature,  $A_1$  and  $r_1$  are temperature dependent material parameters, and  $m_1$  is the temperature independent hardening parameter. Notice that the model accounts for both static and dynamic recovery effects, the second term representing static recovery while the negative part of the first term represents dynamic recovery.

The directional hardening term  $\beta_{ij}$  does not appear as a back stress or kinematic hardening variable, but rather the component of this variable in the direction of the stress is added to the isotropic variable

<sup>†</sup> Equation nos. preceded by B refer to the numbers used in Chapter 6 of this volume (by Bodner).

as shown in eqn (4.4). The evolution of  $\beta_{ij}$  is given by:

$$\dot{\beta}_{ij} = m_2 \left( Z_3 \frac{s_{ij}}{\sqrt{s_{ij}s_{ij}}} - \beta_{ij} \right) \dot{W}_p - A_2 Z^1 \left( \frac{\sqrt{\beta_{ij}\beta_{ij}}}{Z^1} \right)^{r_2} \frac{\beta_{ij}}{\sqrt{\beta_{ij}\beta_{ij}}} \quad (4.7)$$

As in eqn (4.6) for the evolution of the isotropic variable,  $m_2$  represents the hardening rate and  $Z_2$  and  $r_2$  are temperature dependent parameters. In the evolution of the directional internal variable the hardening depends upon the magnitude of the plastic work rate as opposed to the tensor valued plastic strain rate as is the case in most of the other models under consideration. The positive aspect of this is the ability of the model to describe a material in which the hardening rate is an increasing function of the stress level. Also this feature allows the prediction of strain rate history effects as have been reported during strain rate change tests of OFHC copper.<sup>3</sup> In these experiments the stress jump due to a strain rate change was an increasing function of the strain at which the change was performed. This behavior could not be predicted by a model which hardens linearly with the plastic strain rate. As in the isotropic variable, both dynamic and static recovery effects are considered. The direction of both types of recovery is assumed to be in the direction of the variable  $\beta_{ij}$ .

One of the unique features of this model is the manner in which the Bauschinger effect can be described without introducing a subtractive kinematic hardening variable. In eqn (4.4), Bodner introduces directional hardening by adding to the isotropic hardening variable the contribution of a tensor variable,  $\beta_{ij}$ , in the direction of deviatoric stress. This tensor variable  $\beta_{ij}$  is quite similar to the kinematic hardening variables used in other models. In particular, the form of the evolution equation is very similar. The manner in which the variable predicts the Bauschinger effect is best illustrated by considering a somewhat simplified system. In the case of small strain cyclic analysis, the effects of recovery are negligible on the first cycle. We therefore consider the evolution equations for  $Z^1$  and  $\beta_{ij}$ , of the simplified form without recovery terms:

$$\dot{Z}^1 = Z_1 \dot{W}_p \quad (4.8)$$

$$\dot{\beta}_{ij} = m_z Z_3 \dot{W}_p \frac{s_{ij}}{\sqrt{s_{ij}s_{ij}}} \quad (4.9)$$

Now consider the stress-strain behavior depicted in Fig. 1, produced by loading at a constant strain rate from A to C and then

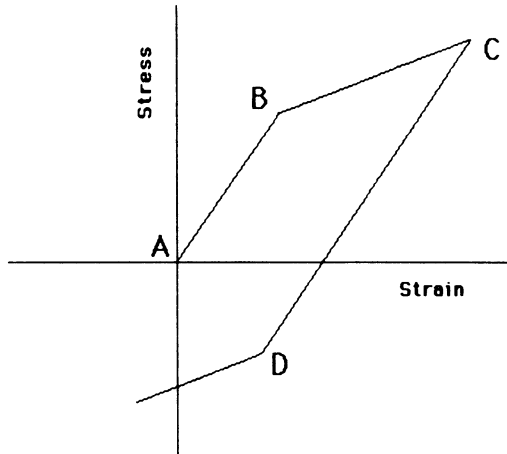


**Fig. 1.** Schematic representation of the stress-strain response for cyclic loading conditions.

reverse loading at the same magnitude of strain rate from C to E. The inelastic strain rate will be near zero from A to B and C to D, and nearly equal to the total strain rate from B to C and D to E. Let us represent the value of each of the variables at point C by  $\sigma^C$ ,  $\beta_{ij}^C$ ,  $Z_D^C$ ,  $Z_Z^C$ . Now, during unloading from C to D, the plastic work rate  $\dot{W}_p$  is essentially zero. Therefore the values of the variables  $\beta_{ij}$  and  $Z_I$  are nearly identical to the values of each at point C, or

$$Z_I^D \doteq Z_I^C \quad (4.10)$$

$$\beta_{ij}^D \doteq \beta_{ij}^C \quad (4.11)$$

However, since the stress is now negative we see from eqn (4.5) that

$$Z_D^D \doteq -Z_D^C \quad (4.12)$$

Therefore, the plastic strain rates at C and D respectively are given by

$$\gamma^C = D_0^2 \exp\left(\frac{-(Z_I^C + Z_D^C)^2}{3|\sigma^C|}\right) \quad (4.13)$$

$$\gamma^D = D_0^2 \exp\left(\frac{-(Z_I^C - Z_D^C)^2}{3|\sigma^C|}\right) \quad (4.14)$$

We see that for this case the directional hardening variable  $Z_D$  behaves analogously to the kinematic hardening variable since it is an

additive contribution to the hardening at C while changing signs at D and acting to decrease the total hardening, thus resulting in the prediction of the Bauschinger effect.

Bodner suggests modifications of this system for two specific considerations. In situations where the stress-strain curve is too square upon stress reversal, the hardening parameter  $m_2$  in the evolution of the directional variable is modified to be of the form

$$m_2 = \left( \frac{\bar{m}_2}{2} \right) [1 + \exp(-m_3 Z^D)] \quad (4.15)$$

This is similar to the approach suggested in the Krieg, Swearngen and Jones model. To account for increased directional hardening for non-proportional loading, Bodner introduces a variable to account for the situation when the direction of the rate of hardening of the directional variable differs from the current value of the variable itself (see eqns (B4.18–25)). This is accomplished by introducing a direction cosine between these directions and appears to be a promising approach.

Neglecting these last two features of the model, Bodner introduces the material parameters  $D_0$ ,  $n$ ,  $Z_0$ ,  $Z_2$ , and  $A_1$  which are temperature dependent as well as the temperature independent parameters  $m_1$ ,  $m_2$ ,  $Z_1$ ,  $Z_3$ ,  $r_1$ , and  $r_2$ . These parameters are determined from uniaxial stress tests under conditions of constant strain rate, creep, and cyclic loading at various strain rates and temperatures. Although the number of parameters appears quite large at first glance, they are determined from a relatively small group of different types of tests. It is important to remember that the number of parameters is not nearly as important as the number of independent tests required to determine the parameters.

This model has been implemented into finite difference and finite element codes and has effectively accounted for rate and temperature effects, in particular in impact problems. The model suffers from the same stiffness problems as the other UCP models discussed in this work and therefore its use becomes very expensive when considering more complex analyses.

## 5. MODEL BY KORHONEN, HANNULA AND LI

The Korhonen, Hannula and Li (KHL) model is stated in four forms: (A) Hart's model for grain matrix deformation; (B) an extension of

Hart's model to a multiaxial loading case; (C) an extension of Hart's model for transient deformation; and (D) an extension of the state variable description for grain boundary sliding. The comments here will be centered on the form B of the basic model, called the KHL-B model.

The KHL-B model is described by eqns (1)–(7) and (10)–(20) of Chapter 2 (Korhonen, Hannula and Li). These 18 equations involve the variables  $s_{ij}$ ,  $s_{ij}^a$ ,  $s_{ij}^f$ ,  $\sigma$ ,  $\sigma^a$ ,  $\sigma^f$ ,  $e_{ij}^p$ ,  $a_{ij}$ ,  $\alpha_{ij}$ ,  $\varepsilon$ ,  $a$ ,  $\alpha$ ,  $\sigma^*$ ,  $T$  and time. In the three-dimensional case, this would involve 45 scalar components, which in turn implies a considerable computer memory storage size if the model were used in structural analyses. For a structural model of 4000 twenty-node brick elements ( $20 \times 20 \times 10$ ) with eight Gauss point integration in each brick, this would require a minimum storage of  $4000 \times 8 \times 45$  or 1.4 million locations just for the material information! This turns out, however, to be only an apparent shortcoming of the KHL-B model. Most of the variables listed appear only as a convenience in explaining the physical motivation for the model and may be eliminated by mathematical manipulations. This has been carried out and the details are recorded in Appendix A at the end of this chapter. The final equations are listed in the appendix and are repeated here for convenience:

$$\dot{s}_{ij} = 2G(\dot{e}_{ij} - \dot{e}_{ij}^p) \quad (5.1a)$$

$$\dot{e}_{ij}^p = (3/2)\dot{a}^*(T)\left(\frac{\sigma - \sigma_a}{G}\right)^M \frac{s_{ij}}{\sigma} \quad (5.1b)$$

$$\dot{\sigma}_a = \mathcal{M} \left[ \dot{a}^*(T) \left(\frac{\sigma - \sigma_a}{G}\right)^M - \left(\ln \frac{\sigma^*}{\sigma_a}\right)^{-1/\lambda} \left(\frac{\sigma^*}{G}\right)^m f e^{-Q/RT} \right] \quad (5.1c)$$

$$\frac{d}{dt}(\ln \sigma^*) = \Gamma^*(\sigma_a, \sigma^*) - R(\sigma^*, T) \quad (5.1d)$$

$$\sigma = \sqrt{1.5s_{ij}s_{ij}} \quad (5.1e)$$

This is a complete set of equations describing the KHL-B model where  $a^*$  is a function of temperature,  $\Gamma^*$  and  $R$  are functions which depend upon the material, and  $G$ ,  $\mathcal{M}$ ,  $M$ ,  $\lambda$ ,  $m$ ,  $f$  and  $Q$  are material constants.

As noted above, the KHL-B model involves only the variables  $s_{ij}$ ,  $\dot{e}_{ij}$ ,  $\sigma_a$ ,  $\sigma^*$ ,  $T$  and time. (Here we assume that  $\dot{e}_{ij}^p$  is eliminated by substituting the second equation into the first.) The 45 apparent scalar components have collapsed into 16. Since  $T$ , time and  $\dot{e}_{ij}$  are independent variables in the usual displacement formulation of a finite

element structural code, only eight storage locations are required at each point in the body where stresses are calculated in a fully three-dimensional code. Contrary to our initial evaluation, the KHL-B model is very attractive in terms of storage requirements when it is implemented in a structural computer program!

The working equations listed above reveal a considerable amount about the behavior of the model. At first it appears that we have a kinematic-isotropic UCP model where  $\sigma_a$  is the back stress and  $\sigma^*$  is an isotropic hardening parameter.

The quantity  $\sigma_a$  (with an exception to be discussed below) has the usual role of a back stress for the uniaxial stress case for which the model was developed. The first term in the evolutionary equation for  $\sigma_a$  is the scalar strain rate  $\dot{\epsilon}_p$  and is the usual hardening term for the uniaxial case. The quantity  $\dot{\epsilon}_p$  normally is positive when the test specimen is being stretched and negative when the loading direction reverses. The second term in eqn (5.1c) is a recovery term. This uniaxial hardening and recovery behavior for  $\sigma_a$  is to be expected of a back stress. Unfortunately, the multiaxial model has a somewhat different behavior.

The usual back stress would become aligned in the direction in which the deviatoric stress is acting. As noted in the discussion on the skeletal model, the back stress carries the integrated history of deformation and hence, in contrast to  $s_{ij}$ , cannot be instantly changed without accompanying 'instant' deformations of the material. That behavior is not characteristic of the KHL-B model. Let us consider an example.

Consider the case where a stress state  $s_{11} = 100$  MPa has been applied for some time with other components zero. From eqn (5.1e) we find  $\sigma = 122$  MPa, and we furthermore choose a material and prior history such that  $\sigma_a$  has grown to a value  $\sigma_a = 100$  MPa. Then the plastic strain rate vector from eqn (5.1b) is  $\dot{\epsilon}_{11}^p = C(22)^M$  and the other components are zero. The constant  $C$  is a combination of material constants. Values of  $M$  range over 3 to 15, so if we choose  $M = 5$  then  $\dot{\epsilon}_{11}^p = C(5E6)$ . Now the stress state is suddenly changed to  $s_{22} = 0.1$  MPa with the other components zero. From eqn (5.1e) we have  $\sigma = 0.12$  MPa but since  $\sigma_a$  cannot change instantly (as noted in eqn (5.1c)) the value of the back stress is still  $\sigma_a = 100$  MPa. From eqn (5.1b) we now find  $\dot{\epsilon}_{22}^p = C(100)^M$  or with  $M = 5$  we have  $\dot{\epsilon}_{22}^p = C(1E10)$ . The other components of  $\dot{\epsilon}_{ij}^p$  are all zero. This is a large plastic strain rate in the 22-direction for a near-zero  $s_{22}$  stress. But if the stress state is changed only slightly to  $s_{33} = 0.1$  MPa or  $s_{11} =$

$-0.1$  MPa with the other components zero in each case, the strain rate will change to  $\dot{\epsilon}_{33}^p = C(1E10)$  and  $\dot{\epsilon}_{11}^p = -C(1E10)$ , respectively, with the other components zero. These are drastic changes in the plastic strain rate for trivial changes in the near-zero stress state.

It appears that the basic difficulty with the KHL-B model is that the inelastic strain rate has been chosen to be in the direction of the deviatoric external stress. This assumption is used in conventional multiaxial creep models where plasticity and creep are assumed to be independent processes. It is well known that these conventional models have severe shortcomings, but the additional complexities of a unified creep-plasticity model accentuate the shortcomings of that directionality assumption for the example illustrated here.

A second shortcoming of the KHL-B model is that the quantity  $\dot{\epsilon}^p$  is defined to be proportional to the magnitude (or  $L_2$  norm) of the strain rate tensor  $\dot{\epsilon}_{ij}^p$  as given in eqn (16) of Chapter 2. This can only result in a positive  $\dot{\epsilon}^p$ . There cannot be a negative  $\dot{\epsilon}^p$ . The evolutionary equation for  $\sigma_a$  given by eqn (5.1c) has a hardening first term and a recovery second term. Because of the definition of  $\dot{\epsilon}^p$ , however, the first term is always positive. No matter which direction  $\dot{\epsilon}_{ij}^p$  (or  $s_{ij}$ ) is acting, it will always act to increase  $\sigma_a$ . Only the recovery term can act to decrease  $\sigma_a$ . This behavior is unique to the multiaxial KHL models and is not seen in the uniaxial model.

The state variable  $\sigma^*$  enters into the equations in a manner which is unique to this method. As noted in the discussion of the skeletal model, eqn (5.1a) and a corresponding volumetric equation are the only equations which explicitly involve the physically independent and directly measurable quantities strain and external stress. The parameters in the UCP models make their presence felt via the equation for  $\dot{\epsilon}_{ij}^p$ . As noted in eqn (5.1b), the state variable  $\sigma^*$  only influences this equation indirectly through its influence on  $\sigma_a$ . Furthermore, it does not enter into the dominant hardening term in the evolutionary expression for  $\sigma_a$  but only influences recovery of  $\sigma_a$ . The recovery term in eqn (5.1c) is rather complex, but over a limited range of  $(\sigma^*/\sigma_a)$  the recovery term is roughly a power of  $\sigma^*$  times a power of  $\sigma_a$  times a constant. A possible approximation would be  $(\sigma_a \sigma^*)^3$  times a constant. To a first approximation when  $\sigma^*$  is constant, the scalar evolutionary equation for  $\sigma_a$  has a hardening term proportional to plastic strain rate and a recovery term of the order of  $\sigma_a^3$ . It should be noted that this approximation is the form of the evolutionary equation used to describe the back stress in the skeletal model.

This description of the influence of  $\sigma^*$  is admittedly simplistic. The

recovery is accelerated as  $\sigma^*$  grows and slows as  $\sigma^*$  decreases. Equations (5.1c) and (5.1d) are a coupled pair of non-linear ordinary differential equations which must be solved simultaneously. The explanation outlined above only holds when  $\sigma^*$  is nearly constant or when  $\sigma_a$  enters eqn (5.1d) in a weak manner. The simplistic explanation also is not meant to imply that  $(\ln \sigma^*/\sigma_a)^{-1/\lambda}(\sigma^*/G)^m$  should be replaced by a power of  $\sigma^*$  times a power of  $\sigma_a$ . This approximation is merely used in order to place it in context with the skeletal model and hence compare it with the other models. The success of the KHL models could be used to argue that we have merely approximated true physical behavior in our explanation.

The reader should be aware that, although some quirks in this model have been pointed out here, the criticisms have been with the multiaxial generalization which has been applied to the uniaxial model. No criticisms have been directed at the underlying uniaxial model or its micromechanical foundation. The reader should also be aware that the difficulties noted might possibly be eliminated by making small changes in critical places in the mathematical formulation. Speculation on how the multiaxial generalization should be made is beyond the scope of this chapter. It is important, however, to note that the basic uniaxial model is untouched.

## 6. MODEL BY GITTUS

The model described by Gittus<sup>2</sup> has a characteristic which is distinctly different from the other models, and for that reason alone is worth studying. The creep rate  $\dot{\epsilon}$  is described by the equation

$$\dot{\epsilon} = gb\rho v \quad (6.1)$$

where  $b$  is the Burgers vector,  $\rho$  is the density of gliding dislocations and  $v$  is the velocity of these dislocations. The other models can usually be stated in terms of a back stress and a drag stress as state variables, but the Gittus model has defied our attempts to cast it into that form. His model is tied directly to eqn (6.1) and in particular he has used the mobile dislocation density,  $\rho$ , as a fundamental state variable. The development which he follows is principally one of writing expressions which characterize each factor in eqn (6.1) and combining these into a set of governing equations.

In an apparent effort to stay very near the physical observations

from uniaxial testing, Gittus has elected to cast his equations in terms of principal directions. Unfortunately, this places severe restrictions on the implementation of this model into a general three-dimensional structural analysis code. The axes chosen are principal directions of both the stress and the strain tensors, and there is no provision for rotation of these axes with respect to the body as time passes. Because the principal axes of stress and strain generally are not coincident and the axes generally rotate as a body deforms in a visco-plastic manner, the formulation is confined to radial loading/unloading.

The equations governing the Gittus model are presented in his chapter (Chapter 4) and condensed in Appendix B. An attempt was made to state his model in a differential form so that it could be placed in the form of the skeletal model and directly compared with other models. In his chapter several of the working equations are stated in integrated form so that they are applied over a time step in his computer program where certain quantities are assumed to be constant over the step. The differential formulation given as eqn (B16) in Appendix B then is a set of equations which are distinct from his working equations. They are merely the differential form of his which have subsequently been reworked. Equations (B17) are repeated here for convenience; they are for a fixed temperature case:

$$\begin{aligned} \dot{s} &= 2G(\dot{\epsilon} - \dot{\epsilon}_p) \\ \dot{\epsilon}_p &= \left[ \frac{B\dot{\epsilon} + \sqrt{1.5} \frac{\bar{\rho}_F}{\bar{\rho}_L} - \frac{c}{\mu} \frac{\partial \bar{\rho}_\infty}{\partial s}}{1 + \nu B(\sqrt{2/3} s)^n} \right] (\sqrt{2/3} s)^n \nu \quad (6.2) \\ \dot{\bar{\rho}}_F &= -\mu(\bar{\rho}_F - \bar{\rho}_L) \\ \dot{\bar{\rho}}_R &= -\mu(\bar{\rho}_R - 1) \end{aligned}$$

where

$$\begin{aligned} \mu &= \lambda \nu (\sqrt{2/3} s)^n - \gamma \\ \bar{\rho}_L &= \frac{\lambda \nu ((2/3)s)^n \bar{\rho}_\infty - \gamma}{\lambda \nu ((2/3)s)^n - \gamma} \\ B &= B_0(1 - \bar{\rho}_\infty) \end{aligned}$$

and where  $\bar{\rho}_\infty$  as well as  $\partial \bar{\rho}_\infty / \partial s$  are functions of stress and where  $G$ ,  $B_0$ ,  $C$ ,  $n$ ,  $\nu$ ,  $\lambda$  and  $\gamma$  are functions of temperature only.

As previously stated, the mobile dislocation density is used as a state variable. Since dislocations which are blocked due to some obstruction

are readily moved back when the strain rate is reversed, the mobile dislocation density is characterized by a value in the forward direction,  $\bar{\rho}_F$ , and one in the reverse direction,  $\bar{\rho}_R$ . Gittus has elected to use only these two scalar state variables even in the multiaxial case. A set of rules are given which describe how to find new values of  $\bar{\rho}_F$  and  $\bar{\rho}_R$  when the direction of straining is changed. Note that the mobile dislocation density only enters into the working equations (the first two of eqns (6.2)) in the second term of the numerator of eqn (6.2b). If this term is dominant, then the inelastic strain rate is roughly proportional to the mobile forward dislocation density. One could imagine that the mobile dislocation density could somehow be restated in full tensor form,  $\rho_{ij}$ . This leads to the question of how  $\rho_{ij}$  would be related to the back stress,  $\alpha_{ij}$ , of the other models.

There are fundamental differences in the character of  $\alpha_{ij}$  and a conjectured  $\rho_{ij}$ . This is perhaps best illustrated by the behavior of the mobile dislocation densities,  $\bar{\rho}_F$  and  $\bar{\rho}_R$ , and the back stress,  $\alpha_{ij}$ , during a standard creep test. Consider a fully annealed initially isotropic metal which would initially have  $\alpha_{ij} = 0$  and a low initial value of  $\bar{\rho}_F$ . The stress in the specimen is then raised to some value, say  $s_0$ , and held at that stress level. During the process of raising the stress, both the back stress and the mobile dislocation density increase. When the stress is held fixed then the back stress continues to increase toward  $s_0$  but the forward mobile dislocation density decreases. This is schematically illustrated in Fig. 2. Thus we conclude that  $\bar{\rho}_F$  and  $\alpha_{ij}$  cannot be simply related. It might be noted, however, that the general behavior of the reverse mobile dislocation density as noted in the figure does have the same general character as the back stress, increasing throughout the test. It is misleading, however, to draw a parallel between the reverse mobile dislocation density and the back stress in this example where there is no strain reversal because  $\bar{\rho}_R$  does not enter into the governing eqns (6.2a) or (6.2b), either explicitly or implicitly. In contrast, the back stress always enters into the stress rate equation directly by way of the inelastic strain rate. Thus one cannot usefully draw any parallels between  $\bar{\rho}_R$  and  $\alpha_{ij}$ .

The fundamental difference in behavior of the mobile dislocation density and the back stress, as illustrated by this example, leads to the conclusion that there is no simple mathematical relation between the two.

Because of the above observation, it is unwise to force the system of eqn (6.2) into the form of the skeletal model. There are, however, a

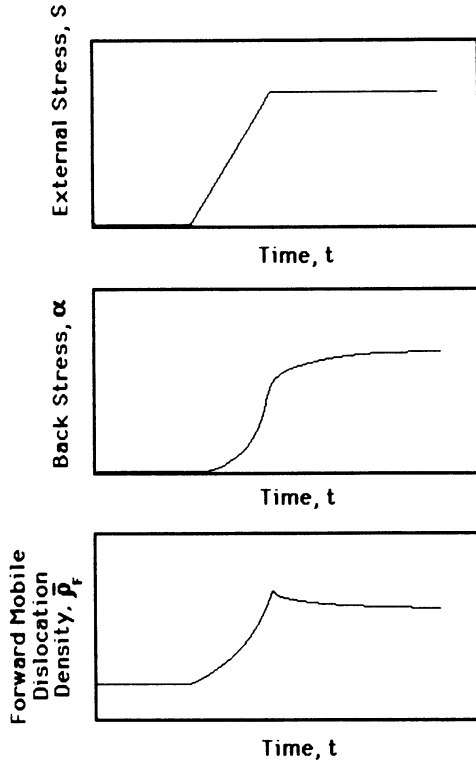


**Fig. 2.** Schematic representation of the behavior of the back stress for the skeletal model with the forward mobile dislocation density as used in the Gittus model; it is noted that the behaviors of the two quantities are qualitatively different.

few observations which can be made directly from eqn (6.2). The first is that the inelastic strain rate increases roughly as a power of stress since  $s^n$  factors out of the numerator. Although  $\bar{\rho}_F$  and  $\bar{\rho}_L$  are both functions of stress, it appears that the ratio is overshadowed by the power function. It is curious that the same stress factor also appears in an additive manner in the denominator. For very large stresses then the inelastic strain rate is a lower effective power of stress than for a small stress where the term in the denominator is ineffective.

A second observation from eqn (6.2) is that the decomposition of the strain rate into elastic and inelastic parts as stated in eqn (6.2a) is not a natural decomposition in this model. This is evidenced by the

appearance of  $\dot{\epsilon}$  in eqn (6.2b). This motion-enhanced inelastic straining is also unique to this model.

In conclusion, although we have been unsuccessful in placing this model into the form of the skeletal model, it is nonetheless an interesting model to study. It is particularly unique in its use of mobile dislocation density as a fundamental state variable. It is felt that Gittus has not been entirely successful in his multiaxial treatment. The theoretical base and the resulting working equations, however, make this a worthwhile model to study in spite of that weakness.

## 7. NUMERICAL DIFFICULTIES WITH THE MODELS

The use of unified creep-plasticity models has not become widespread in structural analysis due mainly to difficulties associated with the efficient implementation into finite element codes. In complex finite element analysis a percentage of the computation time is related to the integration of the constitutive model. The computation times range from a small percentage for linear elastic, to a much greater percentage when inelastic effects are included. The constitutive models are integrated separately from the solution of the boundary value problem through the introduction of an operator split. In this procedure, the balance laws are solved following the assumption that the stress is constant during the time step. This solution yields the strain increment in the case of the implicit code and the symmetric part of the velocity gradient (which is identical to the strain rate for small strains or small enough time increments) in the explicit codes. Then, the constitutive subroutine is solved for the same time step assuming this time that the strain rate is constant during the time step. Therefore, the problem of implementing UCP models of the type described by the skeletal structure in eqns (1.4)–(1.8) reduces to determining an algorithm which efficiently integrates this system of ordinary differential equations for the stress and internal variables, with the constant forcing function,  $\dot{\epsilon}_{ij}$ . These equations have been effectively separated from the geometric problems associated with the solution of the momentum balance equations. While this should be a simple task, unfortunately, this system of equations becomes very stiff in the mathematical sense, in certain regimes.

In this section, we adopt the definition used for mathematical stiffness. We assume that a system of ordinary differential equations is

stiff if it cannot be integrated without loss of stability using an explicit algorithm such as a forward Euler.

The importance of efficient algorithms for the integration of the constitutive subroutine is best illustrated by considering complex analyses. In particular, analysis of the short duration impact of bodies having complex geometries may result in integration of the constitutive subroutine for up to three to four billion times. A particular analysis was performed using the explicit finite element code DYN2D with a finite strain kinematic hardening UCP model of the same form as the skeletal structure described in eqns (1.4)–(1.8). For the purposes of having a base-time with which to compare our numerical algorithms, the same problem was solved using a rate independent bilinear hardening model.

The UCP model was integrated using a forward Euler scheme while the yield surface model employed the radial return technique. The UCP solution required over two orders of magnitude more time than did the classical yield surface plasticity model. This resulted from the inherent mathematical stiffness exhibited by the UCP model. During some of the time steps in which the model behaved in a particularly stiff manner, stability in the constitutive integration required time steps 9 to 10 orders of magnitude smaller than those required by the Courant condition for stability in the code. As a result, 95% of the solution time was now spent in the constitutive subroutine.

When considering the detailed numerical aspects of a system such as eqns (1.4)–(1.8), it is instructive to rewrite the equations for the one-dimensional case of uniaxial stress. We also choose a more specific form for the purpose of illustration. All of the arguments we present are valid for the more general skeletal structure. Therefore, consider a skeletal structure of the following form:

$$\dot{\sigma} = E(\dot{\epsilon} - \dot{\epsilon}^p) \quad (7.1)$$

$$\dot{\epsilon}^p = f\left(\frac{\sigma - \alpha}{R}\right) \quad (7.2)$$

$$\dot{\alpha} = H_\alpha \dot{\epsilon}^p - P_\alpha \alpha \quad (7.3)$$

$$\dot{R} = H_R |\dot{\epsilon}^p| - P_R |R - R_0| \quad (7.4)$$

It is shown that a system such as eqns (7.1)–(7.4) possesses one large eigenvalue,  $\lambda_1$ , which is proportional to

$$\lambda_1 \sim \frac{\partial f(\sigma - \alpha/R)}{\partial(\sigma - \alpha)} \quad (7.5)$$

In most models, the derivative in eqn (7.5) will be an increasing function of  $(\sigma - \alpha)$ . Since the stiffness of a system depends upon the largest negative eigenvalue, we see that this system will be stiff when  $(\sigma - \alpha)$  is very large and non-stiff in situations when  $(\sigma - \alpha)$  is small. This is consistent with previous observations<sup>1</sup> that models of this type are particularly stiff in high stress regions. From eqns (7.2) and (7.5) we see that the stiffness of these equations is inherently coupled to the underlying concept of unified creep-plasticity. Since the existence of an elastic region of space is not assumed, the flow rule  $f[(\sigma - \alpha)/R]$  must be formulated in such a way as to approximate the linear elastic regime in a plasticity model and to display a 'pseudo' yield limit. At small strains or large strain rates, the inelastic strain is essentially zero and grows rapidly with increasing stress, thereby predicting nearly elastic behavior during initial loading as well as for rapidly increasing strain rates or strain rate jumps. The functional form of the function  $f$  required to predict these responses is inherently stiff.

In recent years, several approaches have been developed to integrate UCP models more efficiently. Recently, Banthia and Mukherjee with their one-step Euler integration scheme with variable time step have improved the method by imposing a better time step control. This approach takes advantage of the fact that the equations appear to be stiffer for large strain rates. They choose a time step which is approximately inversely proportional to the strain rate. This scheme is more accurate but slightly less efficient than their previous algorithm.

Tanaka and Miller developed a non-iterative, self-correcting solution method (NONSS) for integration of these types of equations. This method is similar to the Newmark  $\beta$ -method in that a parameter is introduced which determines whether the method is explicit or implicit. This method was recently used on the Bodner equations in a comparative study by Chan *et al.* They concluded that any of the automatic time step control explicit integration schemes performed well if the strain increment was kept below  $10^{-4}$  (in/in). This can be a rather stringent requirement particularly in cases where the strain rate is very large for the large strain problems, resulting in a large number of integrations.

In the impact problem described earlier, a scheme was developed which capitalized upon the fact that not all integration points were stiff for each time step. For each subroutine call at each element, an analytic Jacobian was calculated first. This does not involve too much additional time since most of the functions in the Jacobian are

required for the function evaluation in the model. Based upon the norm of the Jacobian, it was determined whether the system was stiff for that particular integration point and time step. If the system was stable for the forward Euler, this scheme was used. If the forward Euler was not stable as determined by the norm of the Jacobian, the system was integrated using Newton's method. In the large strain impact problem described in this study only 1.3% of the integrations needed to be solved using Newton's method. Even with these improvements, the solution time was still an order of magnitude greater than the classical plasticity solution. However, this saved more than one order of magnitude in computation time compared to using a forward Euler in which the time step was chosen to accommodate the stiffness of the constitutive model.

These numerical difficulties are a serious consideration for engineers performing complex structural analyses with finite element codes. They are constantly confronted with the choice between inexpensive solutions and the use of sophisticated models which accurately describe material response.

## 8. CONCLUSION

This chapter has attempted to compare the various models presented in the preceding chapters based mainly upon their usefulness in finite element analyses. It is apparent from the models discussed that in recent years great advances have been made in bridging the gap between continuum plasticity and the underlying physical mechanisms of the inelastic mechanical response of materials. In this book a representative set of models have been discussed. As noted in the first chapter, the five models presented in the book are by no means an exhaustive set or even meant to be the five best models.

In the future, further advances in this area may reduce the rather large number of independent tests which are required to predict the complexities of this behavior. It is interesting to note that most of the models were not cast in a form addressing the issues of large strain deformation. This is an area in which similar gaps must be bridged between the kinematics of a continuum theory and the large rotations of grains and textures which develop in a material at very large strains. These processes may have as large an effect on the mechanical

response as the other physical mechanisms modeled in these chapters and is definitely an area for further research.

However, the biggest problem which must be overcome, if these models are to become useful design tools, is the efficient implementation into finite element codes of these models.

It is not apparent that an algorithm is imminent which will efficiently integrate these equations. This stems mainly from the numerical stiffness which is inherently coupled with the formulation of unified creep-plasticity models. As discussed earlier, the problem stems partially from the concept of simulating an apparent elastic regime without introducing a yield surface. This concept, in conjunction with the dislocation models of the process, requires that the plastic strain rate be a strongly increasing function of the stress (generally a power law exponential, or hyperbolic sine function). This formulation allows the plastic strain rate to be nearly zero at small stresses, and a nearly linear elastic stress response is predicted. The plastic strain rate then increases rapidly over a small stress change simulating an abrupt yield point. This approach, while accurately describing the material response, leads to the numerical difficulties. Perhaps it would be useful to re-formulate some of these approaches. Recent attempts to cast these models into the structure of yield surface models, to take advantage of the numerical tools available to that formulation, appear quite promising. However, much work is needed to determine the extent of the approximations associated with the approach.

In conclusion, we consider the problems faced by the analyst. The sophistication with which material behavior can be described by the models in this book, coupled with the numerical inefficiency associated with these models, requires more engineering judgement of an analyst than ever before. Since the cost of accurate description can be prohibitive, the analysts must be cautioned against overkill. Much effort is required in parameter studies, concerned not necessarily with the effect of the various model parameters on material response, but rather with the effect these parameters have on a finite element solution. This is strongly problem dependent. If one desires a solution which requires a global deformation or shape change, a sophisticated model is unnecessary. If, however, an accurate description of local stress or ensuing failure is demanded, more sophistication is required. Unfortunately, which of the parameters (strain rate sensitivity, recovery, thermal softening, primary creep, etc.) have the greatest influence on the solution to the boundary value problem is not well

understood. Research in this area is essential both to enhance the use of these models in structural analysis as well as to aid the analyst in choosing the appropriate models demanded by this problem.

### APPENDIX A: REDUCTION OF EQUATIONS FOR THE KHL MODEL CASE B

The case B model of Korhonen, Hannula and Li (KHL) is titled 'An Extension of Hart's Model to a Multiaxial Loading Case'. As implied in the title, most of the equations are simple extensions of their case A model and are taken from that section.

Two equations are missing from the model but are simply implied. The first concerns the volumetric behavior which is elastic and stated as

$$\sigma_{kk} = 3K\varepsilon_{kk} \quad (\text{A1})$$

where  $K$  is the elastic bulk modulus and  $\sigma_{ij}$  and  $\varepsilon_{ij}$  are infinitesimal stress and strain rate tensors. The deviatoric stress and strain rate tensors are defined as

$$s_{ij} = \sigma_{ij} - \sigma_{kk}\delta_{ij} \quad (\text{A2})$$

$$\dot{\varepsilon}_{ij} = \dot{\varepsilon}_{ij} - \dot{\varepsilon}_{kk}\delta_{ij} \quad (\text{A3})$$

where  $\delta_{ij}$  is the Kronecker delta which is zero for  $i \neq j$  and 1 if the two indices are equal. The UCP models are concerned with the deviatoric description. The second implied equation is that the external or mechanical strain rate is the sum of elastic and inelastic parts. The elastic strain rate is defined as  $\dot{s}_{ij}/2G$  so that the resulting equation is:

$$\dot{s}_{ij} = 2G(\dot{\varepsilon}_{ij} - \dot{\varepsilon}_{ij}^p) \quad (\text{A4})$$

where  $G$  is the elastic shear modulus.

There appear to be many dependent and independent variables in the KHL-B model. A list would include  $s_{ij}$ ,  $s_{ij}^a$ ,  $s_{ij}^f$ ,  $\sigma$ ,  $\sigma^a$ ,  $\sigma^f$ ,  $\dot{\varepsilon}_{ij}^p$ ,  $a_{ij}$ ,  $\alpha_{ij}$ ,  $\varepsilon$ ,  $a$ ,  $\alpha$ ,  $\sigma^*$ ,  $T$  and time. This is an imposing list of variables which appears to require 45 scalar storage locations for each of hundreds to thousands of points in a three-dimensional structural model where stresses are computed. In reality, there are not nearly this many variables which must be remembered. In this appendix we will eliminate all but the essential independent and dependent variables.

No simplifications will be made on the model. The KHL-B is actually a very storage efficient model as will be shown below.

The equations describing the KHL-B model are listed in the KHL eqns (1)–(7) and (10)–(20). Rather than restate these equations, the equations will be referenced as they are needed.

An important observation is that the tensor valued quantities  $\alpha_{ij}$ ,  $a_{ij}$ ,  $e_{ij}^p$ ,  $s_{ij}^f$ ,  $s_{ij}^a$  and  $s_{ij}$  are all collinear. This means that  $\dot{\alpha}_{ij}/\sqrt{(\dot{\alpha}_{pq}\dot{\alpha}_{pq})} = \dot{a}_{ij}/\sqrt{(\dot{a}_{pq}\dot{a}_{pq})}$  and so forth for all six tensors.

This collinearity is shown as follows. From eqns (13) and (14) we find

$$\frac{\dot{\alpha}_{ij}}{\dot{a}} = \frac{\dot{a}_{ij}}{\dot{a}} = \frac{3s_{ij}^a}{2\sigma_a} \quad (\text{A5a})$$

From KHL eqn (10) and eqn (A5a) we find

$$\begin{aligned} \dot{e}_{ij}^p &= \dot{\alpha}_{ij} + \dot{a}_{ij} \\ \dot{e}_{ij}^p &= \frac{3s_{ij}^a}{2\sigma_a} \dot{\alpha} + \frac{3s_{ij}^a}{2\sigma_a} \dot{a} \end{aligned}$$

The KHL eqn (1) is substituted to find

$$\frac{\dot{e}_{ij}^p}{\dot{\epsilon}_p} = \frac{3s_{ij}^a}{2\sigma_a} \quad (\text{A5b})$$

The KHL eqn (12) is now used with eqn (A5b) to find

$$\frac{s_{ij}^f}{\sigma_f} = \frac{s_{ij}^a}{\sigma_a} \quad (\text{A5c})$$

The KHL eqn (11) is used with eqn (A5c) and KHL eqn (2) to give

$$\frac{s_{ij}}{\sigma} = s_{ij}^a + \frac{\sigma_f}{\sigma_a} s_{ij}^f \frac{1}{\sigma} = \frac{s_{ij}^a}{\sigma_a} \quad (\text{A5d})$$

Equations (A5a)–(A5d) are now combined to give

$$\frac{\dot{\alpha}_{ij}}{\dot{\alpha}} = \frac{\dot{a}_{ij}}{\dot{a}} = \frac{\dot{e}_{ij}^p}{\dot{\epsilon}_p} = \frac{3s_{ij}^a}{2\sigma_a} = \frac{3s_{ij}^f}{2\sigma_f} = \frac{3s_{ij}}{2\sigma} \quad (\text{A5})$$

This collinearity simplifies the model considerably. It allows us to eliminate  $\dot{\alpha}_{ij}$ ,  $\dot{a}_{ij}$ ,  $\dot{e}_{ij}^p$ ,  $s_{ij}^a$  and  $s_{ij}^f$  by stating them in terms of  $\dot{\alpha}$ ,  $\dot{a}$ ,  $\dot{\epsilon}_p$ ,  $\sigma_a$  and  $\sigma_f$ , respectively, along with the directionality of  $s_{ij}$ .

The back stress  $\sigma_a$  plays an important role in many of the models.

For the purposes of the comparison of models in this chapter, it will be used as a state variable rather than using the anelastic strain,  $a_{ij}$ . This process begins by differentiating the KHL eqn (3):

$$\dot{\sigma}_a = M\dot{a}$$

Then KHL eqn (1) is substituted to obtain

$$\dot{\sigma}_a = M(\dot{\epsilon}_p - \dot{\alpha}) \quad (\text{A6})$$

The KHL eqn (4) is solved for  $\alpha$  and KHL eqn (5) is used to eliminate  $\epsilon^*$  and yield

$$\dot{\alpha} = \left( \ln \frac{\sigma^*}{\sigma_a} \right)^{-1/\lambda} \left( \frac{\sigma^*}{G} \right)^m f e^{-Q/RT} \quad (\text{A7})$$

where  $m$  is the 'inverse slope of the scaling direction' and  $f$  and  $Q$  are material parameters.

The KHL eqn (2) is used to eliminate  $\sigma_f$  in KHL eqn (7) and produce the result

$$\dot{\epsilon}_p = \dot{a}^*(T) \left( \frac{\sigma - \sigma_a}{G} \right)^M \quad (\text{A8})$$

Equations (A7) and (A8) are then used to eliminate  $\alpha$  and  $\epsilon_p$  and eqn (A6) to produce the resulting evolutionary equation for the scalar part of the back stress:

$$\dot{\sigma}_a = M \left[ \dot{a}^* \left( \frac{\sigma - \sigma_a}{G} \right)^M - \left( \ln \frac{\sigma^*}{\sigma_a} \right)^{-1/\lambda} \left( \frac{\sigma^*}{G} \right)^m f e^{-Q/RT} \right] \quad (\text{A9})$$

The hardness parameter,  $\sigma^*$ , is a state variable which is unique to this constitutive model. The evolutionary equation for  $\sigma^*$  is given by KHL eqn (6) which is

$$d(\ln \sigma^*)/dt = \Gamma^*(\sigma_a, \sigma^*) - R(\sigma^*, T) \quad (\text{A10})$$

where  $\Gamma^*(\sigma_a, \sigma^*) = \Gamma(\dot{\alpha}, \sigma^*)\dot{\alpha}$ . Equation (A7) is used to restate this in terms of our chosen variables as

$$\Gamma^*(\sigma_a, \sigma^*) = \Gamma \left[ \left( \frac{\sigma^*}{G} \right)^m f e^{-Q/RT} \left( \ln \frac{\sigma}{\sigma_a} \right)^{-1/\lambda}, \sigma^* \right] \\ \times \left( \frac{\sigma^*}{G} \right)^m f e^{-Q/RT} \left( \ln \frac{\sigma^*}{\sigma_a} \right)^{-1/\lambda} \quad (\text{A11})$$

Equation (A5) is used to eliminate  $s_{ij}^f/\sigma_f$  in KHL eqn (12) and eqn (A8) substituted into the resulting expression to obtain

$$\dot{e}_{ij}^p = (3/2)\dot{a}^* \left( \frac{\sigma - \sigma_a}{G} \right)^M \frac{s_{ij}}{\sigma} \quad (\text{A12})$$

The entire set of differential equations describing the deviatoric behavior predicted by the model are given by eqns (A4), (A5), (A11), (A9) and (A10) and gathered here for convenience:

$$\begin{aligned} \dot{s}_{ij} &= 2G(\dot{e}_{ij} - \dot{e}_{ij}^p) \\ \dot{e}_{ij}^p &= (3/2)\dot{a}^*(T) \left( \frac{\sigma - \sigma_a}{G} \right)^M \frac{s_{ij}}{\sigma} \\ \dot{\sigma}_a &= \left[ \dot{a}^*(T) \left( \frac{\sigma - \sigma_a}{G} \right)^M - \dot{\epsilon}^* \left( \ln \frac{\sigma^*}{\sigma_a} \right)^{-1/\lambda} \right] \\ d(\ln \sigma^*)/dt &= \Gamma^*(\sigma_a, \sigma^*) - R(\sigma^*, T) \\ \sigma &= \sqrt{1.5s_{ij}s_{ij}} \end{aligned} \quad (\text{A13})$$

The dependent and independent variables are time and  $\dot{e}_{ij}$ ,  $s_{ij}$ ,  $\sigma_a$ ,  $\sigma^*$  and  $T$ . The quantity  $\dot{e}_{ij}^p$  is merely used to place the model more conveniently into the standard form of UCP models.

## APPENDIX B: REDUCTION OF EQUATIONS FOR THE GITTUS MODEL

The Gittus model is stated in terms of components in the directions of the principal stress axes. It is assumed that these are also principal strain directions. Tensor quantities such as stresses are then denoted by a single subscript which takes values 1, 2 or 3.

The inelastic strain rate in the Gittus model is composed of two parts, the 'delayed elastic (recoil) strain',  $\dot{\xi}_i$ , and the 'creep strain',  $\dot{\epsilon}_i^c$ . This is taken from eqn (3.32) in Chapter 4 (Gittus) in scalar form to the principal axes differential form

$$\dot{e}_i^p = \dot{\epsilon}_i^c + \dot{\xi}_i \quad (\text{B1})$$

The creep strain rate components are given by Gittus eqns (4.68) and (4.70) as

$$\dot{\epsilon}_i^c = \frac{\bar{\rho}}{\rho_L} \frac{\dot{\epsilon}^{vs}}{\sigma^v} s_i \quad (\text{B2})$$

where  $s_i$  are the principal components of the external deviatoric stress. The stress measure  $\sigma^v$  is related to the magnitude of the deviatoric stress using Gittus eqn (4.59) and the definition of a deviatoric quantity. The result is

$$\sigma^v = \sqrt{2/3} |s_{ij}| \quad (\text{B3})$$

The limiting value of the mobile dislocation density under the prevailing conditions of stress and temperature is given in Gittus eqn (4.63) as

$$\bar{\rho}_L = \frac{\lambda \dot{\epsilon}^{vs} \bar{\rho}_\infty + \gamma}{\mu} \quad (\text{B4})$$

where from Gittus eqns (4.64b) and (4.51)

$$\begin{aligned} \mu &= \lambda \dot{\epsilon}^{vs} + \gamma \\ \gamma &= \exp(E' - Q/RT) \end{aligned} \quad (\text{B5})$$

The quantities  $\lambda$ ,  $\bar{\rho}_\infty$ ,  $E'$  and  $Q$  are material constants,  $R$  is the gas constant and  $T$  is the absolute temperature. The steady creep rate  $\dot{\epsilon}^{vs}$  is given by Gittus eqn (4.60) and eqn (B3) as

$$\dot{\epsilon}^{vs} = v(\sqrt{2/3} |s_{ij}|)^n \quad (\text{B6})$$

where

$$v = \exp(E_a - Q/RT)$$

and where  $n$  and  $E_a$  are material constants. The final quantity needed in order to evaluate eqn (B2) is the mobile dislocation density in the forward direction. This is obtained from the differential equations

$$\dot{\bar{\rho}}_F = -\mu(\bar{\rho}_F - \bar{\rho}_L) \quad (\text{B7a})$$

and

$$\dot{\bar{\rho}}_R = \mu(1 - \bar{\rho}_R) \quad (\text{B7b})$$

The first of these is Gittus eqn (4.65) and the second is found from eqns (4.64) and (4.73). This pair of differential equations is integrated in time and  $\bar{\rho}_F$  used in eqn (B2). If the strain rate is reversed at any time, then the values of  $\bar{\rho}_R$  and  $\bar{\rho}_F$  are switched;  $\bar{\rho}_R$  becomes  $\bar{\rho}_F$  and vice versa. For the case when the strain rate changes in some other way, consult Chapter 4. In any case, eqns (B2)–(B5) can be collapsed to the

equation

$$\dot{\epsilon}_i^c = \sqrt{1.5} \left( \frac{\lambda \dot{\epsilon}^{vs} + \gamma}{\lambda \dot{\epsilon}^{vs} \bar{\rho}_\infty + \gamma} \right) \bar{\rho}_F \dot{\epsilon}^{vs} \frac{s_i}{|s_j|} \quad (\text{B8})$$

where eqn (B6) is used to evaluate  $\dot{\epsilon}^{vs}$  and the differential eqn (B7) is used to evaluate  $\bar{\rho}_F$ .

The delayed elastic strain  $\xi_i$  is taken to be in the direction of the deviatoric stress as noted in Gittus eqn (4.30) which is restated as

$$\xi_i = \frac{1.5}{E^*} s_i \quad (\text{B9})$$

where  $E^*$  is a delayed elastic modulus and is given by Gittus eqns (4.32) and (4.36) and eqn (B4) as

$$\frac{1}{E^*} = \frac{\sqrt{2} l_a \lambda \dot{\epsilon}^{vs} (1 - \bar{\rho}_\infty)}{3 \sqrt{J_2} (\lambda \dot{\epsilon}^{vs} + \gamma)} \quad (\text{B10})$$

Equations (B9) and (B10) are combined to give

$$\xi_i = C(1 - \bar{\rho}_\infty) \frac{\dot{\epsilon}^{vs}}{\lambda \dot{\epsilon}^{vs} + \gamma} \frac{s_i}{|s_j|} \quad (\text{B11})$$

where  $C = (\sqrt{2}/3) l_a \lambda (1 - \bar{\rho}_\infty)$  and where we have used  $|s_j| = \sqrt{2J_2}$ . This is now differentiated under the assumption that we are considering radial loading only:

$$\dot{\xi}_i = \left[ C(1 - \bar{\rho}_\infty) \frac{(\lambda \dot{\epsilon}^{vs} + \gamma) \ddot{\epsilon}^{vs} - \lambda \dot{\epsilon}^{vs} \ddot{\epsilon}^{vs}}{(\lambda \dot{\epsilon}^{vs} + \gamma)^2} - C \frac{\partial \bar{\rho}_\infty}{\partial s} \frac{\dot{\epsilon}^{vs}}{\mu} \right] \frac{s_i}{|s_j|} \quad (\text{B12})$$

Differentiating eqn (B6) under constant temperature conditions and radial loading, we note that only  $\dot{\epsilon}^{vs}$  varies with time:

$$\frac{d}{dt} \dot{\epsilon}^{vs} = n \dot{\epsilon}^{vs} \frac{(s_1 \dot{s}_1 + s_2 \dot{s}_2 + s_3 \dot{s}_3)}{|s_j|^2}$$

If we confine our attention to radial loading and unloading this can be rewritten as

$$\frac{d}{dt} \dot{\epsilon}^{vs} = n \dot{\epsilon}^{vs} \frac{|\dot{s}_i|}{|s_j|} \quad (\text{B13})$$

This expression is substituted into eqn (B12) to give

$$\dot{\xi}_i = \frac{C}{\mu} \dot{\epsilon}^{vs} \left[ \frac{(1 - \bar{\rho}_\infty) \gamma n \dot{s}}{\mu s} - \frac{\partial \bar{\rho}_\infty}{\partial s} \right] \frac{s_i}{s}$$

This expression is now combined with eqns (B8), (B4), (B1) and (A4) to give

$$s_i = 2G e_i - \frac{2GC}{\mu} \dot{\epsilon}^{vs} \left( \frac{(1 - \bar{\rho}_\infty) \gamma n \dot{s}}{\mu s} - \frac{\partial \bar{\rho}_\infty}{\partial s} \right) \frac{s_i}{s} \\ - \sqrt{1.5} 2G \frac{\bar{\rho}_F}{\bar{\rho}_L} \dot{\epsilon}^{vs} \frac{s_i}{s}$$

Now, since we are considering radial loading only, any stress changes are in the direction of  $s_i$  so that we can consider only the magnitude of  $s_i$ . The vector components  $s_i$ ,  $e_i$  and  $\dot{s}_i$  can be replaced by their respective magnitudes and the equation solved for  $s$  as

$$\dot{s} = \frac{2G \left[ \dot{\epsilon} - \dot{\epsilon}^{vs} \left( \sqrt{1.5} \frac{\bar{\rho}_F}{\bar{\rho}_L} - \frac{C}{\mu} \frac{\partial \bar{\rho}_\infty}{\partial s} \right) \right]}{1 + \frac{2GC}{s\mu^2} \gamma n (1 - \bar{\rho}_\infty) \dot{\epsilon}^{vs}} \quad (\text{B14})$$

The right side of this equation is equated to  $2G(\dot{\epsilon} - \dot{\epsilon}_p)$  to give an expression for the inelastic strain rate:

$$\dot{\epsilon}_p = \frac{\frac{2GC\gamma n}{\mu^2 s} (1 - \bar{\rho}_\infty) \dot{\epsilon}^{vs} \dot{\epsilon} + \dot{\epsilon}^{vs} \left( \sqrt{1.5} \frac{\bar{\rho}_F}{\bar{\rho}_L} - \frac{C}{\mu} \frac{\partial \bar{\rho}_\infty}{\partial s} \right)}{1 + \frac{2GC\gamma n}{\mu^2 s} (1 - \bar{\rho}_\infty) \dot{\epsilon}^{vs}}$$

Equation (B6) is now used to give the result:

$$\dot{\epsilon}_p = \frac{B \dot{\epsilon} + \left( \sqrt{1.5} \frac{\bar{\rho}_F}{\bar{\rho}_L} - \frac{C}{\mu} \frac{\partial \bar{\rho}_\infty}{\partial s} \right)}{1 + B \dot{\epsilon}^{vs}} (\sqrt{2/3} s)^n \nu \quad (\text{B15})$$

where

$$B = \frac{2GC\gamma n}{\mu^2} (1 - \bar{\rho}_\infty) \quad (\text{B16})$$

For constant temperature and radial loading then the result is

$$\begin{aligned} \dot{s} &= 2G(\dot{\epsilon} - \dot{\epsilon}_p) \\ \dot{\epsilon}_p &= \left[ \frac{\frac{B\dot{\epsilon}}{s} + \sqrt{1.5} \frac{\bar{\rho}_F}{\bar{\rho}_L} - \frac{C}{\mu} \frac{\partial \bar{\rho}_\infty}{\partial s}}{1 + \frac{\nu B}{s} (\sqrt{2/3} s)^n} \right] (\sqrt{2/3} s)^n \nu \quad (\text{B17}) \\ \dot{\rho} &= -\mu(\bar{\rho}_F - \bar{\rho}_L) \\ \dot{\rho}_R &= -\mu(\bar{\rho}_R - 1) \end{aligned}$$

and various parameters are defined as follows:  $B$  by eqn (B16),  $\bar{\rho}_L$  by eqn (B4),  $\nu$  by eqn (B6) and  $\mu$  by eqn (B5). When the strain rate vector changes sign, the value of  $\bar{\rho}_F$  immediately after the reversal is taken to be the value of  $\bar{\rho}_R$  immediately before the reversal. In a similar way, the value of  $\bar{\rho}_R$  after the reversal is taken to be that of  $\bar{\rho}_F$  before the reversal.

## REFERENCES

1. R. D. Krieg, Numerical integration of some new unified plasticity-creep formulations, in *Proc. 4th SMIRT Conf.*, San Francisco, 1977, paper M6/4\*.
2. J. Gittus, *Creep, Viscoelasticity and Creep Fracture in Solids*, Applied Science Publishers, London, 1975.
3. J. Klepaczko, Thermally activated flow and strain rate history effects for some FCC polycrystalline metals, *Mat. Sci. Eng.*, **18** (1975) 121-36.

# Index

- Acceleration, 17–18
- Activation energy, 147, 149, 151, 201, 234, 285
- Aging, 18, 26
- Aluminum, 186–96, 268
  - alloys, 294
- Aluminum–magnesium alloys, 201
- Aluminum–zinc alloys, 269
- Amorphous solids, 125
- Anelastic deformations, 276
- Anelastic elements, 130
- Anelasticity, 225–31
- Angular yield surface shapes, 49
- Anisotropic deviatoric elastic compliance, 48
- Anisotropic elasticity, 47–8
- Anisotropic plasticity, 45–7
- Anisotropy, 41
- Aspects of behavior, 2, 3
- Asymptotic behavior, 6, 11
- Athermal hardening, 53–5
- Austenitic stainless steel, 198–201
  
- B1900 + Hf, 291, 293
- Back-extrapolation, 6, 15, 20
- Backstress, 306, 309, 322, 323
- Bailey–Orowan equations, 305
- Bailey–Orowan process, 245
- Bauschinger effect, 8, 15, 66–7, 94, 98, 126, 253, 255, 257
  
- Boundary conditions, 38
- Boundary element method, 90
- Bulk behavior, 304
- Burgers vector, 21, 232
  
- Cauchy stress, 30
- Classes of materials, 2
- Cold-rolled sheet, 47
- Constant extension/compression rate test, 108
- Constant-structure flow-kinetics curve, 24
- Constitutive relations for cubic metals or alloys, 76–81
- Cottrell–Jawson solute drag formulation, 162
- Cottrell–Stokes law, 70, 72, 74
- Cottrell–Stokes ratio, 150
- Creep, 58–9, 84
  - constant load, 108
  - irradiation-enhanced, 205, 206
- Creep behavior, 186, 307
- Creep deceleration, 58, 63
- Creep–plasticity interactions, 187–8
- Creep/plasticity unification, 142
- Creep rate *vs.* stress and temperature, 198–9
- Creep strain, 332
- Crystal coordinate system, 30
- Crystal plasticity, 29–36

- Crystallographic slip, 2, 29  
 Cyclic deformation, 143–5  
 Cyclic softening, 125, 173  
 Cyclic straining, 192–3  
 Cyclic stress–strain behavior, 200
- Delayed elastic strain, 332, 334  
   diagram, 225–31  
 Deviatoric behavior, 304  
 Deviatoric strain rate, 305  
 Diagnostic tools, 3  
 Differential constitutive relations,  
   59–61, 83  
 Diffusion, 147–52, 162–3, 234  
 Directional hardening, 143–5, 157–60  
 Dislocation(s), 21, 157, 158, 231  
   arrangement, 63  
   climb, 254  
   creep under multiaxial stresses,  
     224–42  
   density, 63, 65, 174  
   drag, 25  
   dynamics, 22, 273  
   glide, 2  
   models, 245  
   polycrystals, 68  
   storage, 2  
   theory, 28  
   velocity, 235–6  
 Dispersion-strengthened single  
   crystals, 68  
 Drag coefficient, 22  
 Dynamic recovery, 53–6, 63, 279  
 Dynamic strain aging, 145–6
- Elastic bulk modulus, 305  
 Elastic–plastic transition, 81  
 Elastic shear modulus, 305  
 Elastic–viscoplastic constitutive  
   equations, 273  
 Elastic–viscoplastic model, 273  
 Energy storage, 10  
 Equivalent strain, 12–13  
 Equivalent stress, 12–13  
 Evolution kinetics, 16
- $F_{\text{def}}$  equations, 164–9  
 $F_{\text{sol}}$  equations, 178–80  
 Fiber texture, 45  
 Finite difference computer programs,  
   296–7  
 Finite element computer programs,  
   295–6  
 Finite element method, 90  
 Fisher variable, 28  
 Flow chart, 109–15  
 Flow kinetics, 16–28, 82  
 Flow stress, 7, 25, 54, 63, 64, 70, 79,  
   92, 122–3, 156  
   saturation, 55  
   temperature sensitivity of, 284  
   *vs.* strain-rate relation, 28  
   *vs.* temperature, 71–2, 79  
   *vs.* temperature and strain,  
     199–200  
 Flow surface, 36  
 Friction element(s), 131  
   parameters, 110  
 Friction stress, 92, 104  
 Functional relations, 84
- Glide resistance, 64  
 Gliding dislocations, 232  
 Grain boundary element, 133  
 Grain boundary sliding, 101–3, 105,  
   126  
 Grain matrix deformation, 95–8  
 Grain sizes, 29  
 Green–McInnis stress flux, 258
- Haasen plot, 27, 74, 76  
 Hall–Petch equation, 161, 254  
 Hall–Petch plot, 79  
 Hardening, 9, 12, 26, 279  
   rules, 14–15, 48–9, 82  
   transients, 61–3  
 Hart’s model, 89–137  
   multiaxial loading case, 329–32  
   summary and critique, 316–20  
 Hastelloy-X, 282, 291, 293  
 History dependence, 141–2  
 History effects, 190–1

- Hooke's law, 275  
 Hydrostatic pressure, 47
- IN-100, 291  
 Inconel-718, 291  
 Incremental distortion tensor, 31  
 Inelastic behavior of solids, 274  
 Inelastic strain rate, 305, 335  
 Infinitesimal increment of strain, 2  
 Internal stresses, 64–72, 84, 92, 105, 158, 231  
   forward and backward, 66, 69–70  
 Internal structure, 152–3  
 Internal variable model, summary and critique, 308–10  
 Irradiation effects, 204–8  
 Irradiation hardening, 205  
 Isotropic hardening, 12, 14, 15, 48, 145, 154–7, 173, 281  
 Isotropic internal variable, 254–8
- Jerkiness, 16–17
- Kinematic hardening, 14, 48, 66–8, 173, 280  
 Kinematic internal variable, 253–4  
 Kinetic equation, 276, 284  
 Kronecker delta, 305  
 KSR model, 246, 254
- Lankford coefficient, 15  
 Latent hardening, 51–3  
 Lateral hardening, 49  
 Levy–Mises criterion, 228  
 Levy–Mises equations, 224  
 Limit of steady-state saturation, 55  
 Limiting behavior at low strains and low temperatures, 53  
 Load–elongation curve, 73  
 Localization, 17–18  
 Lüders bands, 18
- Machine coordinates, 31  
 Mar-M247, 291, 293
- MARC finite element computer code, 296  
 Material behavior, 27  
 Material constants, 211–12, 286–90  
 Material element, 2  
 Material parameters, 103–7  
   procedure for obtaining, 130–4  
 Material response, 2  
 MATMOD equations, 139–219  
   development of, 141  
   general form of, 142  
   phenomena simulated by, 140  
   phenomenological development of specific equations, 164–85  
   physical and phenomenological bases for, 146–64  
   simulations and predictions, 185–208  
   summary and critique, 310–12  
 Mechanical equation of state (MEDS), 221–43  
   computer program, 242  
   dislocation creep under multiaxial stresses, 224–42  
   reduction of equations, 332–6  
   summary and critique, 320–4  
   yield criteria, 221–4  
 Mechanical threshold, 18–20, 25, 28, 36, 81  
 Microscopic heterogeneities, 16–17  
 Microyield, 5, 8, 14  
 Mobile dislocation density, 21, 22, 231, 234, 237, 238, 322, 333  
 Mohr–Coulomb yield criterion, 222, 223  
 Multiaxial deformation, 11–16  
 Multiaxial directional strain softening, 195–6  
 Multiaxial generalization, 180–5  
 Multiaxial loading, 98  
 Multiaxial relations, 78  
 Multiaxial strain rates, 235–6  
 Multiaxial stresses, dislocation creep under, 224–42
- Negative rate sensitivity, 26  
 Non-iterative self-correcting solution method (NONSS), 210, 326

- Non-recoverable strain, 231–4
- Non-uniform deformation, 16–18
- Normality flow rule, 82
- Normalization, 20–1
- Normalized Taylor factor, 38
- Normalized variables, 84
- Numerical integration methods, 208–11
  
- Occam's Razor, 246
- Orientation change, 31
- Orientation distribution, 47
- Orientation effects, 30, 31
- Orowan stress, 65
- Overstress, 21–2
  
- Path changes, 8, 51
- Path dependence, 50–1
- Peierls forces, 152, 163
- Peierls potential, 125
- Peierls stress, 9, 74, 161
- Persistent slip bands, 174
- Plane-strain rolling, 44
- Plastic anisotropy, 15, 82
- Plastic deformation, 29
- Plastic element(s), 132, 133
  - parameters, 112
- Plastic potential, 32–3, 40, 47
- Plastic strain rate, 307, 315
- Plastic viscosity, 11
- Plasticity, 3, 16, 20
- Polycrystals
  - dislocations in, 68
  - plasticity, 28–48
  - strain hardening in, 245
  - yield surface, 41–5
- Portevin–LeChatelier effect, 180
- Power-law creep, 71
- Power-law flow rule, 245
- Prandtl–Reuss flow law, 275
- Pressure dependence, 9–10
  
- R* Equation, 170
- R*-Value, 15
  
- Rate dependent plasticity model, 245–271
  - behavior of, 268–9
  - determination of constants, 260–6
  - final equations, 258–60
  - general problem, 248–53
  - parameter determination problems, 266–8
  - proposed new model, 253–68
- Rate sensitivity, 8–9, 35–6, 74, 75, 77, 81
- Recovery behavior, 67–8, 75, 307
- Recovery kinetics, 245
- Regimes of variables, 2
- Relaxed constraints, 39, 45, 47
- Remobilisation, 234–5
- René-95, 291
- Resolved stress, 31–3, 37, 49
  
- Saturation stress, 56
- Schmid factor, 31
- Schmid law, 32
- Screw dislocations, 174
- Shear modulus, 20–1
- Shear processes, 21
- Shear stress, 21
- Single crystals, 29, 33–5, 37
  - dispersion-strengthened, 68
- Single-phase materials, 68–72
- Skeletal model, 308
- Slip systems, 30, 34, 35, 40
- Slip theory, 15
- Solute drag, 160–4
- Solute effects, 198
- Stacking-fault energy (SFE), 57
- State variable theories, 89–137
  - summary and critique, 316–20
- Steady-state flow, 143
- Strain aging, 24, 125
- Strain dependence, 27–8
- Strain hardening, 6–8, 14, 51–3, 65, 83, 186
  - constant strain rate, 186–7
  - polycrystals, 245
- Strain hardening rate, 8, 46, 52–4, 59, 63, 74, 77–80
- Strain increment, 2

- Strain rate, 30, 307  
 equations, 164–9  
*vs.* stress diagram, 19
- Strain softening, 155, 186
- Strain time equation, 236–42
- Straining direction, 37
- Stress, 2  
 concentration factor, 105  
 dip test, 261–4  
 dip/rise test, 267  
 direction, 37  
 exponent, 9  
 path, 8  
 recovery, 194  
 relaxation, 26–7, 70, 200  
 reversal, 8, 75, 234–5
- Stress–strain curves, 3, 4, 6–8, 62, 100, 314, 316
- Stress/strain/strain–rate relations, 18
- Stress/strain/strain–rate test, 73–5
- Substructure evolution, 51–64
- Taylor factor, 52, 55
- Temperature dependence, 76, 83, 142
- Temperature effects, 308
- Temperature/material scaling, 56–8
- Temperature sensitivity of flow stress, 284
- Texture evolution, 48–51
- Texture hardening, 49–50
- Texture softening, 49–50
- Thermal activation, 22–5
- Thermodynamic threshold, 10
- Time effects, 25–6
- Transient(s), 7–8, 51, 61–3, 83  
 creep, 80  
 deformation, 98–101
- Tresca hexagon, 11
- Tresca yield criterion, 222, 223
- Twinning, 29
- Two-phase materials, 65–8
- Ultimate tensile strength, 55, 75, 77
- Uniaxial monotonic deformation, 4–10
- Unidirectional strain softening, 194
- Unified creep–plasticity (UCP)  
 models, 245, 253  
 numerical difficulties, 324–7  
 summary and critique, 303–36
- Unified elastic–viscoplastic theory, 273–301  
 applications, 295–8  
 constitutive equations, 275–86  
 evolution equations, 278–84  
 material constants, 286–90  
 modeling of metals, 290–4  
 special problems, 297–8  
 summary and critique, 312–16  
 temperature dependence, 284–6
- Uniform deformation, 18–28
- Unloading and reloading effects, 70, 194–5, 307
- Unstable behavior, 17
- Viscous drag, 21
- Viscous glide, 22
- Voce law, 55
- Volume changes, 9–10
- Volume-conservation criterion, 228
- Von Mises circle, 11
- Von Mises criterion, 12, 221–3
- Von Mises potential, 46
- Von Mises yield surface, 224
- Work hardening, 14, 62, 123–4, 155  
 equation, 114  
 rate, 59
- Work increment, 31–2
- Yield, 4–6, 11, 14, 15  
 criteria, 221–4  
 applicable to metals, 223–4  
 applicable to polymers, 222–3  
 non-requirement of, 274  
 drop, 7  
 point, 27  
 strength, 11  
 stress, 6, 11, 20, 76

**Yield—*contd.***

surface, 11, 14, 15, 20, 33, 34, 36,  
40, 47, 81, 224  
polycrystals, 41–5

**Young's modulus, 310**

**Zener parameter, 58**

**Zircaloy, 201, 204–8**